SPECTRUM EFFICIENT CELLULAR BASE-STATION ANTENNA ARCHITECTURES

Simon C. Swales

A thesis submitted to the University of Bristol in accordance with the requirements for the degree of Doctor of Philosophy in the Faculty of Engineering, Department of Electrical & Electronic Engineering.

November 1990

ABSTRACT

The frequency spectrum is, and always will be, a finite and scarce resource, thus there is a fundamental limit on the number of radio channels which can be made available to mobile telephony. It is essential, therefore, that Cellular Land Mobile Radio systems utilise this commodity efficiently, so that a service can be offered to as large a subscriber community as possible. The public demand for mobile telephony has so far exceeded capacity forecasts for the first generation of mobile cellular communications networks, and analysts are now predicting that there could be 10 million users in the UK alone by the year 2000. Consequently, the next generation of cellular networks and future Personal Communication Networks (PCN's) will be beset with the problem of severe spectral congestion as the subscriber community expands.

In this thesis a multiple beam adaptive base-station antenna is proposed to complement other solutions, such as spectrum efficient modulation, currently being developed to meet the proliferating demands for enhanced capacity in cellular networks. This novel approach employs an antenna array capable of resolving the angular distribution of the mobile users as seen at the base-station site, and then utilising this information to direct beams towards either lone mobiles, or groupings of mobiles, for both transmit and receive modes of operation. The energy associated with each mobile is thus confined to an addressed volume, greatly reducing the amount of co-channel interference experienced from and by neighbouring co-channel cells. In this study, a figure of merit is established for the proposed base-station antenna with respect to a conventional omni-directional antenna. A statistical propagation model is employed and the results indicate that a significant increase in the spectrum efficiency, or capacity, of the network is attainable. The task of resolving the location of the mobile user is fundamental to the operation of the proposed antenna system. Therefore, with the aid of computer simulations and an experimental test rig, the ability to estimate the azimuth bearing of a mobile test source in a typical urban environment is demonstrated. Further to this, the results of the field trials provide a revealing insight into the signal scattering conditions which prevail in an urban locality.

To my mother and to the memory of Baggins

ACKNOWLEDGEMENTS

Over the last three years there have been so many people who have contributed to this piece of work either directly or indirectly, that it is difficult to know where to start the acknowledgements. The best place is usually at the beginning, and so this honour must go to Professor J.P. McGeehan who was the first person at Bristol to seriously consider the potential advantages to be gained with advanced base-station antenna technology, and secured a project funded by the UK SERC. As director of the Centre for Communications Research, Professor McGeehan has also provided invaluable support and made so much possible. I would also like to extend my thanks to the UK SERC for their financial support.

My supervisor over the first two years was Dr. D.J. Edwards, and throughout this period his enthusiasm and input to the project was much appreciated.

For the last two years, the work has been funded as a CASE Award with the Antennas Group at British Telecom Research Labs. (BTRL), Martlesham. The head of the group is Miles Butcher who, as my industrial supervisor, has made a significant contribution to the work. I am also extremely grateful to the other members of the group, and in particular Ian Rose and Roger Stuckey. My special thanks also go to John who runs the long test range, since without his help and endless patience, the array manifold measurements in chapter 6 would not have been as successful.

The construction of the DF test rig and subsequent trials brought the project to a suitable conclusion, and this was achieved with the valuable assistance of many individuals: Philip Mattos of INMOS (Bristol) for the donation of the Transputer Board, John MacLeod for the power amplifiers, Tony Ward and his crew at Graseby Dynamics for many fruitful discussions on the DF process, Geoff Hilton for the patch antenna design, Bob Butler for the dipole array, and finally, Ross Wilkinson and the crew of the "DORMOUSE" hot air balloon for the photograph in figure 6.22. I would like to thank Bob Butler in particular for his assistance throughout the field trials.

My colleagues in the Centre for Communications Research have proved to be invaluable over the last three years, providing a wealth of experience in all aspects of mobile communications. I would like to thank in particular my fellow postgraduates for many inspirational beers.

I would now like to express my special thanks to two people who have been very close to me over the last few years. Firstly to Alison, whose unceasing support is much appreciated. Although a mathematician, her superior grasp of written English has saved many sentences in this thesis and, as a Quantity Surveyor, her skills also proved invaluable, enabling the height of the base-station site to be accurately measured. Also, my thanks go to my flatmate, Darren, for never taking me too seriously, especially through the endless period of writing up.

Finally, I would like to express my special thanks to Dr. Mark Beach, who has contributed in so many ways to this piece of work that it would be impossible to list them all here. As my supervisor for the final year, he has had the unenviable task of reviewing this manuscript, and for this alone, he has my sincerest thanks.

DECLARATION

Unless otherwise acknowledged, the content of this thesis is the original work of the author. None of the work in the thesis has been submitted by the author in support of an application for another degree or qualification at this, or any other University or institute of learning.

Simon C. Swales

COPYRIGHT

CONTENTS

List of Figures ix
List of Tables xiii
Glossary xiv

1 INTRODUCTION 1

1.1 The Evolution of Mobile/Personal Communications 1
1.2 Spectrum Efficiency 5
1.3 Outline of Thesis 8

2 ANTENNA ARRAYS FOR CELLULAR BASE-STATIONS 12

2.1 Adaptive Antenna Arrays 12
2.2 Advanced Base-Station Antenna Design 13
2.2.1 Antenna Diversity 13
2.2.2 Optimum Combining 15
2.2.3 Multiple Beams 18
2.3 The 'Smart' Base-Station Antenna 20

3 POTENTIAL CAPACITY ENHANCEMENT WITH THE "SMART" BASE-STATION ANTENNA 26

3.1 Preliminaries 27
3.2 Modelling the Co-channel Interference Environment 30
3.2.1 Geometrical Propagation Model 32
3.2.2 Statistical Propagation Model - One Co-channel Cell 36
3.2.3 Statistical Propagation Model - Six Co-channel Cells 39
3.3 Conclusions 42

4 DIRECTION FINDING IN THE CELLULAR LMR ENVIRONMENT: AN INTRODUCTION 45

4.1 Angle of Arrival Estimation with Antenna Arrays 46
4.1.1 The Fourier Method (FM) 47
4.1.2 Maximum-Likelihood Method (MLM) 51
4.1.3 Maximum-Entropy Method (MEM) 52
4.1.4 Eigenstructure Methods 55
4.2 Comparison of DF Algorithms 62
4.3 Factors Affecting Performance 65
4.3.1 Array Manifold 65
4.3.2 Temporal Averaging 65
4.3.3 Coherent Multipath 66
4.4 Application in a Cellular Radio Environment 67

5 DIRECTION FINDING IN THE CELLULAR LMR ENVIRONMENT: A COMPUTER SIMULATION STUDY 72

5.1 Urban Communications 73
5.1.1 Local Scattering Environment 73
5.1.2 Co-Channel Interference 79
5.1.3 Mutual Coupling 80
5.1.4 Receiver Channel Mismatch 81
5.1.5 Performance of DF Algorithms in an Urban Environment 82
5.2 Suburban/Rural Communications 101
5.2.1 Discrete Multipath Environment 101
5.2.2 Performance of DF Algorithms in a Suburban/Rural Environment 102
5.3 The Ability to Track a Single Mobile Source 108
5.3.1 Urban Communications 110
5.3.2 Suburban Communications 115
5.3.3 Rural Communications 118
5.4 Simulation of an FDMA Scheme 118

6 DIRECTION FINDING IN THE CELLULAR LMR ENVIRONMENT: AN EXPERIMENTAL SYSTEM 123

6.1 Four Channel DF Receiver 124
6.1.1 Antenna Array 124
6.1.2 RF Front End 131
6.1.3 70 MHz IF Stage 133
6.1.4 Baseband Processing 135
6.1.5 Analogue-to-Digital Conversion 137
6.1.6 Off-line AOA Estimation 141
6.1.7 Mobile Test Source 141
6.2 Array Manifold Measurement 144
6.3 Field Trials 156
6.3.1 Trial I - Cathedral Car Park 161
6.3.2 Trial II - Great George St. 164
6.3.3 Trial III - Charlotte St. South 170
6.3.4 Trial IV - Park St. 175
6.3.5 Trial V - Berkeley Square 179
6.4 Conclusions 185
6.4.1 Comparison of Simulation Results with Field Trials 185
6.4.2 Characteristics of the Urban Environment 187
6.4.3 Implementation Issues 187

7 IMPLEMENTATION ISSUES 191

7.1 Base-Station Hardware 192
7.2 Modulation Format 196
7.2.1 Narrowband Modulation 196
7.2.2 Wideband Modulation 198
7.3 Beamforming 199
7.3.1 Potential Antenna Configuration 202
7.3.2 Fixed Multiple Beams 204
7.3.3 Active Multiple Beams 208
7.3.4 Digital Beamforming 210

8 DISCUSSION 214

8.1 Summary 214
8.2 Future Work 217
8.3 Value Added Services 220
8.4 Concluding Remarks 223

APPENDIX A Adaptive Antenna Array Fundamentals 224

APPENDIX B "The Performance Enhancement of Multi-Beam Adaptive Base-Station Antennas for Cellular Land Mobile Radio Systems", IEEE Transactions on Veh. Technol., Vol.VT-39, No.1, Feb. 1990. 226

APPENDIX C The Basic Signal Model 239

APPENDIX D Formation of the Vector d for KuTu Algorithm 243

APPENDIX E Summary of Algorithms for AOA Estimation 246

APPENDIX F Calculation of Mutual Impedance Matrix for an Antenna Array. 247

APPENDIX G Forward/Backward Spatial Smoothing for AOA Estimation in a Discrete Multipath Environment 249

APPENDIX H Extension of Basic Signal Model for Multiple Sources in an FDMA Communications Scheme 255

APPENDIX I Calculation of SNR at Receiver Input 261

APPENDIX J List of Publications 264

LIST OF FIGURES

CHAPTER 1

Fig. 1.1: Hexagonal cellular layout with a 7 cell cluster. 3
Fig. 1.2: Cell splitting a hexagonal floor plan. 5
Fig. 1.3: Cell sectorisation using directional antennas: (a) 120° ; (b) 60°. 6
Fig. 1.4: Controlling energy overspill using antenna arrays. 7

CHAPTER 2

Fig. 2.1: Tracking mobiles with multiple beams. 18
Fig. 2.2: Rejection of co-channel interference with: (a) optimum combining; (b) single independent beam. 21
Fig. 2.3: Multiple beam assignment within a cell. 22
Fig. 2.4: The "smart" base-station antenna concept. 22

CHAPTER 3

Fig. 3.1: Two co-channel cells. 27
Fig. 3.2: Hexagonal cellular layout with a 7 cell cluster. 28
Fig. 3.3: Contour defining interference regions. 33
Fig. 3.4: Contour defining interference regions with fading and shadowing. 37
Fig. 3.5: Relative spectral efficiency as a function of the number of beams/sectors formed. 41

CHAPTER 4

Fig. 4.1: Radiation pattern for an eight element array. 50
Fig. 4.2: Geometrical representation of Direction Finding with a three element antenna array. 56
Fig. 4.3: The mobile propagation environment. 68

CHAPTER 5

Fig. 5.1: Three typical mobile radio scenarios: (a) urban; (b) suburban; (c) rural. 74
Fig. 5.2: The scattering environment. 75
Fig. 5.3: Resulting spatial spectra with the reference urban scenario: (a) FM, MLM & MEM; (b) MUSIC, JoDeG & KuTu. 84
Fig. 5.4: Resulting spatial spectra for the MUSIC algorithm with varying numbers of scatterers. 87
Fig. 5.5: Resulting spatial spectra for the MUSIC algorithm with a varying spread of scatterers. 87
Fig. 5.6: Resulting spatial spectra for the MUSIC algorithm with different SNR's. 89
Fig. 5.7: Resulting spatial spectra for the KuTu, JoDeG and MUSIC algorithms when the SNR is 0dB. 89
Fig. 5.8: Resulting spatial spectra for the KuTu and MUSIC algorithms with 2 signal sources of SNR=10dB. 90
Fig. 5.9: Resulting spatial spectra for the MUSIC algorithm with different numbers of snapshots K. 92
Fig. 5.10: Variation of the input SNR. 92
Fig. 5.11: Resulting spatial spectra for the MUSIC algorithm with and without mutual coupling. 93

Fig. 5.12: Resulting spatial spectra for the KuTu and JoDeG algorithms with mutual coupling. 94
Fig. 5.13: Resulting spatial spectra for the MUSIC algorithm with amplitude uncertainty. 95
Fig. 5.14: Resulting spatial spectra for the KuTu and JoDeG algorithms with σ_γ=0.1. 96
Fig. 5.15: Resulting spatial spectra for the MUSIC algorithm with phase uncertainty. 96
Fig. 5.16: Resulting spatial spectra for MUSIC, KuTu and MEM algorithms when the modified steering vector is employed. 97
Fig. 5.17: Resulting spatial spectra for the MUSIC algorithm with a co-channel source located at $+30^\circ$. 99
Fig. 5.18: Resulting spatial spectra for FM, MLM and MEM algorithms with a SINR of 10dB. 99
Fig. 5.19: Resulting spatial spectra with three co-channel sources (SINR=10dB). 100
Fig. 5.20: Resulting spatial spectra for the MUSIC algorithm in suburban and rural environments: (a) no spatial smoothing; (b) spatial smoothing. 104
Fig. 5.21: Results of applying spatial smoothing with MUSIC in the rural environment for ideal and practical arrays. 106
Fig. 5.22: Resulting spatial spectra for the MUSIC algorithm in a suburban environment with and without spatial smoothing. 108
Fig. 5.23: Results in mobile urban environment with the MUSIC algorithm. 111
Fig. 5.24: Results in mobile urban environment with the MLM algorithm. 111
Fig. 5.25: Results in mobile urban environment with the KuTu algorithm. 112
Fig. 5.26: The MUSIC algorithm in the mobile urban environment with two interfering co-channel sources. 114
Fig. 5.27: The MLM algorithm in the mobile urban environment with two interfering co-channel sources. 114
Fig. 5.28: Results of mobile suburban environment with the MEM algorithm (no spatial smoothing). 116
Fig. 5.29: Results of mobile suburban environment with the FM algorithm (no spatial smoothing). 116
Fig. 5.30: Results in mobile suburban environment with the MEM algorithm with spatial smoothing applied. 117
Fig. 5.31: Movement of mobiles in a simulated FDMA scheme. 120

CHAPTER 6

Fig. 6.1: Four channel DF receiver architecture. 125
Fig. 6.2: Four element antenna arrays for DF receiver: (a) the dipole array; (b) the patch array. 126
Fig. 6.3: Antenna pattern measurement. 127
Fig. 6.4: Azimuth radiation patterns for each element of the dipole array. 128
Fig. 6.5: Dimensions of a single microstrip patch antenna element: (a) top view; (b) cross section. 129
Fig. 6.6: Azimuth radiation patterns for each element of the patch array. 130
Fig. 6.7: Dimensions of microstrip interdigital bandpass filter design. 132
Fig. 6.8: Testing the receiver chain in the anechoic chamber. 136
Fig. 6.9: The complete DF receiver hardware: (a) RF front end; (b) IF to baseband downconversion unit. 138
Fig. 6.10: Schematic of data acquisition hardware. 140

Fig. 6.11: Processes involved in array data acquisition. 140
Fig. 6.12: Block diagram of complete AOA estimation process. 142
Fig. 6.13: Mobile test source. 143
Fig. 6.14: Measuring the array manifold. 146
Fig. 6.15: Setup for measurement of array manifold. 147
Fig. 6.16: Dipole array and RF front end mounted on turntable. 147
Fig. 6.17: Effective radiation patterns for each channel with: (a) the dipole array; (b) the patch array. 149
Fig. 6.18: Phase errors across the dipole array for each channel at elevations of $\psi = 0^\circ$, 5° and 10°. 151
Fig. 6.19: Phase errors across the patch array for each channel at elevations of $\psi = 0^\circ$, 5° and 10°. 152
Fig. 6.20: Estimated AOA's from manifold data ($\psi=0^\circ$) with the MUSIC algorithm: (a) the dipole array; (b) the patch array. 154
Fig. 6.21: View of Clifton from the base-station site. 157
Fig. 6.22: Aerial photograph of the test area (Clifton). 157
Fig. 6.23: Map of Clifton area showing the test routes followed by the mobile. 159
Fig. 6.24: Measured fading signal envelopes in all four channels. 160
Fig. 6.25: Spatial spectra for Trial I with the dipole array and the MLM algorithm. 162
Fig. 6.26: Spatial spectra for Trial I with the patch array: (a) measured data; (b) simulated data. 163
Fig. 6.27: The view of Great George St. from the start of Trial II. 165
Fig. 6.28: The view towards the base-station from the end of Trial II. 165
Fig. 6.29: Estimated bearings for Trial II with: (a) the dipole array; (b) the patch array. 167
Fig. 6.30: Spatial spectra for frame 0 of Trial II with the dipole array. 168
Fig. 6.31: Spatial spectra for frame 4 of Trial II with the patch array. 169
Fig. 6.32: Spatial spectra for frame 10 of Trial II with the dipole array. 170
Fig. 6.33: The view from the end of Charlotte St. South down Charlotte St. 171
Fig. 6.34: The view of Park St from the start of Trial IV. 171
Fig. 6.35: Estimated bearings for Trial III with: (a) the dipole array; (b) the patch array. 173
Fig. 6.36: Spatial spectra for frame 3 of Trial III with the dipole array. 174
Fig. 6.37: Spatial spectra for frame 2 of Trial III with the patch array. 174
Fig. 6.38: Estimated bearings for Trial IV with: (a) the dipole array; (b) the patch array. 176
Fig. 6.39: Spatial spectra for frame 1 of Trial IV with the dipole array. 177
Fig. 6.40: Spatial spectra for frame 3 of Trial IV with the dipole array. 177
Fig. 6.41: Spatial spectra for frame 6 of Trial IV with the dipole array. 179
Fig. 6.42: Berkeley Square (trial V) as viewed from base-station site. 180
Fig. 6.43: The view back from the end of Trial V. 180
Fig. 6.44: Estimated bearings for Trial V with: (a) the dipole array; (b) the patch array. 181
Fig. 6.45: Spatial spectra for frame 4 of Trial V with the dipole array. 183
Fig. 6.46: Spatial spectra for frame 5 of Trial V with

the patch array. 183
Fig. 6.47: Spatial spectra for frame 11 of Trial V with the dipole array. 184

CHAPTER 7

Fig. 7.1: Simplified block diagram of base-station hardware for the American AMPS system. 193
Fig. 7.2: Broadband linear power amplifier. 195
Fig. 7.3: Multiple beam antenna array. 200
Fig. 7.4: Beamforming network for single beam operation. 201
Fig. 7.5: Potential antenna configurations:
(a) 16 beams in 4 zones.
(b) 12 beams in 3 zones. 202
Fig. 7.6: 4x8 patch array for proposed base-station antenna. 203
Fig. 7.7: The Rotman lens feeding a linear array. 205
Fig. 7.8: Lossless 8 element, 8 beam Butler matrix beamforming network. 206
Fig. 7.9: Schemetic of 'smart' base-station antenna employing RF beamforming. 207
Fig. 7.10: Active beamforming network. 209
Fig. 7.11: Schematic of full digital implementation of proposed base-station system. 211

CHAPTER 8

Fig. 8.1: Closing the loop. 218
Fig. 8.2: User location with two base-station antennas. 221
Fig. 8.3: Overlapping cell boundaries. 223

APPENDICES

Fig. A.1: An adaptive antenna array. 225
Fig. C.1: Linear array with a single incident plane wave. 240
Fig. F.1: Representation of an antenna array. 248
Fig. G.1: Forward/Backward subarraying. 251
Fig. H.1: An antenna array with a tapped delay line. 255
Fig. H.2: Channel allocation for an FDMA type scheme. 259
Fig. I.1: Parameters for calculation of input SNR. 262

LIST OF TABLES

CHAPTER 3

Table 3.1: Comparison of fixed sector directional antennas with omni-directional antenna using geometrical model. 36

CHAPTER 5

Table 5.1: Reference urban scenario. 83
Table 5.2: Results of peak search on spectra from reference urban scenario. 85
Table 5.3: Results of peak search for the MUSIC algorithm with varying numbers of scatterers. 86
Table 5.4: Results of peak search for the MUSIC algorithm with varying spread of scatterers. 86
Table 5.5: Results of peak search for the MUSIC algorithm with different SNR's. 88
Table 5.6: Results of peak search for the MUSIC algorithm with different numbers of snapshots. 91
Table 5.7: Results of peak search for the MUSIC algorithm with one co-channel source. 98
Table 5.8: Reference suburban scenario. 103
Table 5.9: Results of peak search for the MUSIC algorithm in suburban & rural environments with one coherent multipath. 105
Table 5.10: Error statistics for mobile urban scenario. 112
Table 5.11: Error statistics for mobile urban scenario with two co-channel sources. 113
Table 5.12: Error statistics for mobile suburban scenario with no spatial smoothing. 115
Table 5.13: Error statistics for mobile suburban scenario with spatial smoothing. 117
Table 5.14: Set-up for mobile sources in simulated FDMA scheme. 120
Table 5.15: Error statistics for urban and non-urban environments in an FDMA scheme. 121

CHAPTER 6

Table 6.1: Measured parameters of RF front end. 133
Table 6.2: Measured response of IF filter and amplifier. 134
Table 6.3: AOA error statistics for measured manifold data. 153
Table 6.4: AOA error statistics for different types of data processing with alternative manifolds. 155
Table 6.5: Details of test routes. 158

CHAPTER 7

Table 7.1: System parameters for 1st generation UK & USA networks. 194

APPENDICES

Table G.1: Properties of spatial smoothing techniques. 254

GLOSSARY OF PRINCIPAL SYMBOLS

a_m	Complex amplitude of mth signal.
$\mathbf{a}(k)$	Signal-in-space vector.
a	Erlangs of offered traffic.
A	Area of a cell in km^2.
$\mathbf{b}(\theta_m)$	Direction vector associated with mth source.
B	Direction matrix.
B	Blocking probability.
B_t	Total available signal bandwidth for communications network (MHz).
B_c	Frequency channel spacing (MHz).
C	Number of cells in a cluster.
d	Spacing between adjacent elements in an antenna array (m).
d	Steering vector for KuTu DF algorithm
D	Co-channel reuse distance (km).
$\mathbf{e}_i$	The ith eigenvector of the array covariance matrix, **R**.
$\mathbf{E}_N$	Matrix of noise eigenvectors.
$\mathbf{E}_S$	Matrix of signal eigenvectors.
E	Spectrum efficiency.
E_r	Relative spectrum efficiency.
ϕ	Inter element phase shift across the array (radians).
γ	Propagation path loss slope.
Γ	Diagonal matrix of receiver channel mismatches.
I	Identity matrix.
K	Number of snapshots.
η	Loading factor of a cell (number of erlangs/channel).
λ_m	Wavelength of mth signal source (m)
λ_i	The ith eigenvalue of the array covariance matrix, **R**.
M	Number of signals incident on to the antenna array.
N	Number of elements in the antenna array.
N_c	Number of channels allocated per cell.
pdf	Probability density function.
p_r	Protection ratio.
p_R	20 $log_{10} p_r$ (dB)
$P(s_w \leq p_r s_i)$	Probability of co-channel interference occurring (outage probability).

$P(\phi)$	Spatial spectrum
Q	Co-channel reuse ratio.
θ_m	Angle of arrival of mth source off the array broadside (degrees).
$\mathbf{R}$	Array covariance matrix.
$\hat{\mathbf{R}}$	Sampled covariance matrix.
R	Cell radius (km).
$\mathbf{s}(k)$	Received signal vector across the antenna array.
SINR	Signal-to-interference-plus-noise ratio (dB).
SNR	Signal-to-noise ratio (dB).
σ	Standard deviation in dB of the log-normal shadowing pdf.
$\mathbf{u}$	Ideal steering or weight vector.
$\mathbf{u}'$	Modified steering vector.
$\mathbf{w}$	General steering vector.
$\mathbf{w}_o$	Optimised steering vector
$\mathbf{x}(k)$	Observed signal vector across the array.
$\mathbf{Z}_o$	Normalised impedance matrix of an antenna array.

CHAPTER 1

INTRODUCTION

"Imagine a time when, instead of having a home telephone number, an office telephone number and an answering machine that gives a number where you can be contacted when you go away for the weekend, you have just one personal telephone number, and a tiny portable telephone that you can carry with you in a handbag or pocket wherever you go."

- The Independent Newspaper
Tues. 24th October 1989 [1].

This is a vision of the future which is increasingly being portrayed by communication system operators and the media. Many even predict that a pocket sized telephone that is affordable to a mass market will be available by the end of the century, turning the realms of science fiction into reality. This will dramatically affect the way we lead our lives, raising many issues which have, as yet, to be addressed. However, with a potential market place of millions of users, there are massive profits to be made, and so the next decade will witness a rapid growth in the communications industry.

1.1 THE EVOLUTION OF MOBILE/PERSONAL COMMUNICATIONS

In many recent conferences and journals [2][3][4], there have been papers outlining current trends in the evolution of mobile communications, predicting future developments and the move towards personal communications. These developments, and the estimated few years before their introduction, would have seemed inconceivable in the late 60's. In these pioneering days of mobile radio communication it was simply possible to allocate new radio channels to each mobile radio system as it was installed. As the number of installations increased however, the limited amount of radio spectrum allocated to these services rapidly diminished and frequency, or channel

reuse was introduced. This was the first step towards meeting the growing public demand for mobile telephony, and involved reusing channels in different geographical regions which were separated by distances sufficient to ensure that *co-channel interference* did not occur anywhere within the service area of the base-station. Co-channel interference is the phenomenon which occurs when a mobile receives a strong enough signal from a distant base-station with the same channel allocation, sufficient to cause interference. Initially no systematic plan of frequency reuse existed and there was no automatic transfer of calls in progress as the mobile moved from one service area to another, a technique known as *handover*. Hence, the concept of Cellular Radio Communication evolved [5], providing a service to an ever increasing user community.

The term *cellular* is derived from the way the service area is divided up into small cells, each cell being served by its own base-station with a dedicated set of channel frequencies. The base-station is connected to a mobile-services switching centre (MSC) which initiates call setup, controls access to the conventional telephone network, monitors the mobile calls in progress and performs, as necessary, call handovers with adjacent cells. Thus the cellular network can be considered as a wireless extension to the existing telecommunication network. The power transmitted by each base-station is controlled in such a way that only the local cell is served while co-channel interference is kept to an acceptable minimum. In principle, the spacing of transmitter sites need not be regular, although in order to aid network planners, an array of identical regular polygons which closely approximate the ideal circular cell are employed. The most popular shape, and the one readily identified with cellular technology, is the regular hexagon. Figure 1.1 shows a possible frequency reuse plan with a seven cell repeat. Each cell labelled with the same number is served by the same set of channel frequencies, and the group of cells amongst which all of the available frequencies are divided is known as a *cluster*. Through frequency reuse, a cellular mobile radio system in a given coverage area can handle a number of simultaneous calls, greatly exceeding the total number of allocated channel frequencies.

Cellular Mobile Radio was first introduced into the UK in 1985 with the Total Access Communication System (TACS) [6] which is derived from the American Advanced Mobile Phone Service standard (AMPS) and operates at 900 MHz. The system has experienced a phenomenal level of growth, with over

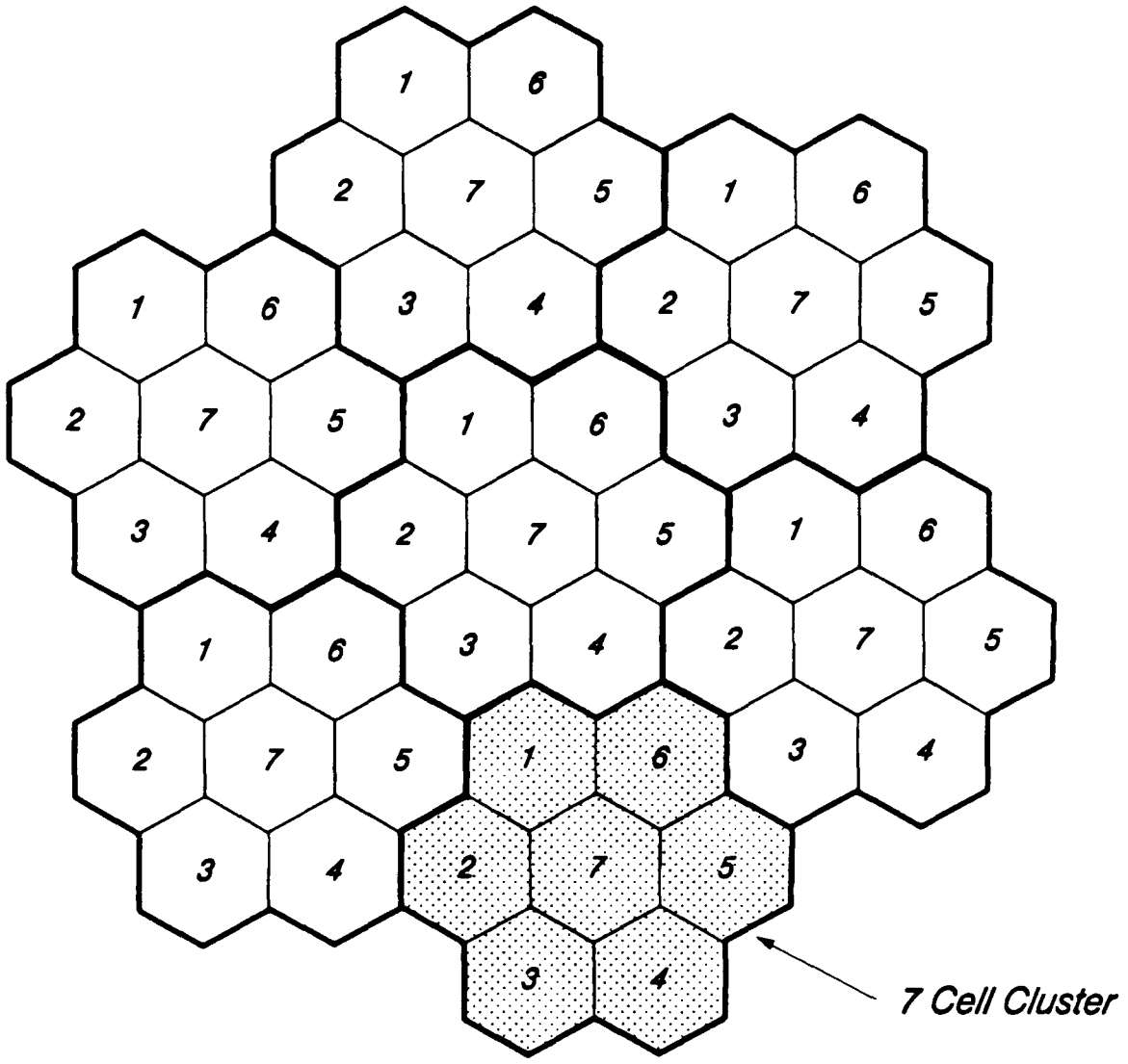

Figure 1.1: Hexagonal cellular layout with a 7 cell cluster.

one million users currently subscribing to the network. This rapid growth has produced problems for the network operators though, since with only a limited capacity available, the quality of service was degraded as some areas became saturated. This, combined with high costs, produced many complaints from users early on in the evolution of the TACS system [7]. This was alleviated to some extent with the provision of additional channels early in 1988 with the new E-TACS system. In America, Japan and other European countries similar cellular systems were being developed and installed and the dominant choice for the modulation scheme for these first generation systems was narrowband frequency modulation (FM). Unfortunately, FM does not utilise the available spectrum very efficiently and consequently the next generation of systems will employ more spectrally efficient narrowband digital modulation techniques, e.g. the proposed US narrowband digital linear system [8][9] and the 2nd Generation Pan-European cellular network [10][11].

The Pan-European system, specified by the Groupe Spéciale Mobile (GSM),

is in the advance stages of development and is due to come into operation at the end of 1991. The system will operate in the 900 MHz band, employing a multi-carrier time division multiple access (TDMA) scheme supporting eight channels/carrier. A carrier spacing of 200 kHz is to be used with GMSK (Gaussian Minimum Shift Keying) modulation providing a total of 1000 full duplex channels in the available 50 MHz bandwidth. The implementation of TDMA technology is particularly attractive because it opens up new possibilities for pocket sized cellular telephones since many of the large analogue components can be dispensed with [10]. Wideband modulation techniques have also been considered as alternatives to the narrowband schemes described above and in particular Code Division Multiple Access (CDMA). This is a well established modulation and multiple access scheme based on spread spectrum communications and, although primarily employed in the military sector, has recently been proposed as a contender for the next generation of mobile radio systems [12]. A spread spectrum system operates by imprinting onto the baseband data a unique spreading signal, or code, which has a much greater bandwidth than the data signal. This enables the same spectrum to be reused in each cell and, since the transmitted bandwidth greatly exceeds the coherent bandwidth of the mobile channel, the level of fading experienced by the data signal is now greatly reduced, i.e. an inherent frequency diversity action. The potential cost savings and increased capacity make this a particularly attractive option.

Over the next five years there will be three regional second generation systems operating in Europe, USA and Japan. Therefore, in order to provide truly universal personal communications, the third generation of systems must move towards a world standard, e.g. the European Commission's RACE Mobile programme. Recently, the UK Government granted licenses to three new operators to develop personal communications networks (PCN's) operating around 1.8 GHz. The three systems will probably use cellular technology based initially on the GSM standard. Hence, with all these different operators, the next decade is going to witness some fierce competition for the largest share of the market. This, combined with the rapid advances in technology envisaged, as well as competition from cordless telephony and telepoint services (e.g. the UK CT2 standard), may well enable the personal communications dream to become a reality by the turn of the century.

1.2 SPECTRUM EFFICIENCY

One of the most critical factors which will affect the ultimate capacity and performance of present day and future generation systems is the limited frequency allocation for these services. The promise of large blocks of new spectrum being released will serve to reduce this problem and has been heralded to some extent with the recently granted PCN licenses in the UK. Unfortunately, with the current rate of expansion, there is no room for complacency, and so the frequency spectrum must still be treated as a valuable commodity and employed as efficiently as possible. A measure often used to assess the efficiency of spectrum utilisation is the *number of voice channels per megahertz of available bandwidth per square kilometre*. This defines the amount of traffic that can be carried within the system and is directly related to the ultimate capacity of the network. Hence, as traffic demands increase, the spectrum efficiency of the network must also increase if the quality and availability of service is not to be degraded. At present this is accomplished in areas with a high traffic density by employing a technique known as *cell splitting*. An area formerly regarded as a single cell is restructured as a region containing several cells as illustrated in figure 1.2. This ensures that there are the same number of channels in a reduced coverage area, and consequently increases the spectrum efficiency. The cellular concept allows for a continuous growth in traffic demand using the cell splitting technique, although there is a practical limit on the

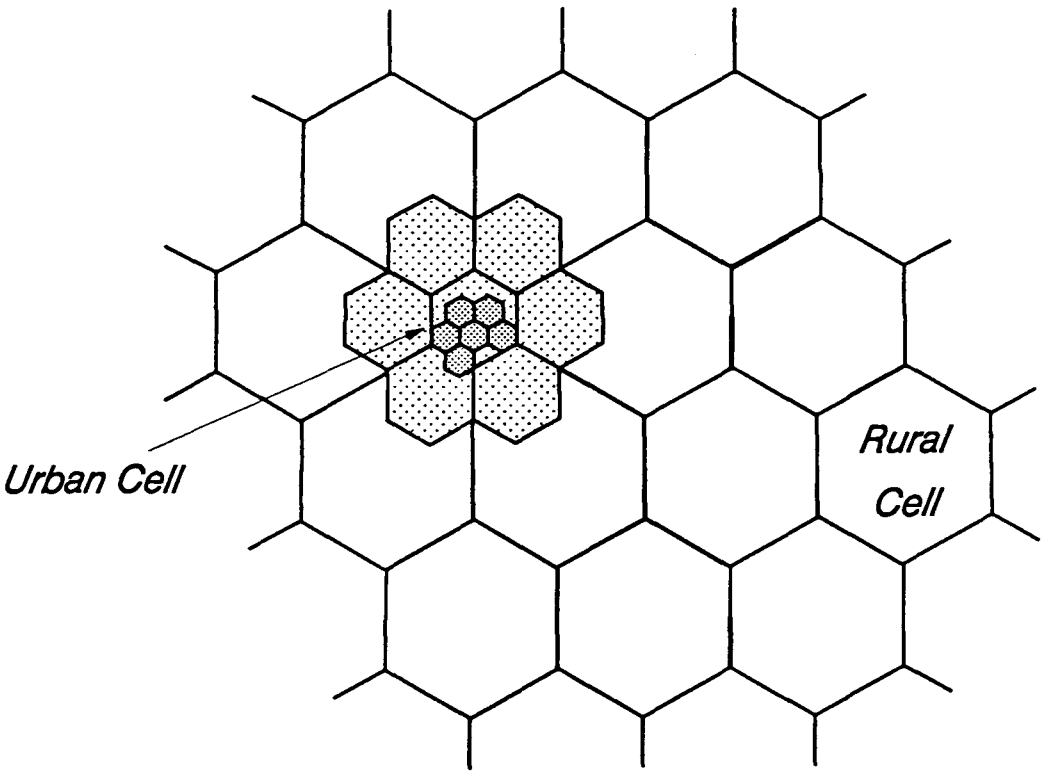

Figure 1.2: Cell splitting a hexagonal floor plan.

minimum acceptable cell size. As the cell sizes are reduced, the handover rate increases, which in turn reduces the *trunking efficiency* of the network, i.e. the rate at which calls can be handled. This has already occurred in Central London [7] where the planned cell radius of 7 km has been reduced to 1.75 km to meet with growing public demand for service. At present it appears unlikely that the cells can be reduced any further and so placing a limit on the number of users that can have simultaneous access to the system. Within the GSM format for the next generation systems, there will be a facility for incorporating much smaller *microcells* (30 - 200 m in radius) within larger *macrocells* (1 - 15 km in radius) to increase the traffic handling capabilities of the system. The handover problem will be very severe within the microcells, therefore it can be envisaged that these will deal mostly with the slower moving pedestrian traffic.

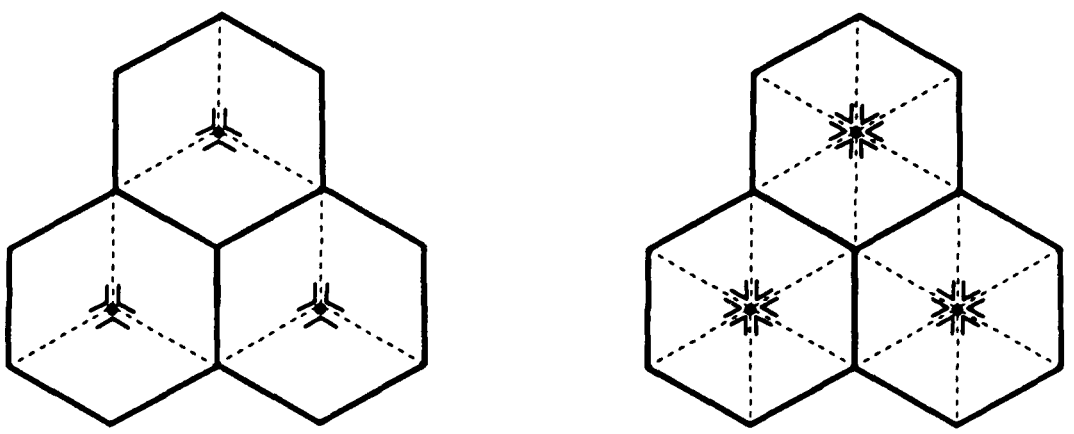

Figure 1.3: Cell sectorisation using directional antennas: (a) 120° ; (b) 60°.

Cell splitting has the added disadvantage of increasing the infrastructure costs since more base-station sites must be acquired. An alternative approach employs a technique known as *cell sectorisation*. Directional antennas are used at the base-station site to illuminate a fixed sector of the cell as shown in figure 1.3 for 120° and 60° beamwidth antennas. Each sector is then assigned a subset of the channel frequencies allocated to the original cell. With the signal energy now confined to a reduced coverage area, there is clearly a reduction in the co-channel interference that is transmitted or received since the front-to-back ratio of a directional antenna is typically 20 dB or greater. This manifests itself as a reduction in the minimum separation of co-channel cells and so allows more channels to be deployed in each cell, increasing the spectrum efficiency.

Unfortunately, a different form of handover is now introduced as the mobile circumnavigates the cell, limiting the overall capacity. In spite of this additional control overhead, this technique not only reduces co-channel interference but makes very effective use of the base-station site.

The omni-directional and sector antennas described above can be realised as a series fed collinear array of cylindrical dipoles [13], with corner reflectors providing the required directional properties of the sector antennas. In the early development of cellular systems, cell sizes were relatively large and so the emphasis was on providing high gain antennas to ensure sufficient coverage. With the advent of smaller cells, this is no longer a priority and the emphasis is now on reducing the amount of signal energy transmitted into (or received from) neighbouring cells, i.e. *spillover*. This can be achieved using fixed phased array antennas, with carefully controlled amplitude tapers and sidelobe levels [13], a technique originally developed for radar. The directional vertical radiation pattern can now be carefully controlled and even tailored for individual cells as illustrated in figure 1.4.

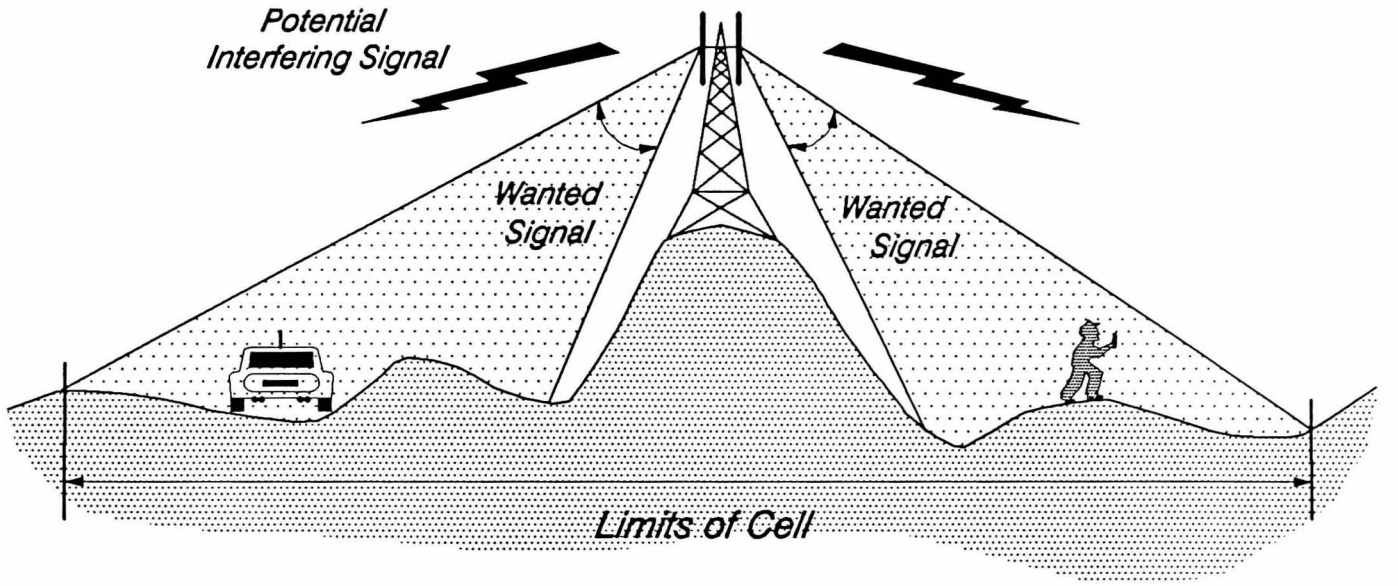

Figure 1.4: Controlling energy overspill using antenna arrays.

Cell splitting and cell sectorisation are currently employed in the present generation of cellular systems to increase spectrum efficiency although their ultimate use will be limited due to the reduction in the trunking efficiency of the network. Hence, with the number of subscribers able to have simultaneous access to these systems still well below long term forecasts, this places great emphasis on finding alternative techniques to maximise the spectrum efficiency of future generation systems. There have

already been significant developments in terms of spectrum efficient modulation schemes as described earlier, and there is also an abundance of material appearing in the technical literature proposing novel solutions and many of the most viable are described in the text of Lee [14]. Two popular techniques employ adaptive power control and dynamic channel allocation. The former approach ensures that the transmitted power levels are controlled to keep the received signals at an acceptable minimum, and consequently reduces the levels of co-channel interference. The latter approach works by exchanging a channel which is experiencing an excessive level of interference for an idle channel with less interference. Both of these techniques have been shown to be effective in reducing the levels of co-channel interference, enabling co-channel cells to be placed closer together and increasing the spectrum efficiency.

The application of *adaptive antenna arrays* in civil land mobile radio systems has hitherto received little attention, especially in view of the significant advances made in this field for both military and satellite communications. In this thesis a multiple beam adaptive base-station antenna array is proposed to complement other solutions, such as spectrum efficient modulation, currently being developed to meet the proliferating demands for enhanced capacity in cellular networks.

1.3 OUTLINE OF THESIS

Chapter 2 begins with an overview of the application of antenna arrays in cellular land mobile radio. A number of current proposals are discussed before presenting the concept of a multiple beam adaptive base-station antenna system. A figure of merit for the proposed base-station antenna with respect to conventional omni-directional and fixed sector directional antennas is established in **chapter 3**. The analysis is based on the ability of the proposed antenna system to reduce the level of co-channel interference and gives a measure of the capacity advantage that could be achieved if it were to be incorporated into an existing cellular framework.

A fundamental requirement of the proposed base-station antenna system is the ability to determine the angular position of individual mobile users within each cell. Therefore **chapter 4** considers a direction finding (DF)

approach in the cellular land mobile radio environment with an array of antenna elements. The techniques considered have been extensively employed in radar and sonar for many years and consequently the technology is well advanced, although their application in the severe propagation conditions found in land mobile radio has yet to be fully appraised. A computer simulation suite is developed in **chapter 5** and is employed to demonstrate the ability of the antenna system to determine the azimuth bearing of a mobile source in a number of different environments (urban, suburban and rural). A comparison is then made between the direction finding techniques introduced in chapter 4. The construction of a linear four element DF receiving array is discussed in **chapter 6.** Field trials are carried out to demonstrate the principles of direction finding in a typical urban locality. A single mobile source was employed and the results are compared with the simulation results from the previous chapter.

Having considered in some detail the process to determine the mobile user's location within a cell, **chapter 7** addresses a number of implementation issues which would affect the ultimate realisation of the proposed base-station antenna system. The beamforming aspect in particular is discussed and potential system architectures are presented. Finally in **chapter 8,** a summary of the work is presented. This includes a discussion on the feasibility of the proposed antenna system bearing in mind current developments in cellular communications, as well as giving some recommendations for future work.

REFERENCES

[1]: *"A Pocket-sized Revolution in Telephones"*, The Independent newspaper, Tuesday 24th October 1989, page 14.

[2]: G. Vincent, *"Personal Communications - The Dream and The Reality"*, IEE Review, Sept. 1990, pp.299-303.

[3]: W.H.W. Tuttlebee, *"Technology Innovation Requirements for Personal Communications"*, IEE Fifth International Conference on Radio Receivers & Associated Systems, University of Warwick, 24th - 26th July 1990. (Not bound in Proceedings.)

[4]: J. Thompson, *"Shades of Mobility"*, Keynote Paper, IEEE 1989 Workshop on Mobile & Cordless Communications, King's College - University of London, Sept. 1989, pp.3-11.

[5]: V.H. MacDonald, *"The Cellular Concept"*, The Bell System Technical Journal, Vol.58, No.1, Jan. 1979, pp.15-41.

[6]: E. Beddoes and M. Pinches, *"Cellular Radio Telephony - The Racal-VODAFONE Network in Great Britain"*, The Ericsson review No.3, 1987.

[7]: *"Car Phone Users Stuck in a Jam"*, Sunday Observer, 31st July 1988, page 9.

[8]: J.A. Tarello and G.I. Zysman, *"Modulation Techniques for Digital Cellular Systems"*, Proceedings of 38th IEEE Vehicular Technology Conference, Philadelphia, USA, 15th - 17th June 1988, pp.245-248.

[9]: J. Uddenfeldt, K. Raith and B. Hedberg, *"Digital Technologies in Cellular Radio"*, Proceedings of 38th IEEE Vehicular Technology Conference, Philadelphia, USA, 15th - 17th June 1988, pp.516-519.

[10]: F. Lindell, J. Swerup and J. Uddenfeldt, *"Digital Cellular Radio for the Future"*, The Ericsson Review, No.3, 1987.

[11]: D.M. Balston, *"Pan-European Cellular Radio: or 1991 and all that"*, Electronics & Communication Engineering Journal, Jan/Feb 1989, pp.7-13.

[12]: A. Salmasi, *"An Overview of Advanced Wireless Telecommunication Systems Employing Code Division Multiple Access"*, IEEE International Symposium on Spread Spectrum Techniques and Applications, King's College London, 24th - 26th Sept. 1990, pp.18-24.

[13]: P.C. Carlier, *"Antennas for Cellular Phones"*, Communications International, Dec. 1987, pp.43-46.

[14]: W.C.Y. Lee, *"Mobile Cellular Telecommunications Systems"*, McGraw-Hill, 1989.

CHAPTER 2

ANTENNA ARRAYS FOR CELLULAR BASE-STATIONS

2.1 ADAPTIVE ANTENNA ARRAYS

The flexibility offered by an array of antenna elements over a single sensor has long been exploited in a range of applications. The earliest radars were developed during World War II, and these made use of antenna array technology to enhance their ability to detect and locate targets. Since then, advances in digital computing, and the ability to perform real time signal processing, has seen the emergence of the adaptive antenna array. This may be defined as an array that is capable of modifying its radiation pattern, frequency response, or other parameters, by means of internal feedback control while the antenna system is operating. A general description of the fundamental operation of an adaptive antenna array is included in Appendix A, but can be briefly summarised as follows. The signals received at each element in the array are weighted and then summed to form the array output, given by

$$y(t) = \mathbf{w}^T\mathbf{x}(t) \tag{2.1}$$

where $\mathbf{w}$ is a vector of complex weights (i.e. phase and amplitude control) and $\mathbf{x}(t)$ is the received signal vector (T denotes the transpose operation). The weights are chosen to satisfy the particular requirements of the receiver.

Some of the earliest work concerning adaptive antenna arrays employed a self-phasing antenna system which reradiated signal energy in the direction from which it arrived [1]. This "retrodirective" system operated without prior knowledge of the direction it was required to transmit, and was applied in point-to-point satellite communications. One of the most important applications of this technology however, is the ability of the system to steer a null, that is a reduction in sensitivity in a certain angular direction, towards a source of interference. Normally the presence of undesired signals, whether as deliberate electronic countermeasures, RF interference or natural noise sources, causes a degradation in the received

signal-to-noise ratio (SNR). Hence the widespread interest in adaptive antenna systems which have the ability to detect the presence of interference, and to then suppress it whilst simultaneously enhancing reception of the desired signal. The first practical implementation of electronically steering nulls in the direction of unwanted signals, or jammers, was the Howells-Applebaum Side-Lobe Canceller for radar. This work started in the 1950's, and a fully developed system was reported in open literature in 1976 by Applebaum [2]. At about the same time Widrow [3] independently developed an approach for controlling an adaptive array using the least-mean-squares minimisation technique, now known as the LMS algorithm. Since this pioneering work, there has been a considerable amount of research activity in the field of adaptive antenna arrays [4][5][6], particularly for reducing the jamming vulnerability of military radar and communication systems. Other applications include seismology, sonar, radio astronomy and tomography, however to date there has been little attention to the application of such techniques in the area of civil Land Mobile Radio (LMR).

Adaptive antenna arrays cannot simply be integrated into any arbitrary communications system, since a control process must be implemented which exploits some property of either the wanted, or interfering, signals. In general, adaptive antennas adjust their directional beam patterns so as to maximise their signal-to-noise ratio at the receiver output. Applications have included the development of receiving systems for acquiring desired signals in the presence of strong jamming, a technique known as *Power Inversion* [7]. Systems have also been developed for the reception of Frequency Hopping signals [8][9], TDMA (time division multiple access) satellite channels [10] and spread spectrum signals [11]. Of particular interest for cellular schemes, is the development of adaptive antenna arrays for the reception of multiple wanted signals [12].

In the following sections, some examples of the application of antenna array technology in cellular land mobile radio systems are given. The emphasis is to reduce the level of co-channel interference received at the base-station antenna, thereby achieving greater frequency reuse and enhanced capacity.

2.2 ADVANCED BASE-STATION ANTENNA DESIGN

2.2.1 Antenna Diversity

Space diversity combining is an established method for combatting the effects of multipath (Rayleigh) fading in mobile radio [13]. Although the techniques are not strictly related to the adaptive antenna array principles, where the emphasis is on the reduction of interference, antenna diversity can be employed effectively to reduce the effects of co-channel interference. The increase in the output signal-to-interference-plus-noise ratio (SINR) reduces the frequency reuse distances required for a given performance criterion, thus increasing the spectrum efficiency and capacity of the network. Hence as an introduction to the application of antenna arrays for mobile radio, a short discussion on the merits of diversity combining will be presented.

In general, diversity combining requires a number of transmission paths, all carrying the same message but having independent fading statistics. This can be achieved in a number of ways [13], however space diversity using antenna arrays potentially offers the largest benefits in narrowband systems. The basic requirement is that the antenna spacing is sufficient to provide uncorrelated signals at each element. Correct combination of the received signal channels (or branches) then results in a signal with improved SNR, which increases as the number of elements in the array increases. There are a number of combining methods, the simplest being *selection diversity* where the receiver with the highest baseband SNR is connected to the receiver output. *Maximal ratio combining* is an alternative technique where each branch signal is amplitude weighted in proportion to its own signal voltage to noise power ratio before being co-phased and then summed. This offers a significant improvement over selection diversity but at the expense of complexity in the receiver hardware required.

When there are many co-channel interferers, the incoherent sum of their contributions is equivalent to stationary Gaussian noise. Hence, the coherent combination of the desired signal results in an increase in the output SINR. Henry and Glance [14] proposed a scheme utilising space diversity reception at the base-station only. Employing adaptive retransmission using time division [13] allows only a single antenna element to be deployed at the mobile, but still provides diversity action in both the mobile-to-base and base-to-mobile directions. This is achieved by weighting the transmitted

signal from the base-station with the complex conjugate of the received signal vector, and time sharing a single channel for both directions of transmission. It was proposed that a three cell repeat pattern could be accommodated using only 3 or 4 elements at the base-station. In order to overcome shadowing, each cell would be covered by three base-stations located on alternate cell corners (hexagonal layout assumed). Here each base-station site would comprise of three 120° sector antennas. Yeh and Reudnik [15] proposed a scheme employing diversity at both the mobile and the base-station. It was shown that complete frequency reuse could be provided with a 20 branch diversity combiner at the mobile and a 67 branch diversity combiner at the base-station. Various other proposals were considered requiring fewer elements but at the expense of spectrum efficiency. In both the above schemes maximal ratio combining was assumed.

The main factor affecting the realisation of diversity combining antenna arrays at the base-station is the requirement for uncorrelated signals at each element. A correlation coefficient as high as 0.7 though will still enable most of the advantages of diversity combining to be obtained [13] and, at the mobile antenna, this can be achieved with an element spacing of the order of half a wavelength ($\lambda/2$) [13]. Hence at the mobile space diversity is fairly straight forward to implement, although when antennas are this close together, the effects of mutual coupling must be considered. Vaughan [16] has estimated that when mutual coupling is present a correlation coefficient of < 0.5 would be necessary when using maximal ratio combining. The main drawbacks of space diversity combining at the mobile are the cost and the inconvenience of the extra hardware since, for the same grade of service, it would have to be installed at all mobiles. This is not such a problem at the base-station antenna but in order to provide the necessary decorrelation between the antenna elements of a horizontal array, spacings of the order of $15\text{-}20\lambda$ (> 5m at 900 MHz) would be necessary if the signal were incident broadside onto the array [17]. In-line incidence would require an even greater separation, and antenna arrays of this size would be difficult to implement, becoming rather impractical and uneconomical.

Two branch diversity can be obtained by exploiting the two orthogonal polarisations of the received signal and, unlike space diversity, there are no restrictions on the positioning of the antenna elements. Lee [18] has demonstrated the viability of such a scheme in suburban field trials with both vertically and horizontally polarised antenna elements at the base and

mobile. It was demonstrated that Rayleigh fading signals received at the two base-station antennas were sufficiently decorrelated to enable diversity action to be successfully implemented. Kozono [19] has also carried out field trials in an urban/suburban environment and demonstrated polarisation diversity reception when a signal radiated from a single vertically polarised mobile antenna was received by a dual polarised ($\pm 45^{\circ}$) base-station antenna. The diversity gain is obtained from the rotation of the polarisation of the signal through multipath propagation, at the expense of a reduction in the received signal level with respect to the vertically polarised component.

2.2.2 Optimum Combining

The primary use of adaptive antennas has been for reducing the jamming vulnerability of military communication systems. Hence the same technology could be employed to reject undesired or co-channel signals in a cellular communications environment. Marcus and Das [20] have considered this approach, and further postulated that 20 dB of interference rejection could reduce the reuse distance between co-channel sites by as much as 40%. This would actually increase the number of available channels by a factor of ≈ 2.8. It was suggested that a continuous (sub-audible) tone control squelch signal used in many LMR systems in the USA at the time, could be utilised to provide the beam steering information. The analysis was entirely theoretical, based on the results of studies into the interference rejection abilities of arrays reported in open literature [21]. The chosen LMR scenario contained a single co-channel cell and the calculations included only the propagation path loss associated with the mobile radio channel. It was recognised by the authors that there were limitations in the approach, especially since the antenna could not reject signals incident from the same azimuth direction as the desired signal. However, it was stressed that experimental work would be necessary to verify their claims, although as yet, the authors have published no further related work.

The operation of the null steering array of Marcus and Das is more generally referred to as adaptive beamforming [22]. In particular, when the signalling environment is unknown, as is the case in mobile radio, optimum beamforming or optimum combining techniques are employed. Here the weights are chosen based on the data received at the array, the aim being to optimise the response of the array so that the output contains reduced contributions

from noise and interference sources, whilst maintaining the original gain of the antenna in the direction of the wanted signal. Appendix A contains a general description of the operation of an adaptive antenna array and includes a brief discussion on optimum beamforming.

Since the null steering approach of Marcus and Das, the potential utilisation of optimum combining methods has been considered in more detail at both the base-station and the mobile. Vaughan [23] has studied the possibilities for optimum combining at the mobile and concluded that, although feasible, there are many practical limitations that have to be overcome. In conventional adaptive beamforming, the wanted signals and interferers are considered as resolvable point sources, thus enabling the antenna pattern to be adapted accordingly. In a built up, urban environment this is not the case since the close proximity of buildings and other local scatterers around the mobile ensures that the wanted signals plus interference are distributed, and incident from all around the mobile. Hence, with the number of sources greatly exceeding the available degrees of freedom of the array, the radiation pattern cannot be adapted to effectively reject all the interferers. However, by considering the optimum combining of array branch signals, as opposed to discrete spatial signals, a solution is obtained. The movement of the vehicle also presents a problem since this causes the signalling environment to change rapidly and places a limit on the adaption time of the array weights. Finally, the use of pseudo-noise codes in a spread spectrum communication system [11] was suggested to obtain the benefits of optimum combining at the mobile. Unfortunately, the cost and complexity of implementation at every mobile would be great, rendering such a scheme impractical for the moment. However, as the demands for high spectrum efficiency and capacity grow, optimum combining at the mobile may have to be considered.

Perhaps of more relevance to the present discussion is the proposal of Winters [24] for the implementation of optimum combining at the base-station. The realisation of this approach would require a spread spectrum communication system [11] employing the LMS adaptive array [3]. Adaptive retransmission with time division [13] was also proposed in order to obtain the benefits in the base-to-mobile direction. In the analysis, Winters compares the performance of optimum combining with maximal ratio combining using computer simulations, and shows that optimum combining increases the output SINR ratio by several decibels. This performance enhancement is

obtained by considering only the strongest interferers, the remaining interferers being considered as lumped interference that is uncorrelated between antennas, the sum being approximated as thermal noise.

Throughout the analysis, Winters assumes that the signals received at each element in the array are independent. Hence, as well as increasing the output SINR, optimum combining will also combat multipath fading, but at the expense of increased antenna spacing. This will also reduce considerably the chances of the signal being in line with an interfering source since received signal phases are independent of vehicle location. Under normal operating conditions, if the angular separation between the interfering signals and desired signals is too small, the array cannot null one signal whilst enhancing reception of another.

One of the main limitations of this approach is the large antenna size that would be required, making the base-station antenna impractical in many situations. Also, it was proposed that a LMS adaptive array would be used at the base-station, employing spread spectrum communications for the mobile-to-base link in order to generate the reference signal in the feedback loop. The application of spread spectrum communications within a code division multiple access (CDMA) scheme is currently receiving renewed interest for the next generation of cellular communication networks [25]. The main reason for this is the potential capacity enhancement that can be achieved, and a simple demonstration system has already been developed by Qualcomm in America. Hence, the practical realisation of base-station optimum combining may well be possible in future cellular networks.

An alternative approach to the reference signal based technique of Winters has been proposed by Andersson *et al* [26]. The proposed method employs a high resolution direction finding step to estimate the angles of arrival of the signal sources incident onto the array, followed by a linear combination of the sensor outputs to extract only the wanted signal components. This later step is termed the *linear least squares estimate* (LLSE) and overcomes the problem of signal cancellation when coherent multipath is present [22]. Further details of this technique can be found in [27]. The proposal would employ a conventional antenna array, with element spacings of the order of half a wavelength. Hence, the signals at each element will be virtually completely correlated (assuming a well sited base-station antenna, away from local scatterers), and the receiver will not

be able to combat multipath fading.

2.2.3 Multiple Beams

A multiple beam adaptive antenna array has been proposed by Telecom Australia [28][29][30] for enhancing the number of simultaneous users accessing future generation cellular networks. It is suggested that each mobile is tracked in azimuth by a single narrow beam for both mobile-to-base and base-to-mobile transmissions, as illustrated in figure 2.1. The directive nature of the beams ensures that in a given system the mean interference power experienced by any one user, due to other active mobiles, would be much less than that experienced using conventional wide coverage base-station antennas. It has already been stressed that high capacity cellular networks are designed to be interference limited, and so the adaptive antenna would considerably increase the potential user capacity.

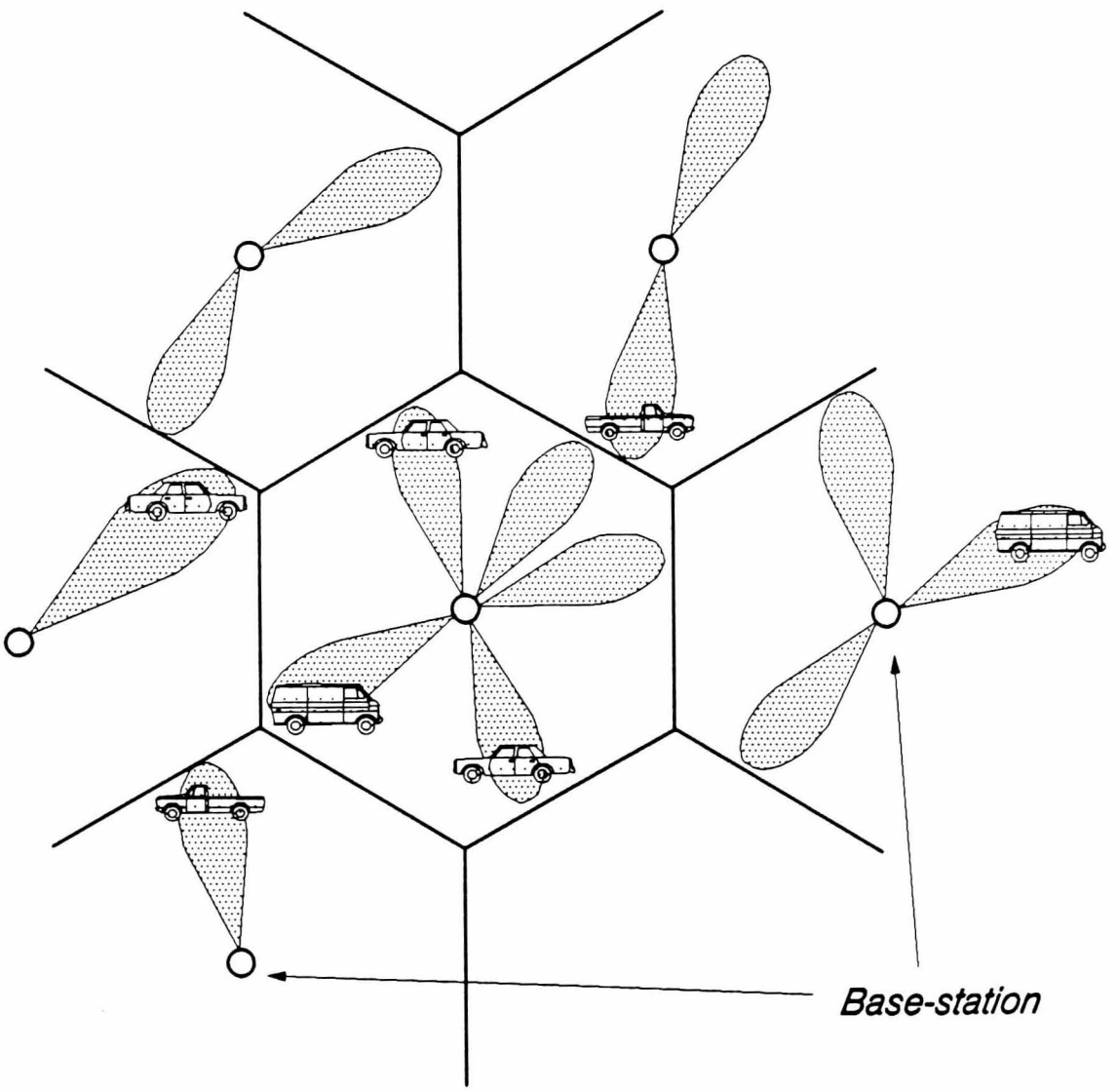

Figure 2.1: Tracking mobiles with multiple beams.

A simplified analysis was carried out to ascertain the potential capacity advantage of the multiple beam antenna over a conventional omni-directional system. A hypothetical fast frequency hopping code division multiple access (FFH/CDMA) network was assumed, and the results showed that the proposed multi-beam base-station, in the form of a 3.5m diameter cylindrical array, could provide an increase in spectrum efficiency or capacity by factor of 30 or more. The analysis assumed a uniform user distribution, with complete frequency reuse for the omni-directional antenna, i.e. adjacent cells are co-channel cells. Complete frequency reuse was then assumed for each of the beams formed by the adaptive array, i.e. adjacent beams are co-channel beams. Results were quoted for idealised and non-idealised antenna beam patterns. It was recognised that serving each active mobile with an individual antenna beam is unnecessary and indeed would be impractical since, with the exception of a TDMA scheme, a separate beamforming network would be required for each user. Thus a commutating multiple fixed beam antenna was proposed, with overlapping beams ensuring good coverage over the complete cell. The authors claim that the loss in capacity would not be significantly different from the conceptual antenna, with the task of tracking the mobiles reduced to measuring the signal levels at the beam ports, switching beams whenever necessary. The lens fed commutating single beam circular array of Boyns *et al* [31] was mentioned as a possibility, utilising an alternative lens feed to obtain multiple beam operation, e.g. the linear lens fed arrays described by Archer [32].

A CDMA scheme [25] would best suit the operation of the proposed system, requiring fewer additional overheads for incorporation into an existing network. However, complete frequency reuse within each beam would significantly increase the level of co-channel interference in a frequency division or time division multiple access scheme (FDMA or TDMA). It was therefore suggested that this problem could be overcome by employing dynamic channel allocation to eliminate the so called *common zones*. This however would introduce additional handovers, reducing the trunking efficiency and available capacity of the network as the mobile circumnavigates the cell. There are numerous challenges to be met in the realisation of this scheme, but unfortunately no further work by the authors has appeared in open literature to date.

2.3 THE 'SMART' BASE-STATION ANTENNA

In the preceding section, different proposals for utilising antenna array technology at the base-stations of a cellular communication network were discussed. The ultimate aim of each proposal was to reduce the level of co-channel interference in order to increase the spectrum efficiency and ultimate capacity of the network. Spatial diversity with maximal ratio combining, although mitigating the effects of multipath fading, would require large antenna structures and so would be impractical in many situations. Adaptive beamforming or optimum combining on the other hand, may offer a possible solution as long as the method is not used to combat multipath fading directly. Unfortunately the proposals of Vaughan and Winters both require reference signals which are highly correlated with the desired signals only, thus restricting their operation to systems such as spread spectrum communications utilising the LMS adaptive array. Andersson *et al* however, have proposed an alternative technique which does not require the generation of a reference signal [26], although the computational overheads would be increased. The approach proposed by Telecom Australia [28] moves away from truly adaptive beamforming, utilising a fixed beam solution. This would dramatically reduce the computational overheads required with optimum combining, but at the expense of complexity in the base-station hardware.

Figure 2.2 illustrates how both the optimum combining technique and fixed beam solution would combat co-channel interference. With optimum combining, the base-station antenna adapts its radiation pattern so as to place nulls on the interferers. The maximum number of nulls is determined by the number of elements in the array, although Winters [24] has demonstrated that even if the number of interferers exceeds the number of elements, the few decibels increase in the output SINR would make possible large increases in channel capacity. The simpler single beam approach however, offers a very attractive alternative since the signal energy is constrained only towards the wanted mobile with the received level of co-channel interference governed by the sidelobes. The approach proposed by Telecom Australia is along these lines, utilising multiple fixed beams to cover the cell. The process of switching calls from beam to beam is then achieved by constantly monitoring the signal levels at each of the beam ports. If however the base-station already knew the distribution of mobiles within its coverage area, it would then be in a position to form an optimum set of beams, confining the signal energy associated with a given mobile to an *addressed volume*. This concept

can be further illustrated by considering the sequence of events in figure 2.3. The scenario depicted is realistic of many operational systems where there are lone mobiles, or groups of mobiles, dispersed throughout the cell. Using the spatial distribution of the users acquired by the array on reception, the antenna system can dynamically assign single narrow beams to illuminate the lone mobiles, and broad beams to the numerous groupings along the major highways. It can be seen that by constraining the energy associated with each mobile to an addressed volume, the level of co-channel interference experienced from and by neighbouring co-channel cells is greatly reduced, thereby increasing the spectrum efficiency and ultimate capacity of the network.

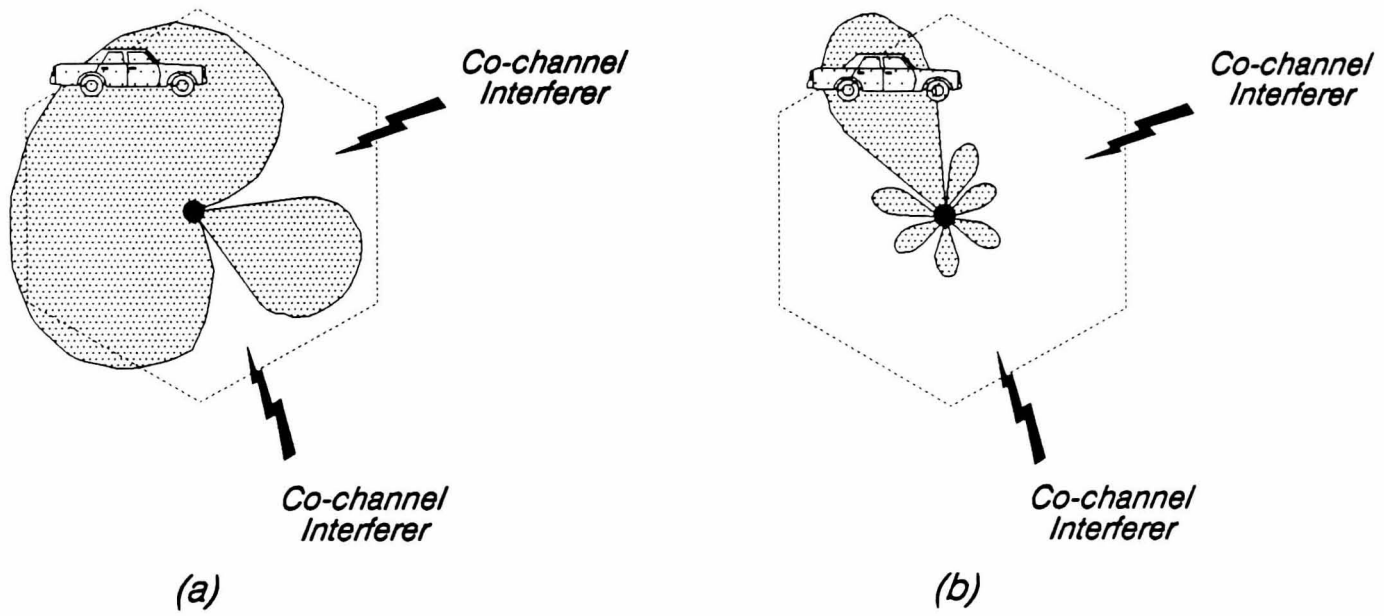

Figure 2.2: Rejection of co-channel interference with: (a) optimum combining; (b) single independent beam.

The realisation of such an adaptive base-station antenna requires an architecture capable of locating and tracking the mobiles, and a beamforming network thus capable of producing the multiple independent beams. The former requirement can be broadly classified as that of a direction finding, or spatial estimation problem. These two tasks are illustrated in figure 2.4 as a source estimation or direction finding (DF) processor and a beamformer. The complete system architecture has been referred to as the "smart" base-station antenna since this very aptly describes the operation of the proposed antenna system to be outlined in more detail in the following sections. Although more computationally intensive than the proposal by Telecom Australia, the additional knowledge of the mobile locations potentials offers a variety of *Value Added Services* (VAS). This particular aspect will be considered briefly in chapter 8. Brookner and Howell [33], and Gabriel [34] have proposed a

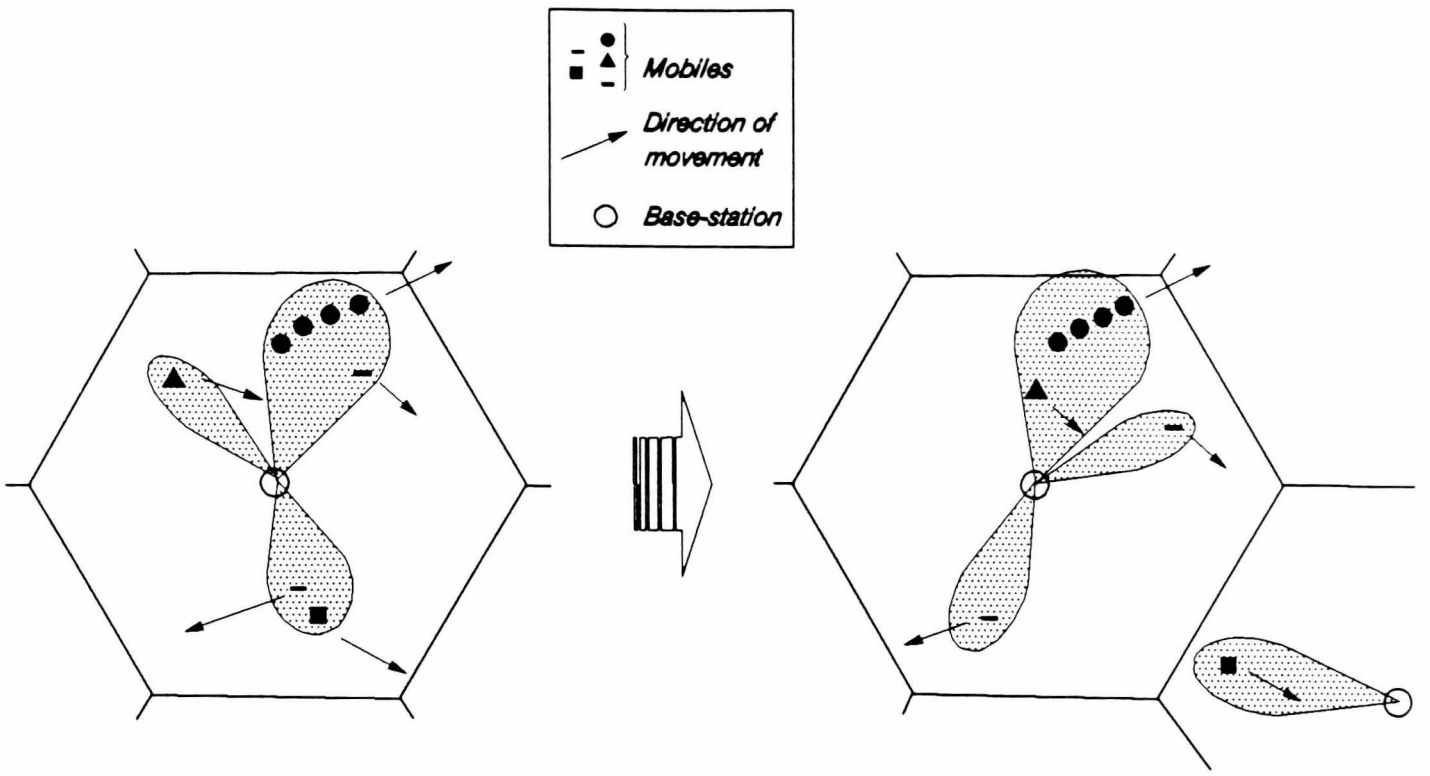

Figure 2.3: Multiple beam assignment within a cell.

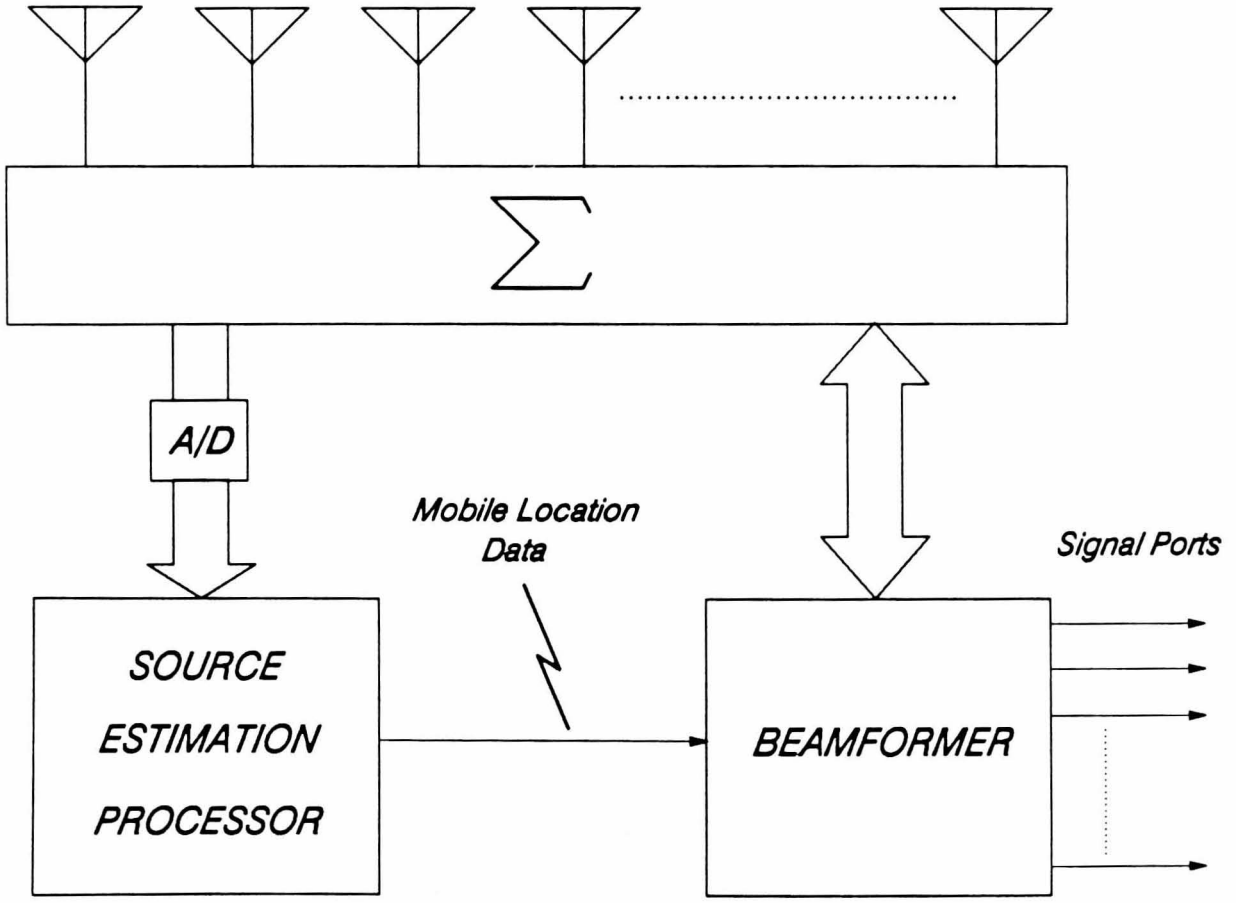

Figure 2.4: The "smart" base-station antenna concept.

similar system concept to enable the stable nulling of interference sources in the mainbeam region of an array antenna. Spatial estimation techniques were employed to estimate the angles of arrival of potential interfering sources and, once armed with this knowledge, beams could be assigned to the interferers and the combined output subtracted from the mainbeam to effectively and efficiently cancel the interference.

REFERENCES

[1]: L.C. Van Atta, *"Electromagnetic Reflector"*, U.S. Patent 2908002, October 6th 1959.

[2]: S.P. Applebaum, *"Adaptive Arrays"*, IEEE Transactions on Antennas & Propagation, Vol.AP-24, No.5, Sept. 1976, pp.585-598.

[3]: B. Widrow, P.E. Mantey, L.J. Griffiths and B.B. Goode, *"Adaptive Antenna Systems"*, Proceedings of IEEE, Vol.55, No.12, Dec. 1967, pp.2143-2159.

[4]: R.A. Monzingo and T.W. Miller, *"Introduction to Adaptive Arrays"*, John Wiley & Sons, 1980.

[5]: J.E. Hudson, *"Adaptive Array Principles"*, Peter Peregrinus Ltd., 1981.

[6]: W.F. Gabriel, *"Adaptive Arrays - An Introduction"*, IEEE Proceedings, Vol.64, No.2, Feb. 1976, pp.654-666.

[7]: R.T. Compton, *"The Power Inversion Adaptive Array: Concept and Performance"*, IEEE Transactions on Aerospace & Electronic Systems, Vol.AES-15, No.6, Nov. 1979, pp.803-814.

[8]: L. Acar and R.T. Compton, *"The Performance of an LMS Adaptive Array with Frequency Hopped Signals"*, IEEE Transactions on Aerospace & Electronic Systems, Vol.AES-21, No.36, May 1985, pp.360-371.

[9]: K. Bakhru and D.J. Torrieri, *"The Maximin Algorithm for Adaptive Arrays and Frequency-Hopping Communications"*, IEEE Transactions on Antennas & Propagation, Vol.AP-32, No.9, Sept. 1984, pp.919-928.

[10]: R.T. Compton, R.J. Huff, W.G. Swarner and A.A. Ksienski, *"Adaptive Arrays for Communication Systems: An Overview of Research at the Ohio State University"*. IEEE Transactions on Antennas & Propagation, Vol.AP-24, No.5,Sept. 1976, pp.599-607.

[11]: R.T. Compton, *"An Adaptive Antenna in a Spread Spectrum Communication System"*, Proceedings of IEEE, Vol.66, No.3, March 1978, pp.289-298.

[12]: M.A. Beach, *"An Adaptive Antenna Array for Multiple Spread Spectrum Signal Sources"*, PhD Thesis, Department of Electrical & Electronic Engineering, University of Bristol, August 1988.

[13]: W.C. Jakes, *"Microwave Mobile Communications"*, John Wiley & Son, 1974.

[14]: P.S. Henry and B.S. Glance, *" A New Approach to High Capacity Digital Mobile Radio"*, The Bell System Technical Journal, Vol.60, No.8, Oct. 1981, pp.1891-1904.

[15]: Y.S. Yeh and D.R. Reudink, *"Efficient Spectrum Utilisation for Mobile Radio Systems Using Space Diversity"*, IEEE Transactions on Communications, Vol.COM-30, No.3, March 1982, pp.447-455.

[16]: R.G. Vaughan and J. Bach Andersen, *"Antenna Diversity in Mobile Communications"*, IEEE Transactions on Vehicular Technology, Vol.VT-36, No.40, Nov. 1987, pp.149-172.

[17]: W.C.Y. Lee, *Antenna Spacing Requirement for a Mobile Radio Base-Station Diversity"*, The Bell System Technical Journal, Vol.50, No.6, July-Aug. 1971, pp.1859-1876.

[18]: W.C.Y. Lee and Y.S. Yeh, *"Polarisation Diversity System for Mobile Radio"*, IEEE Transactions on Communications, Vol.COM-20, No.5, Oct. 1972, pp.912-923.

[19]: S. Kozono, T. Tsuruhara and M. Sakamoto, *"Base-Station Polarisation Diversity Reception for Mobile Radio"*, IEEE Transactions on Vehicular Technology, Vol.VT-33, No.4, Nov. 1984, pp.301-306.

[20]: M.J. Marcus and S. Das, *"The Potential Use of Adaptive Antennas to Increase Land Mobile Frequency Reuse"*, IEE 2nd International Conference on Radio Spectrum Conservation Techniques, 6th - 8th Sept. 1983, CP224, Birmingham, UK, pp.113-117.

[21]: R.T. Compton, *"An Experimental Four-Element Adaptive Array"*, IEEE Transactions on Antennas & Propagation, Vol.AP-24, No.5, Sept. 1976, pp.697-706.

[22]: B.D. Van Veen and K.M. Buckley, *"Beamforming: A Versatile Approach to Spatial Filtering"*, IEEE Acoustics, Speech & Signal Processing (ASSP) Magazine, April 1988, pp.4-24.

[23]: R.G. Vaughan, *"On Optimum Combining at the Mobile"*, IEEE Transactions on Vehicular Technology, Vol.VT-37, No.4, Nov. 1988, pp.181-188.

[24]: J.H. Winters, *"Optimum Combining in Digital Mobile Radio with Co-channel Interference"*, IEEE Transactions on Vehicular Technology, Vol.VT-33, No.3, Aug. 1984, pp.144-155.

[25]: *"CDMA Cellular - The Next Generation"*, PacTel Cellular & Qualcomm, Inc., Seminar Notes, San Diego, USA, Nov. 1989.

[26]: S. Andersson, M. Milnert, M. Viberg and B. Wahlberg, *"An Adaptive Array for Mobile Communication Systems"*, Report Lith-ISY-I-1077, Linköping University, Sweden, March 3rd 1990.

[27]: B. Ottersten, R Roy and T. Kailath, *"Signal Waveform Estimation in Sensor Array Processing"*, Proceedings of 23rd Asilomar Conference on Signals, Systems & Computing, Nov. 1989, pp.787-791.

[28]: Telecom Australia, *"Base-station Antennas for Future Cellular Radio Systems"*, Review of Activities 1985/6, pp.41-43.

[29]: W.S. Davies, R.J. Lang and E. Vinnal, *"The Challenge of Advanced Base-Station Antennas for Future Cellular Mobile Radio Systems"*, IEEE International Workshop on Digital Mobile Radio, Melbourne, Australia, 10th March 1987.

[30]: W.S. Davies, R.J. Lang and E. Vinnal, *"Proposed Advanced Base-Station Antennas for Future Cellular Mobile Radio Systems"*, Australian Telecomms. Research, Vol.22, No.1, 1988, pp.53-60.

[31]: J.E. Boyns, C.W. Gorham, A.D. Munger, J.H. Provencher and J. Reindel, *"Step-Scanned Circular-Array Antenna"*, IEEE Transactions on Antennas & Propagation, Vol.AP-18, No.5, Sept. 1970, pp.590-595.

[32]: D.H. Archer, *"Lens-Fed Multiple Beam Arrays"*, Microwave Journal, Sept. 1984, pp.171-195.

[33]: E. Brookner and J.M. Howell, *"Adaptive-Adaptive Array Processing"*, Proceedings of the IEEE, Vol.74, No.4, April 1986, pp.602-604.

[34]: W.F. Gabriel, *"Using Spectral Estimation Techniques in Adaptive Processing Antenna Systems"*, IEEE Transactions on Antennas & Propagation, Vol.AP-34, No.3, March 1986, pp.291-300.

CHAPTER 3

POTENTIAL CAPACITY ENHANCEMENT WITH THE "SMART" BASE-STATION ANTENNA

The previous chapter introduced the concept of an intelligent base-station antenna system to reduce the level of co-channel interference in cellular communication networks. This novel approach employs an antenna array which is capable of resolving the angular distribution of the mobile users as seen at the base-station site, and then using this information to direct beams towards either the lone mobiles, or groupings of mobiles, for both transmit and receive modes of operation. In subsequent chapters the realisation of such an antenna is considered in some detail therefore, as a precursor to this study, this chapter considers the integration of an idealised multiple beam adaptive antenna system into an existing cellular network.

The aim here is to provide a figure of merit for the proposed system in terms of the increase in spectrum efficiency that can be achieved relative to conventional antenna systems. In an earlier study, a comparison was made with conventional omni-directional base-station antennas[1] and since this was the subject of a recent publication, only a summary of the work will be presented here. (The full paper has been included in Appendix B for reference.) A theoretical approach is adopted which models the conventional and proposed antenna systems in a typical mobile radio environment, enabling the spectrum efficiencies to be calculated for a given level of performance. Geometrical and statistical propagation models are employed and a unique insight is given into the benefits of employing the "smart" base-station antenna. In addition to this, the scope of the previous study is extended to include the performance enhancement offered by fixed sector directional antennas which are currently favoured by system operators as a means of reducing co-channel interference.

1: Work carried out in collaboration with Beach.

3.1 PRELIMINARIES

In order to enable a direct comparison to be made between different base-station antenna architectures in a cellular network, it is necessary to develop models for the propagation characteristics of the mobile radio channel. The effects of co-channel interference can then be included to establish the minimum distances between the co-channel cells to prevent co-channel interference. This distance governs how efficiently the available spectrum can be deployed, and also determines the overall capacity of the network. Consider the situation depicted in figure 3.1 with a single interfering co-channel cell separated from the wanted cell by a distance D. Co-channel interference will occur (at either the mobile or the base-station) when the ratio of the wanted signal envelope, s_w, to the interfering signal envelope, s_i, is less than some *protection ratio*, p_r, i.e. when

$$s_w \leq p_r s_i \tag{3.1}$$

where the protection ratio is defined for the modulation scheme employed. If the two base-stations are sufficiently far apart so that co-channel interference does not occur, then D is termed the *reuse distance* and, if the cells have a radius R, the *co-channel reuse ratio* is defined as

$$Q = D / R \tag{3.2}$$

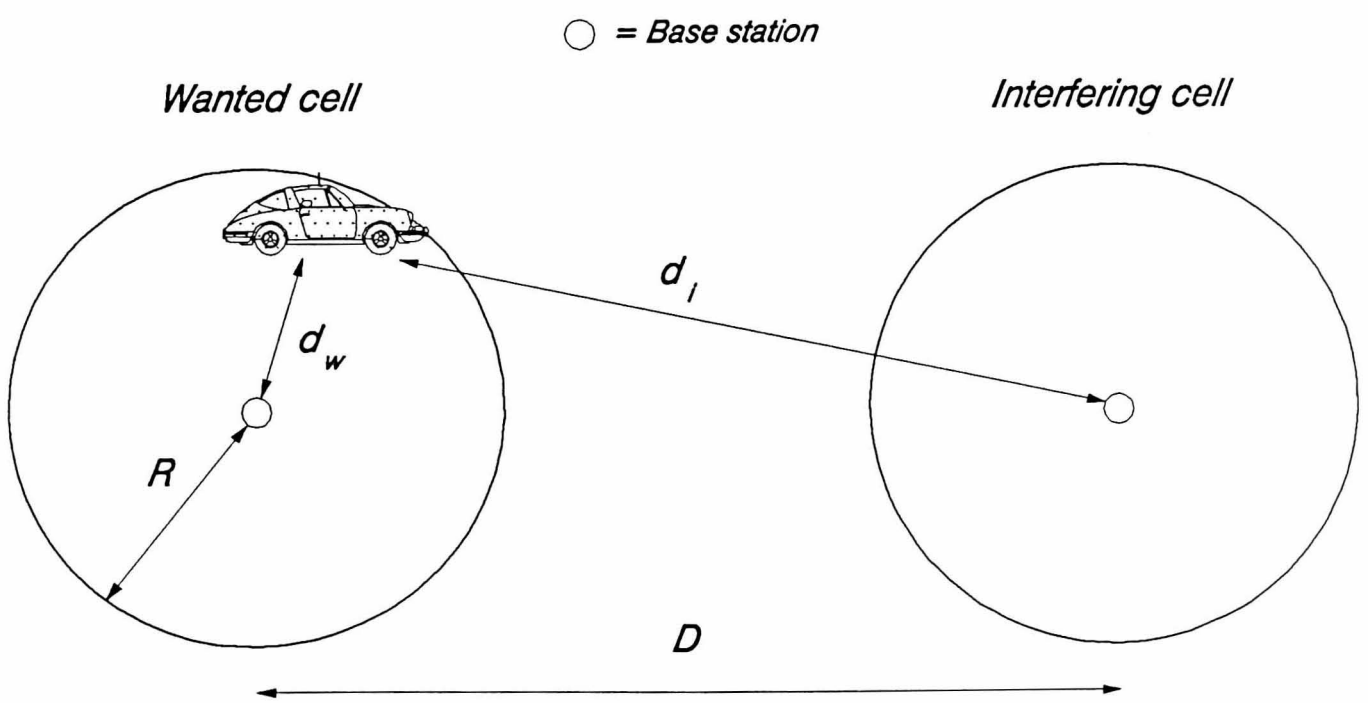

Figure 3.1: Two co-channel cells.

The level of acceptable co-channel interference governs the value of this parameter and hence the overall spectrum efficiency of the network. From this definition of the reuse distance, it is now possible to calculate the number of cells that can be established before reusing the channels, i.e. the cluster size C. If a hexagonal cellular geometry is assumed, then the cluster size is related to the co-channel reuse ratio by [1]

$$C = Q^2 / 3 \qquad (3.3)$$

A hexagonal cellular layout with a seven cell cluster is shown in figure 3.2. The use of regular hexagons restricts the cluster sizes to certain integer values only, e.g. $C = \{1,3,4,7,9,12,13,16,19,21,\cdots\}$, but note that in each case the first tier of co-channel interferers will always contain six cells which are separated from the wanted base-station by at least the reuse distance D.

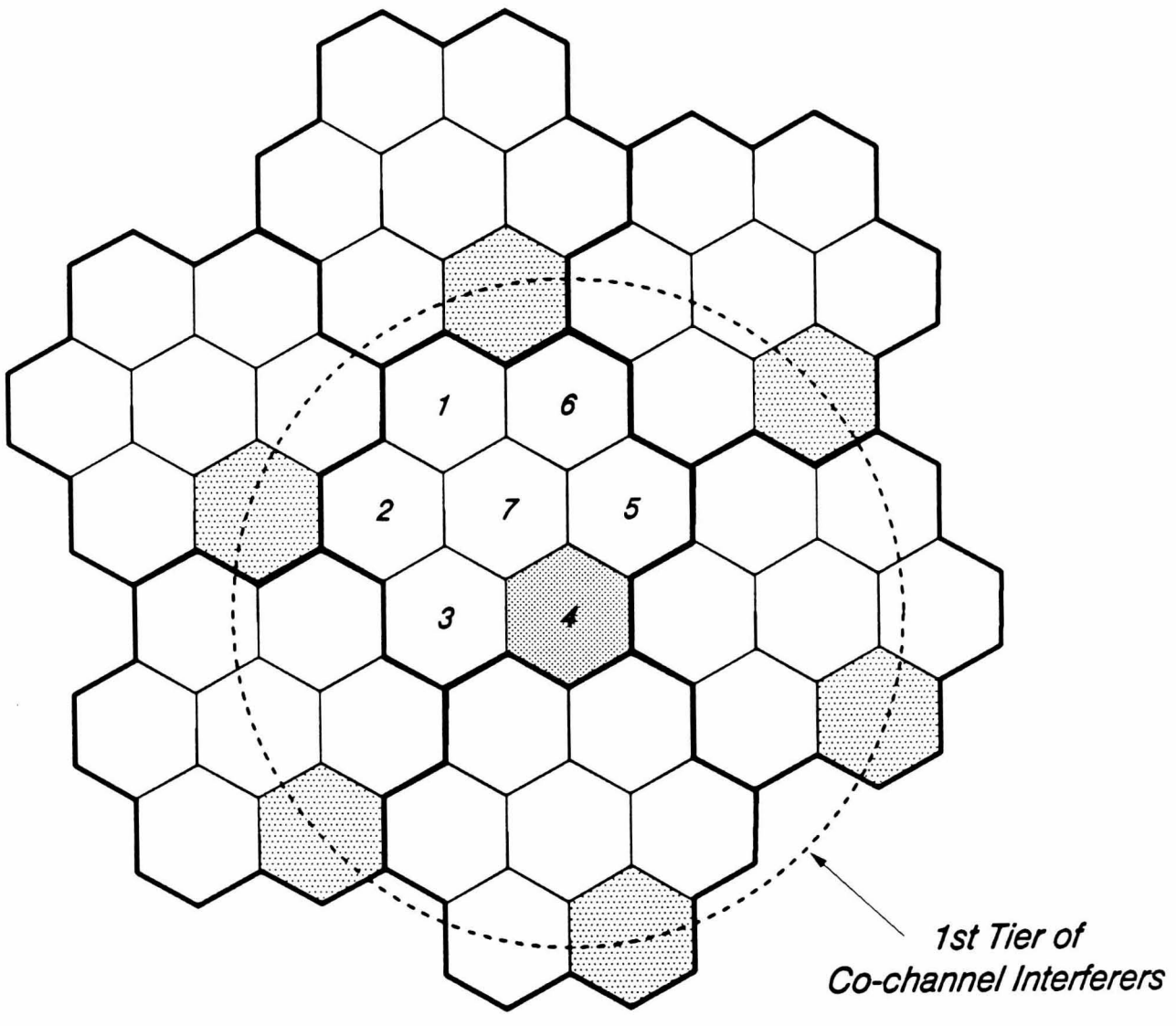

Figure 3.2: Hexagonal cellular layout with a 7 cell cluster.

Once the cluster size has been determined for a particular system architecture, the spectrum efficiency can now be calculated [2]. This gives a direct measure of the spectrum utilisation and can be expressed in terms of the number of voice channels/MHz of bandwidth/km^2, i.e.

$$E = \frac{B_t/B_c}{B_t(CA)} = \frac{1}{B_c CA} \qquad (3.4)$$

where

B_t is the total available bandwidth (MHz).
B_c is the channel spacing in MHz.
C is the number of hexagonal cells per cluster.
A is the area of a hexagonal cell in km^2.

An alternative measure of the spectrum efficiency of a network can be expressed in terms of erlangs/Mhz/km^2 where the erlang is a measure of the traffic intensity[2]. It can be shown that the two definitions are directly related [3] but since the former is simpler to manipulate, this expression is adopted here.

To enable a direct comparison to be made between two different base-station antenna systems, it is necessary to assume that an identical modulation scheme can be employed in both cases, and also that the hexagonal cell areas are the same. Thus $E \propto 1/C$ and the relative spectrum efficiency of system 1 with respect to system 2 can be expressed as

$$E_r = \frac{E_1}{E_2} = \frac{1/C_1}{1/C_2} = \frac{C_2}{C_1} \qquad (3.5)$$

When a comparison is to be made with a network containing fixed sector antennas, it is important to note that the cluster size in equation (3.5) refers to the number of hexagonal cells in each cluster and not the total number of sectors. This is a trivial point but often the sectors are referred to as cells which results in a different value for the number of cells in a cluster.

2: Erlangs give a measure of the quantity of traffic on a channel or group of channels per unit time.

3.2 MODELLING THE CO-CHANNEL INTERFERENCE ENVIRONMENT

In this section various co-channel models previously adopted by a number authors are briefly discussed before applying them to the different antenna systems. Each antenna system is required to operate within the same network and the following assumptions apply in each case:

(i) A cellular network consisting of hexagonal cells with channel reuse every C cells.

(ii) Centrally located base-station antennas.

(iii) A uniform distribution of users per cell.

(iv) A blocking probability of B in all cells.

(v) Idealised base-station antenna patterns providing uniform gain over the required coverage area.

(vi) The same modulation scheme is employed with each antenna system.

The blocking probability B in assumption (iv) is the fraction of attempted calls that cannot be allocated a channel. For example, if there are "a" erlangs of traffic offered, the actual traffic density is equal to a(1 - B) erlangs. This gives an *outgoing channel usage efficiency* or *loading factor* of

$$\eta = \frac{a(1-B)}{N_c} \tag{3.6}$$

where N_c is the total number of channels allocated per hexagonal cell. Hence, on average, the number of active channels in each cell is $N_c\eta$. (A similar expression was used by Daikoku and Ohdate [4].) In Appendix B, the number of channels is denoted by N which is also used later to represent the number of elements in the antenna array. Therefore the subscript "c" has been added here to avoid any confusion.

In the following analysis regarding the spectrum efficiency of the "smart" base-station antenna system, several assumptions have been made concerning the implementation of the system. These are as follows:

(i) The antenna system can generate any number, m, of ideal beams.

(ii) Each beam has a beamwidth of $2\Pi/m$, and a gain equal to the idealised omni/sectoral antenna.

(iii) Each beam only carries the channels that are assigned to the mobiles within its coverage area.

(iv) The necessary base-station hardware is available to enable beamforming and vehicle location.

These assumptions imply a somewhat hypothetical adaptive antenna system, with the m beams providing coverage of the complete cell area. This approach can be justified however since a uniform user population has been assumed for each antenna system. It is recognised that a dynamic, non-uniform user distribution will affect the results presented here, although if the adaptive base-station antenna system has complete control over the beam patterns, a situation similar to that depicted in figure 2.3 could be envisaged. Hence there would be directions in which little or no signal energy is radiated or received, reducing the levels of co-channel interference. This renders the above assumption as a worst case situation in terms of the transmission and reception of co-channel interference.

Another factor which will have a significant bearing on the results, is the assumption that all three systems to be considered (omni-, sectoral and multiple beam) employ idealised antennas, with uniform patterns providing identical coverage areas. In practice this will not be the case, and the effects of sidelobes and non-uniform patterns will result in increased levels of co-channel interference. This is especially true with the sector antennas and the multiple beam system. Also, in an urban or suburban mobile environment, the antenna pattern will be very different from the free space antenna pattern due to the reflections off surrounding buildings. In particular for directional antenna patterns, the free space front-to-back ratio (> 20 dB) could be reduced quite dramatically [5]. This is the result of the strong signal radiated in front being reflected from the surrounding buildings so that the energy can be received by a mobile behind the antenna. Similarly, the signal transmitted from a mobile behind the antenna could be received in the forward direction due to reflections. For these reasons, the resulting spectrum efficiencies for the different systems must be considered as the performance upper-bounds.

Two different categories of co-channel interference model were employed as the basis for this study and they can be summarised as follows:

- A **geometrical model** which considers the relative geometry of the transmitter and receiver locations and takes into account only the propagation path loss associated with the mobile radio channel.

- A **statistical model** in which the propagation effects such as fading and shadowing are included in a statistical fashion

Hammuda [3] has carried out an extensive investigation into the merits of these different models and favoured the geometrical approach which considers only the 1st tier of six interfering co-channel cells. However, this is with the proviso that the value of the protection ratio used is subjectively evaluated for the modulation scheme under fading and shadowing conditions. The main drawback of the geometrical approach is that it does not easily allow for a direct comparison between the competing base-station antenna technologies. However, the statistical approach readily lends itself to this task, although the results tend to give a rather pessimistic outlook, requiring larger clusters sizes for a given level of performance. In spite of these shortcomings, the results of applying both of these models will be discussed in the following sections. Finally note that in the analysis only the base-to-mobile link is considered, although the same principles can be developed for the mobile-to-base link.

3.2.1 Geometrical Propagation Model

This model is essentially the same as that presented by Lee [6] and only takes into account the propagation path loss, i.e. the area mean signal level experienced at the mobile, and is assumed to be proportional to the distance from the base-station raised to a power γ. It is recognised that with the advent of smaller cells, the propagation path loss is close to the free-space value [7], however it is envisaged that the proposed system architecture will initially operate within larger cells. Therefore, in the analysis presented in Appendix B, the commonly used approximation that the received signal power is inversely proportional to the fourth power of range was used [8]. Using the definition for the occurrence of co-channel interference given in equation (3.1), it is possible to draw a contour defining a region where

co-channel interference never occurs and a region where it always occurs. This contour depends on the protection ratio and, for the two co-channel cells shown in figure 3.1, the locus is defined by

$$\frac{d_i}{d_w} = \sqrt{p_r} \qquad (3.7)$$

where d_i and d_w are the distances between the mobile and the wanted and interfering base-station antennas respectively as given in figure 3.1. The contour given by equation (3.7) above is illustrated in figure 3.3 and, in the worst-case position which is in a direct line between the two transmitters as shown, the co-channel reuse ratio can be defined as

$$Q = \frac{D}{R} = 1 + \frac{d_i}{d_w} = 1 + \sqrt{p_r} \qquad (3.8)$$

This idea can be extended to the situation with more than one interferer, but the result is essentially the same, i.e. the maximum spectrum efficiency obtainable with an omni-directional base-station antenna is governed by the protection ratio, and hence the modulation scheme employed.

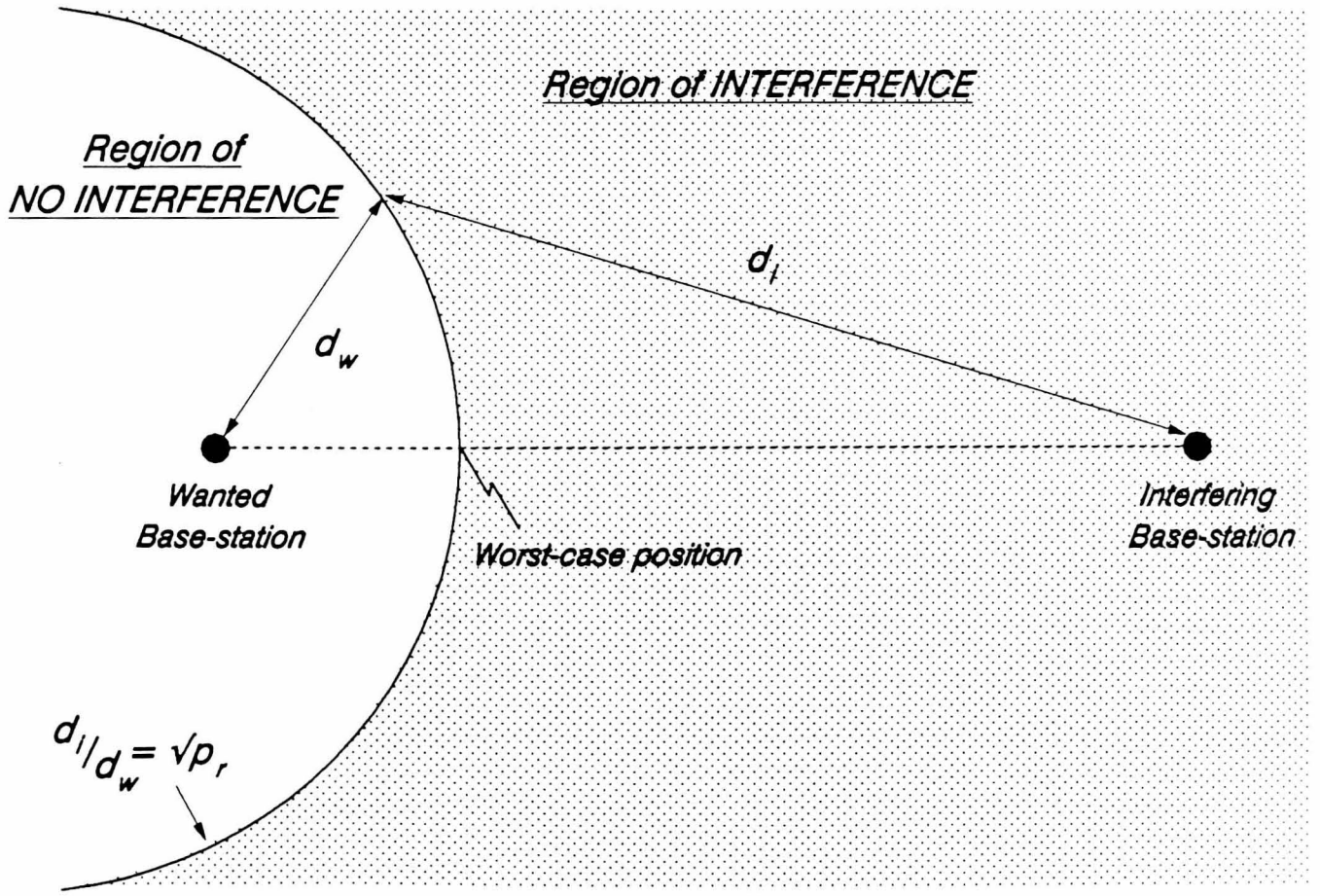

Figure 3.3: Contour defining interference regions.

A: Multiple Beams Versus Omni-directional

In order to compare the performance of the proposed multiple beam base-station antenna with a conventional omni-directional antenna, the model must be extended to consider the probability of co-channel interference occurring, i.e. $P(s_w \leq p_r s_i)$. This is often called the *outage probability*, and is the probability of failing to achieve satisfactory reception in the presence of interference. Within the region of no interference the outage probability is zero for both the antenna systems. However, if the mobile were to stray into the outer region of interference, the outage probability would depend on the proximity of the interfering cells and whether or not the active co-channel[3] is in the co-channel beams that are aligned onto the wanted mobile. For the simple case with only two co-channel cells as depicted in figure 3.3, the outage probability within the region of interference can be expressed as

$$P(s_w \leq p_r s_i) = \frac{\eta}{m} \qquad (3.9)$$

where η is the loading factor as defined in equation (3.6) and the omni- case is given by m = 1. Hence a hypothetical situation could now be envisaged where, if m is large enough to satisfy a given outage criterion, complete channel reuse would be possible (D/R=2) for any modulation scheme, e.g. a 10% outage criterion could be satisfied with only ten beams (m=10) in a fully loaded system. The outage probability for the case with six interferers is given in equation (16) of the paper in Appendix B and is quoted only for the limited region around the wanted cell where none of the co-channel cells alone can interfere with the wanted mobile. As the mobile moves further away from the wanted cell, one or other of the co-channel cells will dominate and the probability of co-channel interference occurring will increase. The actual value will depend on the position of the mobile, therefore significantly more beams would be required for complete channel reuse than in the simplified example given above for two co-channel cells. This clearly illustrates the difficulty in applying the geometrical model since the spectrum efficiency obtainable with the proposed base-station antenna system is not immediately apparent.

3: The "active co-channel" is the channel that has also been allocated to the wanted mobile.

B: Sectoral Versus Omni-directional

Lee [6] has successfully employed the geometrical model to compare the performance of fixed coverage sector antennas with omni-directional antennas. The two configurations considered divided the cell up into three and six sectors, with the base-station employing three 120° or six 60° beam directional antennas respectively. It was shown that with a seven cell cluster, the wanted mobile would only experience interference from two co-channel cells out of the six in the first tier of interferers with 120° sectors, and from only one cell if 60° sectors were employed. Hence the received level of co-channel interference is reduced, enabling the co-channel cells to be placed closer together and increasing the overall spectrum efficiency. If the distances between each co-channel cell and the wanted mobile are assumed to be equal, and the wanted mobile is at the edge of the cell boundary, then the co-channel reuse factor Q is as defined by Lee [6]. This result was given in equation (15) of Appendix B, but was quoted incorrectly and should read as

$$Q = \left[6\left(s_w/s_1\right)^2\right]^{\gamma} \qquad (3.10)$$

since the notation used in the paper defines $\left(s_w/s_1\right)$ as the ratio of the signal envelopes in volts. Hence, for a given protection ratio, a value of Q can be calculated and the spectrum efficiency determined. The approximation used in equation (3.10) assumes that the distances between the co-channel base-stations and the wanted mobile are identical and equal to the co-channel reuse distance D. Clearly as the cluster size is reduced, this approximation will no longer be valid, and the value of Q given by equation (3.10) may not be large enough to maintain a signal-to-interference ratio greater than the protection ratio. Also note that when the cluster size is small, the number of interferers in the first tier for 120° and 60° sector antennas may be greater than the values given above. With this in mind, the cluster sizes required to satisfy protections ratios of 8 dB and 20 dB with both the 120° and 60° sectoral antennas have been calculated. The mobile was placed in the worst-case position, i.e. at the cell boundary closest to the co-channel interfering cells, and the distances between the mobile and the wanted and interfering cells calculated. For a given cluster size, the signal-to-interference power ratio must satisfy the following equation

$$\frac{S_w}{S_I} = \frac{d_w^{-\gamma}}{\sum_{i=1}^{n} d_i^{-\gamma}} \geq p_r \qquad (3.11)$$

where the upper case S denotes the signal power and n is the number of interfering cells. The results are presented in table 3.1 below for 120° and 60° sectors and, as expected, the sector antennas provide a significant improvement in terms of increasing the spectrum efficiency. This gain however is at the expense of an increase in the handover rate since the mobiles will have to cross cell boundaries more frequently. This particular aspect will be addressed in more detail in the following sections.

Antenna Type		Cluster Size C	E_r
360°	$p_R = 8$ dB	3	1.0
	$p_R = 20$ dB	9	1.0
120°	$p_R = 8$ dB	1	3.0
	$p_R = 20$ dB	4	2.3
60°	$p_R = 8$ dB	1	3.0
	$p_R = 20$ dB	3	3.0

Table 3.1: Comparison of fixed sector directional antennas with an omni-directional antenna using geometrical model.

3.2.2 Statistical Propagation Model - One Co-channel Cell

In the previous section it was possible to define two distinct regions of operation using the geometrical model as illustrated in figure 3.3. In practice however, such a well defined contour is unlikely, and a more realistic impression is given in figure 3.4 with small pockets of interference even occurring quite close to the wanted base-station. In order to predict the co-channel interference, a model is now required which includes all the signal variations. There has been much debate, and still is, as to the best models to employ [9], although the general conclusion is that

the statistics of the signal can be represented by a combination of Rayleigh and log-normal statistics in the form of a Rayleigh distribution with a log-normally varying mean. The Rayleigh fading represents the rapid signal variations caused by the multipath effects and the log-normal fading represents the slower variations of the received signal, known as shadowing, due to the changes in the local terrain.

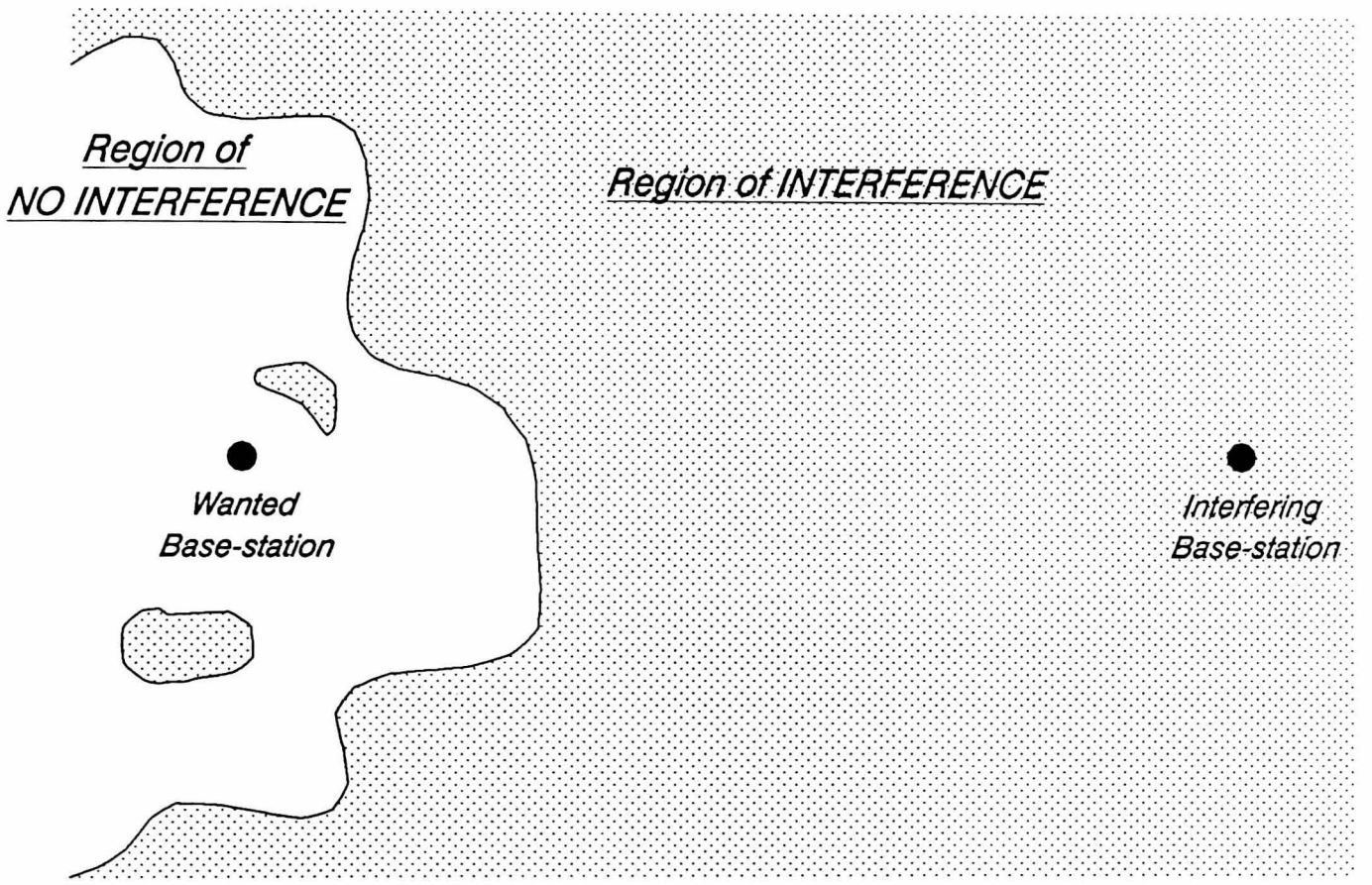

Figure 3.4: Contour defining interference regions with fading & shadowing.

The Rayleigh fading of the signal envelope, s, relative to the local mean $\bar{s}$ ($\bar{s}$ = <s>), is represented by the following probability density function

$$P(s/\bar{s}) = \frac{\Pi s}{2\bar{s}^2} \exp\left[-\frac{\Pi s^2}{4\bar{s}^2}\right] \qquad (3.12)$$

The log-normal variation of the local mean $\bar{s}$ is about the area mean m_d, where $m_d = <\bar{s}_d>$, the mean of $\bar{s}_d$ ($m_d = 20log_{10}m$ and $s_d = 20log_{10}s$). The area mean is governed by the propagation path loss and so is approximately proportional to the inverse of the distance from the base-station raised to the power γ as described earlier. Hence the log-normal shadowing probability density function (pdf) is given by

$$P(\bar{s}_d) = \frac{1}{\sqrt{2\Pi}\ \sigma} exp\left[\frac{-(\bar{s}_d - m_d)^2}{2\sigma^2}\right] \qquad (3.13)$$

The standard deviation σ describes the degree of shadowing, and typically varies from 6 to 12 dB in urban areas, the larger value being associated with very built up inner city areas. The combined pdf can now be expressed as

$$P(s) = \int_{-\infty}^{\infty} P(s/\bar{s}) \cdot P(\bar{s}_d)\ d\bar{s}_d \qquad (3.14)$$

and by substituting $\bar{s} = 10^{(\bar{s}_d/20)}$ (from $\bar{s}_d = 20log_{10}\bar{s}$) into equation (3.12), it becomes

$$P(s) = \sqrt{\Pi/8\sigma^2} \int_{-\infty}^{\infty} \frac{s}{10^{\bar{s}d/20}} exp\left[\frac{\Pi s^2}{4\times10^{\bar{s}d/20}}\right] exp\left[\frac{-(\bar{s}_d - m_d)^2}{2\sigma^2}\right] d\bar{s}_d \qquad (3.15)$$

Numerous studies have been undertaken to analyse the statistics of co-channel interference originating from a single co-channel cell, and have been carefully reviewed. The approach adopted here was that presented by French [10] (see Appendix B for more details). Now, instead of two distinct interference regions, the effects of co-channel interference can be described by outage probability contours as described in Appendix B for a single co-channel cell. The effect of including a multiple beam antenna is to reduce the value of each contour by a factor of m (m being the number of beams). Therefore, for a given outage criterion, either the service area can be increased or the co-channel cell can be placed closer. Hence the co-channel reuse ratio is reduced, requiring fewer cells per cluster and increasing the overall spectrum efficiency. The results for different numbers of beams in a fading and shadowing (σ = 6dB) environment with 70% loading (η = 0.7) and an outage probability of 1% are summarised in figure 11 of Appendix B. There is clearly a significant improvement in the spectrum efficiency, however the effect of multiple interferers has not been considered. Therefore, in order to present a more realistic study and facilitate a comparison with fixed sector directional antennas, the next section will concentrate on an extended model.

3.2.3 Statistical Propagation Model - Six Co-channel Cells

The main problem in developing an accurate model with many co-channel cells is predicting the distribution from the sum of multiple interfering signals. A commonly used approximation is to consider only the slower variations of the signals, i.e. the shadowing, although it must be recognised that the instantaneous effects due to the fast Rayleigh fading will affect the overall system performance. The total interference is then a power sum of statistically independent random variables which are log-normally distributed. The resulting distribution can be approximated to be also log-normally distributed [11] and this has been verified by Cox with Monte Carlo computer simulations [12]. Muammar and Gupta [13] have also considered the case where only Rayleigh fading is present (i.e. $\sigma = 0$) and approximated the overall distribution with a normal distribution.

There have been numerous studies which have considered co-channel interference originating from multiple co-channel cells (see Appendix B). However, the work of Muammar and Gupta [13] was adopted since the analysis is a direct extension of the single co-channel analysis of French [10]. Only the first tier of six interfering co-channel cells was taken into account, even though there are many other tiers of interferers present. Cox [12] has shown that the difference in the ratio of the average signal to average co-channel interference when considering only one tier or a large number of tiers is only a few dB. Therefore, approximating the total number of interferers by only the first tier is a valid approach, especially if the cluster sizes become quite large.

The wanted mobile in the central cell receives a signal envelope s_w from the wanted base-station, as well as n interfering signals s_i from the active co-channel cells (the maximum number being six in this case). The probability of co-channel interference occurring and there being n interfering co-channel cells can be expressed as

$$P\big((\text{co-channel interference}) \cap (\text{n active co-channels})\big)$$
$$= P(S_w \leq p_r S_I / n) \cdot P(n) \qquad (3.16)$$

where S_w and S_I are the wanted signal power and the total interfering signal

power respectively[4]. ($S_w \leq p_r S_I/n$) is the *conditional outage probability* (the probability of co-channel interference given that there are n active interferers) and $P(n)$ is the probability density function of n. The total outage probability is then the probability of co-channel interference occurring with any number of interferers up to n=6, and so can be expressed as

$$P(S_w \leq p_r S_I) = \sum_n P(S_w \leq p_r S_I/n) \cdot P(n) \qquad (3.17)$$

Equations for the conditional outage probability are given in the paper in Appendix B, as well as in the referenced work of Muammar and Gupta [13]. The *origination probability* of Daikoku and Ohdate [4] was employed as the probability density function of n, $P(n)$, and this is simply the probability that n co-channel interfering cells are using the same channel as the wanted mobile. Since only the base-to-mobile link is being considered, the origination probability with multiple independent beams is simply the probability that the n co-channel beams aligned onto the wanted mobile contain the active co-channel. Therefore, the origination probability can be expressed as

$$P(n) = \binom{6}{n} \left(\frac{\eta}{m}\right) \left(1 - \frac{\eta}{m}\right)^{6-n} \qquad (3.18)$$

where η is the loading factor as defined in equation (3.6) and m is the number of beams formed by the adaptive base-station (the omni- case is given by m=1). Note that for the mobile-to-base link, the level of interference experienced by the wanted base-station antenna is governed by the number of co-channel cells covered by an individual beam. In this respect, the results for the two links will be different but since the interference is greater in the base-to-mobile link, this will dominate the overall performance. The results for the mobile-to-base link are similar to the situation with fixed sector antennas to be discussed below.

The results for different numbers of beams in a fading and shadowing (σ = 6dB) environment with 70% loading (η = 0.7) and an outage probability of 1% are summarised in figure 3.5 and again show clearly the significant increases in spectrum efficiency that can be made. Consider now two different

---

4: Note that the equivalent equations in Appendix B should also be expressed in terms of the signal powers as opposed to the signal envelopes.

antenna configurations which employ fixed sector directional antennas with beamwidths of 120° and 60° respectively. Lee [6] has already established that the number of interferers in the first tier is reduced to two and one respectively (a valid assumption for cluster sizes greater than seven) hence, in equations (3.17) and (3.18) above, the maximum number of interferers n can be adjusted accordingly. If the traffic loading in each sector is then assumed to be identical to that in the previous analysis, i.e. the number of erlangs carried per channel is the same, and taking m = 1, the relative spectrum efficiency of sector antennas with respect to a conventional omni-directional antenna can be calculated in the same way. The results are presented in figure 3.5 and are very similar to a multiple beam antenna employing an equivalent number of beams. Further sectorisation will not increase the spectrum efficiency since, with only one tier of interferers considered, there will always be at least one source of co-channel interference. Hence, in using this model, there is an upper-bound to the

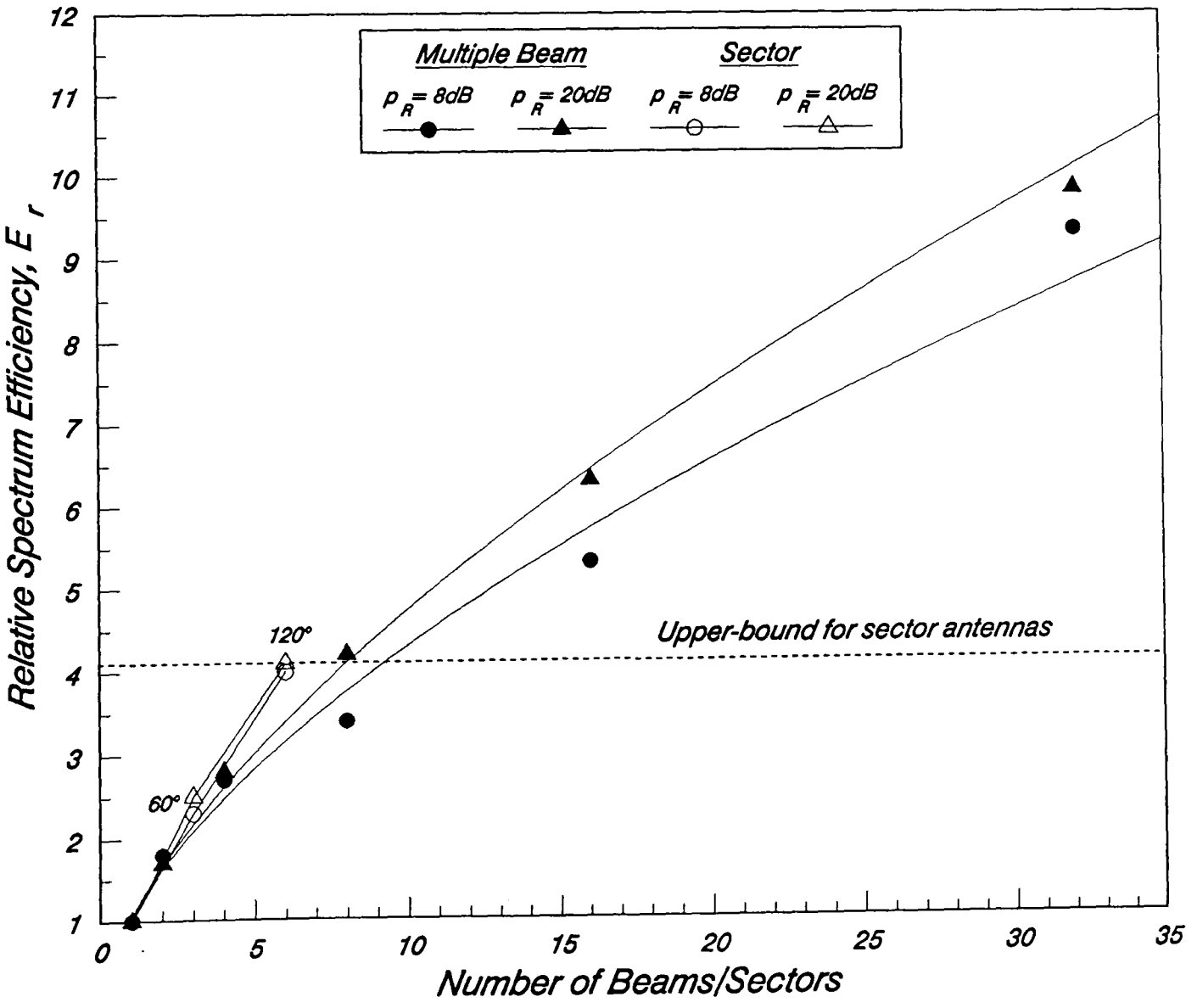

Figure 3.5: Relative spectrum efficiency as a function of the number of beams/sectors formed.

capacity advantage that can be achieved with sector antennas as shown in figure 3.5. In a more extensive model, further tiers of interferers would have to be considered as well as including such effects as the reduction in the front-to-back ratio discussed earlier.

Heeralall and Hughes [14] have proposed some novel cellular patterns employing fixed sector antennas. In their study, the cluster size was not restricted to the usual values for hexagons, and significant performance enhancements were reported. In spite of this, the main problem associated with fixed sector antennas is still to be addressed, namely the increased number of handovers required as the mobile circumnavigates the cell. This results in a reduction in the trunking efficiency of the network and will ultimately restrict the number of subscribers able to access the system as traffic demands rise. The multiple beam base-station antenna does not suffer from this problem since the process of switching the mobile from beam to beam is transparent to the user and does not require any channel switching. Even in the worst-case, with only fixed multiple beams covering the cell, the additional knowledge of the mobile's location enables the base-station to switch beams only when required to maintain signal contact.

3.3 CONCLUSIONS

The study presented in this chapter has demonstrated the feasibility of a multiple beam adaptive base-station antenna for cellular communications networks. A comparison made with the conventional omni-directional base-station antenna has shown a marked improvement in the spectrum efficiency and capacity that can be obtained, e.g. an idealised eight beam antenna system could provide at least a threefold increase in spectrum efficiency. The performance of the proposed system is also equivalent to a network employing fixed sector antennas with the same number of sectors as beams. However, the potential capacity enhancement with fixed sector antenna systems is limited, as well as significantly reducing the trunking efficiency of the network. An additional advantage of the proposed system is that it can provide extra capacity as the traffic demands rise by simply increasing the beamforming capabilities of the system (see figure 3.5). This is in contrast to the current approach of cell splitting. Not only does cell splitting reduce the trunking efficiency but the infrastructure costs are increased

significantly since new base-station sites must be acquired.

Hence this preliminary investigation has produced some very encouraging results and, as discussed above, the key to achieving the proposed increases in spectrum efficiency lies with the ability to locate the azimuth bearing of a mobile within the cell. Therefore the following chapters will concentrate on this particular aspect. The model that was adopted though was far from extensive since it only took into account the propagation characteristics of the mobile radio channel and ignored many of the other factors affecting the transmission performance. For example, power control at the base-station was not considered, and Palestini and Zingarelli [15] have shown that this can significantly increase the overall spectrum efficiency. The model that was adopted in this study also included the effects of non-ideal antenna radiation patterns. This would have a significant effect on the performance of the proposed system and so will have to be considered in any further investigations. Another factor that was not considered was the additional requirement that the received wanted signal must also achieve a satisfactory signal-to-noise ratio (SNR). This is determined by the receiver noise level and was considered by Sowerby and Williamson [16]. Finally the inclusion of a realistic traffic model, with a non-uniform distribution of mobiles and handovers, will enable an assessment of the trunking efficiencies of the different system architectures [17][18].

REFERENCES

[1]: V.H. MacDonald, *"The Cellular Concept"*, The Bell System Technical Journal, Vol.58, No.1, Jan. 1979, pp.15-41.

[2]: D.N. Hatfield, *"Measures of Spectral Efficiency in Land Mobile Radio"*, IEEE Transactions on Electromagnetic Compatibility, Vol.EMC-19, No.3, Aug. 1977, pp.266-268.

[3]: H. Hammuda, J.P. McGeehan and A. Bateman, *"Spectral Efficiency of Cellular Land Mobile Radio Systems"*, Proceedings of 38th IEEE Vehicular Technology Conference, Philadelphia, USA, 15th - 17th June 1988, pp.616-622.

[4]: K. Daikoku and H. Ohdate, *"Optimal Channel Reuse in Cellular Land Mobile Radio Systems"*, IEEE Transactions on Vehicular Technology, Vol.VT-32, No.3, Aug. 1983, pp.217-224.

[5]: W.C.Y. Lee, *"Mobile Cellular Telecommunications Systems"*, McGraw-Hill, 1989.

[6]: W.C.Y. Lee, *"Elements of Cellular Mobile Radio Systems"*, IEEE Transactions on Vehicular Technology, Vol.VT-35, No.2, May 1986, pp.48-56.

[7]: J.H. Whitteker, *"Measurements of Path Loss at 910 MHz for Proposed Microcell Urban Mobile Systems"*, IEEE Transactions on Vehicular Technology, Vol.VT-37, No.3, Aug. 1988, pp.125-129.

[8]: W.C. Jakes, *"Microwave Mobile Communications"*, John Wiley & Son, 1974.

[9]: J.D. Parsons and J.G. Gardiner, *"Mobile Communication Systems"*, Blackie & Son Ltd., 1989.

[10]: R.C. French, *"The Effect of Fading and Shadowing on Channel Reuse in Mobile Radio"*, IEEE Transactions on Vehicular Technology, Vol.VT-28, No.3, Aug. 1979, pp.171-181.

[11]: S.C. Schwartz and Y.S. Yeh, *"On the Distribution Function and Moments of Power Sums with log-normal Components"*, Bell System technical Journal, Vol.61, No.7, Sept. 1982, pp.1441-1462.

[12]: D.C. Cox, *"Co-Channel Interference Considerations in Frequency Reuse Small Coverage Area Radio Systems"*, IEEE Transactions on Communications, Vol.COM-30, No.1, Jan. 1982, pp.135-142.

[13]: R. Muammar and S.C. Gupta, *"Co-channel Interference in High Capacity Mobile Radio Systems"*, IEEE Transactions on Communications, Vol.COM-30, No.8, Aug. 1982, pp.1973-1978.

[14]: S. Heeralall and C.J. Hughes, *"High capacity Cellular Patterns for Land Mobile radio Using Directional Antennas"*, IEE Proceedings, Vol.136, Pt.I, No.1, Feb. 1989, pp.75-80.

[15]: V. Palestini and V. Zingarelli, *"Outage Probability in Cellular Mobile Radio"*, CSELT Technical Reports, Vol.XVI, No.6, Oct. 1988, pp.543-554.

[16]: K.W. Sowerby and A.G. Williamson, *"Outage Probability Calculations for a Mobile Radio System Having Multiple Rayleigh Interferers"*, Electronic Letters, Vol.23, No.11, 21st May 1987, pp.600-601.

[17]: R.A. Guérin, *"Channel Occupancy Time Distribution in a Cellular Radio System"*, IEEE Transactions on Vehicular Technology, Vol.VT-35, No.3, Aug. 1987, pp.89-99.

[18]: W. Mende, *"On the Handover Rate in Future Cellular Systems"*, 8th European Conference on Electrotechnics, EUROCON88, Stockholm, Sweden, 13th -17th June 1988, pp.358-361.

CHAPTER 4

DIRECTION FINDING IN THE CELLULAR LMR ENVIRONMENT: AN INTRODUCTION

In chapter 2, the application of an antenna array in a cellular communications network was discussed, with particular emphasis on reducing the level of co-channel interference, and thereby enhancing the spectrum efficiency of the network. The concept of a "smart" base-station antenna system was then introduced, and chapter 3 focused on the potential capacity advantage that could be achieved by employing such a system. Having established that there are significant capacity gains to be made, the next stage is to consider the practical realisation of the antenna system. It is clear that there are two fundamental tasks that must be accomplished at the base-station site: the estimation of the source locations within the cell, and the formation of a number of multiple independent beams based on this information. Both of these functions can be readily implemented using an antenna array and this is the subject of the present and subsequent chapters.

This chapter concentrates on the source estimation process, and introduces some of the signal processing techniques which can be employed to determine the azimuth bearing of a signal source. The techniques described have previously been employed extensively in radar and sonar systems, and their application in a mobile radio environment is considered here. The key factors which affect the ability of these techniques to accurately estimate the source directions are discussed, before briefly commenting on the propagation characteristics encountered in mobile radio. Although no particular modulation scheme, or access technique, has been specified in conjunction with the proposed antenna system, the signal processing techniques to be outlined in this chapter operate with narrowband signals. Consequently, this study is restricted to networks employing narrowband frequency division multiple access (FDMA), or time division multiple access (TDMA). Operation within a wideband modulation format is considered briefly in chapter 7.

4.1 ANGLE OF ARRIVAL ESTIMATION WITH ANTENNA ARRAYS

Antenna arrays have been employed extensively in a number of applications and have already been introduced as an adaptive beamformer in chapter 2. In this chapter, another application is considered in some detail, and that is the estimation of the angle of arrival (AOA) of the signal waveforms incident onto the array. Many other parameters regarding the signal environment can also be determined using an antenna array, e.g. the number of signals incident onto the array, the signal strengths and the signal polarisations. However, the main interest of this present study is the determination of the azimuth bearings of the signal sources, thus enabling the distribution of users within a cell to be mapped. AOA estimation is the classical problem in radar, sonar and seismic applications and Haykin [1] provides an in depth review of many of the signal processing techniques currently employed.

One of the simplest approaches exploits the duality that exists between frequency estimation from a time domain data sequence, and angle estimation from a spatially sampled data sequence. This is mathematically equivalent to estimating the spatial Fourier Transform across the array and determining the location of local maxima. The disadvantage of this technique is that the resolution of two or more sources is limited by the size of the aperture, hence the estimation accuracy can only be improved by increasing the aperture of the array. This solution is of only limited use since it requires increasing the physical size of the array. However, a description of this Fourier Method (FM), or conventional beamforming as it is sometimes called, is included in the next section as a precursor to some of the more sophisticated approaches which are often referred to as *superresolution* techniques.

Before proceeding it is worth briefly mentioning Maximum Likelihood (ML) estimation [1], since it can be considered as an optimum approach. Firstly, the conditional probability density function of the observed data across the array given the unknown parameters (e.g. the AOA) is formulated. This defines the likelihood function of the data and the maximum likelihood estimates are the values of the unknown parameters which maximise this function. In other words, the estimate provides the parameters which were most likely to have caused the observed signal vector across the array. Given sufficient observations of the data, the estimate will attain the true value and will

satisfy the Cramér-Rao bound. This defines the lower bound on the variance of the parameter estimate. For this reason it is often referred to as the optimum approach, however it does require the solution of a non-linear optimization problem which is time consuming, impractical and, in many instances, unnecessary. Hence, the following study will be restricted to many suboptimal approaches which are considered to be more pertinent to the application in mind. Appendix C contains the signal and noise model for an environment containing a multiplicity of non-coherent and/or coherent narrowband sources incident onto a uniformly spaced linear array. This model is contained in an Appendix for convenience since it will be repeatedly referred to during the following sections.

4.1.1 The Fourier Method (FM)

The spatial Fourier Transform of the observed signal vector **x** across an N element linear array defines the spatial spectrum and can be expressed as

$$X(\phi) = \sum_{n=1}^{N} x_n . exp\left[-j(n-1)\phi\right] \tag{4.1}$$

where

$$\phi = \frac{2\pi d}{\lambda} \sin \theta \tag{4.2}$$

is the inter element phase shift produced by a narrowband signal source with wavelength λ, incident at an angle θ off the array broadside (see Appendix C). The time domain equivalent for a data sequence x(n) is given by the Discrete Fourier Transform, i.e.

$$X(f) = \sum_{n=0}^{N-1} x(nT) . exp\left[-j2\pi fnT\right] \tag{4.3}$$

Hence, the dual of frequency in the time domain is

$$f = \sin \theta \tag{4.4}$$

and the dual of time sampling is

$$T = \frac{d}{\lambda} \tag{4.5}$$

The squared magnitude, $|X(\phi)|^2$, is termed the *periodogram* and the expectation of this gives the power spectrum. Hence the periodogram of equation (4.1) provides the basis of a method for estimating the power spectrum of the energy sources illuminating the array, and determining their *angle of arrival* (AOA).

Equation (4.1) above can be realised in a fairly straightforward manner if it is recognised that the exponential terms are a series of complex weights, with unity amplitude, applied to the outputs of the array elements. If a steering or weight vector **u** is defined as

$$\mathbf{u} = \begin{bmatrix} 1 \\ exp(j\phi) \\ exp(j2\phi) \\ \vdots \\ exp(j(N-1)\phi) \end{bmatrix} \qquad (4.6)$$

then the spatial spectrum, $X(\phi)$, is given by the summation of the weighted outputs of each element as follows

$$X(\phi) = \sum_{n=1}^{N} u^*_n . x_n$$

$$= \mathbf{u}^\dagger \mathbf{x} \qquad (4.7)$$

where * denotes the complex conjugate and † denotes the complex conjugate transpose. Closer inspection of equation (4.6) reveals that the weight vector can be simply realised by a set of phase shifters connected to the array elements.

Given the angular spectrum, $X(\phi)$, the angle of arrival of the signal sources can be estimated by locating the spectral peaks, that is the values of ϕ for which the magnitude of $X(\phi)$ attains a maximum. In order to demonstrate this consider a single source, incident at an angle θ_m off the array broadside, in a noiseless environment. The received signal is given by

$$s_{nm} = a_m exp[j(n-1)\phi_m] \qquad n = 1,2,\cdots,N \qquad (4.8)$$

where a_m denotes the complex amplitude of the signal received at the first element of the array. Substituting equation (4.8) into (4.1), and replacing x_n and $X(\phi)$ with s_{nm} and $S_m(\phi)$ respectively, the angular spectrum of this source equals

$$S_m(\phi) = a_m \sum_{n=1}^{N} exp\left[-j(n-1)(\phi-\phi_m)\right] \tag{4.9}$$

Recognising this as a geometric progression it can be expressed as

$$S_m(\phi) = a_m \left[\frac{1 - exp\left[-jN(\phi-\phi_m)\right]}{1 - exp\left[-j(\phi-\phi_m)\right]} \right]$$

$$= a_m exp\left[-j(N-1)(\phi-\phi_m)/2\right] \frac{\sin\left[N(\phi-\phi_m)/2\right]}{\sin\left[(\phi-\phi_m)/2\right]} \tag{4.10}$$

If the phase reference is at the centre of the array, this can be written as

$$S_m(\phi) = a_m \frac{\sin\left[N(\phi-\phi_m)/2\right]}{\sin\left[(\phi-\phi_m)/2\right]}$$

$$= a_m W(\phi-\phi_m) \tag{4.11}$$

where

$$W(\phi) = \frac{\sin\left[N(\phi)/2\right]}{\sin\left[(\phi/2)\right]} \tag{4.12}$$

The function $W(\phi)$ represents the familiar radiation pattern of a uniformly illuminated linear array. A plot of $W(\phi)$ against ϕ is shown in figure 4.1 for an eight element array. The pattern exhibits a mainlobe, or beam, of finite width, and several sidelobes. Referring to equation (4.11), it can be seen that a peak in the spectrum will occur when $\phi = \phi_m$, i.e. when the steering vector given by equation (4.6) is in the same direction as the incident signal. Hence the Fourier method is equivalent to sweeping a beam defined by **u** across the array aperture and observing the peaks at the array output. The term *conventional beamforming* has also been applied to this approach for obvious reasons. Using the notation of Haykin [1], a standard beamwidth is defined as the angular separation between the main lobe and the first null, i.e. $2\pi/N$ radians. An alternative definition of the beamwidth is the 3dB

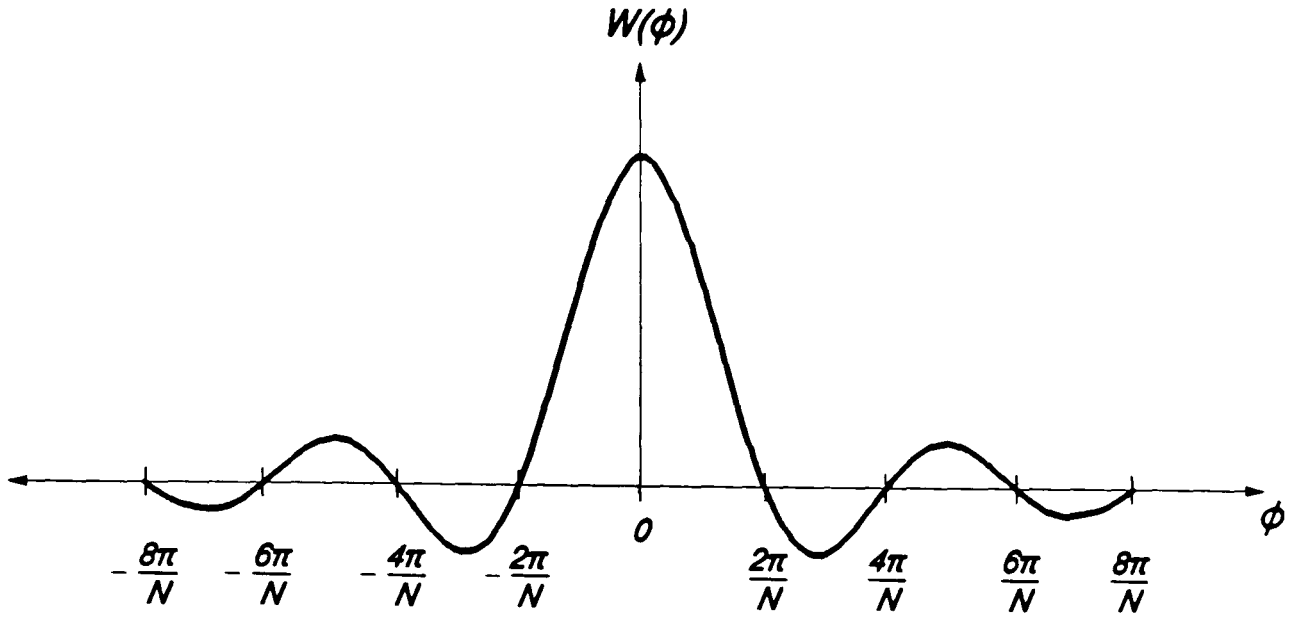

Figure 4.1: Radiation pattern for an eight element array.

beamwidth which, for the broadside beam of a linear array, is defined as [2]

$$\Delta\theta_{3dB} \cong \sin^{-1}\left(\frac{0 \cdot 886\lambda}{Nd} \right) \tag{4.13}$$

As can be seen in figure 4.1, the finite width of the array aperture (N) means that the source appears to come from a dominant, but diffuse direction, as well as false directions corresponding to the sidelobes. The sidelobes are due to the equal weighting assumed for each sensor output. The comparable result in time-series analysis occurs when a rectangular window is applied to a sinusoidal signal and the spectrum computed. If the weights are tapered, the sidelobes can be reduced, but at the expense of a wider mainlobe.

When there are a multiplicity of sources incident on the array the principle of superposition may be used to extend the result in equation (4.11). Thus, for M sources, the complete angular spectrum becomes

$$S(\phi) = \sum_{m=1}^{M} a_m \, W(\phi - \phi_m) \tag{4.14}$$

When the sources are separated from each other by two or more standard beamwidths, the magnitude of the angular spectrum $|S(\phi)|$ exhibits a corresponding number of distinct peaks, located according to the angles of arrival of the sources. If however, the sources are separated by between one and two standard beamwidths, distinct peaks may or may not appear, and herein lies the problem of the Fourier method. Two sources are not able to be

resolved unless the physical size of the array is increased.

Returning to the vector notation used to represent the angular spectrum in equation (4.7), the periodogram or the power spectrum of the received signal at sampling instant k can be expressed as

$$P_{FM}(\phi) = E\left[\left|X(\phi)\right|^2\right] = E\left[\left(\mathbf{u}^\dagger \mathbf{x}(k)\right)\left(\mathbf{u}^\dagger \mathbf{x}(k)\right)^\dagger\right]$$

$$= \mathbf{u}^\dagger E\left[\mathbf{x}(k)\mathbf{x}^\dagger(k)\right] \mathbf{u}$$

$$= \mathbf{u}^\dagger \mathbf{R} \mathbf{u} \qquad (4.15)$$

where $\mathbf{R}$ is defined as the array covariance matrix (see Appendix C). $P_{FM}(\phi)$ gives an estimate of the total signal power in the direction defined by ϕ, and the peaks that occur in this spectrum as the steering vector $\mathbf{u}$ is scanned give an indication of the angles of arrival of the signal sources.

In spite of its limitations, this traditional approach to bearing estimation has many advantages. It is very straight forward to implement and, since it is fairly insensitive to parameter variations, it is robust.

4.1.2 Maximum-Likelihood Method (MLM).

It is possible to obtain a set of weights (or steering vector) to achieve a higher degree of resolution by adapting them to the particular signal and noise fields present at the array aperture. A technique known as the maximum-likelihood method (MLM) for spectral estimation, originally developed for seismic array frequency wave-number analysis, accomplishes this and was first reported by Capon [3]. Strictly speaking it is not a true maximum-likelihood estimate, but the name MLM is retained for historical reasons. (It is also sometimes referenced as the Capon spectral estimate.) In time-series analysis, the technique is defined as a filter designed to only pass the power in a narrowband about the signal frequency of interest, and to minimise or reject all other frequency components in an optimum manner. This is equivalent to steering an antenna beam which will only pass signals from a particular direction, rejecting energy from all other directions. If the beam steering vector is defined as $\mathbf{w}$ then the energy contained within the beam is defined as

$$P = \mathbf{w}^{\dagger}\mathbf{R}\mathbf{w} \tag{4.16}$$

where $\mathbf{R}$ is the array covariance matrix. A steering vector $\mathbf{w}$ has to be found which minimises the beam energy subject to the constraint that

$$\mathbf{w}^{\dagger}\mathbf{u} = 1 \tag{4.17}$$

The vector $\mathbf{u}$ is as defined in equation (4.6) and represents an ideal plane wave in the required look direction. The purpose of this constraint is to fix the processing gain in the required look direction to unity. That is to say, only a signal arriving from that direction will be undistorted at the array output. The solution of this constrained optimisation problem requires the use of a Lagrange multiplier [4] and the resulting optimised steering vector is given by

$$\mathbf{w}_o = \frac{\mathbf{R}^{-1}\mathbf{u}}{\mathbf{u}^{\dagger}\mathbf{R}^{-1}\mathbf{u}} \tag{4.18}$$

This can be related to classical adaptive antenna array terminology by recognising that $\mathbf{w}_o$ gives the optimised array weights in adaptive beamforming [5], i.e. $\mathbf{w}_o = \mu\mathbf{R}^{-1}\mathbf{u}$ with $\mu = (\mathbf{u}^{\dagger}\mathbf{R}^{-1}\mathbf{u})^{-1}$. By substituting equation (4.18) into (4.16), the minimum beam energy, or residual output power, is given by

$$P_{ML}(\phi) = \frac{1}{\mathbf{u}^{\dagger}\mathbf{R}^{-1}\mathbf{u}} \tag{4.19}$$

As the steering vector $\mathbf{u}$ is swept through the directions of interest, equation (4.19) above gives the estimated angular or spatial spectrum for a given covariance $\mathbf{R}$, i.e. narrow peaks in the spectrum will define the AOA's of the incident signals. In a similar way to the Fourier estimate, $P_{FM}(\phi)$, the peak values reflect the true power levels of the sources.

4.1.3 Maximum Entropy Method (MEM)

The Burg Maximum Entropy Method (MEM) for spectral estimation in time series analysis has been shown to be equivalent to a *least mean square* (LMS) error linear prediction. Following the analysis of Gabriel [5], a linear prediction filter predicts the next value in a data sequence from a set of past values. LMS minimisation of the error between the true value and the

predicted value defines the optimum filter weights. When the error has been minimised, the power spectrum is equivalent to white noise. Thus, with the uncertainty in the error maximised, the result is a *maximum entropy* filter.

Alternatively, the output sequence is estimated from past values with the driving process assumed to be a white noise sequence of zero mean and variance σ^2. The process is sometimes referred to as *autoregressive* (AR) since the output sequence is a linear regression on itself with the input noise representing the error. Based on the analysis of Kay and Marple [6], the output power spectral density is given by

$$P_{ME}(f) = \frac{\sigma^2 \Delta t}{|A(f)|^2} \qquad (4.20)$$

where A(f) is the Discrete Fourier transform of the optimum filter weights, Δt is the sampling period and $\sigma^2 \Delta t$ is the power spectral density of the noise. The peaks (poles) of the unknown spectrum will occur at the zeros of the filter function. Hence the input sequence is modelled as a discrete all-pole linear prediction filter.

This has also been termed a deconvolution filter since it estimates the unknown spectrum directly from the reciprocal of the filter transfer function. This is in contrast to conventional window Fourier Transform methods, where the unknown spectrum is estimated by the convolution of the spectrum with the window filter transfer function. It is this convolution which smears or destroys the fine detail obtained with the MEM method for spectral estimation.

The preceding discussion considered spectral estimation in the time domain, however conversion of the MEM method for application with an adaptive antenna array is straight forward. It was demonstrated by Gabriel [5] that the linear predictor filter was identical in configuration to the Applebaum *sidelobe canceller* [7]. Here the signal arriving at a single main beam element is predicted from the weighted auxiliary elements. The optimised weights are then obtained after several successive snapshots across the array aperture. Convergence to the optimum weights may require several snapshots, depending on the algorithm chosen to calculate the weights. A popular method is the *Weiner prediction filter* where the optimum weights are given by

$$\mathbf{w}_o = \mu \mathbf{R}^{-1} \mathbf{c}^* \tag{4.21}$$

where $\mathbf{R}$ is the array covariance matrix, $\mathbf{c}^*$ is the quiescent weight steering vector, and μ is a scalar quantity. For the Applebaum sidelobe canceller, the quiescent weight vector is

$$\mathbf{c}^* = [1\ 0\ 0\ 0\ 0\ \cdots\ 0]^T \tag{4.22}$$

T denoting the transpose operation. Hence, in the noiseless quiescent state, only a single main beam element will be active. This element is usually different from the rest and of a much larger gain. However, the location of the main beam is arbitrary, e.g. it could be a weighted summation of some or all of the elements depending on the application and the desired main beam response. Gabriel [5], for example, proposed a circular array with an omni-directional main beam response and the phase reference at the centre of the array.

Since the input white noise has a power spectrum equal to a constant, the estimated spatial spectrum can now be derived from equation (4.20) as

$$P_{ME}(\phi) = \frac{1}{|W_o(\phi)|^2} = \frac{1}{|\mathbf{u}^\dagger \mathbf{w}_o|^2}$$

$$= \frac{1}{(\mathbf{u}^\dagger \mathbf{w}_o \mathbf{w}_o^\dagger \mathbf{u})} \tag{4.23}$$

where $W_o(\phi)$ is the spatial Fourier transform of the optimum array weights (equation (4.7)). The spatial spectrum is obtained by sweeping the steering vector $\mathbf{u}$ across all the directions of interest with sharp peaks indicating the location of sources of signal energy. It must be emphasised that this does not represent a true antenna pattern, since no combination of element weights could produce such sharply defined peaks. Physically, the spatial spectrum defined above is the inverse of the true adapted antenna pattern, with the nulls placed on the signal sources now representing the peaks in the spatial spectrum. Consequently, the heights of the peaks will not correspond to the signal power levels. However, in general, they will be proportional to the square of the signal power [8].

4.1.4 Eigenstructure Methods

These methods utilise the special eigenstructure of the array covariance matrix **R**, and obtain a much clearer insight into the AOA estimation problem. Pisarenko [9] was the first to exploit this, and it has since been extended by many authors, notably Schmidt [10][11] and Bienvenu and Kopp [12]. The signal and noise model considered is as described in Appendix C, with the additive noise component assumed to be spatially white, i.e. of equal power and uncorrelated from sensor to sensor. The observed signal vector is given in equation (C.6) and can be expressed in the form

$$\mathbf{x}(k) = \left[\mathbf{b}(\theta_1)\ \mathbf{b}(\theta_2)\ \cdots\ \mathbf{b}(\theta_M)\right]\mathbf{a}(k) + \mathbf{v}(k) \tag{4.24a}$$

where

$$\mathbf{b}(\theta_m) = \begin{bmatrix} 1 \\ exp(j\phi_m) \\ exp(j2\phi_m) \\ \vdots \\ exp(j(N-1)\phi_m) \end{bmatrix} \tag{4.24b}$$

and

$$\phi_m = \frac{2\Pi d}{\lambda} \sin \theta_m \tag{4.24c}$$

The $\mathbf{b}(\theta_m)$ (m=1,2,$\cdots$,M) are termed the *direction vectors* and represent the response of an ideal array to the mth signal source. Together they comprise the direction matrix **B** associated with the M signal sources. In practice, the response of the array to a single source will not produce the ideal vector given in equation (4.24b) since each element in the array will have a different amplitude and phase response at different AOA's. Mutual coupling will also have an effect and collectively they are referred to as the *array manifold*, i.e. the response of the antenna array to a single source as a function of the angle of arrival. More details about the effect a non-ideal array manifold on the performance of the DF algorithms will be given in section 4.3.1.

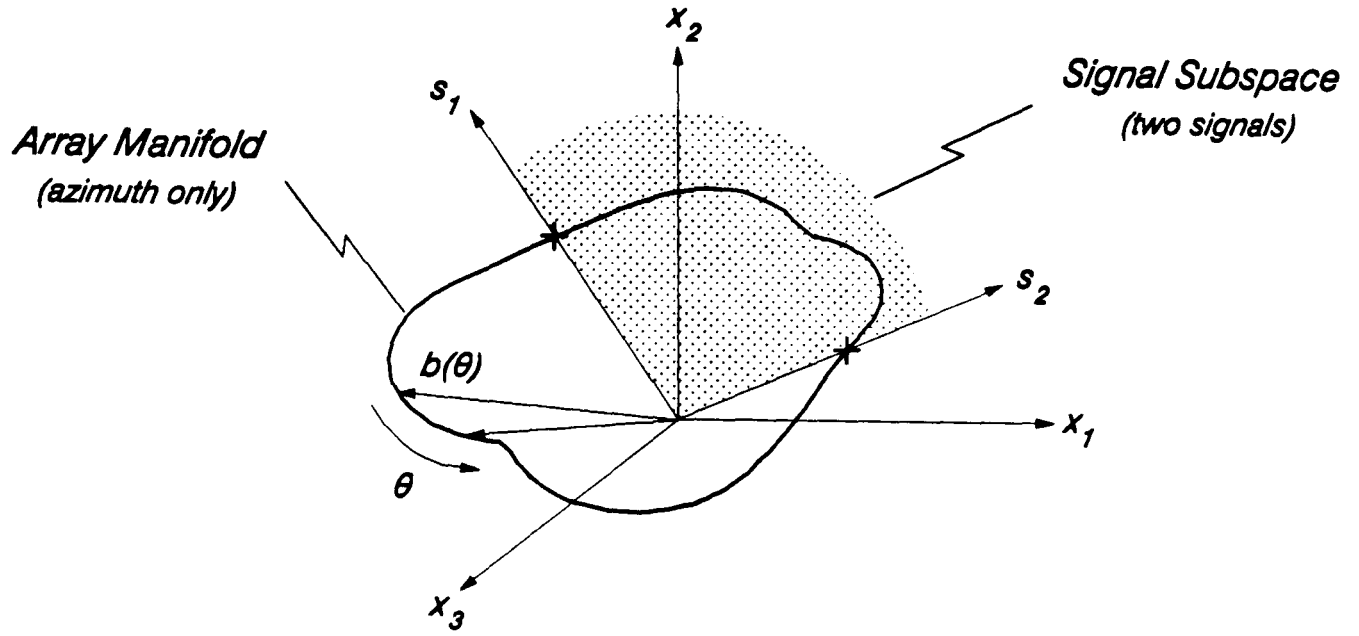

Figure 4.2: Geometrical representation of Direction Finding with a three element antenna array.

In order to visualise the concept, consider the response of the array to a single source as a vector tracing out a path in N dimensional space as the source AOA varies. This is illustrated in figure 4.2 for the simple case of three antenna elements, the coordinate axis representing each element. Hence, if there is a single source, $\mathbf{s}_1$, incident onto the array, the intersection of the source vector and the array manifold determines the AOA of the source. When two sources are incident, the resultant vector is contained within a plane, depicted in figure 4.2 as the *signal subspace*. The source AOA's are then given by the intersection of the array manifold with the signal subspace as indicated in the figure. This simple concept can now be extended to consider many more dimensions and sources, the principle of determining the source AOA's remaining the same. Many algorithms have been developed to determine the intersection of the signal subspace and the array manifold and three of the most popular techniques will now be presented. These exploit the characteristics of the eigenstructure of the array covariance matrix which is given by

$$\mathbf{R} = \mathbf{B}\mathbf{R}_a\mathbf{B}^{\dagger} + \sigma^2\mathbf{I} \tag{4.25}$$

Let $\{\lambda_1 > \lambda_2 > \cdots > \lambda_N\}$ and $\{e_1, e_2, \cdots e_N\}$ be the eigenvalues and the corresponding set of orthonormal eigenvectors of $\mathbf{R}$. Since the noise covariance is assumed to be equal to $\sigma^2\mathbf{I}$, the minimum eigenvalues of $\mathbf{R}$ are all equal to σ^2, the noise variance, with a multiplicity of N-M [10][11], i.e.

$$\lambda_{M+1} = \lambda_{M+2} = \cdots = \lambda_N = \sigma^2 \tag{4.26}$$

Let $\mathbf{E}_N$ be the matrix constructed of the associated noise eigenvectors

$$\mathbf{E}_N = [\mathbf{e}_{M+1}\ \mathbf{e}_{M+2}\ \cdots\ \mathbf{e}_N] \tag{4.27}$$

and $\mathbf{E}_S$ the matrix containing the remaining M signal eigenvectors.

$$\mathbf{E}_S = [\mathbf{e}_1\ \mathbf{e}_2\ \cdots\ \mathbf{e}_M] \tag{4.28}$$

A: The MUSIC Algorithm

Consider first of all the MUSIC algorithm (**MU**ltiple **SI**gnal Classification) described by Schmidt [10][11]. It was demonstrated that the noise subspace eigenvectors, given in equation (4.27), are orthogonal to the space spanned by the source direction vectors $\mathbf{b}(\theta_m)$, i.e. the signal subspace of figure 4.2. Hence

$$\mathbf{B}^\dagger \mathbf{e}_i = 0 \qquad i=M+1,\cdots,N \tag{4.29}$$

In geometrical terms, the N-M noise eigenvectors are said to span an N-M dimensional subspace, referred to as the *noise subspace*, with the remaining M signal eigenvectors contained within the *signal subspace*. Hence, in terms of equation (4.29) above, the direction vectors are said to be orthogonal to the noise subspace. For further information and proof of these statements, refer to the extensive work of Schmidt [10][11][13][14].

Exploiting the orthogonality between the direction vectors and the noise subspace, the MUSIC angular or spatial estimate is expressed as

$$P_{MU}(\phi) = \frac{1}{\mathbf{u}^\dagger \mathbf{E}_N \mathbf{E}_N^\dagger \mathbf{u}} \tag{4.30}$$

As the steering vector $\mathbf{u}$, given by equation (4.6), is swept across the array aperture, peaks in the spectrum will occur whenever $\mathbf{u} = \mathbf{b}(\theta_m)$, i.e. when the steering vector is orthogonal to the noise subspace, the intersection of the

array manifold (ideal in this case) and the signal subspace has been determined. The key steps of this algorithm are as follows:-

1: Calculate the eigenstructure of **R**.

2: Determine the number of signals **M** from equation (4.26), i.e. from knowledge of the number of noise eigenvalues.

3: Form the noise eigenvector matrix $\mathbf{E}_N$ and define the noise subspace.

4: Evaluate $P_{MU}(\phi)$ and determine the AOA's from the peaks in the spectrum.

An experimental system was also built by Schmidt to verify the theoretical performance of the MUSIC algorithm [15]. The results showed that the AOA's of signal sources, all located within a single beamwidth of the array, could be accurately measured and the signal strength estimated. A very interesting aspect of the experiments was the so called READ algorithm. Once the signal AOA and strength were calculated, an optimum set of weights was applied to the array to suppress all but one of the incident sources and reconstruct the selected signal. In this way, a separate array output was generated for each signal. This algorithm is of particular interest here, since it is very similar to the proposal in figure 2.4, i.e. once the AOA's of the incident sources are resolved, an optimum set of weights, or beams, are generated to recover the signals individually.

It is worth mentioning briefly at this point the work by Brandwood [16][17] into methods of obtaining the MUSIC DF function from the array covariance matrix **R** without having to resort to eigenanalysis. The proposed algorithms produce very similar results to the conventional MUSIC approach, but dramatically reduce the amount of computation that is required since eigen-decomposition is no longer necessary. They also reduce the complexity of the practical implementation of the DF function since the algorithms will lend themselves more readily to forms of parallel processing. The purpose of this study however, is only to assess the viability of DF in a mobile radio environment, and so consequently these algorithms will not be considered in any more detail at this stage. Although, if at a later date a commercially viable system is required, such factors as computational load and complexity will be of great importance, and the alternative non-eigenvector methods will merit further investigation.

B: The JoDeG Algorithm

This algorithm was developed by Johnson and DeGraaf [18] and is very similar to the MUSIC algorithm of Schmidt. (The name "JoDeG" has been chosen here to identify this approach and, as can been seen, it is derived from the names of the authors.) As an introduction to this approach, consider the underlying principle behind most of the current high resolution DF techniques. That is to find a steering vector, $\mathbf{w}$, which minimises the energy in the beam subject to the constraint that $\mathbf{w}^{\dagger}\mathbf{z} = 1$, where $\mathbf{z}$ is the constraint vector. The energy contained in the beam is expressed in equation (4.16) and is reiterated here for convenience

$$P = \mathbf{w}^{\dagger}\mathbf{R}\mathbf{w} \tag{4.31}$$

The solution to this optimisation problem was obtained in section 4.1.2 for the MLM approach (also termed the *minimum energy* scheme in [18]). Here, the constraint vector, $\mathbf{z}$, was simply the vector that would result when an ideal plane wave was incident onto the array. Hence, the gain of the steering vector in the look direction is fixed to unity and, by minimising the energy in the beam, the contribution from any source incident from another direction is reduced. Johnson and DeGraaf took this a step further by considering a general constraint vector, $\mathbf{z}$. This results in an optimum weight vector of

$$\mathbf{w}_o = \frac{\mathbf{R}^{-1}\mathbf{z}}{\mathbf{z}^{\dagger}\mathbf{R}^{-1}\mathbf{z}} \tag{4.32}$$

giving the energy in the beam, or spatial spectrum, as

$$P = \frac{1}{\mathbf{z}^{\dagger}\mathbf{R}^{-1}\mathbf{z}} \tag{4.33}$$

They further postulated that there must be suitable choice for $\mathbf{z}$ which would maximise the spatial resolution. Consider the constraint vector in the form of

$$\mathbf{z} = \mathbf{C}\mathbf{u} \tag{4.34}$$

with $\mathbf{u}$ representing a plane wave (equation (4.6)). The resulting energy in the beam when steered towards the source would be

$$P = \frac{1}{\mathbf{u}^{\dagger}\mathbf{C}^{\dagger}\mathbf{R}^{-1}\mathbf{C}\mathbf{u}} \tag{4.35}$$

The choice of constraint vector, $\mathbf{z}$, is then reduced to finding a matrix $\mathbf{C}$ which contains $\mathbf{u}$ in its null space, i.e. $\mathbf{Cu} = 0$. As already discussed, the eigenvectors associated with the N-M smallest eigenvalues are orthogonal to all of the signal direction vectors $\mathbf{b}(\theta_m)$ (m=1,$\cdots$,M) contained within the signal subspace. Hence define the matrix $\mathbf{C}$ as the outer product of these noise subspace eigenvectors

$$\mathbf{C} = \sum_{i=M+1}^{N} \mathbf{e}_i \mathbf{e}_i^{\dagger} \tag{4.36}$$

Consequently, since the M signal subspace eigenvectors are orthogonal to the noise subspace eigenvectors, $\mathbf{Ce}_i = 0$ for i=1,$\cdots$,M. More importantly however, the direction vectors $\mathbf{b}(\theta_m)$, defined in equation (4.24b), will also lie in the null space of $\mathbf{C}$, i.e. $\mathbf{Cb}(\theta_m) = 0$ (m=1,$\cdots$,M). Hence, as the steering vector $\mathbf{u}$ is swept through the source locations, peaks will occur in the beam energy function defined in equation (4.35) above. If the array covariance matrix $\mathbf{R}$ is expressed in terms of its eigenvectors and eigenvalues as

$$\mathbf{R} = \sum_{i=1}^{N} \lambda_i \mathbf{e}_i \mathbf{e}_i^{\dagger} \tag{4.37}$$

and similarly the inverse of $\mathbf{R}$ as

$$\mathbf{R}^{-1} = \sum_{i=1}^{N} \frac{1}{\lambda_i} \mathbf{e}_i \mathbf{e}_i^{\dagger} \tag{4.38}$$

then, because of the orthogonality of the eigenvectors, the beam energy can be simply expressed as

$$P_{JO}(\phi) = \frac{1}{\sum_{i=M+1}^{N} \frac{1}{\lambda_i} |\mathbf{u}^{\dagger}\mathbf{e}_i|^2} \tag{4.39}$$

and this defines the spatial spectrum for the JoDeG algorithm. The MUSIC algorithm can be obtained in a similar fashion utilising a slightly modified $\mathbf{C}$ matrix. Expressing the MUSIC spatial spectrum, given by equation (4.30), in a different form gives

$$P_{MU}(\phi) = \frac{1}{\sum_{i=M+1}^{N} |u^{\dagger} e_i|^2} \tag{4.40}$$

Johnson and DeGraaf carried out extensive comparisons between the MLM, MUSIC and their own eigenvector algorithm (hereafter referred to as the JoDeG algorithm), and their observations will be discussed in section 4.2.

C: The KuTu Algorithm

The final method to be considered is based upon the algorithm developed by Kumaresan and Tufts [19]. It is sometimes referred to as the *minimum norm* method but for the purpose of this analysis it shall be known as the "KuTu" algorithm. The authors considered a general approach to the AOA estimation problem and postulated that if a vector **d** could be found which exhibited the following property

$$\mathbf{b}^{\dagger}(\theta_m)\ \mathbf{d} = 0 \qquad m=1,\cdots,M \tag{4.41}$$

then it would be possible to estimate the source bearings since a polynomial D(z) given by

$$D(z) = \sum_{n=0}^{N-1} d_{n+1} z^{-n} \tag{4.42}$$

will have zeros at $exp(j\phi_m)$, m=1,···,M, thus indicating the AOA's of the M signals. A spatial spectrum can then be defined as

$$P_{KU}(\phi) = \frac{1}{|u^{\dagger} d|^2} \tag{4.43}$$

with peaks indicating the location of the signal sources.

The noise subspace eigenvalues exhibit the orthogonality described by equation (4.41) and the MUSIC and JoDeG algorithms exploit this property. Unfortunately, when the array covariance matrix, **R**, is estimated from a finite number K of data snapshots, i.e. $\hat{\mathbf{R}}$ in equation (C.8), the noise

eigenvalues will not all equal σ^2 as given by equation (4.26), especially at low signal-to-noise ratios. Hence, in practice, the MUSIC and JoDeG algorithms utilise the N-M eigenvectors corresponding to the eigenvalues that are closest to σ^2 in order to obtain the best possible estimate of the source bearings. Kumaresan and Tufts proposed a method of finding a vector **d** spanning the whole noise subspace of **R**. In other words, a vector **d** is required which is a linear combination of the N-M noise subspace eigenvectors. Constraining the first element of **d** to unity and minimising the Euclidean length ensures that the N-M zeros of D(z) not corresponding to the signal sources are less susceptible to noise, and will be uniformly distributed (approximately) around the unit circle. This greatly reduces the tendency for spurious peaks occurring in the spatial estimate, especially at low signal-to-noise ratios, and provides more accurate estimates of the actual source bearings. A more detailed description of the properties of D(z) can be found in the paper by Kumaresan and Tufts [19]. The vector **d** can be generated from either the signal subspace or noise subspace eigenvectors (E_s and E_n in equations (4.28) and (4.27)) and the results are briefly summarised in Appendix D.

4.2 COMPARISON OF DF ALGORITHMS

Numerous authors have made comparisons between the above angular estimation techniques in a multiple signal environment, and some of their findings will now be briefly discussed. The performance is usually based on the following criteria:-

- **Resolution** The ability to resolve two or more sources correctly.
- **Bias** The error in the location of the spectral peak.
- **Variabilty** The range of bearings over which the estimated AOA can be expected to vary.
- **Robustness** The susceptibility to non-ideal operating conditions, i.e. when have coherent signals or array calibration errors.

Lacoss [8] provides one of the earliest studies into the the MLM and MEM methods, and although the emphasis was on frequency estimation, the results are still relevant to this discussion. As already mentioned, the main

problems with the Fourier method are a consequence of the inherent "windowing" applied to the array aperture. This has the same effect as in time series analysis, with the smearing of detail reducing the resolution and leading to false peaks due to the sidelobes in the spectrum. The cause of this is that the window does not depend upon the true spectrum of the received data. The MLM and MEM methods do not suffer from this problem since they do not have fixed window functions associated with them. When estimating the power from a particular direction, the effects of power from other directions are minimised. In this respect they can be considered as data adaptive techniques, and can be termed as high resolution estimates, with narrow peaks in the spectrum indicating a source location. In general the peak values in the MLM method (as well as the Fourier method) indicate the actual power level of the incident signal. The peaks in the MEM spectrum tend to be proportional to the square of the power, although the area below the peak does give an indication of the power level [8]. Schmidt [11] has carried out computer simulations comparing the MLM, MEM and MUSIC algorithms. The MUSIC algorithm proved to be the superior, giving very sharply resolved peaks with no bias error, i.e. no offset from the actual angle of arrival. The MLM method, although having no bias error, produced poorly defined peaks and hence a reduced resolution. The MEM produced fairly sharp peaks but with quite large bias errors. Also, the increased resolution of the MEM method is at the expense of increased ripple in the sidelobes [4].

Evans [20] has applied the MLM and MEM methods to the resolution of radar targets, in particular the resolution of low angle terrain scattering or multipath. An experimental nine element array was employed and the results confirm the findings just mentioned, the MEM proving to have the higher resolution capabilities. In a subsequent publication [21], Evans *et al* compared the performance of many high resolution algorithms in typical terrain scattering environments. In particular, they studied the effects of multipath reflections on the accuracy of the estimates. The results were taken from extensive computer simulations, as well as field trials, and confirm many of the properties already mentioned. The problem with multipath reflections is that if the wanted signal and the reflected signal are in phase, or 180° out of phase, poor resolution will result, whereas a 90° phase difference ensures correct resolution of the two signals. More will be said about the problem of coherent multipath in section 4.3.3.

The superior resolution of the eigenstructure approach has made them the

most popular techniques, although if the eigen-decomposition of the covariance matrix given in equations (4.37) and (4.38) is used, all of the algorithms can be expressed in terms of their eigenvalues and eigenvectors. Clarke [22], for example, preferred this approach and formed a general equation relating all of the most popular algorithms.

Johnson [18] carried out a thorough examination of the MLM, MUSIC and JoDeG algorithms with the aid of computer simulations. The main difference between MUSIC and JoDeG is in the assumptions made about the noise field. In particular, the eigenvalues which represent the noise level (equation (4.26)). The MUSIC algorithm assumes that they are all equal, and this has the effect of "whitening" the background noise, resulting in a flatter spectrum. In general though the algorithms perform equally well, the only exception being when the number of signals to be estimated (M) is chosen incorrectly. The MUSIC algorithm tends to produce the same number of peaks as the number of estimated sources M, hence overestimating or underestimating M will produce misleading results. In contrast, the JoDeG algorithm is less sensitive to the choice of M and underestimating M will produce a spatial spectrum resembling the MLM estimate. This effect can be seen by substituting equation (4.38) into (4.19) and, if the number of sources is chosen to be zero, then the JoDeG and MLM algorithms are identical.

The computer simulation work of Kumaresan and Tufts [19] compared the KuTu algorithm with MUSIC and the following observation can be made. At low signal-to-noise ratio the resolution performance of the KuTu algorithm, in terms of correctly resolving two closely spaced sources, is superior. This can be attributed to the method of choosing the polynomial D(z) described earlier.

There have been many other detailed studies into the statistical performance of these techniques based on the four criteria highlighted at the beginning of this session. Brandwood [23] for example has presented extensive results from computer simulations on the performance of the MUSIC, MLM and FM algorithms. To date however, their application in a mobile radio environment has received little or no attention. Consequently, further comment on the merits of individual techniques will be reserved until the results of the computer simulations in the next chapter have been presented.

4.3 FACTORS AFFECTING PERFORMANCE

4.3.1 Array Manifold

The performance of all of these techniques is strongly dependent upon the assumptions made about the response of the array. The signal model developed in Appendix C assumed an ideal situation, with the phase information contained within the direction matrix **B** indicating perfect reception of the incident plane waves with ideal antenna elements. Generally, this will not be the case, and the response of the array to a single source must be measured as a function of the angle of arrival. This calibration process determines the *array manifold* and will include both the effects of mutual coupling and any amplitude/phase differences between the array receiver channels, as well as any errors in the positions of the antenna elements. Clarke [24] has demonstrated that even minor calibration errors can confuse the analysis, although the results from computer simulations carried out by Brandwood [23] show that the techniques performed reasonably well, even with quite substantial channel matching errors. Hence, in chapter 5, computer simulations will be used to further analyse this phenomenon and determine the robustness of the DF algorithms.

Measurement of the array manifold can be costly and time consuming, especially if frequent re-calibration is required. A potential solution would be to incorporate a more thorough model of the array manifold and to then estimate the correct array response on-line. This approach has been considered briefly by Clarke [24] and in more detail by Weiss and Friedlander [25].

4.3.2 Temporal Averaging

In all of the preceding analysis, use of the array covariance **R** has been assumed although, in practice, it is the sampled covariance matrix $\hat{\mathbf{R}}$, given by equation (C.8), which is employed. This involves taking a number of *snapshots*[1] K across the array and averaging. K is sometimes referred to as the *time bandwidth product* [4]. Generally speaking, the larger the number of

---

1: A snapshot is defined as one simultaneous sampling of the complete array aperture.

snapshots, the more valid the assumption about the additive noise being spatially and temporally white, and the greater the resolution and accuracy of the Direction Finding techniques.

4.3.3 Coherent Multipath

The resolution performance of all the above algorithms depends very strongly on the degree of correlation that exists between the signal sources to be resolved. If the sources are highly correlated, as would be the case with multipath reflections, the algorithms' performance is severely degraded in terms of the number of signals that can be successfully resolved. Bresler and Macovski [26] have investigated this problem in some detail and have determined the *resolution capacity* of a uniform linear array as a function of the coherency of the signal sources. If the sources are completely uncorrelated then the resolution capacity is one less than the number of elements in the array (N - 1). Gabriel [27] has also addressed this problem, and demonstrated that if a Doppler shift existed between coherent sources, then it would be possible to resolve them. Alternatively, a Doppler shift could be induced between the sources by sideways movement of the array aperture at each sampling instant or snapshot. In many cases this would not be practical or feasible, and so it was proposed that a reduced-dimension sample covariance matrix could be formed by synthetically shifting a subaperture across the complete array. This type of forward-backward averaging proved to be extremely effective, enabling the resolution of two coherent sources within a single beamwidth of the array.

Evans *et al* [21] proposed a similar preprocessing scheme, referred to as *spatial smoothing*, which effectively decorrelates the signals. Shan *et al* [28] provide a more complete analysis of this approach and, in conjunction with the MUSIC algorithm, present simulation results demonstrating its performance. A more thorough treatment of this technique will be given in the following chapter with the aid of computer simulations. Johnson [29] has considered a general approach to antenna array design for DF applications, by estimating the amount of temporal averaging and spatial smoothing that is required to ensure resolution of two completely coherent sources. Design curves were generated based on the performance of the MUSIC algorithm.

4.4 APPLICATION IN A CELLULAR RADIO ENVIRONMENT

In urban cellular communications, there is seldom a line of sight path between the base-station and the mobile, and hence radio communications is obtained by means of diffraction and reflection of the transmitted signal energy. This produces a complicated signal pattern causing the field strength to vary greatly throughout the cell, and the received signal at the moving mobile to fluctuate very rapidly. This is generally attributed to the superposition of two different classifications of signal fading phenomenon; *fast fading* (or just fading) due to the multipath nature of the received signal, and *slow fading* (shadowing), the slower variations of the received signal due to variations in the local terrain. As a result of this, the signal arriving at the mobile antenna can be assumed to be incident from all directions.

The base-station antenna on the other hand is usually well sited, high above any local scatterers, and so the angles of arrival (AOA's) of the incident signals are much closer to the direct line path between the mobile and base as shown in figure 4.3. It is for this reason that the use of fixed sector directional antennas at the base-station is made possible. However, the angular spread of the received signals is very dependent on the local scatterers in the vicinity of the mobile, as well as the distance of the mobile from the base. A spread of only 1° or 2° has been reported by Jakes with the mobile at distances of greater than 1.5 miles [27]. In an urban environment the buildings are in close proximity and so it is reasonable to expect that the angular spread is kept low. However, as the mobile moves into more open suburban areas this tends not to be the case, with line of sight propagation more likely, as well as discrete multipath reflections from more distant objects.

This range of operating conditions provides a very unique and significant challenge to the DF process, especially in the highly cluttered 'city centre' type environment. The primary task of the DF process however, is to only provide sufficient knowledge of the mobile locations within a cell to satisfy the beamforming requirements of the proposed base-station antenna. In an ideal situation, the mobiles can be accurately pinpointed, enabling the width of the beams covering the mobiles to be kept to a minimum. This will reduce the potential for the reception and transmission of co-channel interference and increase the level of performance that can be achieved (see

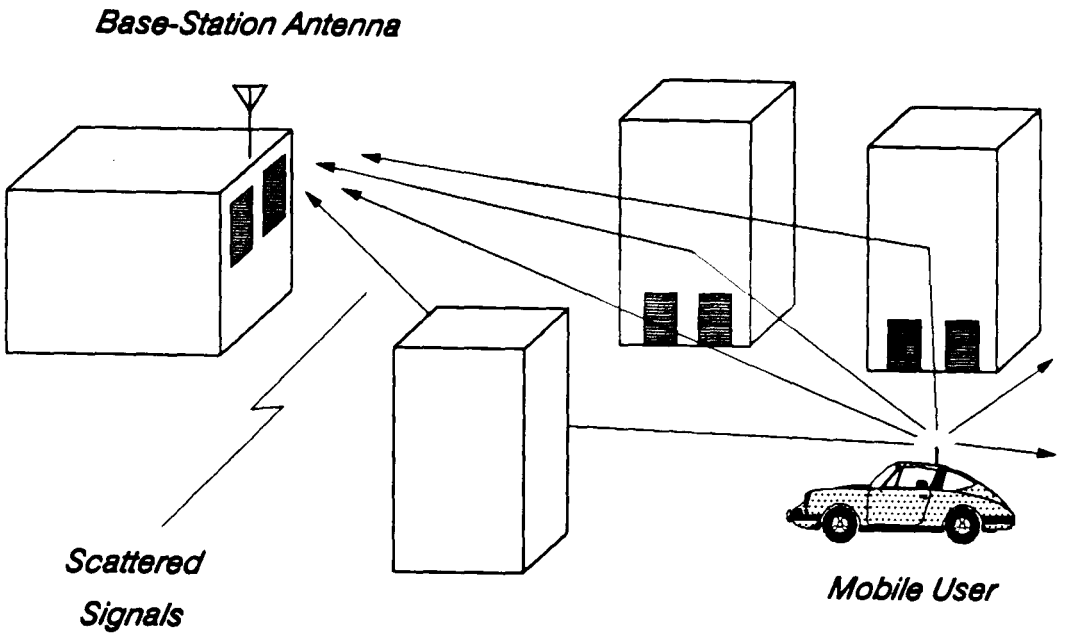

Figure 4.3: The mobile propagation environment.

chapter 3). Unfortunately this is not the case, and the degree of scattering in an urban locality will have a major effect on the potential capacity enhancement; if the angular spread of the signals is too large, the beams covering the mobiles will have to be made wider, increasing the level of co-channel interference. Also, the number of incident wave fronts incident at the base-station antenna array will be much greater than the available array degrees of freedom, although if the angular spread of these signals is low enough it would be impossible to estimate the AOA of each wave front. A reasonable assumption then would be that the combined effect will give a strong indication of the mobile source location within the limited degrees of freedom available. As the mobile moves into suburban areas, the scattering model may not be so relevant, with multipath reflections producing distinct coherent signals over a much larger angular spread. This would then necessitate some sort of spatial smoothing as described earlier.

Consider now a typical mobile communications environment where there could be up to 100 mobiles within a cell, each communicating with a central base-station antenna. An array with the necessary degrees of freedom to enable the resolution of all of these mobiles is unreasonable and unnecessary since each mobile is assigned a unique channel. Assuming a narrowband modulation format, this would correspond to a particular frequency allocation (e.g. a frequency division multiple access scheme) or time slot (e.g. a time division multiple access scheme), and it is sufficient to distinguish each mobile. Hence, the chosen DF algorithm need only search within each channel for a single mobile, dramatically reducing the hardware requirements. The

choice of the number of elements must also take into account the beamforming requirements of the system, since as the number of elements increases, the number of beams that can be generated also increases, thus offering the potential for increased efficiency and capacity. This particular aspect is addressed in more detail in Chapter 7.

In summary then, the chosen DF algorithm will have to locate a single mobile source within each narrowband communications channel, and in the next chapter models of the different mobile communication environments will be developed and included within a computer simulation suit. This then will enable an objective assessment of the different DF algorithms to be made. (A summary of all the algorithms to be studied is included in Appendix E for reference.) Direction finding with a wideband modulation format, e.g. a code division multiple access scheme employing wideband spread spectrum communications, is discussed briefly in chapter 7.

REFERENCES

[1]: S. Haykin, Ed., *"Array Signal Processing"*, Prentice Hall, Inc., 1985.

[2]: A.W. Rudge, K. Milne, A.D. Olver and P. Knight, *"The Handbook of Antenna Design - Volume 2"*, Peter Peregrinus Ltd., 1983.

[3]: J. Capon, *"High-resolution Frequency-Wavenumber Spectrum Analysis"*, IEEE Proceedings, Vol.57, No.8, Aug. 1969, pp.1408-1418.

[4]: Don H. Johnson, *"The Application of Spectral Estimation Methods to Bearing Estimation Problems"*, IEEE Proceedings, Vol.70, No.9, Sept. 1982, pp.1018-1028.

[5]: W.F.Gabriel, *"Spectral Analysis and Adaptive Array Superresolution Techniques"*, IEEE Proceedings, Vol.68, No.6, June 1980, pp.654-666.

[6]: S.M. Kay and S.L. Marple, Jr, *"Spectrum Analysis - A Modern Perspective"*, IEEE Proceedings, Vol.69, No.11, Nov. 1981, pp.1380-1419.

[7]: S.P. Applebaum, *"Adaptive Arrays"*, IEEE Transactions on Antennas & Propagation, Vol.AP-24, No.5, Sept. 1976, pp.585-598.

[8]: R.T. Lacoss, *"Data Adaptive Spectral Analysis Methods"*, Geophysics, Vol.36, No.4, Aug. 1971, pp.661-675.

[9]: V.F. Pisarenko, *"The Retrieval of Harmonics from a Covariance Function"*, Geophysics Journal Royal Astronomical Society, Vol.33, 1973, pp.347-366.

[10]: R.O. Schmidt, *"A Signal Subspace Approach to Emitter Location and Spectral Estimation"*, Ph.D dissertation, Dept. Electrical Eng., Stanford University, Stanford, CA, USA, Nov. 1981.

[11]: R.O. Schmidt, *"Multiple Emitter Location and Signal Parameter Estimation"*, IEEE Transactions on Antennas & Propagation, Vol.AP-34, No.3, March 1986, pp.276-280.

[12]: G. Bienvenu and L. Kopp, *"Source Power Estimation Method Associated with High Resolution Bearing Estimation"*, Proceedings IEEE International Conference on Acoustics, Speech & Signal Processing, ICASSP81, Atlanta, USA, 1981, pp.153-156.

[13]: R.O. Schmidt, *"New Mathematical Tools in Direction Finding and Spectral Analysis"*, Proceedings SPIE 27th Annual Symposium, Aug. 23 1983, San Diego, USA, pp.7-19.

[14]: R.O. Schmidt, *"Eigenvector Methods in Signal Processing"*, Proceedings SPIE National Society Optical Engineering (USA), Highly Parallel Signal Processing Architectures, Vol.614, Jan. 1986, pp.13-23.

[15]: R.O. Schmidt and R.E. Franks, *"Multiple Source DF Signal Processing: An Experimental System"*, IEEE Transactions on Antennas & Propagation, Vol.AP-34, No.3, March 1986, pp.281-290.

[16]: D.H. Brandwood, *"Noise Space Projection and Economical Methods for Obtaining the MUSIC DF Function Without Eigenanalysis"*, IEE Fifth International Conference on Antennas & Propagation, ICAP87, pp.415-418.

[17]: D.H. Brandwood, *"Noise-Space Projection: MUSIC Without Eigenvectors"*, IEE Proceedings, Vol.134, Pt.H, No.3, June 1987, pp.303-309.

[18]: Don H. Johnson and S.R. DeGraaf, *"Improving the Resolution of Bearing in Passive Sonar Arrays by Eigenvalue Analysis"*, IEEE Transactions on Acoustics, Speech & Signal Processing, Vol.ASSP-30, No.4, Aug. 1982, pp.638-647.

[19]: R. Kumaresan and D.W. Tufts, *"Estimating the Angles of Arrival of Multiple Plane Waves"*, IEEE Transactions on Aerospace & Electronic Systems, Vol.AES-19, No.1, Jan. 1983, pp.134-139.

[20]: J.E. Evans, *"Aperture Sampling Techniques for Precision Direction Finding"*, IEEE Transactions on Aerospace & Electronic Systems, Vol.AES-15, No.6, Nov, 1979, pp.891-895.

[21]: J.E. Evans, J.R. Johnson and D.F. Sun, *"High Resolution Angular Spectrum Estimation Techniques for Terrain Scattering Analysis and Angle of Arrival Estimation"*, Proceedings of 1st Acoustics, Speech & Signal Processing (ASSP) Workshop on Spectral Estimation, Canada, 1981, pp.5·3·1-5·3·10.

[22]: I.J. Clarke, *"Comparison of Advanced Signal Processing Algorithms"*, IEE Colloquium on Direction Finding Systems in Their Operational Environment, Digest No.1986/10, 21st Jan. 1986, pp.9/1-9/9.

[23]: D.H. Brandwood, *"Adaptive Array Techniques for Direction Finding"*, Fourth International Conference on Antennas & Propagation, ICAP85, pp.246-250.

[24]: I.J. Clarke, *"Robustness of Eigen Based Analysis Techniques Versus Iterative Adaption"*, IEE International Conference on Radar, RADAR 87, London, U.K., 19th - 21st Oct. 1987, pp.84-88.

[25]: A.J. Weiss and B. Friedlander, *"Direction Finding in the Presence of Mutual Coupling"*, Proceedings of 22nd Asilomar Conference on Signals, Systems & Computers, USA, 1988, pp.598-602.

[26]: Y. Bresler and A. Macovski, *"On the Number of Signals Resolvable by a Uniform Linear Array"*, IEEE Transactions on Acoustics, Speech & Signal Processing, Vol.ASSP-34, No.6, Dec. 1986, pp.1361-1375.

[27]: W.F. Gabriel, *"Adaptive Superresolution of Coherent RF Spatial Sources"*, Proceedings of 1st Acoustics, Speech & Signal Processing (ASSP) Workshop on Spectral Estimation, Canada, 1981, pp.5·1·1-5·1·7.

[28]: T. Shan, M. Wax and T. Kailath, *"On Spatial Smoothing for Direction-of-Arrival Estimation of Coherent Signals"*, IEEE Transactions on Acoustics, Speech & Signal Processing, Vol.ASSP-33, No.4, Aug. 1985, pp.806-811.

[29]: R.L. Johnson, *"Antenna Array Design for Covariance-Based Direction-Finding Methods"*, IEEE Transactions on Antennas & Propagation, Vol.AP-36, No.11, Nov. 1988, pp.1537-1544.

[30]: W.C. Jakes, *"Microwave Mobile Communications"*, John Wiley & Son, 1974.

CHAPTER 5

DIRECTION FINDING IN THE CELLULAR LMR ENVIRONMENT: A COMPUTER SIMULATION STUDY

In chapter 4, a number of signal processing techniques were introduced from which the spatial spectrum of the signals incident onto an antenna array can be generated. The peaks in the spatial spectrum define the angles of arrival (AOA's) of the received signals, and enable the distribution of signal sources around the array to be determined. These so called direction finding (DF) algorithms have been employed extensively in radar and sonar, although to date, their application in a mobile radio environment has not been considered. In this chapter, a computer simulation suite is developed in order to assess the performance of the six DF algorithms outlined in chapter 4 for a variety of operating conditions typical of a mobile radio environment. A uniform linear antenna array comprising of four elements with half wavelength spacing is considered, and the DF algorithms applied to resolve the bearing of a single mobile source. This particular set-up was chosen to enable a comparison to be made between the simulation results, and the results obtained from the field trials presented in the following chapter. The antenna array is assumed to be located at a typical uncluttered base-station site and, since the array is linear, provides uniform coverage over a 180° sector.

In section 4.4 the land mobile radio (LMR) propagation environment was briefly discussed, with particular attention given to the spread of the received signals at a base-station antenna site. This phenomenon is a result of the buildings and other scattering objects[1] in the immediate vicinity of the mobile. In a typical urban environment, a line of sight path would generally not be available, with the presence of continuous lines of buildings along the streets ensuring that signal reception at the base-station is predominantly from reflections, with some diffraction of the signal energy around buildings. Therefore it can be seen that the urban

---

1: Including other vehicles, both stationary and mobile.

environment potentially offers a significant challenge to the direction finding process, and the task of providing sufficient knowledge of the mobile locations to satisfy the beamforming requirements of the proposed base-station antenna system. It would be unreasonable to expect the array to correctly resolve all of the scattered wavefronts incident at the base-station since this would require an excessive number of antenna elements, although if the degree of scattering is only a few degrees, the combined effect of all the scattered wavefronts would probably give a strong indication of the actual location of the mobile source.

In suburban and rural areas, the scenario changes, with line of sight propagation more likely, as well as the occurrence of discrete multipath reflections from distant objects not in the immediate vicinity of the mobile. These three general classifications of the different operating conditions that can be encountered in mobile radio are briefly summarised in figure 5.1 and, in the following sections, models for each of them are outlined. The effects of co-channel interference are also included, as well as the mutual coupling characteristics of the array and receiver channel mismatches. The resolution performance of all six DF algorithms is then assessed in the different environments with a stationary and mobile source. Finally, some recommendations are made regarding the suitability of the various DF algorithms for the different mobile radio environments discussed.

5.1 URBAN COMMUNICATIONS

5.1.1 Local Scattering Environment

Following the analysis of Jakes [1], the local scatterers in the immediate vicinity of the mobile can be assumed to be uniformly distributed around the mobile at a small distance away. Figure 5.2 illustrates a possible scenario with the scatterers uniformly spaced on a circle, radius r, surrounding the mobile. Other possible models could include the direction of motion of the mobile with respect to the line of sight path to the base-station, e.g. the scatterers could lie on an ellipse with the major axis along the direction of motion. This would probably more closely resemble the scattering in a typical urban street, however the simplified model depicted in figure 5.2 will be sufficient for the purposes of this study.

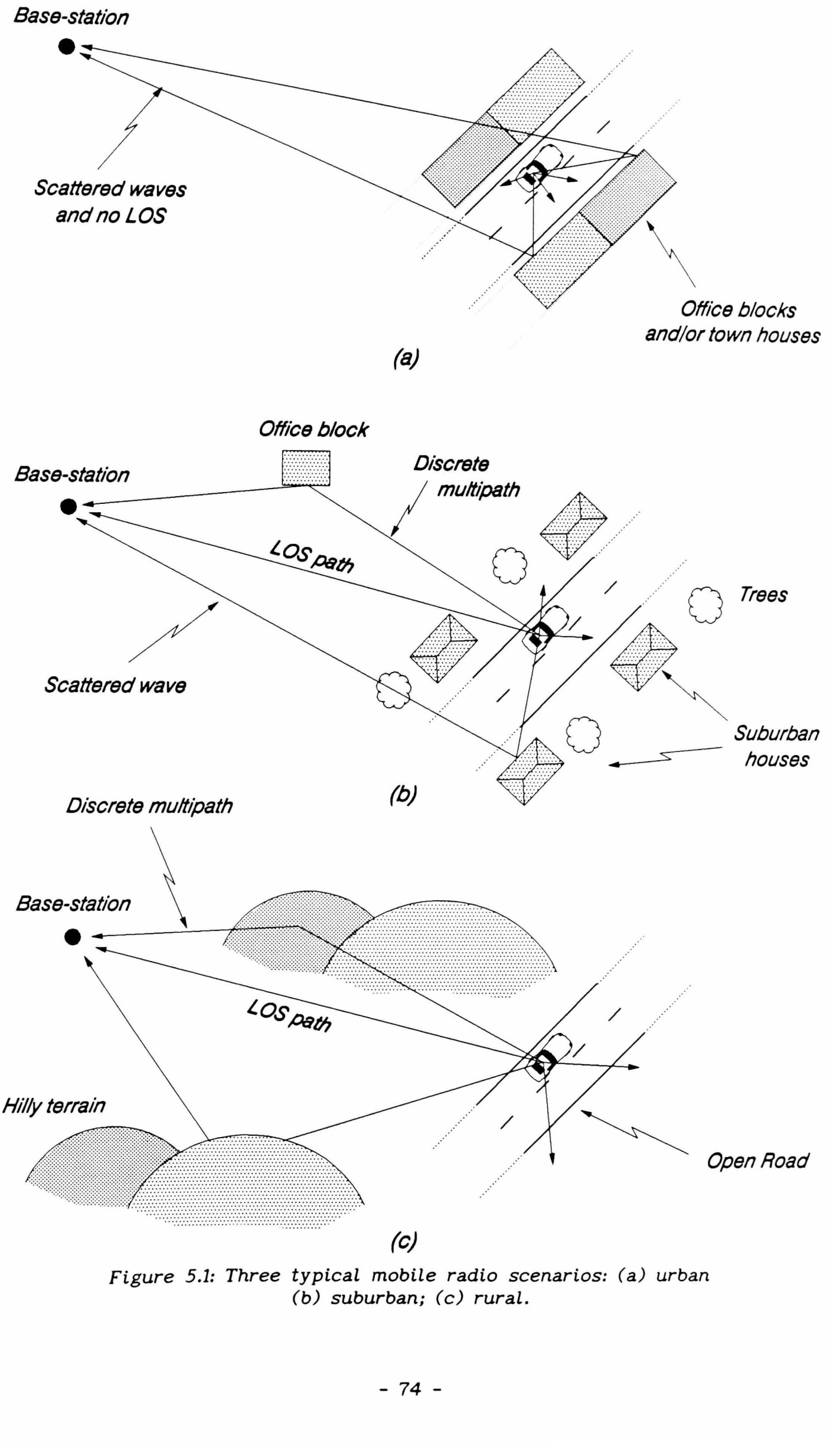

Figure 5.1: Three typical mobile radio scenarios: (a) urban (b) suburban; (c) rural.

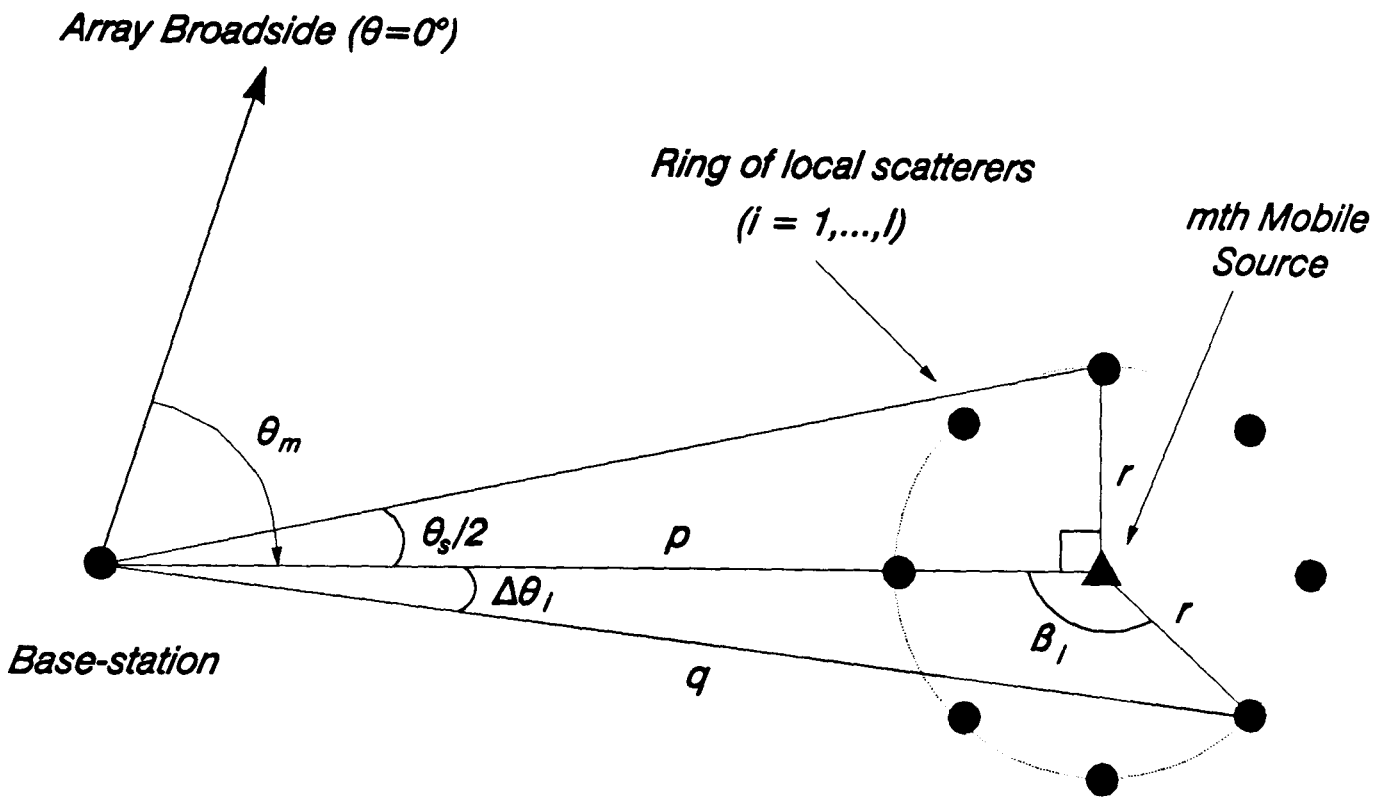

Figure 5.2: The scattering environment.

The distance between the mobile and base-station is p and it is assumed that p » r. If there are a total of I scatterers, then the angle β_i is given by

$$\beta_i = \frac{2\pi i}{I} \qquad i=1,\cdots,I \tag{5.1}$$

and employing the *sine rule* gives

$$\frac{\sin\Delta\theta_i}{r} = \frac{\sin\beta_i}{q} \tag{5.2}$$

The radius of the scattering circle can be calculated from the angular spread of the scatterers, θ_s, as

$$r = p \tan(\theta_s/2) \tag{5.3}$$

Since p » r it can be assumed that p ≅ q and, if θ_s is assumed to be small, the following are also true

$$\sin\Delta\theta_i \cong \Delta\theta_i$$

$$\tan\left(\theta_s/2\right) \cong \theta_s/2 \tag{5.4}$$

Hence, the change in the bearing θ_m of the mth mobile source due to each scatterer can be expressed as

$$\Delta\theta_i = \left(\theta_s/2\right)\sin\beta_i \tag{5.5}$$

Substituting in the expression for β_i, given by equation (5.1), the bearing of each scatterer off the array broadside is given by

$$\begin{aligned}\theta_{m,i} &= \theta_m + \Delta\theta_i \\ &= \theta_m + \left(\theta_s/2\right)\sin\left(\frac{2\pi i}{I}\right) \qquad i=1,\cdots,I \ ; \ m=1,\cdots,M\end{aligned} \tag{5.6}$$

The local scatterers will introduce a random amplitude and phase onto the signal after the reflection. Therefore, using the notation developed in Appendix C and following the analysis of Lee [2], each scattered signal incident at the base-station can be expressed as

$$a_{m,i}(k) = A_{m,i}\,exp\left(j\alpha_{m,i}\right)\cdot a_m(k) \qquad i=1,\cdots,I \ ; \ m=1,\cdots,M \tag{5.7}$$

where k denotes the time sampling instant and $a_m(k)$ is the original baseband signal transmitted by the mth mobile. For the purposes of the simulation it is assumed that $a_m(k)$ is constant and that

$$E\left[\left|a_m(k)\right|^2\right] = 1 \tag{5.8}$$

The attenuation factor $A_{m,i}$ and phase shift $\alpha_{m,i}$ are assumed to be independent random variables and, for the situation where both the mobile and scatterers are moving, will be unique at each sampling instant. The phase components will be uniformly distributed between 0 and 2π and, for the purposes of the simulation, the attenuation factors will be Rayleigh distributed. In reality this will not be the case and the attenuation factor, or more correctly the reflection coefficient, will depend upon the type of scatterers surrounding the mobile, i.e. whether they are static (buildings) or moving (vehicles) [2].

For each mobile source the total combined signal incident at each element of the base-station antenna array will be given by

$$s_{nm}(k) = \sum_{l=1}^{I} a_{m,l}(k) exp\left[j(n-1)\phi_{m,l} \right] \tag{5.9}$$

where

$$\phi_{m,l} = \frac{2\pi d}{\lambda} \sin \theta_{m,l} \tag{5.10}$$

and the $\theta_{m,l}$ are as given in equation (5.6). For the general case with M mobile sources, each with I local scatterers, the signal observed at each sensor is then given by

$$x_n(k) = \sum_{m=1}^{M} s_{nm}(k) + v_n(k)$$

$$= \sum_{m=1}^{M} \sum_{l=1}^{I} a_{m,l}(k) exp\left[j(n-1)\phi_{m,l} \right] + v_n(k) \tag{5.11}$$

where $v_n(k)$ is the additive sensor noise. Hence, the observed signal vector, already defined in equation (C.6) for a non-scattering environment, is given by

$$\mathbf{x}(k) = \left[\mathbf{b}(\theta_{1,1}) \cdots \mathbf{b}(\theta_{M,I}) \right] \mathbf{a}(k) + \mathbf{v}(k) \tag{5.12a}$$

where

$$\mathbf{a}(k) = \left[a_{1,1}(k) \cdots a_{M,I}(k) \right]^T \tag{5.12b}$$

is the MIx1 signal-in-space vector and

$$\mathbf{b}(\theta_{m,l}) = \left[1 \; exp(j\phi_{m,l}) \; exp(j2\phi_{m,l}) \cdots exp(j(N-1)\phi_{m,l}) \right]^T \tag{5.12c}$$

is the Nx1 direction vector associated with the ith scatterer of the mth source. The sampled covariance matrix, $\hat{\mathbf{R}}$, can then be generated as in equation (C.8).

Note that the resulting signal envelope received at each element will exhibit the characteristic Rayleigh fading indicative of mobile radio

communications. The validity of this model however has increasingly come into question [3], especially when the received signal is very strong or very weak. Many alternative statistical models have been proposed based on measured data (e.g. the Nakagami distribution and the Weibull distribution [3]), and would appear to provide the best representation of the multipath environment throughout the entire fading signal range. In order for the fading to exhibit Rayleigh behaviour, the following assumptions must be true [3]:

- The scattering waves must be randomly varying in phase and be of near equal power.
- The phases of the scattered waves must be uniformly distributed between 0 and 2π.
- There must be a minimum of five scattering waves.

In the majority of urban and suburban environments, the last two assumptions will probably apply, although for the initial assumption, it is unlikely that a situation will occur when all the scattered components would have nearly equal powers. Also, the presence of a steady direct signal or strong discrete reflection (see section 5.2 later) would affect the nature of the relative phase of the signals. Measured data however does support the Rayleigh model, even if only over a limited range, and so since this study is primarily to investigate the angular spread of the signals received at the base-station, the Rayleigh model for the scattering environment will be sufficient. The effects of shadowing (the long term fading caused by variations in the local terrain) will not be considered at this stage since only a limited number of samples are required to carry out the bearing estimation process. It is generally agreed that this can be accurately represented by a log normal distribution.

Hence, it is now possible to simulate a scattering environment, defined by the number and spread of the scatterers, I and θ_s respectively. If the additive sensor noise is assumed to be a spatially and temporally white random process with zero mean and variance σ^2, and that $E\left[\left|s_m(k)\right|^2\right] = 1$ for each signal source, then the input signal-to-noise ratio for each source as measured at the reference element in the array (i.e. n = 1) can be expressed as

$$SNR = E\left[\left| \sum_{l=1}^{I} a_{m,l}(k) \right|^2\right] / \sigma^2$$

$$= \left| \sum_{l=1}^{I} A_{m,l} exp(\alpha_{m,l}) \right|^2 / \sigma^2 \qquad (5.13)$$

5.1.2 Co-channel Interference

Mobile sources in neighbouring co-channel cells which occupy the same channel as the wanted mobile will produce spurious peaks in the spatial spectrum, giving rise to ambiguities in the DF results. This phenomenon is similar to that caused by hostile jammers in military radar systems. Therefore, in order to generate a realistic model of the mobile communications environment, it is necessary to include the effects of co-channel interference.

Consider a single mobile source (M = 1) with J interfering co-channel sources present. Using equation (5.9), the signal incident at each element in the array will now be given by

$$s_{nm}(k) = \sum_{l=1}^{I} a_{m,l}(k) exp\left[j(n-1)\phi_{m,l}\right] + \sum_{j=1}^{J} a_j(k) exp\left[j(n-1)\phi_j\right] \qquad (5.14)$$

where the interferers are assumed to be point sources from distinct directions θ_j. The complex amplitude a_j of the interferers will be modelled with a Rayleigh envelope and a uniformly distributed phase component. The observed signal vector $\mathbf{x}(k)$ given in equation (5.12) can then be rearranged to include the direction vectors for the co-channel sources, and the resulting sampled covariance matrix generated in the normal way. The input signal-to-interference-plus-noise ratio (SINR) measured at the reference element is given by

$$\text{SINR} = \frac{E\left[\left|\sum_{i=1}^{I} a_{m,i}(k)\right|^2\right]}{\sigma^2 + E\left[\left|\sum_{j=1}^{J} a_j(k)\right|^2\right]} \qquad (5.15)$$

5.1.3 Mutual Coupling

The effect of mutual coupling between antenna elements on the performance of adaptive antenna arrays has been studied in some detail by Gupta and Ksienski [4]. The result with well known adaptive array algorithms, such as the LMS algorithm, is to decrease both the output signal-to-interference-plus-noise ratio (SINR) as well as the speed of adaption of the array. In terms of estimating the angle of arrival of one or more sources of signal energy, mutual coupling also has a very detrimental effect, distorting the received signal vectors and the resulting covariance matrix. All of the DF algorithms discussed in chapter 4 exploit the sampled covariance matrix and so mutual coupling will affect the AOA estimates from each algorithm to a greater or lesser degree (see the results presented in section 5.1.5 below). The effect on the MUSIC algorithm has been studied extensively by Weiss and Friedlander [5] and Yeh *et al* [6][7], the results of computer simulations showing a severe degradation in the estimation performance. Hence, in order to provide a comparison with the other algorithms, a model of the mutual coupling in an antenna array is required, and the approach employed by Gupta [4] was adopted. A linear N element array is considered as a N+1 terminal linear bilateral network responding to an external source and the resulting output voltage (defined as a vector) is given by

$$\mathbf{v} = \mathbf{Z}_o^{-1}\mathbf{v}_o \qquad (5.16)$$

where $\mathbf{Z}_o$ is the normalised impedance matrix and $\mathbf{v}_o$ is the vector of open circuit voltages across the antenna terminals. A full derivation for this equation is included in Appendix F. $\mathbf{Z}_o^{-1}$ can be considered as a transformation matrix, transforming the open circuit antenna voltages to the actual output voltages. In most of the papers analysing and comparing the performance of various DF algorithms, the degree of coupling is assumed to be negligible and

so is not included in the simulations. Thus $\mathbf{Z}_0^{-1}$ would be equivalent to the identity matrix, corresponding to the situation when the elements in the array are spaced sufficiently far apart.

Using the basic signal model developed in Appendix C, the open circuit signal voltages at the output of an array are given by the received signal vector **s** in equation (C.5). In order to include the effects of mutual coupling, the observed signal vector **x** given by equation (C.6) can be modified by substituting in equation (5.16) as follows

$$\mathbf{x}(k) = \mathbf{Z}_0^{-1}\mathbf{B}\mathbf{a}(k) + \mathbf{v}(k) \tag{5.17}$$

The output of each element is then the sum of all the incident plane waves plus the contribution from neighbouring elements. Each of the direction vectors $\mathbf{b}(\theta_m)$ in **B** are distorted by $\mathbf{Z}_0^{-1}$, hence by employing the ideal steering vector **u** (equation (4.6)) to estimate the spatial spectrum, errors in the AOA estimate will occur. Yeh *et al* demonstrated that the effects of mutual coupling could be removed by employing a modified steering vector $\mathbf{Z}_0^{-1}\mathbf{u}$. This however assumes that the mutual coupling between the elements is known already, e.g. from the measurement of the array manifold (as discussed in section 4.3.1) or estimated on-line. This latter approach is discussed in the following section.

5.1.4 Receiver Channel Mismatch

The model developed above includes only the effects of mutual coupling, and therefore no longer assumes perfect reception of the signal sources by an ideal antenna array. The remaining DF receiver behind each antenna element has not been taken into account though, and the model must be extended to consider any phase and amplitude mismatch that may occur between the receiver channels, as well as any phase and gain uncertainties of the antenna elements. Taking the expression for the signal received at each element in the array (equation (C.4)), and incorporating the relative gain, γ_n, and phase, ψ_n, associated with each element gives

$$x_n(k) = \sum_{m=1}^{M} \gamma_n exp\left[j\psi_n\right] \cdot a_m exp\left[j(n-1)\phi_m\right] + v_n(k) \tag{5.18}$$

The observed signal vector $\mathbf{x}$ then becomes

$$\mathbf{x}(k) = \Gamma \mathbf{B} \mathbf{a}(k) + \mathbf{v}(k) \tag{5.19}$$

where

$$\Gamma = \mathrm{diag}\left\{ \gamma_1 exp(j\psi_1) \quad \gamma_2 exp(j\psi_2) \quad \cdots \quad \gamma_N exp(j\psi_N) \right\} \tag{5.20}$$

Mutual coupling effects can then also be included to give

$$\mathbf{x}(k) = \mathbf{Z}_0^{-1} \Gamma \mathbf{B} \mathbf{a}(k) + \mathbf{v}(k) \tag{5.21}$$

The coupling matrix $\mathbf{Z}_0^{-1}$ is very sensitive to environmental factors and consequently will vary with time. Thus it would be desirable to estimate $\mathbf{Z}_0^{-1}$ and Γ on line, and Weiss and Friedlander [5] have proposed an iterative procedure for achieving this. Having estimated $\mathbf{Z}_0^{-1}$ and Γ, the ideal steering vector $\mathbf{u}$ (equation (4.6)) used in all of the DF algorithms can then be modified as follows

$$\mathbf{u}' = \mathbf{Z}_0^{-1} \Gamma \mathbf{u} \tag{5.22}$$

This approach looks like providing a viable alternative to measuring the array manifold and merits further investigation.

5.1.5 Performance of DF Algorithms in an Urban Environment

In this section the performance of the DF techniques discussed in chapter 4 are assessed in a typical scattering urban environment. The test scenario defined in table 5.1 forms the basis for comparison, as well as enabling a study to be carried out on the effects of varying the different parameters. The number of scatterers was chosen initially as six since this is the minimum requirement for a typical urban profile as defined by GSM [8].

Antenna Array	• No. of elements, • Element spacing, • Mutual coupling, • Channel mismatch,	N=4 d=0.5λ —— ——
Signal Environment	• No. of sources, • Source AOA, • Input SNR, • Line of sight path, • No. of scatterers, • Angular spread, • No. of co-channels,	M=1 $\theta_1=0^\circ$ SNR=20dB None I=6 $\theta_s=10^\circ$ J=0
Signal Processing	• No. of snapshots, • Spatial smoothing,	K=50 ——

Table 5.1: Reference urban scenario.

The resulting spatial spectra with the above scenario for each of the DF algorithms introduced in chapter 4 are illustrated in figure 5.3, and table 5.2 summarises the results of a peak search. The angular resolution is to within one degree, and the spectra are all relative to their peak value, the location of which determines the estimated AOA of the source, θ_{est}. Knowledge of the number of sources present is required by the eigenstructure methods (MUSIC, JoDeG and KuTu), and this was provided by the application of the information theoretic criteria, an approach adopted by Wax and Kailath [9]. In essence, the number of signals is determined as the value which minimises a chosen criteria, hence avoiding the need for subjective decisions. In section 4.1.4, the choice was based on inspection of the eigenvalues of the sampled covariance matrix, and determining the minimum values which are associated with the noise. In practice they are never all equal to the noise variance (as given by equation (4.26)) and so the choice is based on subjective judgment and the setting of threshold levels. Applying the information theoretic criteria overcomes this uncertainty and throughout the simulation, the choice of M, the number of signals present, was based on the results of applying the MDL criteria given in the paper of Wax and Kailath [9].

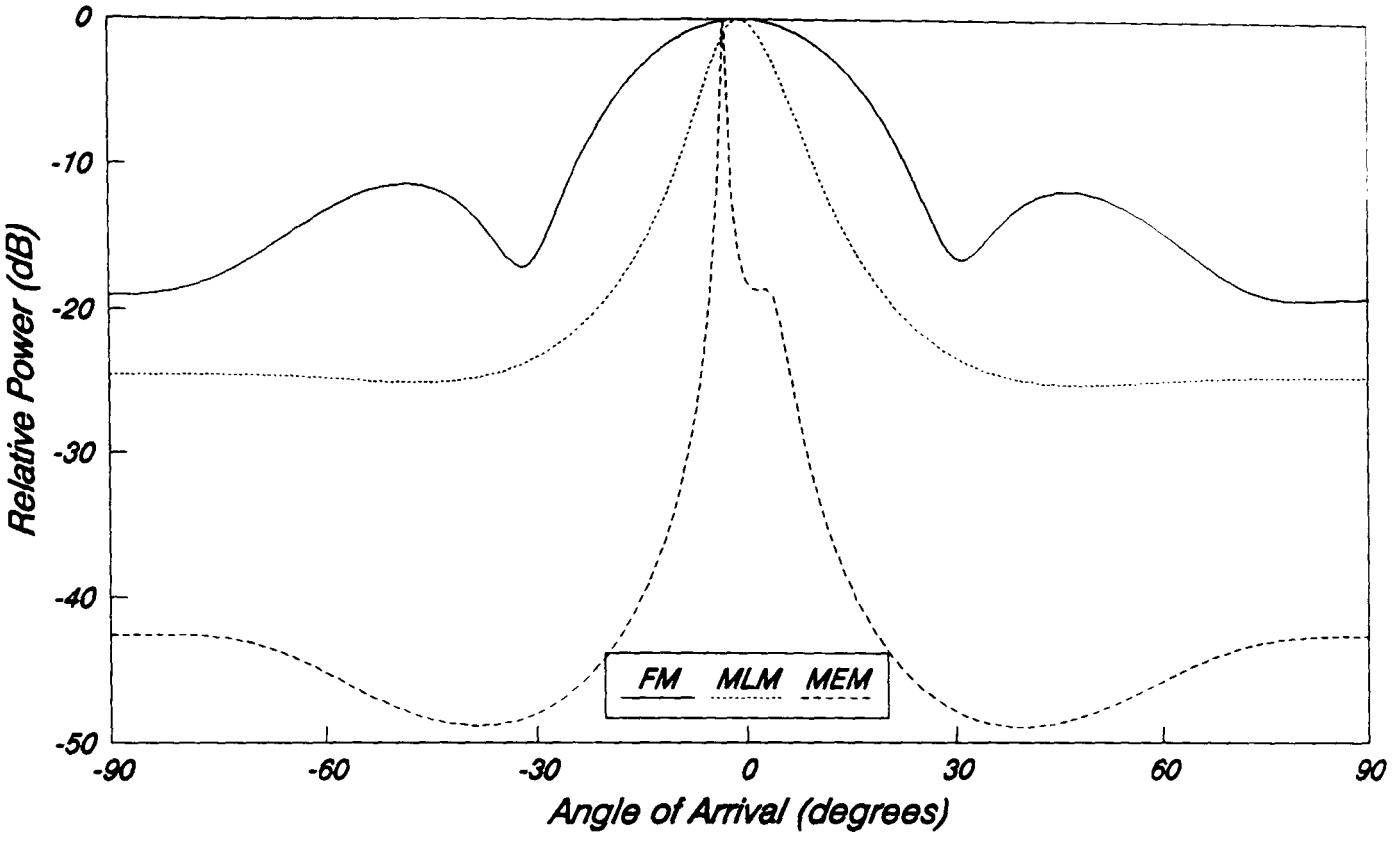

Figure 5.3: Resulting spatial spectra with the reference urban scenario: (a) FM, MLM, and MEM; (b) MUSIC, JoDeG and KuTu.

Algorithm	θ_{est}	Other peaks
FM	0°	——
MLM	-1°	——
MEM	-3°	——
MUSIC	-3°	$+4^{\circ}$ (-0.4dB)*
JoDeG	-3°	$+4^{\circ}$ (-0.2dB)
KuTu	-3°	$+4^{\circ}$ (-0.7dB)

* Level below main peak.

Table 5.2: Results of peak search on spectrums from reference urban scenario.

Figure 5.3a shows the response of the Fourier Method (FM), the Maximum-likelihood Method (MLM) and the Maximum Entropy Method (MEM), clearly illustrating the attributes discussed in section 4.2. The FM approach has the characteristic wide main beam and high sidelobes, and although there is a smearing of detail, the peak is correctly located at a bearing of 0°. The MLM approach produces a more sharply defined peak at -1°, although fails to provide any more information on the scattering environment. The MEM approach gives a very sharply defined peak, although it is at the very limit of its resolution capabilities since it is unable to resolve more than one source. Figure 5.3b shows the results of applying the eigenstructure techniques, and clearly demonstrates their improved resolution capabilities, with all three having peaks at -3° and $+4^{\circ}$ (the MDL criteria indicating that two sources are present). In fact the responses are almost identical except for the increased ripple in the sidelobes of the KuTu response, a characteristic mentioned earlier.

A: The Scattering Environment

In order to assess the validity of the urban scattering model, the first step is to assess the sensitivity of the results to the number of scatterers I and their angular spread θ_s. Figure 5.4 shows the resulting spatial spectra for different numbers of scatterers when the MUSIC algorithm is employed, and

the results of a peak search are included in table 5.3. This illustrates clearly that increasing the number of scatterers above six has little effect, whereas with less than six the effect is more pronounced, with one of the scatterers dominating.

The results of varying the spread of the scatterers are shown in figure 5.5. Again the MUSIC algorithm was employed, and the results of a peak search are given in table 5.4. With a spread of 2° the source becomes indistinguishable from a point source at a bearing of 0°, although the shoulder in the spectrum suggests that this is not so. In fact the MDL criteria still indicates that two sources are present. Increasing the spread to 10° and 30° produces only two strong peaks in the spectrum, even though there are three degrees of freedom available. Also note that the location of the peaks is less than the extremities of the scattering sources. This is because the SNR of each of the scattered components is too low to enable them to be resolved individually, their combined effect resulting in only the two peaks.

I	θ_{est}	Other peaks
3	$+3^\circ$	-4° (-2.7dB)
6	-3°	$+4^\circ$ (-0.4dB)
30	-3°	$+4^\circ$ (0 dB)

Table 5.3: Results of peak search for the MUSIC algorithm with varying numbers of scatterers.

θ_s	θ_{est}	Other peaks
2°	0°	——
10°	-3°	$+4^\circ$ (-0.4dB)
30°	-10°	$+10^\circ$ (-4.0dB)

Table 5.4: Results of peak search for the MUSIC algorithm with varying spread of scatterers.

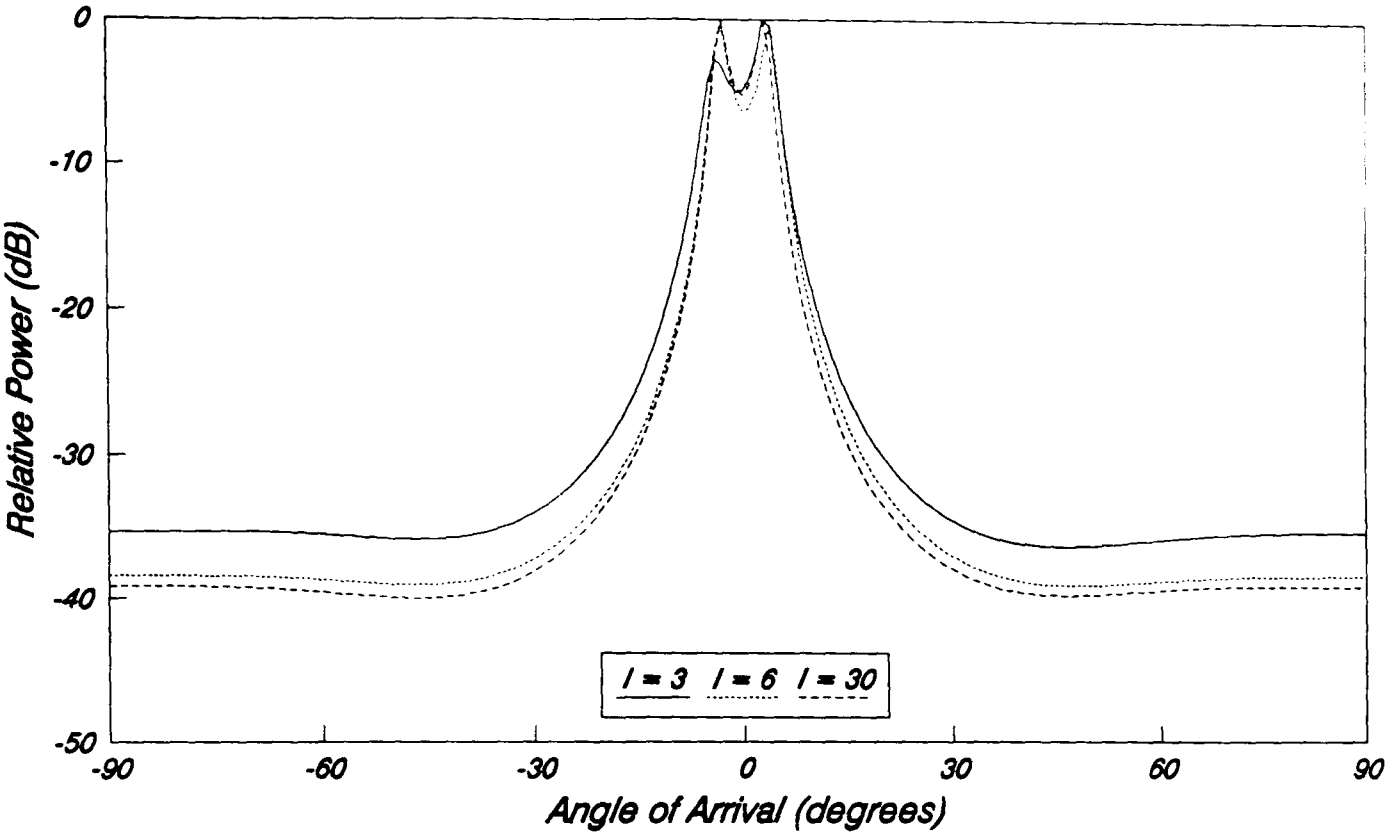

Figure 5.4: Resulting spatial spectra for the MUSIC algorithm with varying numbers of scatterers.

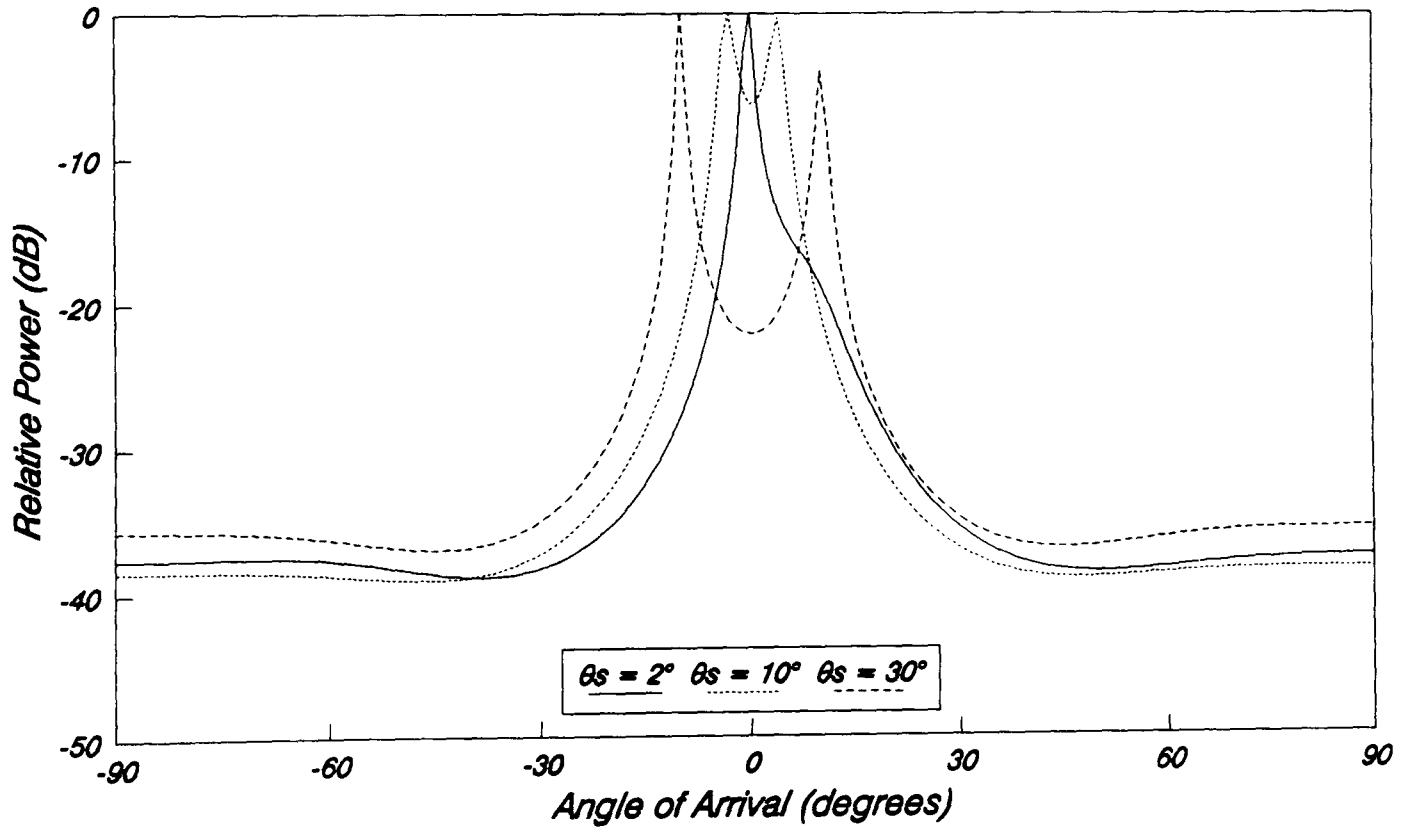

Figure 5.5: Resulting spatial spectra for the MUSIC algorithm with a varying spread of scatterers.

B: Input SNR

The input SNR is defined in equation (5.13) and is derived from the combination of all the scattered waves from the wanted source incident at the reference element of the array. The resulting spectra for different SNR's with the MUSIC algorithm are given in figure 5.6, and the results of a peak search are presented in table 5.5. At values greater than 20 dB, the only noticeable effect is a lower sidelobe level, and an increased distinction between the two peaks. With a SNR of 10 dB, the MDL criteria still indicates that two sources are present, even though only a single peak is generated. Notice however the shoulder in the spectrum. At a level of 5 dB, only a single source is detected by the MDL criteria, as is apparent from the lone peak in the spectrum.

SNR	θ_{est}	Other peaks
20 dB	-3°	$+4^{\circ}$ (-0.4dB)
10 dB	-3°	$+5^{\circ}$ (-4.4dB)
5 dB	-1°	——

Table 5.5: Results of peak search for the MUSIC algorithm with different SNR's.

The performance of the other algorithms at a low SNR is also very enlightening, especially with the eigenstructure methods. Figure 5.7 shows the resulting spatial spectra for these methods at a SNR of 0 dB and clearly shows the superior performance of the KuTu algorithm over MUSIC and JoDeG. The remaining three algorithms all successfully indicate the presence of the source but with much higher sidelobes. The superior performance of the KuTu algorithm at low SNR's is also made apparent when required to resolve two closely spaced sources located at $+3^{\circ}$ and -3° off the array broadside. With no local scatterers present and each source with a SNR of 10 dB, the resulting spectra for the KuTu and MUSIC algorithms are shown in figure 5.8. The KuTu algorithm correctly indicates both sources (peaks located at -2° and $+4^{\circ}$) while MUSIC can only indicate a single source (located at $+1^{\circ}$) even though the MDL criteria correctly indicates that two are present.

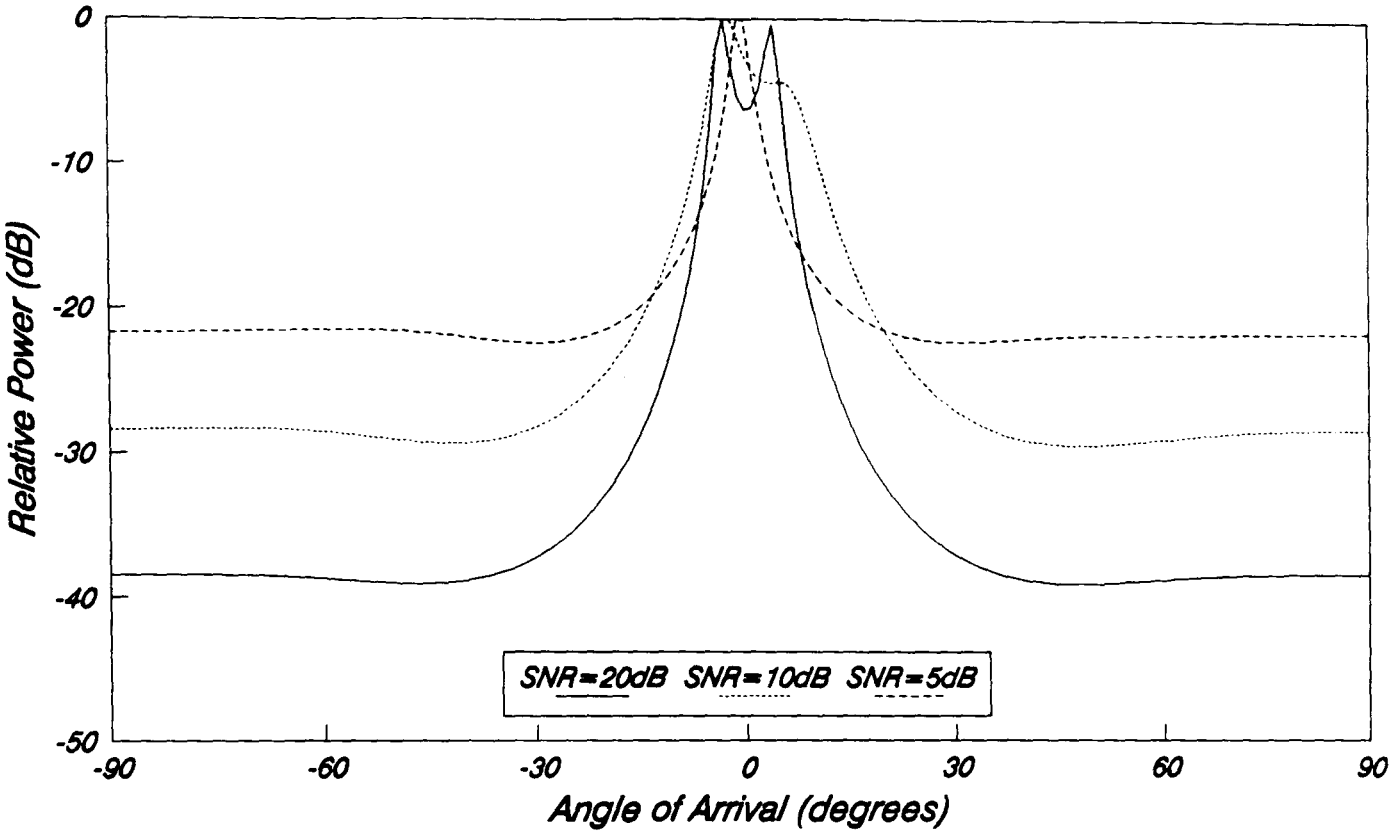

Figure 5.6: Resulting spatial spectra for the MUSIC algorithm with different SNR's.

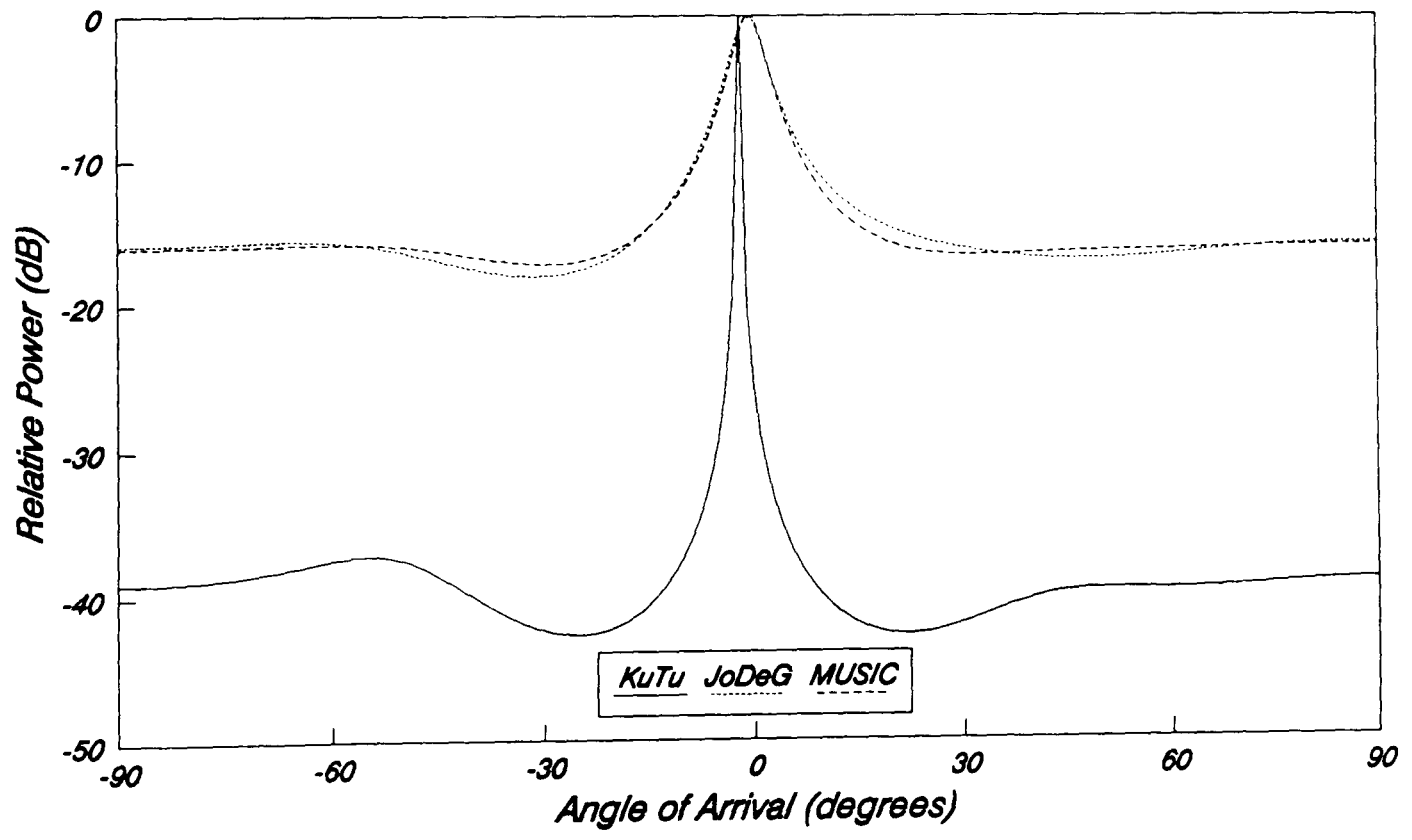

Figure 5.7: Resulting spatial spectra for the KuTu, JoDeG and MUSIC algorithms when the SNR is 0dB.

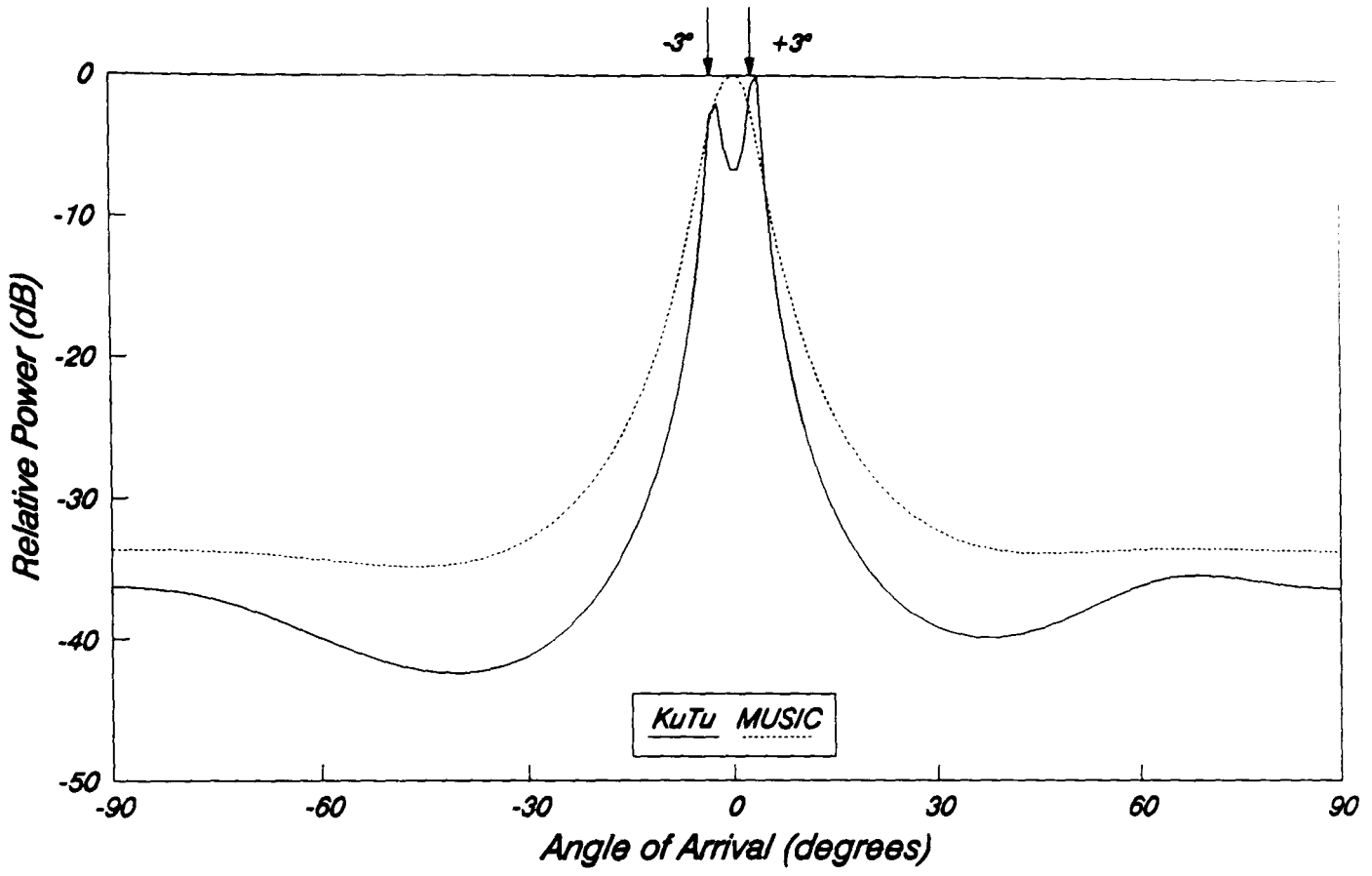

Figure 5.8: Resulting spatial spectra for the KuTu and MUSIC algorithms with 2 signal sources of SNR=10dB.

C: Temporal Averaging

The number of snapshots required to obtain a stable estimate of the source direction is a very important factor in the realisation of practical DF base-station antenna since the larger the number of snapshots required, the greater the processing time for each DF scan. The results of applying the MUSIC algorithm for different numbers of snapshots are shown in figure 5.9, and the peak locations are given in table 5.6. When $K \geq 50$ there is very little difference in the resulting spectrum, although as K is reduced, the number of peaks that can be resolved is reduced to only one at K = 10. None of the other algorithms can provide any further information on the scattering environment at such low numbers of snapshots. The input SNR is plotted in figure 5.10 over a 100 snapshot frame and illustrates very clearly the characteristic fading experienced with the mobile radio communications channel.

K	θ_{est}	Other peaks
50	-3°	$+4^{\circ}$ (-0.4dB)
20	$+2^{\circ}$	-3° (-0.5dB)
10	$+2^{\circ}$	——

Table 5.6: Results of peak search for the MUSIC algorithm with different numbers of snapshots.

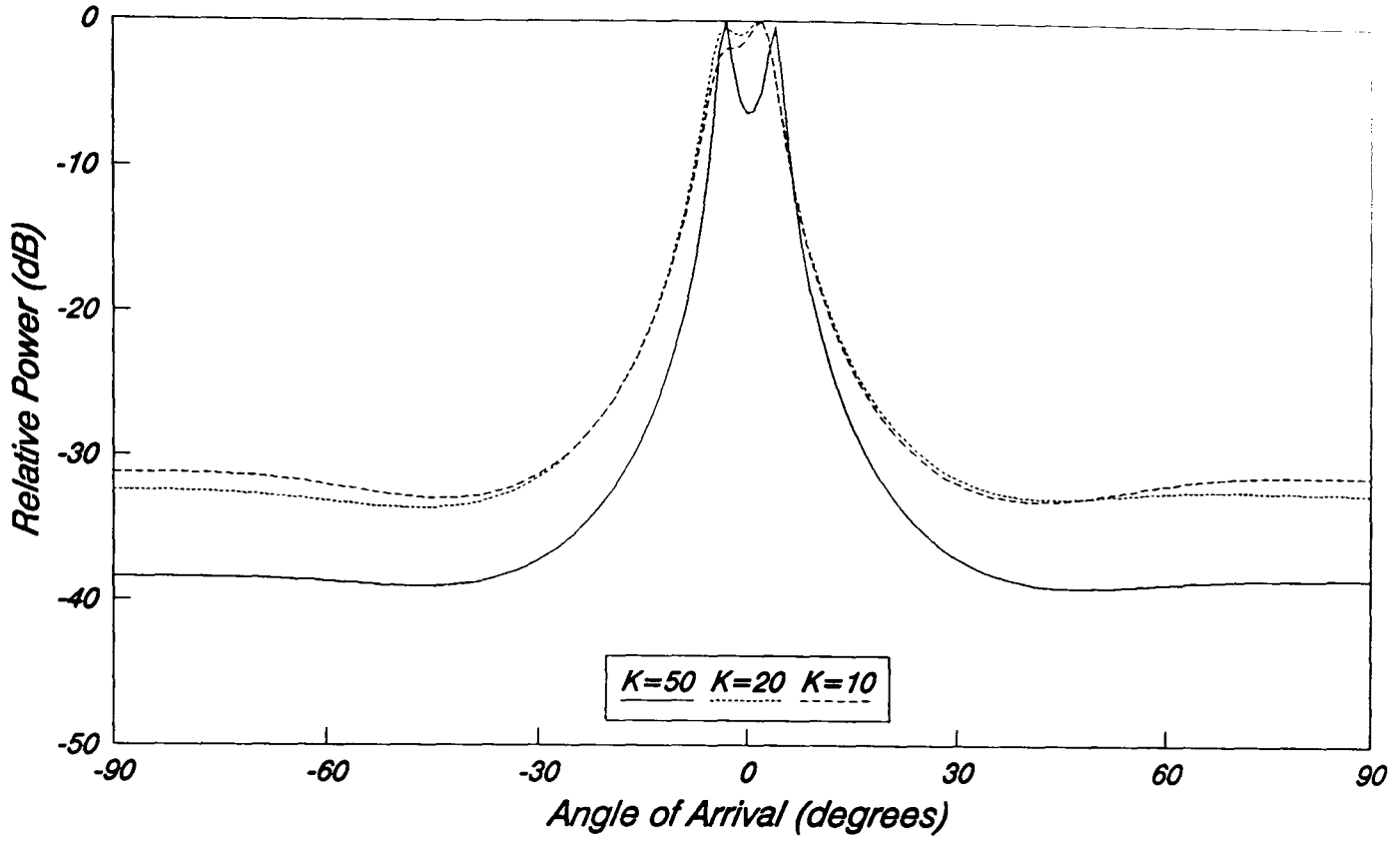

Figure 5.9: Resulting spatial spectra for the MUSIC algorithm with different numbers of snapshots K.

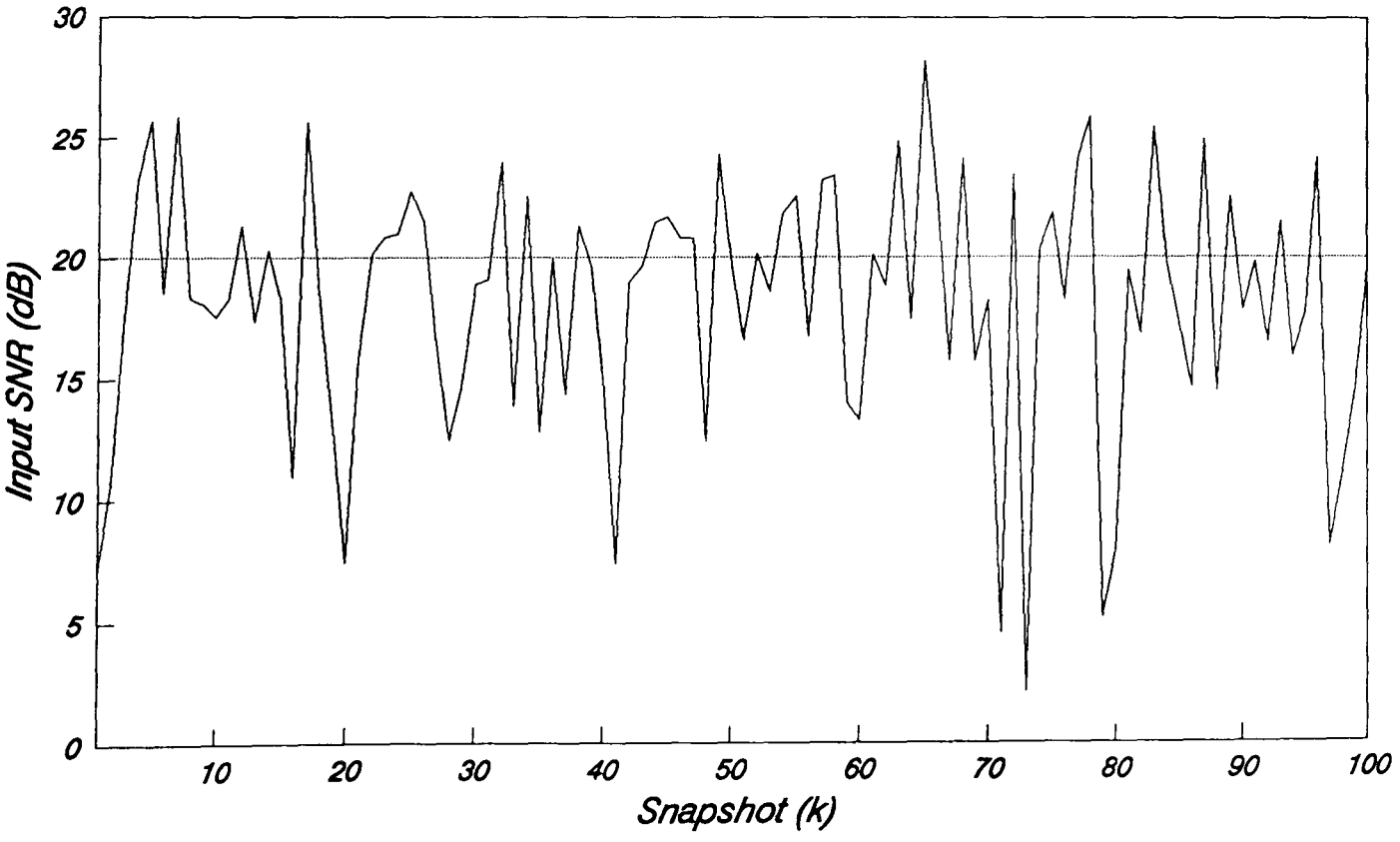

Figure 5.10: Variation of the input SNR.

D: Mutual Coupling

Consider now the effect that mutual coupling has on the ability of the DF algorithms to successfully locate a signal source. In Appendix F, the mutual impedance matrix for an antenna array was formulated and, for the purpose of this simulation, was calculated for half wavelength centre-fed dipoles [10]. The load impedance was assumed to be the complex conjugate of the self impedance of the antenna elements and the results of applying the MUSIC algorithm with and without mutual coupling are shown in figure 5.11. Notice the smearing of detail and the presence of only a single peak (located at 0°) when mutual coupling is included, even though the MDL criteria indicates that two sources are present. Figure 5.12 shows the response of the KuTu and JoDeG algorithms when mutual coupling is present, further demonstrating the extremely detrimental effect that mutual coupling has on the DF performance of the algorithms. The JoDeG spectrum is very similar to that produced by MUSIC, with a peak at 0°. However, the effect of mutual coupling on the KuTu algorithm is very noticeable, with increased sidelobe ripple and a peak located at -5°. The response of the FM and MLM algorithms shows very little difference from the responses shown in figure 5.3, although the MEM approach produces a response similar to that for the KuTu algorithm, with increased ripple and a peak located at -6°.

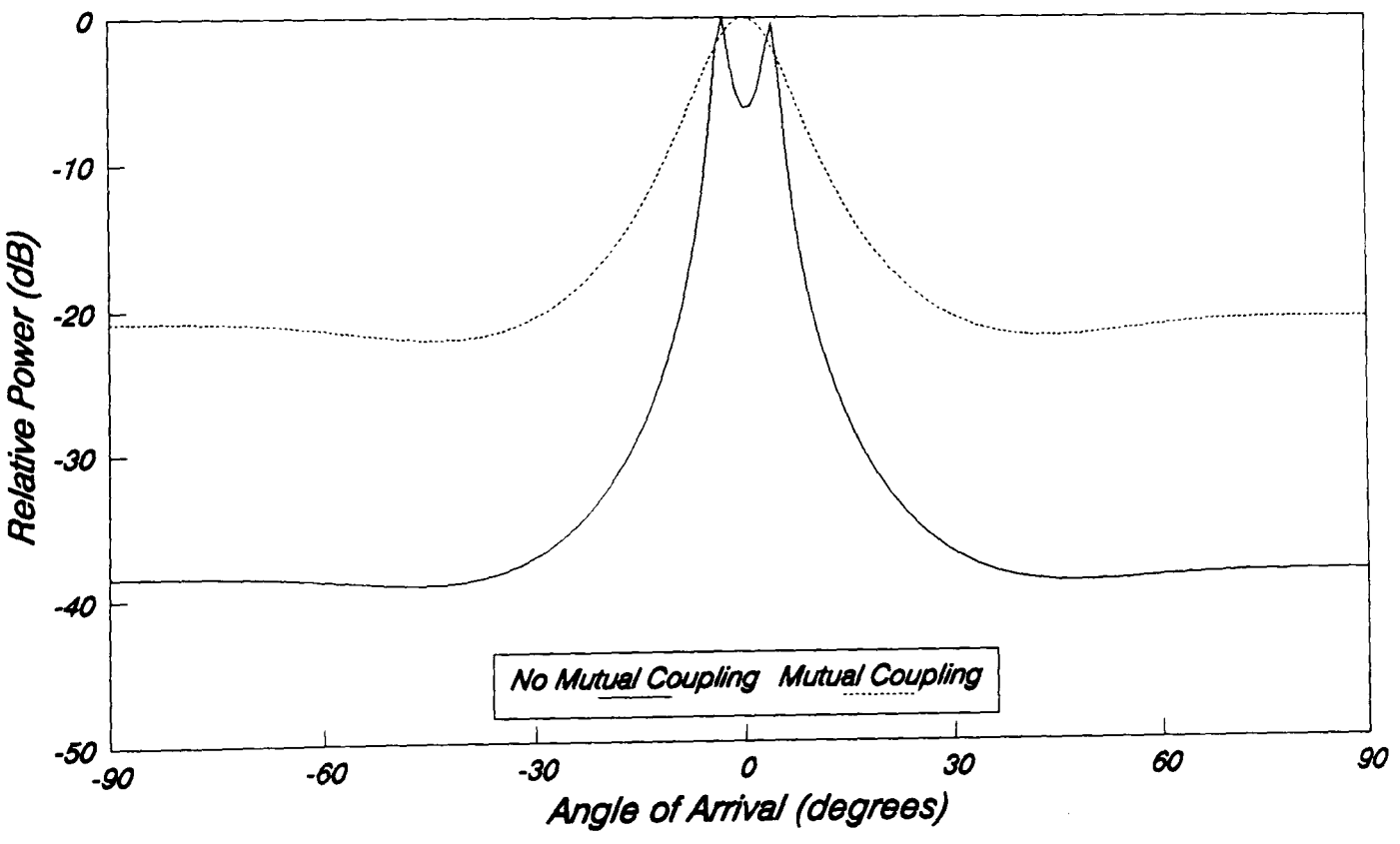

Figure 5.11: Resulting spatial spectra for the MUSIC algorithm with and without mutual coupling.

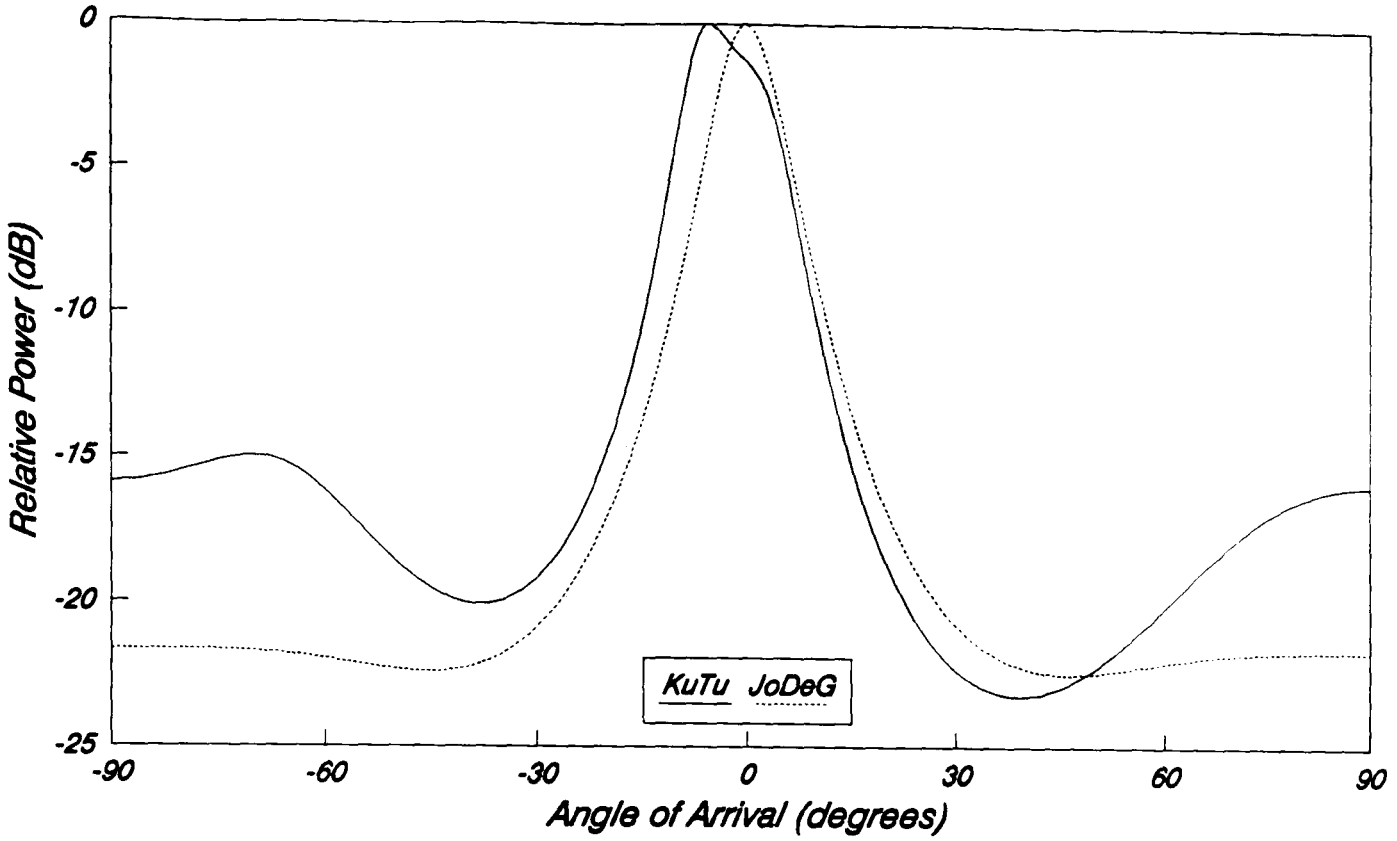

Figure 5.12: Resulting spatial spectra for the KuTu and JoDeG algorithms with mutual coupling.

E: Channel Mismatch

In order to study the effects of gain and phase uncertainties of the antenna elements, as well as the complete receiver chain, the approach adopted by Weiss and Friedlander has been employed [5]. This involves generating values for the gain γ_n and phase ψ_n of each element, and then perturbing them from the ideal by a random variable with a specified variance. The two equations to be used are given by

$$\gamma_n = \left[(\alpha_n - 0.5)\sigma_\gamma \sqrt{12} + 1 \right] \qquad n=1,\cdots,N \qquad (5.23)$$

$$\psi_n = \left[(\beta_n - 0.5)\sigma_\psi \sqrt{12} \right] \qquad n=1,\cdots,N \qquad (5.24)$$

where α_n and β_n are uniformly distributed random numbers between zero and one. Hence, γ_n and ψ_n will be uniformly distributed about one and zero respectively, with a variance of σ_γ^2 and σ_ψ^2.

The results of applying the MUSIC algorithm with different amplitude standard deviations are shown in figure 5.13, clearly demonstrating the

severe effects that this type of mismatch can have on the AOA estimate. The results of applying the KuTu and JoDeG algorithms when $\sigma_\gamma = 0.1$ are illustrated in figure 5.14. The JoDeG response is almost identical to that produced by MUSIC, with the smearing of detail causing errors in the AOA estimate. However, the KuTu algorithm still produces two sharp peaks, and so it would appear that this algorithm is less sensitive to gain mismatches. The MEM algorithm also performs quite well in terms of resolving two peaks but at the expense of increased ripple in the sidelobes. Figure 5.15 shows the results of varying the phase standard deviation, σ_ψ, with the MUSIC algorithm, again clearly illustrating the adverse effects this has on the AOA estimation process. The results also indicate that the KuTu algorithm is less sensitive to phase uncertainties than MUSIC or JoDeG.

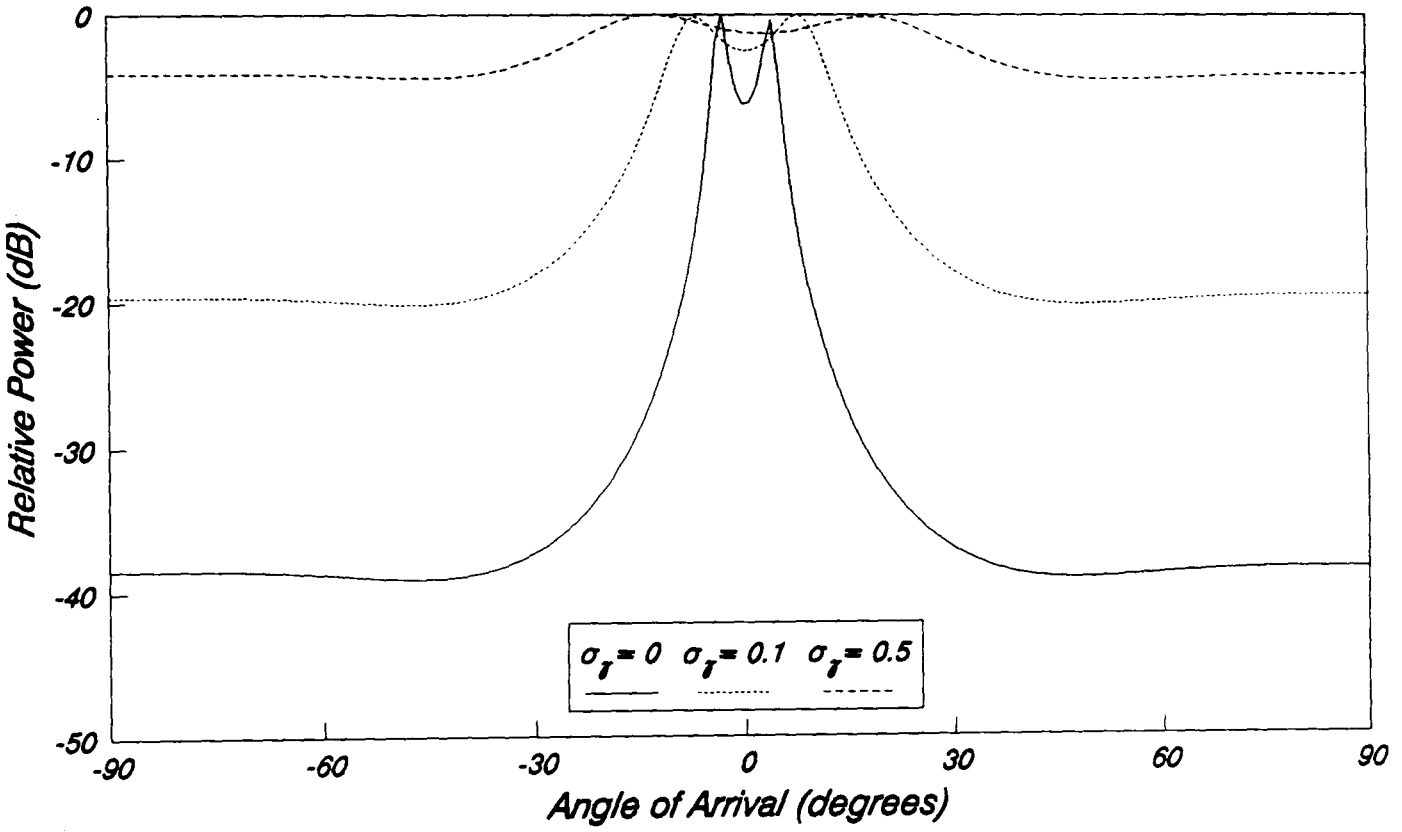

Figure 5.13: Resulting spatial spectra for the MUSIC algorithm with amplitude uncertainty.

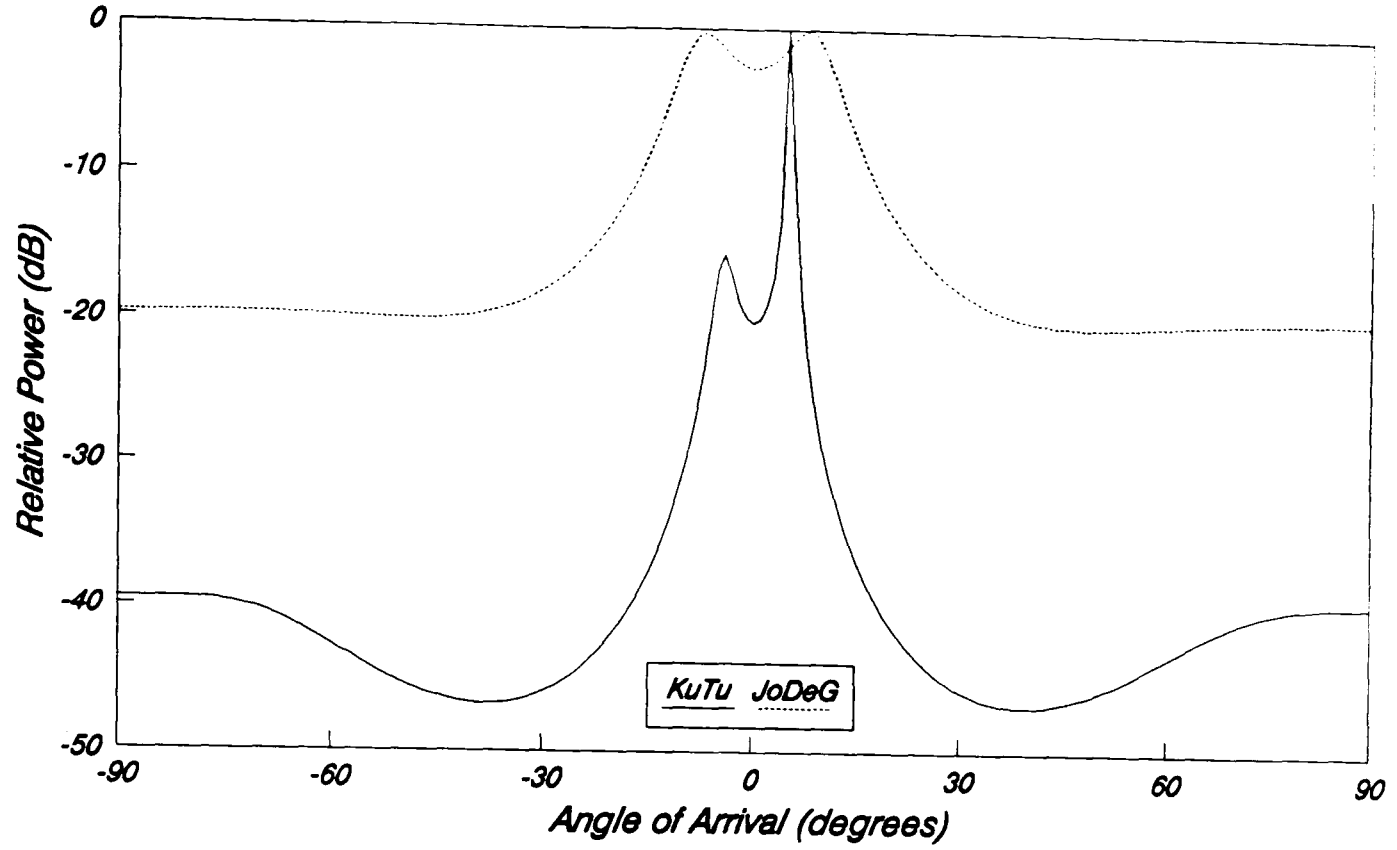

Figure 5.14: Resulting spatial spectra for the KuTu and JoDeG algorithms with $\sigma_\gamma = 0.1$.

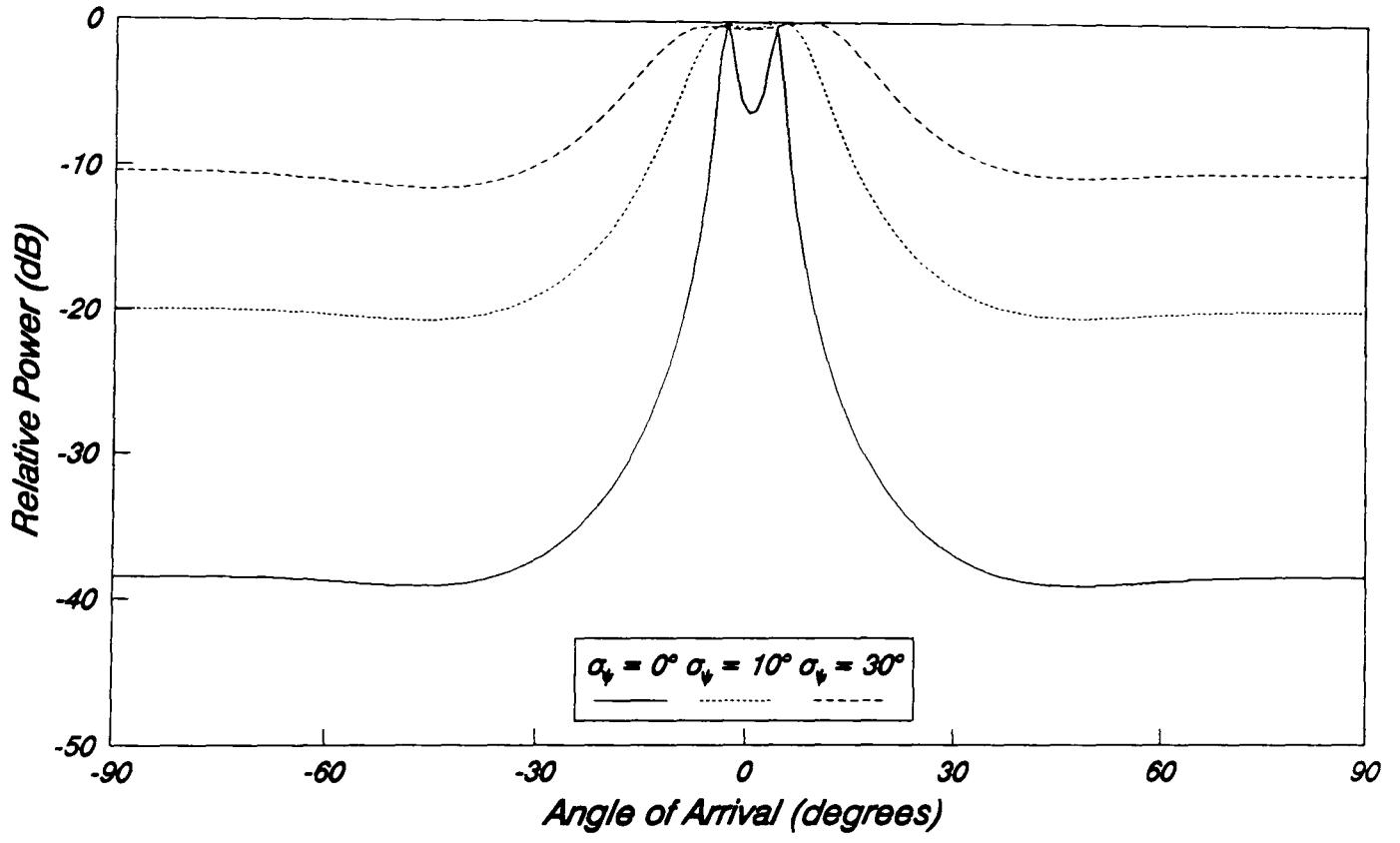

Figure 5.15: Resulting spatial spectra for the MUSIC algorithm with phase uncertainty.

In section 6.2 the results of the manifold measurement of an experimental DF receiver are presented and the effects of mutual coupling and receiver mismatches are considered in more detail. The result of measuring the array manifold is to generate the modified steering vector given in equation (5.22), and thus remove the effects of an imperfect DF receiver. Direct application of equation (5.22) when mutual coupling and mismatches are simulated does reproduce the spectra of figure 5.3, although the MEM and KuTu algorithms do have a tendency to produce a spurious peak as shown in figure 5.16. Here mutual coupling has been included, as well as both amplitude and phase uncertainties defined by $\sigma_\gamma = 0.1$ and $\sigma_\psi = 10^\circ$.

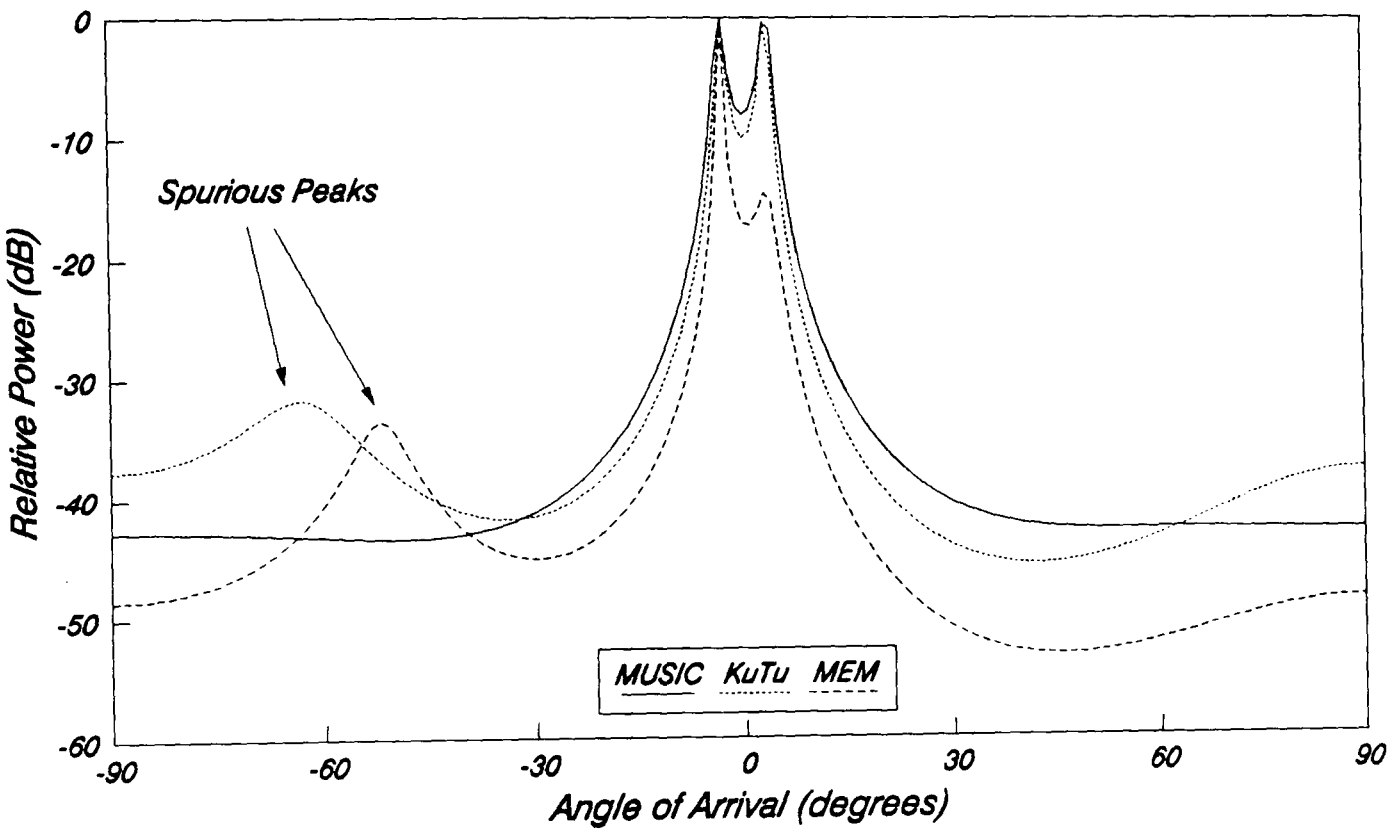

Figure 5.16: Resulting spatial spectra for the MUSIC, KuTu and MEM algorithms when the modified steering vector is employed.

F: Co-channel Interferers

Consider now the presence of a single interfering source at +30° off the array broadside with the reference urban scenario outlined in table 5.1. The results of applying the MUSIC algorithm at different SINR (defined in equation (5.15)) are shown in figure 5.17, and the locations of the peaks are included in table 5.7. Note the gradual emergence of the extra peak due to the co-channel interferer (given by θ_{ccl} in table 5.7) as the SINR reduces. The JoDeG and KuTu algorithms produce very similar results and the responses of the other three are given in figure 5.18 with, as expected, only the MEM method having sufficient resolution capabilities to clearly indicate the presence of the co-channel source.

SINR	θ_{est}	θ_{ccl}	Other peaks
18 dB	+5°	——	-1° (-9.2dB)
15 dB	+5°	+27° (-25 dB)	-1° (-2.4dB)
10 dB	-1°	+28° (-16 dB)	+4° (-0.5dB)

Table 5.7: Results of peak search for the MUSIC algorithm with one co-channel source.

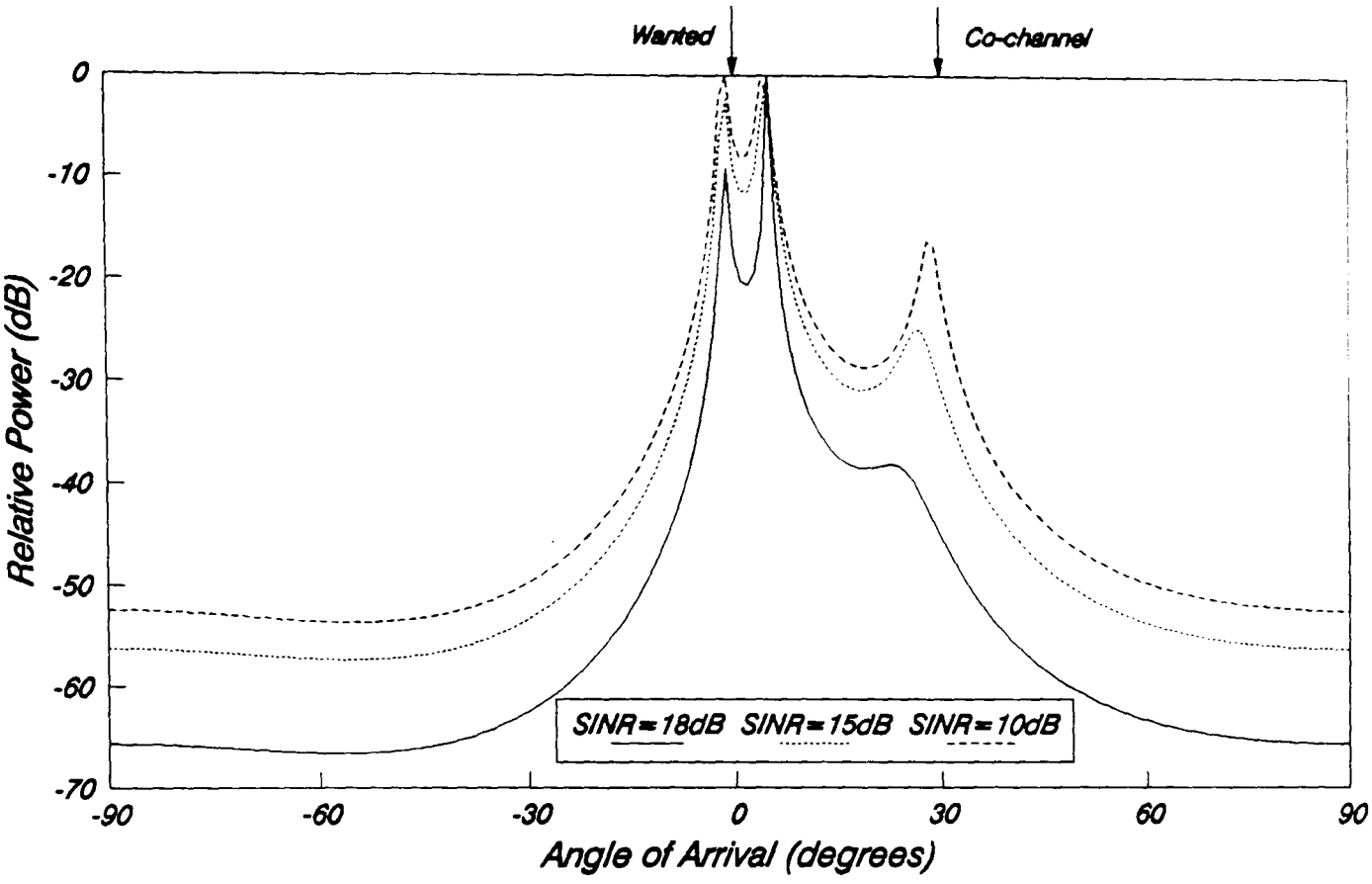

Figure 5.17: Resulting spatial spectra for the MUSIC algorithm with a co-channel source at +30°.

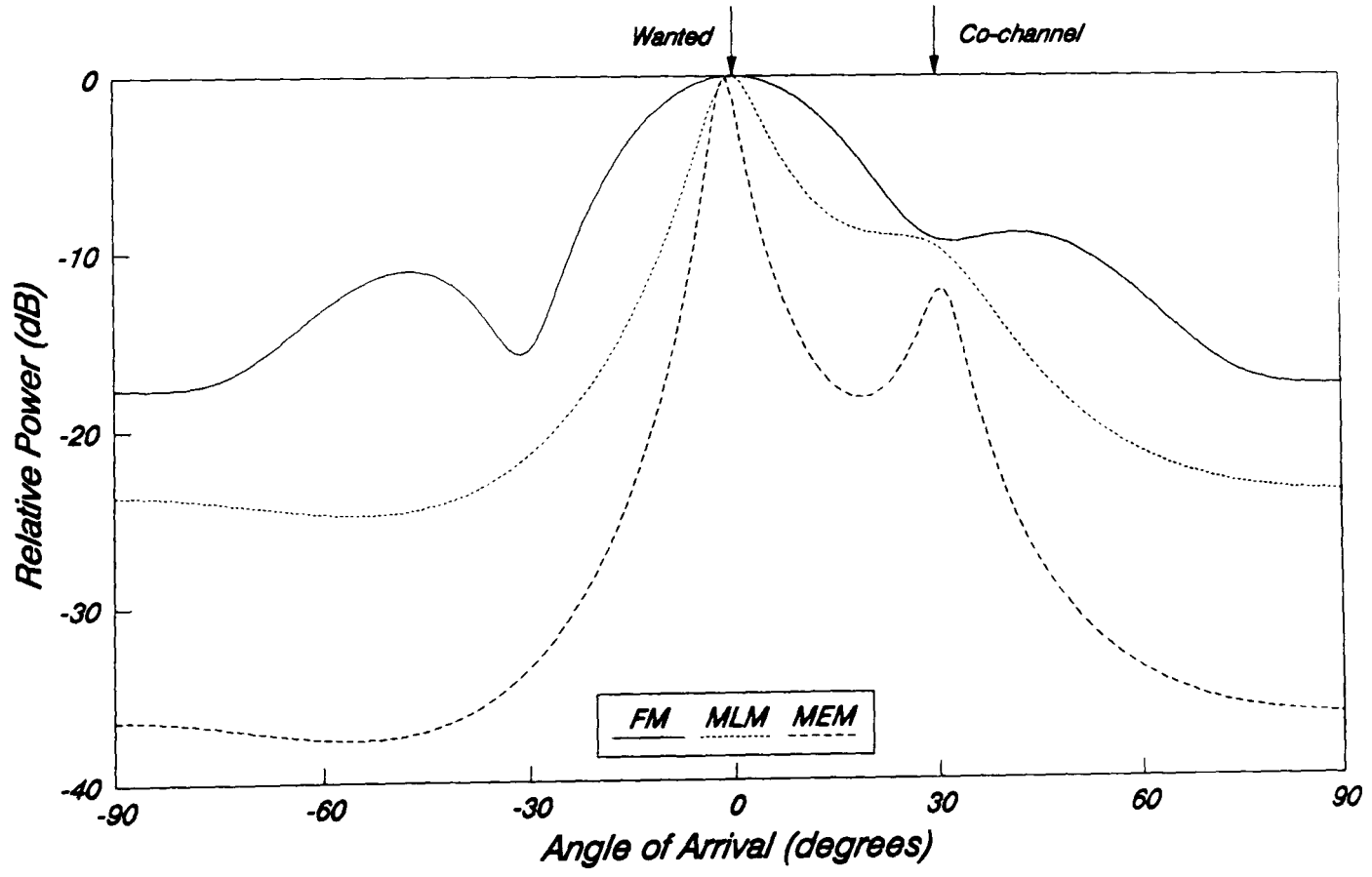

Figure 5.18: Resulting spatial spectra for the FM, MLM and and MEM algorithms with a SINR of 10dB.

One foreseeable problem is if the total number of sources exceeds the available array degrees of freedom, i.e. M > (N-1). Even though there are a large number of scattered waves incident onto the array, the combined effect is to produce one or two peaks as shown in figure 5.3. The presence of only a single co-channel source presents the array with no problems, and even with two co-channel interferers at a modest SINR (10 dB), three peaks occur in the MUSIC spectrum, correctly indicating the presence of all three sources. If an extra co-channel source is now introduced (⇒ J = 3), the array degrees of freedom will be exceeded, possibly causing ambiguities in the resulting spectrum. This scenario was considered with a SINR of 10 dB and the results for the MUSIC, MLM and FM algorithms are shown in figure 5.19. Note that the combined effect of the scattered waves dominates, and only a single peak is produced (co-channel sources located at -80°, -30° and +30°). The KuTu and MEM algorithms also produce a single peak but there is an excessive amount of ripple in the sidelobe region, possibly leading to an ambiguous estimate. Note that the MDL criteria indicates the presence of only two sources for this scenario.

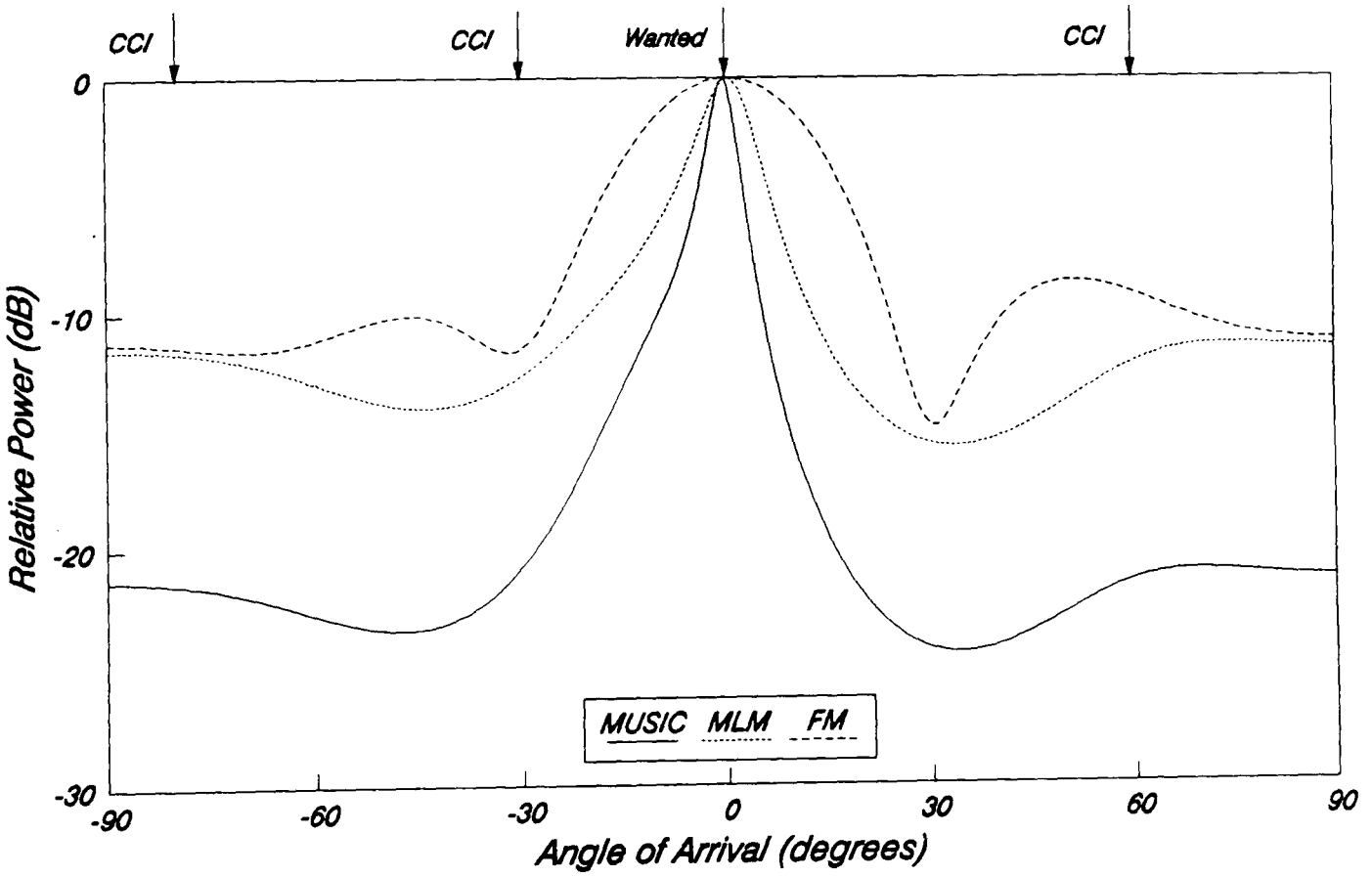

Figure 5.19: Resulting spatial spectra with three co-channel sources (SINR=10dB)

5.2 SUBURBAN/RURAL COMMUNICATIONS

5.2.1 Discrete Multipath Environment

A typical suburban environment would be in a small town or the out-lying districts of a city with scattered houses, small buildings and trees in the immediate vicinity of the mobile as depicted in figure 5.1b. Hence, as well as a direct path towards the base-station being more likely to occur, there will be discrete reflections from distant buildings in addition to the scattered reflections from nearby scatterers. In order to simulate this behaviour, the model developed above for an urban environment can be simply extended to include a direct line of sight component and discrete multipath reflections from more diverse directions.

If there are H discrete reflections associated with each mobile source, then the signal received at each element in the array for a single source (M = 1) is given by

$$s_{nm}(k) = \sum_{i=0}^{I} a_{m,i}(k) exp\left[j(n-1)\phi_{m,i}\right] + \sum_{h=1}^{H} a_{h}(k) exp\left[j(n-1)\phi_{h}\right] \qquad (5.25)$$

where the discrete reflections are from directions θ_h and the line of sight signal is given by i = 0. For the purpose of this simulation, the magnitude of both the line of sight component and the multipath signal will be constant, with the multipath signal power received at the base-station defined relative to the total wanted signal power (i.e. the combination of the line of sight and the scattered components). The multipath signals will also be completely coherent with the direct signal, hence the phase of each will be identical at each sampling instant. The observed signal vector given in equation (5.12) can then be rearranged to include the direction vectors for the discrete multipath reflections, and the resulting sampled covariance matrix generated in the same way.

The problem of coherent multipath reflections causing ambiguous AOA estimates was briefly mentioned in section 4.3, as well as introducing a method of overcoming it. The technique is called *spatial smoothing* and employs spatial averaging to decorrelate the signals. Many authors have studied the benefits of such a scheme [11][12][13[14] and a full description is included in Appendix G. The published results from computer simulations

clearly demonstrate that spatial smoothing enables coherent signals to be resolved successfully, although this is at the expense of a reduction in the array degrees of freedom (see Appendix G). The scattering scenario discussed in section 5.1.1 for the urban environment is an example of a special type of multipath phenomenon since the reflections introduce some sort of random perturbation onto the signal. Thus, even though the array covariance matrix may still be non-diagonal, it will be non-singular, enabling the sources to be potentially resolved. The presence of discrete multipath reflections however, which are highly correlated with the wanted signal, will confuse the AOA estimation process. Hence the spatial smoothing technique will be employed to investigate the ability to resolve coherent signal sources in a suburban environment.

In a rural environment there will be fewer obstacles like trees or buildings in the propagation path, with open farm land and fields predominating as depicted in figure 5.1c. Hence, signal reception at the base-station antenna will primarily be from line of sight propagation, with diffraction of the signal energy in more hilly terrains. The task of the AOA process is then greatly simplified, although the presence of hills may well introduce coherent reflections, causing some ambiguities which could be removed by employing spatial smoothing techniques.

5.2.2 Performance of DF Algorithms in a Suburban/Rural Environment

The reference suburban test scenario for the following simulations is outlined in table 5.8 below. Note that the only major change to the urban environment given in table 5.1 is to include a single coherent multipath signal at a bearing of -30° as well as a line of sight path for the wanted signal. Also, the number of scatterers in the vicinity of the mobile has been reduced to three in order to provide a more realistic representation of a typical suburban locality. In order to simulate a rural environment the scenario will be identical to the suburban set-up except there will be no local scatterers.

Antenna Array	• No. of elements, • Element spacing, • Mutual coupling, • Channel mismatch,	N=4 d=0.5λ —— ——
Signal Environment	• No. of sources, • Source AOA, • Input SNR, • Line of sight path, • No. of scatterers, • Angular spread, • No. multipaths,	M=1 $\theta_1=0^\circ$ SNR=20dB Yes I=3 $\theta_s=10^\circ$ Q=1 $\theta_m=-30^\circ$
Signal Processing	• No. of snapshots, • Spatial smoothing,	K=50 ——

Table 5.8: Reference suburban scenario.

A: Single Coherent Multipath Signal

The reference suburban test scenario outlined in table 5.8 was simulated with the multipath component 10 dB below the total wanted signal (line of sight plus scatterers). A similar set-up was then chosen for the rural environment, but with no local scatterers, and in order to enable a direct comparison with the suburban results, the line of sight component was given a SNR of +14 dB with the multipath signal -4 dB below. The results of applying the MUSIC algorithm to both of these scenarios are given in figure 5.20a. No spatial smoothing was employed at this stage and this is apparent from the result with the rural type environment, since only a single peak is generated. (The MDL criteria also indicated a single source.) The result from the suburban environment is very interesting since the multipath component has been successfully detected, as well as the line of sight signal. Hence, the presence of the scattered signals enables the coherent component to be resolved.

The results of applying the complex conjugated backward array in addition to the forward array (forward/backward spatial smoothing in Appendix G) are shown in figure 5.20b. Again the MUSIC algorithm was employed

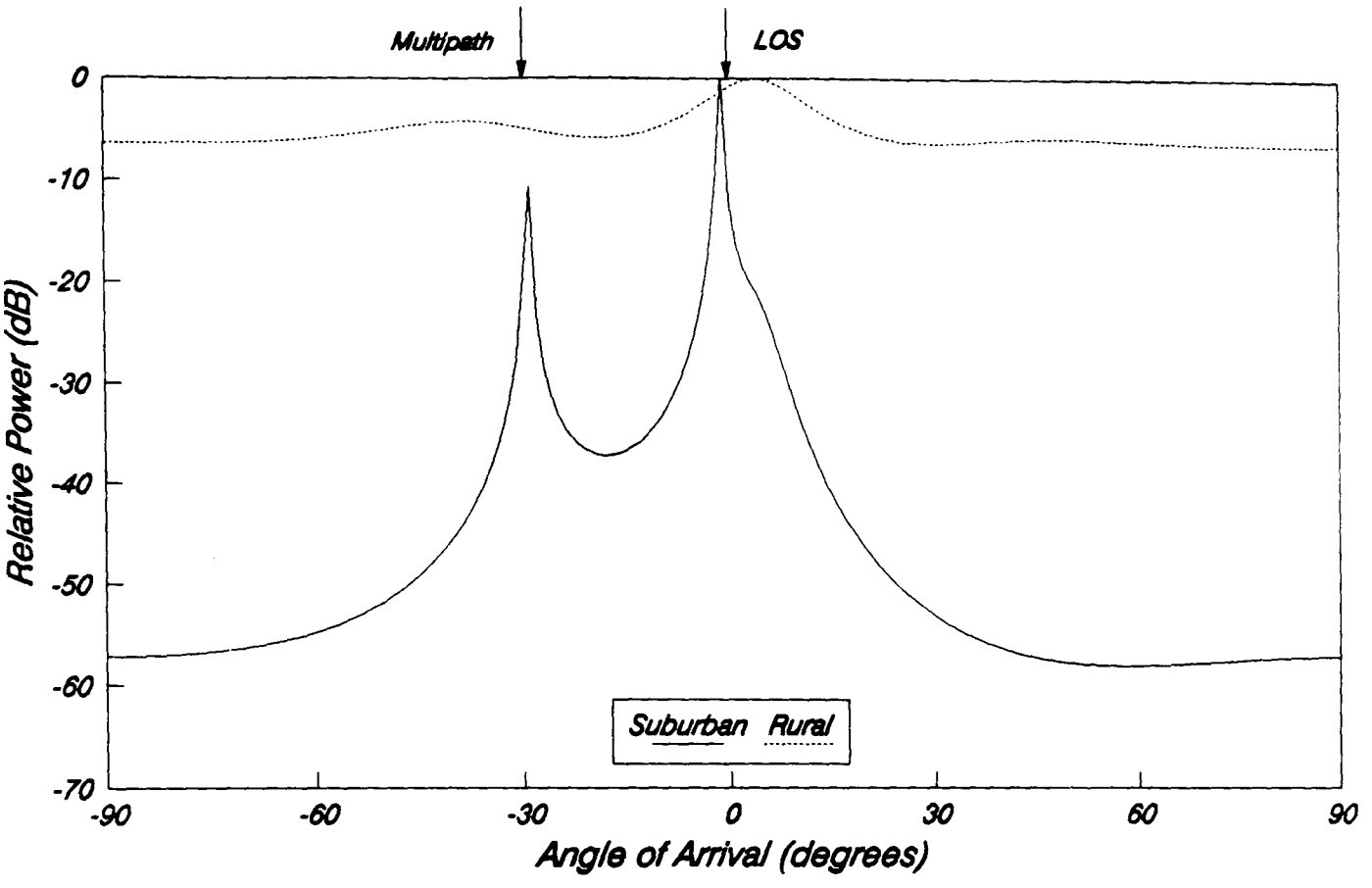

(a)

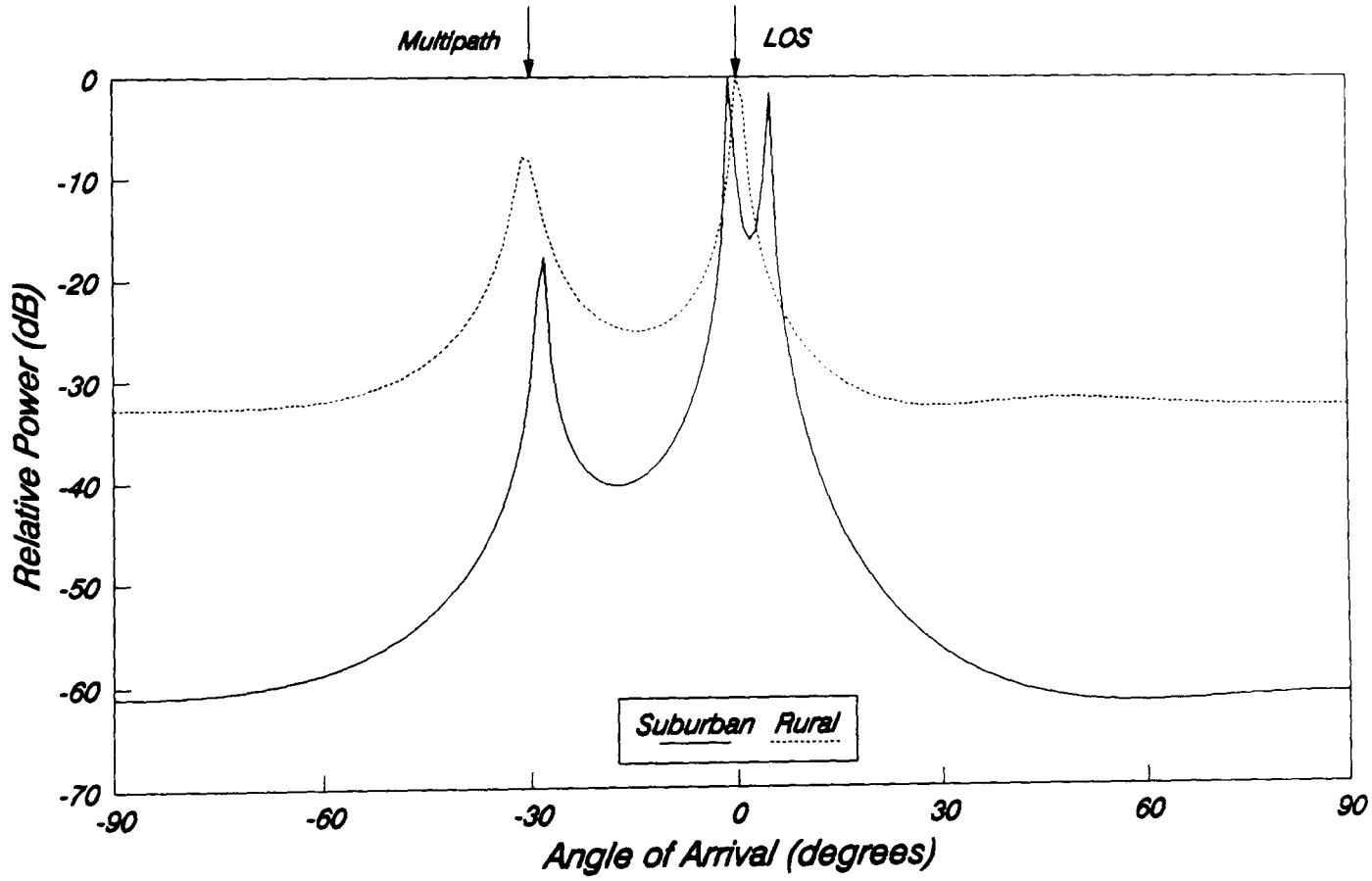

(b)

Figure5.20: Resulting spatial spectra for the MUSIC algorithm in suburban and rural environments: (a) no spatial smoothing; (b) spatial smoothing.

and, in the case of the rural environment, successfully allows the location of the two coherent signals. (The MDL criteria now correctly indicates two sources.) The spectrum for the suburban environment also indicates the presence of the coherent multipath, as well as producing two peaks in the vicinity of the wanted signal which can be attributed to the scattered components. The results of a peak search for the spectra in figure 5.20 are included in table 5.9 below.

Scenario	θ_{est}	θ_{mult}	Other peaks
SUBURBAN (No Smoothing)	-1°	-29° (-11 dB)	——
SUBURBAN (Smoothing)	-1°	-29° (-16 dB)	$+5^{\circ}$ (-3 dB)
RURAL (No Smoothing)	$+4^{\circ}$	——	——
RURAL (Smoothing)	0°	-30° (-4 dB)	——

Table 5.9: Results of peak search for the MUSIC algorithm in suburban and rural environments with one coherent multipath.

Unfortunately, the correct application of the spatial smoothing technique requires that the direction vectors of a signal source at each subarray differ only by a constant phase term (see Appendix G). When mutual coupling is present however, this property will not hold, and spatial smoothing cannot be applied directly. This is very noticeable in figure 5.21, where forward/backward spatial smoothing, in conjunction with the MUSIC algorithm, has been applied to the rural environment for both the ideal array and an array with mutual coupling and receiver mismatches (σ_{γ} = 0.1 and $\sigma_{\psi} = 10^{\circ}$). The latter result was generated by employing the modified steering vector $\mathbf{u}'$ given in equation (5.22), and clearly demonstrates the reduction in performance.

Yeh *et al* [7] have addressed this problem and proposed an alternative to employing the modified steering vector. This involves premultiplying the array covariance matrix $\mathbf{R}$ with the mutual impedance matrix $\mathbf{Z}_0$, i.e.

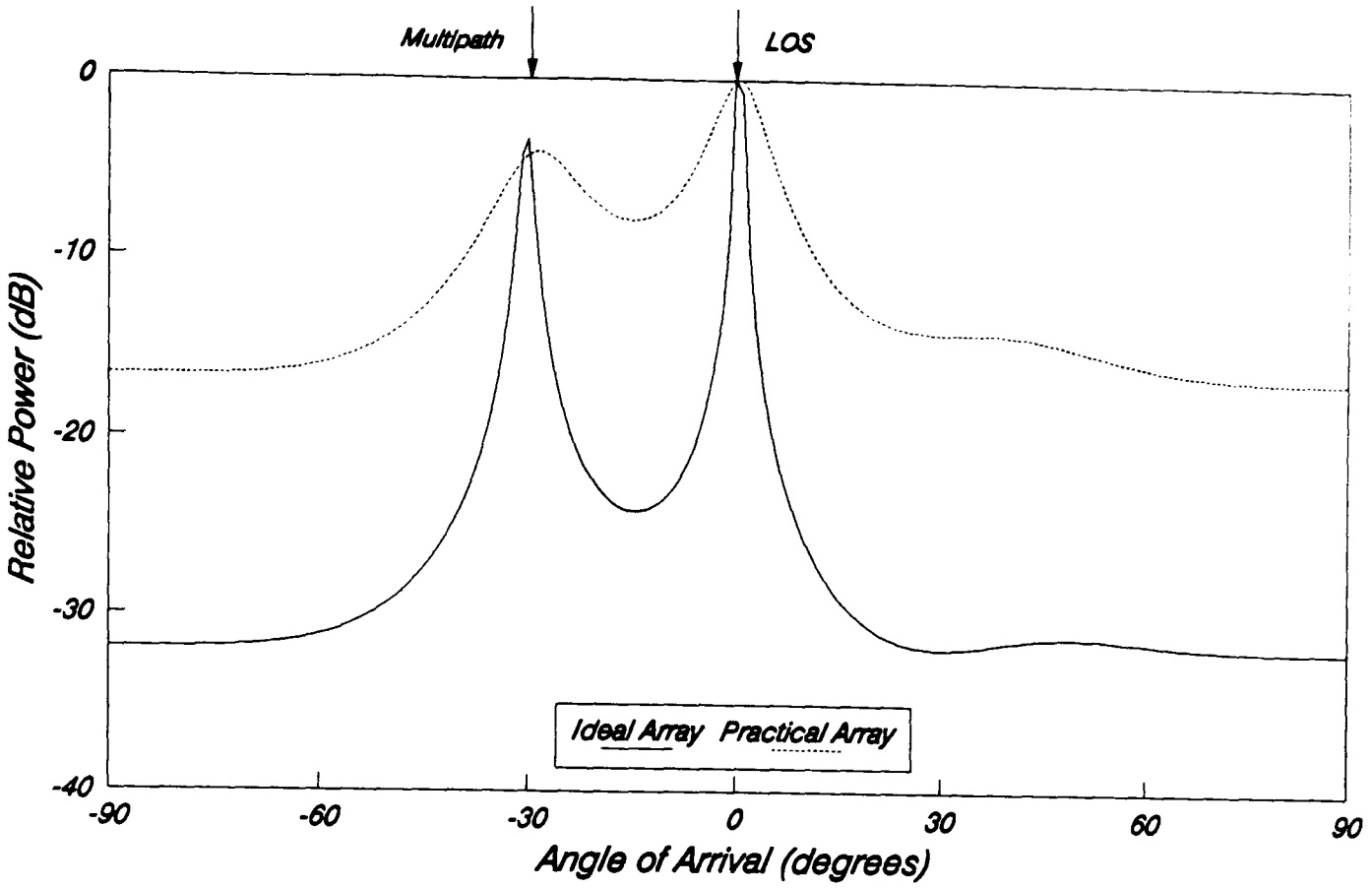

Figure 5.21: Results of applying spatial smoothing with MUSIC in the rural environment for ideal and practical arrays.

$$\mathbf{R}' = \mathbf{Z}_0 \mathbf{R} \mathbf{Z}_0^{\dagger} \tag{5.26}$$

$$= \mathbf{Z}_0 E\left[\mathbf{x}(k)\mathbf{x}(k)^{\dagger}\right] \mathbf{Z}_0$$

Hence substituting in the expression for $\mathbf{x}(k)$ in equation (5.17), and assuming independent noise, gives

$$\mathbf{R}' = \mathbf{B}\mathbf{R}_a\mathbf{B}^{\dagger} + \sigma^2 \mathbf{Z}_0 \mathbf{Z}_0^{\dagger} \tag{5.27}$$

Spatial smoothing can now be applied successfully to the modified covariance matrix $\mathbf{R}'$ in the normal manner, and this is demonstrated with the aid of computer simulations by Yeh *et al* [7]. Unfortunately, the results of the array manifold measurement, to be discussed in section 6.2, clearly show that the phase errors introduced by the combined effects of mutual coupling and receiver mismatches depends on the angle of arrival of the signal source. This suggests therefore that in practice the mutual coupling matrix is not a constant, thus requiring in the case of the eigenstructure algorithms, the

complete eigen-decomposition of the modified covariance matrix $\mathbf{R}'$ at each AOA of interest. This would dramatically increase the computational overheads, potentially making the proposed technique unusable in the present application.

B: Two Coherent Multipaths

Without any preprocessing of the data, there are three degrees of freedom available with a four element array, i.e. the DF algorithms can search for up to three uncorrelated signals. Spatial smoothing with subarrays of three elements ($N_s = 3$), and applying either the forward or backward techniques reduces the degrees of freedom to two, although a combination of both could potentially increase this to the integer part of 2N/3. Unfortunately, with only four elements in the array, this reduces to two again. Therefore, in this section, the problem of an additional discrete multipath component is considered.

The resulting spatial spectra for the suburban environment with an additional multipath component at $+60^\circ$ are shown in figure 5.22. Both the multipaths were 10 dB below the total wanted signal and the two responses shown are with and without spatial smoothing applied. The smoothing employed was the forward/backward technique with no subarraying, i.e. $N_s = 4$. The results clearly show that even with spatial smoothing of the data, the MUSIC algorithm fails to resolve the multipath components, although still successfully detects the presence of the wanted signal. The other algorithms all perform in a similar fashion, with the degree of resolution depending on their individual attributes. The result of applying spatial smoothing though, is very dependent on the position of the multipath components and, in some cases, can have a very detrimental effect leading to ambiguous estimates.

The results of applying spatial smoothing in a rural type environment with two coherent multipath sources is very dependant on the source locations. This is to be expected since with only four elements in the array, the available degrees of freedom for successful application of spatial smoothing have been exceeded. Hence in order to provide the sufficient resolution capabilities for operation in a rural environment, an array with a larger number of elements may have to be employed.

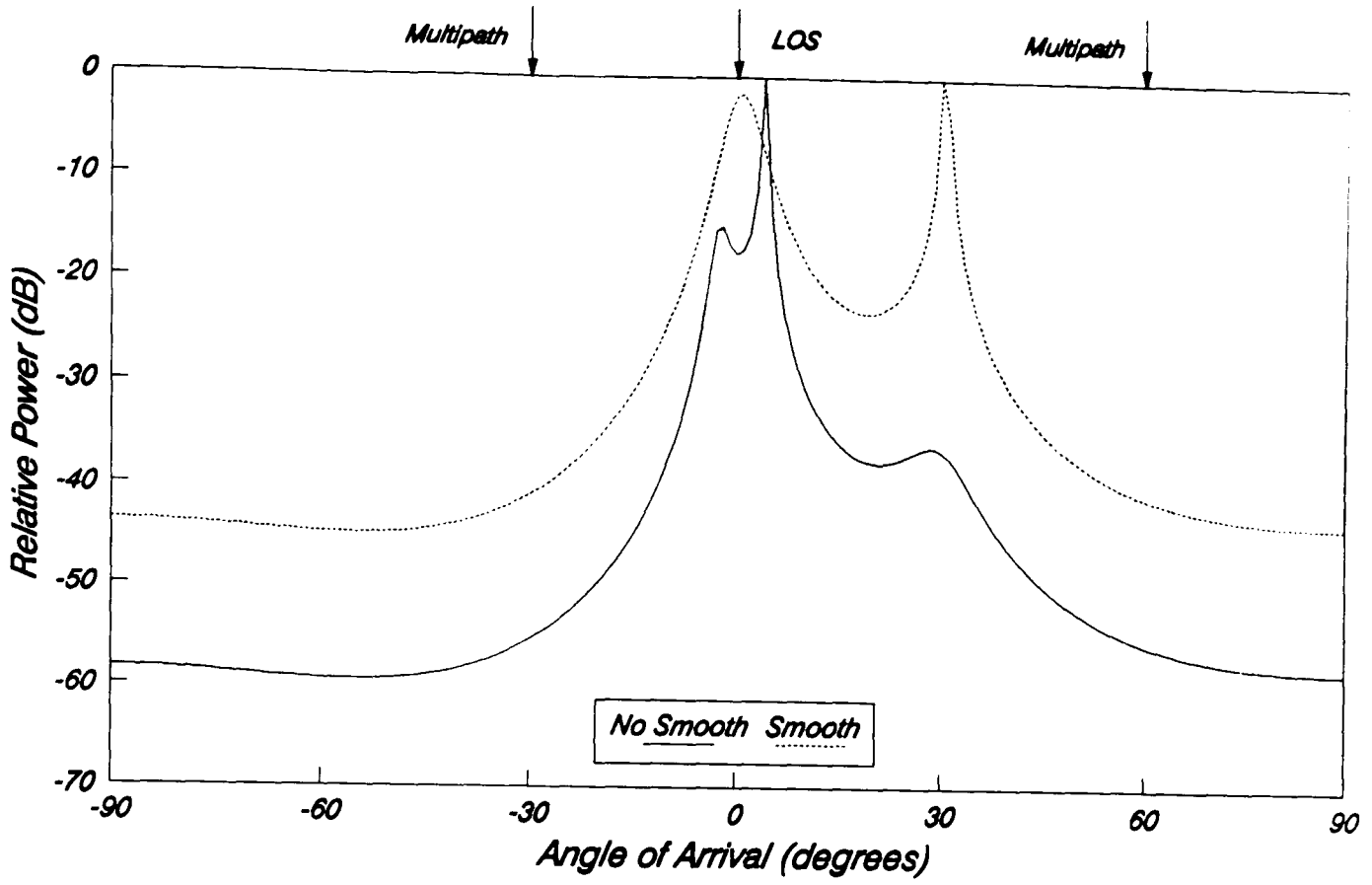

Figure 5.22: Resulting spatial spectra for the MUSIC algorithm in a suburban environment with and without spatial smoothing.

5.3 THE ABILITY TO TRACK A SINGLE MOBILE SOURCE

In the preceding analysis a static mobile scenario was considered and the following general observations can be made from each of the operational environments investigated.

Urban Environment

The presence of a large numbers of scatterers (≥ 6) in the immediate vicinity of the mobile, with no line of sight path, presents a unique problem for the DF processor. Complete resolution of all the scattered wavefronts is not possible, as was demonstrated, with only the higher resolution techniques (**MUSIC**, **JoDeG**, **KuTu** and **MEM**) indicating the presence of more than one incident wavefront. Consequently, the error in the estimated AOA of the wanted mobile is very dependent on the spread of the scatterers. This was not the case with the lower resolution techniques (**FM** and **MLM**), which tended to average out the effect of the scattered wavefronts and indicate the presence of a single source at approximately the correct bearing. Hence, in this type

of environment, accurate AOA estimation does not necessarily require the highest resolution DF algorithms.

Urban Environment with Co-channel Interferers

When a co-channel interfering source is present only the higher resolution techniques (**MUSIC, JoDeG, KuTu** and **MEM**) can successfully determine the bearing. If the total number of sources exceeds the degrees of freedom available, the combined effect of the scatterers associated with the wanted mobile tends to dominate, enabling the bearing to be successfully estimated with all the algorithms.

Suburban Environment

The presence of discrete multipath signals with a high degree of correlation with the wanted line of sight signal traditionally causes many problems for the DF processor as explained earlier. However, the presence of one or more scattered waves, as well as the line of sight component, ensures that the bearing of the wanted signal can be determined. Also, the higher resolution techniques can indicate the presence of the additional multipath component. Hence, spatial smoothing techniques are not absolutely necessary in this type of environment.

Rural Environment

Without the presence of any scattered waves, coherent multipath does become a problem. Hence, spatial smoothing techniques must be applied, with the higher resolution algorithms producing the superior results.

The most suitable choice of DF algorithm clearly depends on the environment in which it must operate and so in order to provide a more statistical basis for comparison, the mobile was made to follow a predefined path in each of the operational environments considered so far. Previously, the same seed for the random number generator was used for each simulation run in order to produce consistent results. Therefore, for each iteration of the mobile run, a different seed was used. This enables the results of applying all the DF algorithms to be compared based on the statistical nature of the error between the estimated and actual source bearings over a number of iterations, e.g. the mean error, the root mean square (RMS) error and the standard deviation, σ. In the following sections, each of the signal environments is considered in turn, with the mobile moving from -30° to $+30^{\circ}$

in 3° steps. In order to provide a realistic environment, mutual coupling and receiver mismatches were included ($\sigma_{\gamma} = 0.1$ and $\sigma_{\psi} = 10^{\circ}$ [5]) and the modified steering vector $\mathbf{u}'$ given in equation (5.22) employed to simulate the measured manifold response.

5.3.1 Urban Communications

The first scenario to be considered was defined in table 5.1 for a typical urban environment and the statistical results for all the DF algorithms are presented in table 5.10. If the RMS error and standard deviation are considered, these results clearly illustrate that the lower resolution techniques (FM and MLM) provide the most accurate estimate of the mobile's bearing. The resulting spatial spectra for the MUSIC algorithm are given in figure 5.23 and exhibit the characteristic clustering of peaks in the vicinity of the mobile. In contrast, the spatial spectra for the MLM algorithm given in figure 5.24 have only a single peak and hence provide a more reliable estimate for the bearing of the mobile source[2].

The results for both the FM and MLM techniques are slightly worse than if an ideal array was assumed, i.e. an array with no mutual coupling and no receiver mismatches. Hence, by employing the modified steering vector the resultant peaks are marginally wider, an effect more noticeable with the FM technique. The KuTu algorithm produces a relatively large mean error which could possibly be attributed to the presence of spurious peaks in the spectra as shown in figure 5.25. The spectrum produced by the MEM also produced these extra peaks, although with an ideal array this phenomenon was not apparent. Hence the effect can be attributed to the use of the modified steering vector when mutual coupling and receiver mismatches are present.

2: Note that the amplitude scale is in dB as before but has not been included since the plots are only required to illustrate the effects of applying each algorithm in a different mobile scenario.

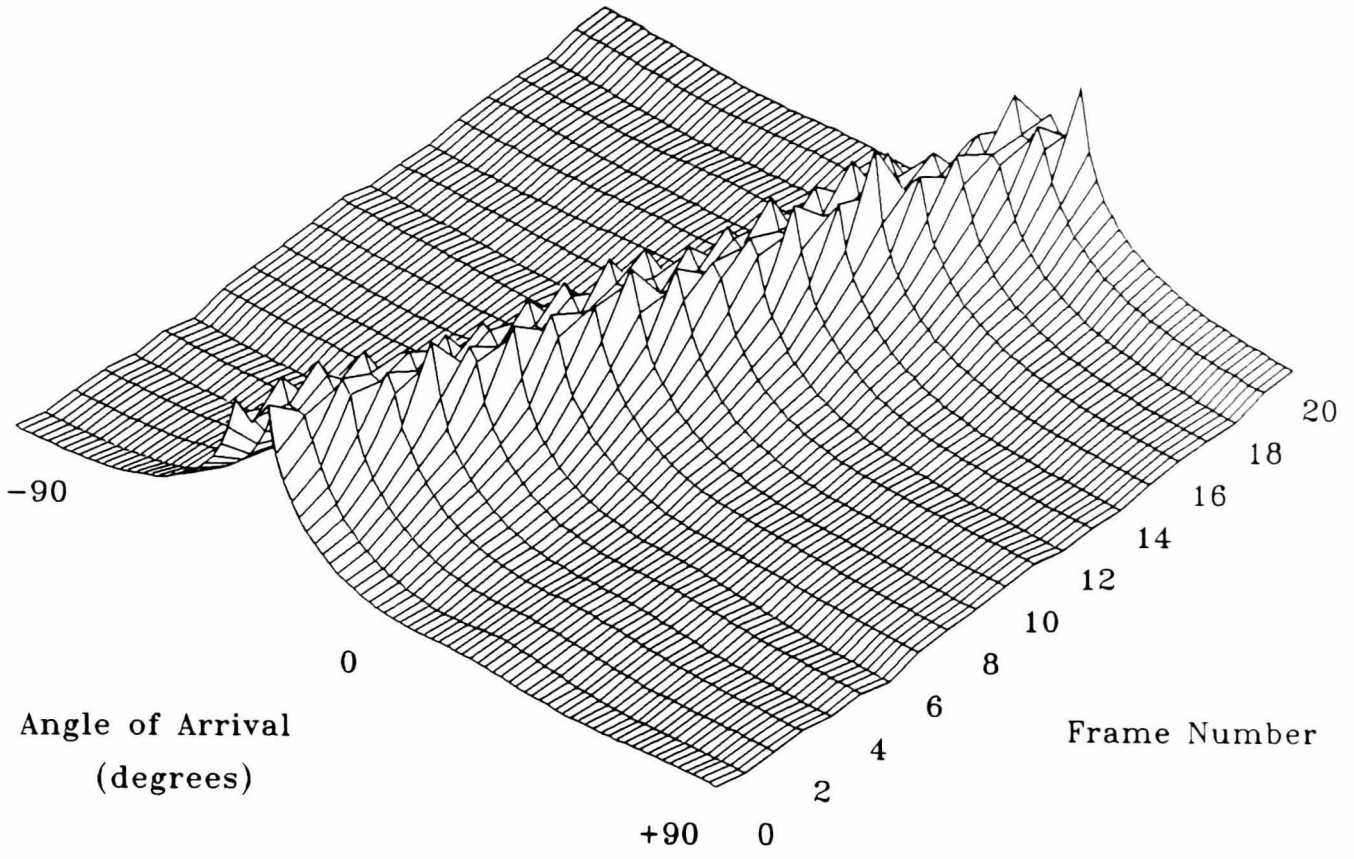

Figure 5.23: Results in mobile urban environment with the MUSIC algorithm.

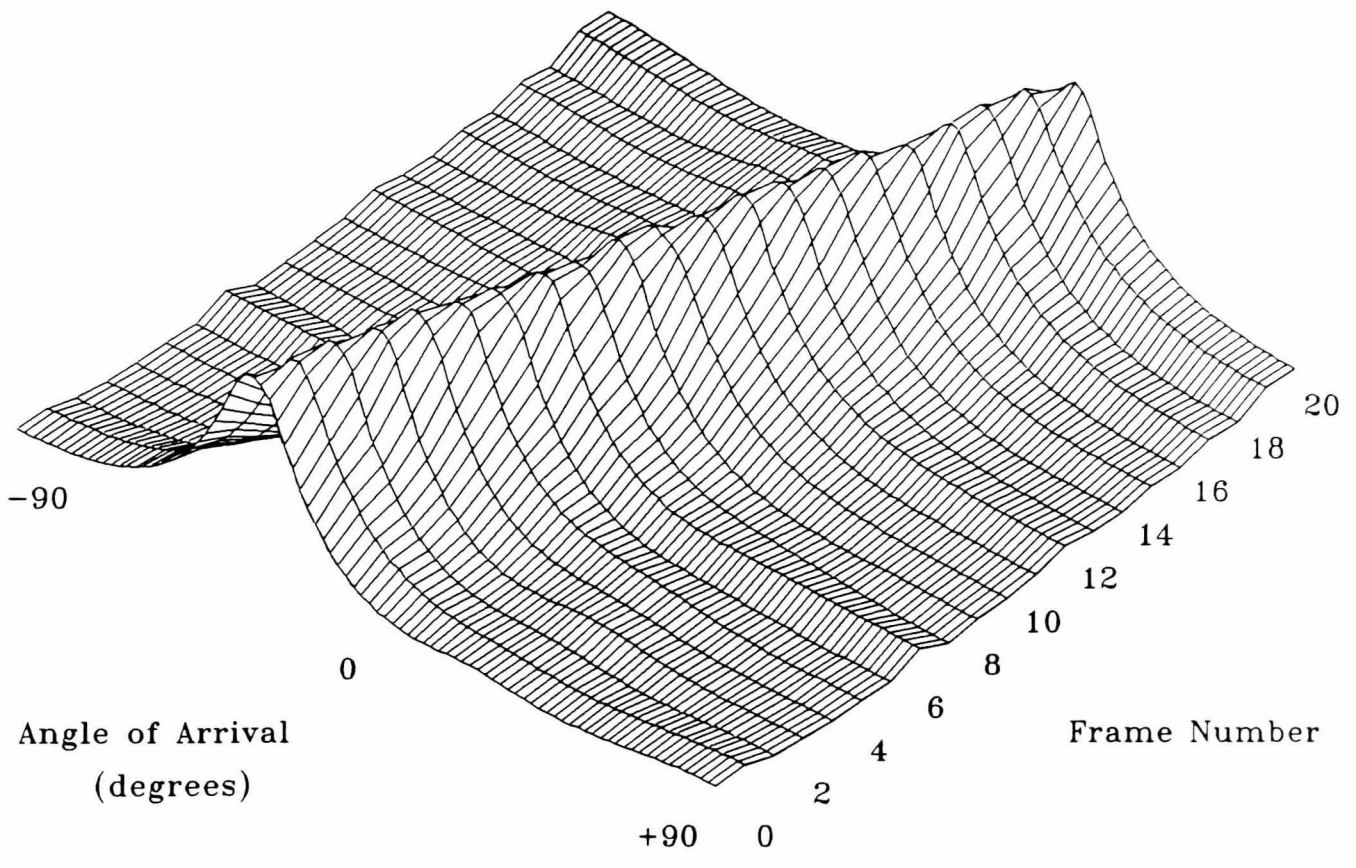

Figure 5.24: Results in mobile urban environment with the MLM algorithm.

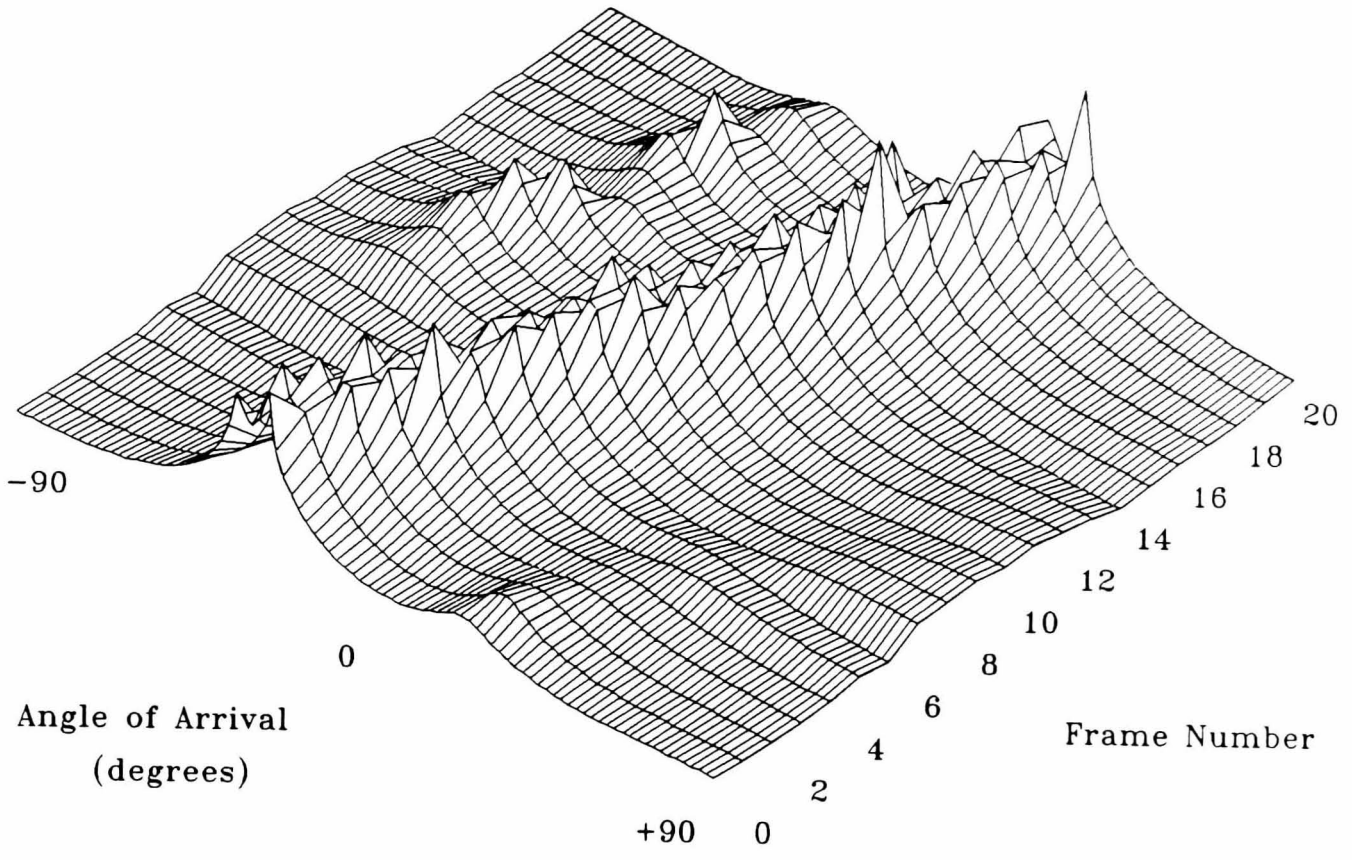

Figure 5.25: Results in mobile urban environment with the KuTu algorithm.

Algorithm	Error Statistics (degs.)		
	Mean	RMS	σ
FM	-0.1	1.5	1.5
MLM	-0.3	1.2	1.2
MEM	-0.2	3.2	3.2
MUSIC	-0.1	3.5	3.5
JoDeG	-0.3	3.5	3.5
KuTu	2.3	3.6	2.8

Table 5.10: Error statistics for mobile urban scenario.

The results when a single co-channel source was located at a bearing of 0° (SINR = 10 dB) were very similar to those described above, with the MLM and FM algorithms producing the superior estimates of the mobile's bearing. However, inclusion of an additional co-channel source at -60° produced some interesting results. Again the SINR was set at 10 dB and the statistical results are presented in table 5.11. There is a slight reduction in the errors for all the algorithms when compared with the results in table 5.10 with no co-channel interference. This effect is most noticeable with the MLM technique and can be attributed to the reduction in the available degrees of freedom when extra sources are present. The resulting spatial spectra for the MUSIC algorithm are given in figure 5.26 and show the presence of all three sources of signal energy, although the estimate for the co-channel sources is inconsistent and on some occasions the peak associated with either co-channel source dominates. This phenomenon was also noticeable with the other eigenstructure techniques and the MEM algorithm, and could possibly lead to a false indication of the mobile's bearing. This was not the case with the MLM technique as illustrated in figure 5.27. Notice the smoother response enabling a more consistent estimate of the mobile's bearing.

Algorithm	Error Statistics (degs.)		
	Mean	RMS	σ
FM	-0.1	1.4	1.3
MLM	0.2	0.8	0.7
MEM	0.4	2.4	2.3
MUSIC	0.7	3.0	2.9
JoDeG	0.8	3.0	2.9
KuTu	-0.7	3.0	2.9

Table 5.11: Error statistics for mobile urban scenario with two co-channel sources.

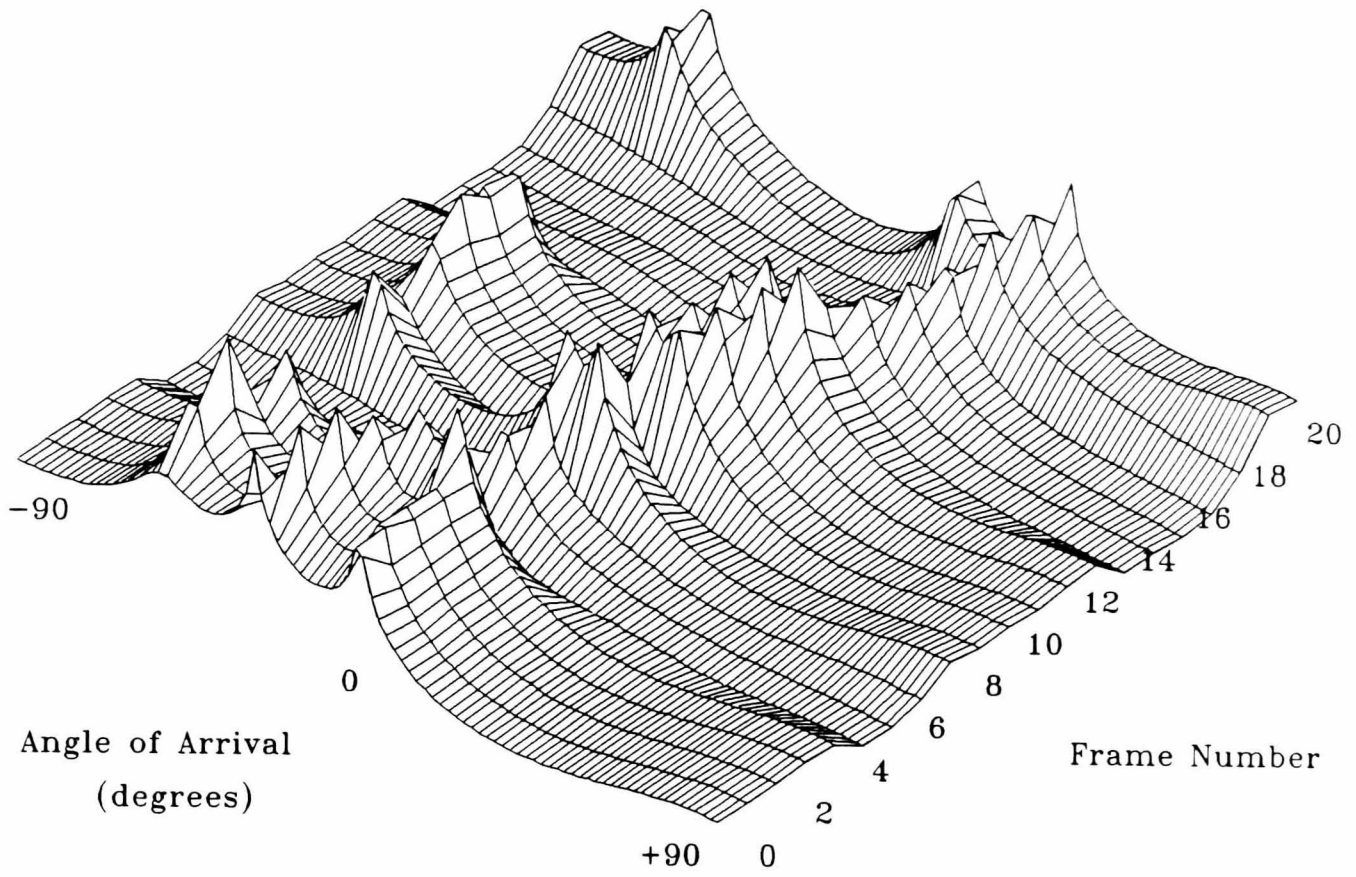

Figure 5.26: The MUSIC algorithm in the mobile urban environment with two interfering co-channel sources.

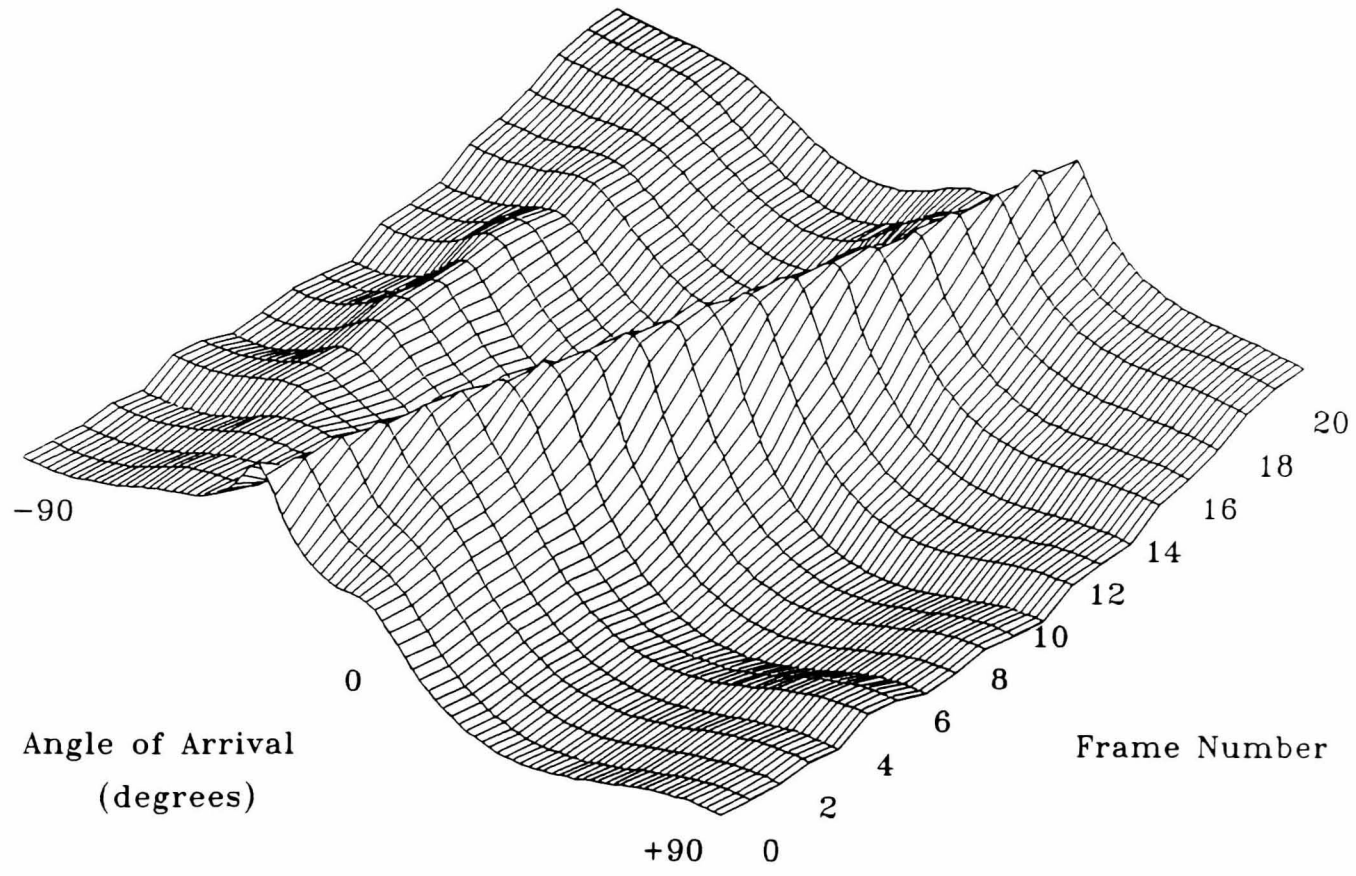

Figure 5.27: The MLM algorithm in the mobile urban environment with two interfering co-channel sources.

5.3.2 Suburban Communications

Consider operation in a suburban type environment, which is as defined in table 5.8, but with a single discrete multipath component located at a fixed bearing of -40° and -10 dB below the total wanted signal. The statistical results without spatial smoothing are given in table 5.12 with the MLM algorithm again proving to be superior in terms of correctly estimating the bearing of the mobile source. The MEM algorithm gives the worst results which can be attributed to the strong presence of the multipath component which is evident in the spatial spectra of figure 5.28. The peak associated with the multipath signal is also occasionally stronger than the peak indicating the wanted source. The results for the FM technique are also presented in figure 5.29 and the spectra clearly show the characteristic main beam and sidelobes.

Algorithm	Error Statistics (degs.)		
	Mean	RMS	σ
FM	-0.3	1.9	1.9
MLM	0.2	1.0	1.0
MEM	-1.7	4.8	4.5
MUSIC	-0.8	3.0	2.9
JoDeG	-1.3	3.2	2.9
KuTu	-0.8	3.0	2.9

Table 5.12: Error statistics for mobile suburban scenario with no spatial smoothing.

The statistical results when spatial smoothing[3] was employed are presented in table 5.13. As expected, the performance of all the algorithms is degraded since spatial smoothing cannot be applied directly when mutual coupling between antenna elements is present (see section 5.2.2). The only exception to this is with the MEM technique, although if the resulting spatial spectra illustrated in figure 5.30 are considered, this can be possibly attributed to the presence of spurious peaks. Note again that these peaks are not present when an ideal array is employed with spatial smoothing.

3: Forward and backward spatial smoothing with no subarraying.

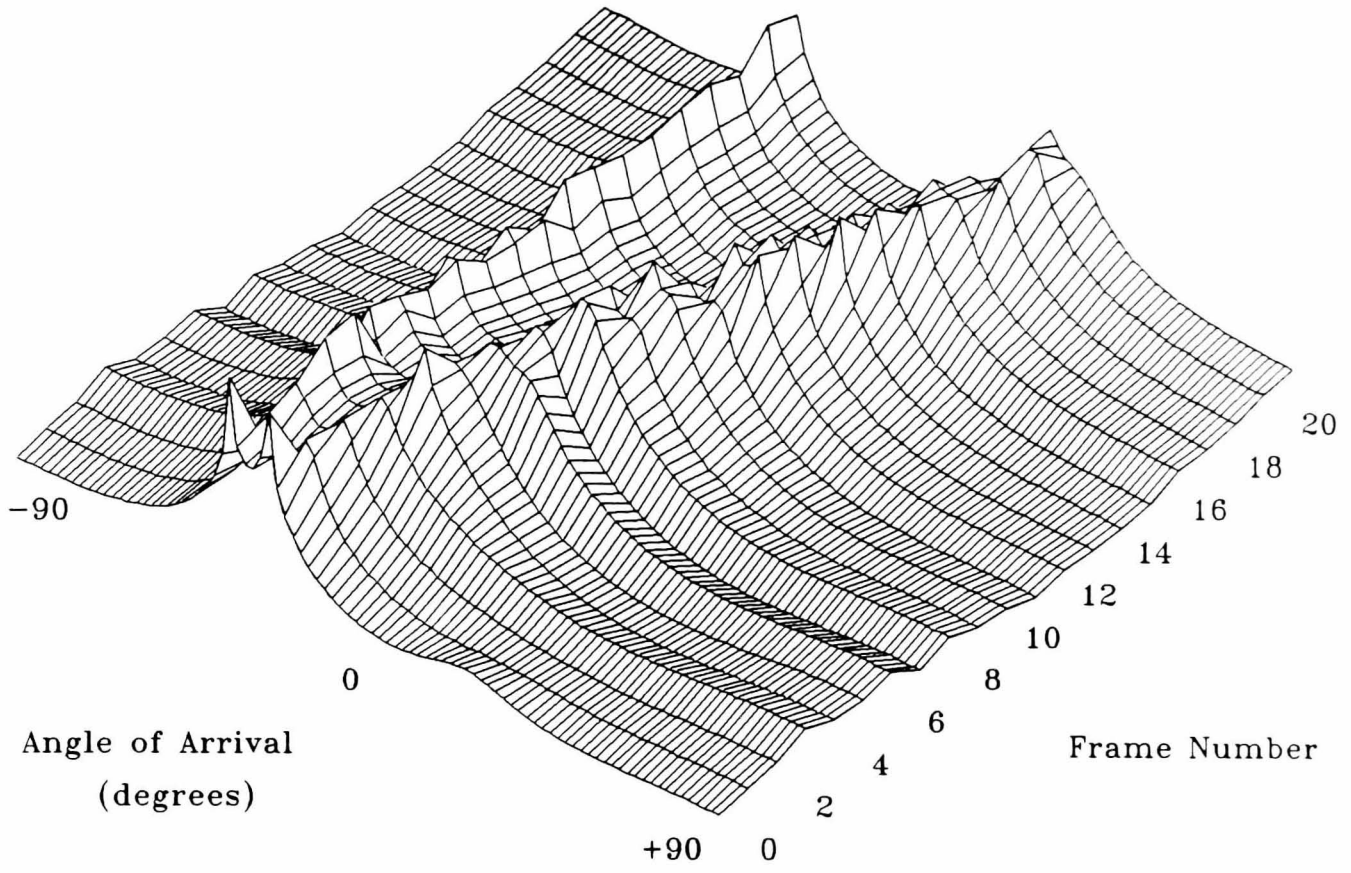

Figure 5.28: Results in mobile suburban environment with the MEM algorithm (no spatial smoothing).

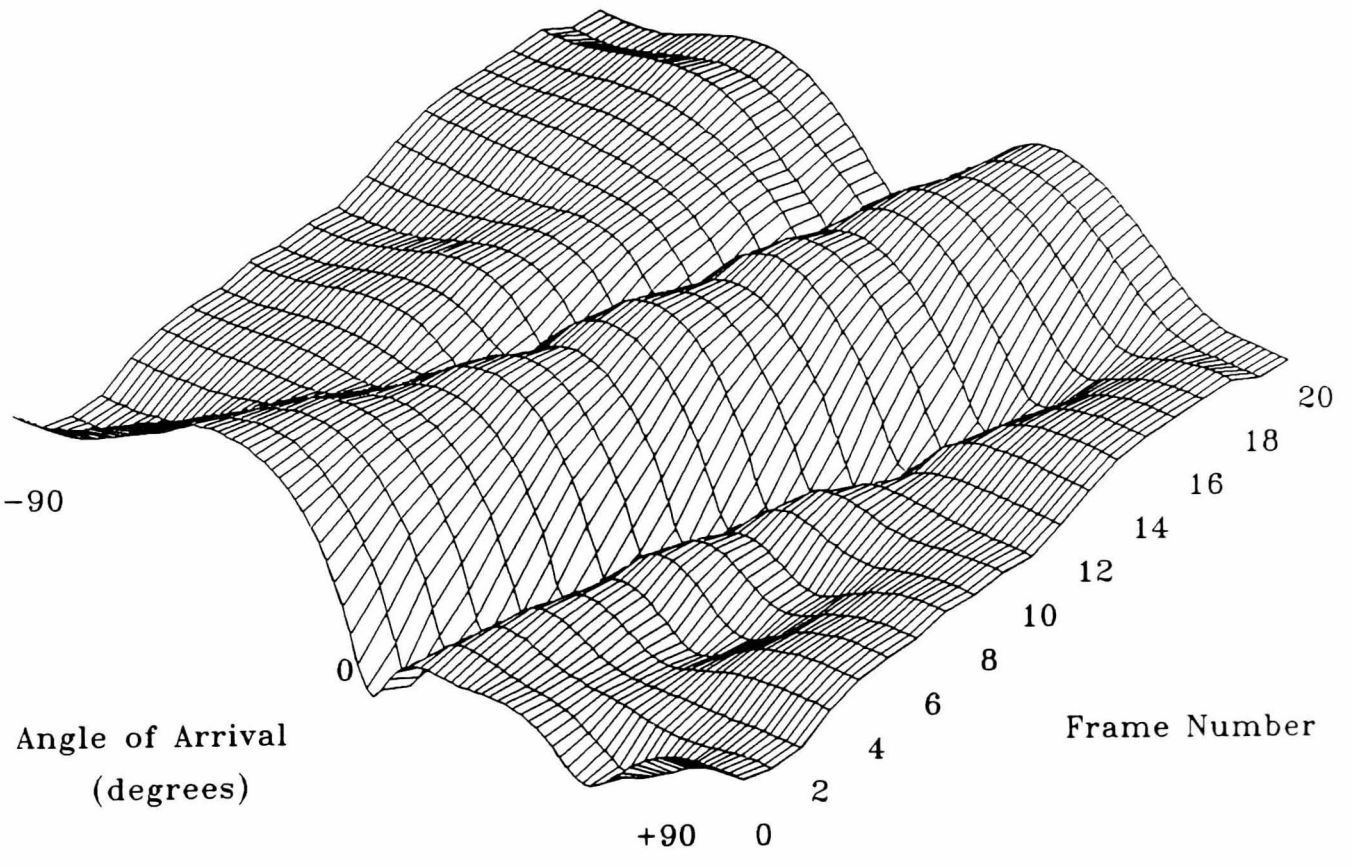

Figure 5.29: Results in mobile suburban environment with the FM algorithm (no spatial smoothing).

Algorithm	Error Statistics (degs.)		
	Mean	RMS	σ
FM	-0.4	2.3	2.2
MLM	0.1	1.0	1.0
MEM	2.3	2.7	1.5
MUSIC	0.7	4.1	4.0
JoDeG	0.7	4.1	4.0
KuTu	1.7	4.4	4.1

Table 5.13: Error statistics for mobile suburban scenario with spatial smoothing.

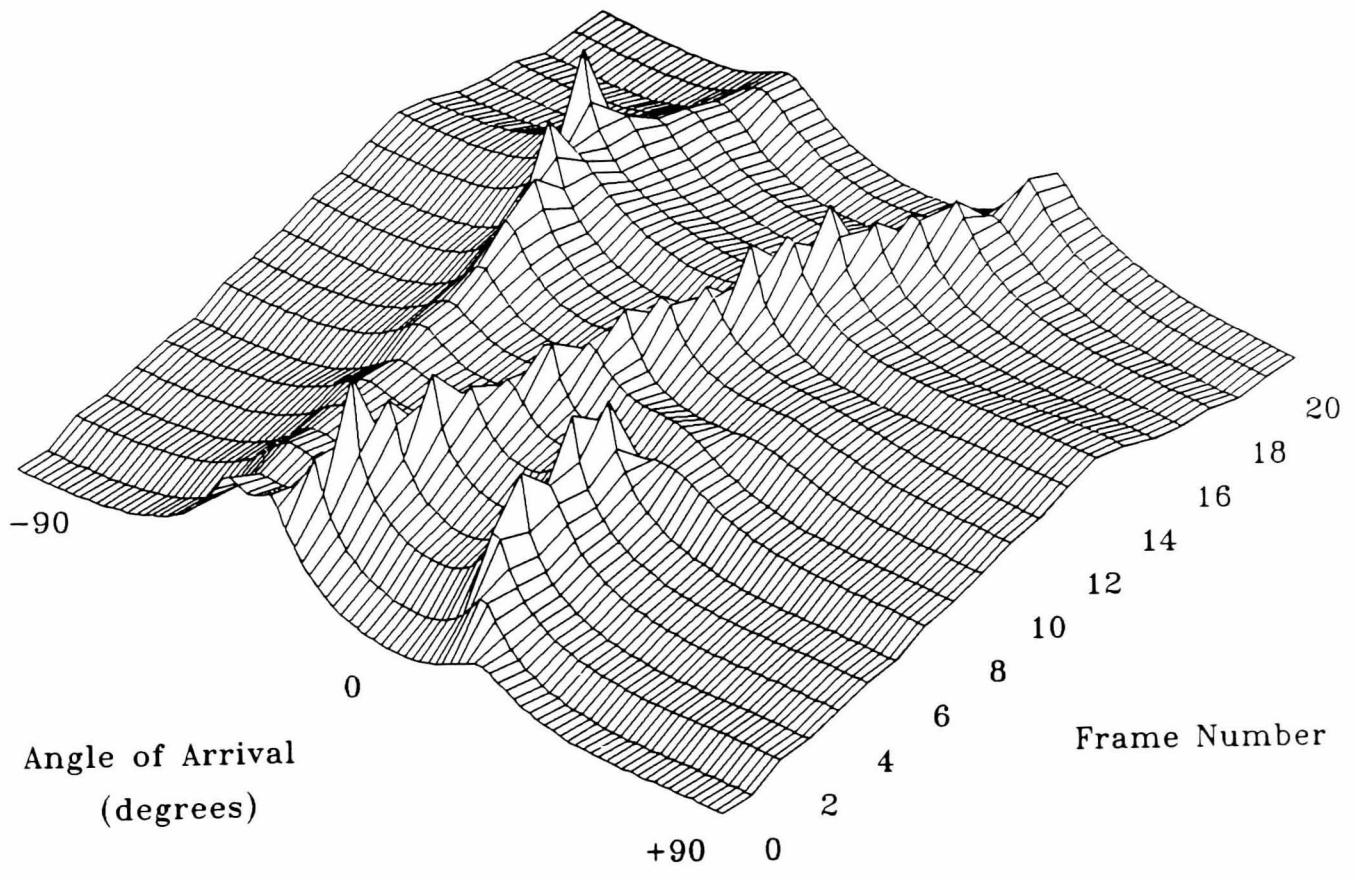

Figure 5.30: Results in mobile suburban environment with the MEM algorithm with spatial smoothing applied.

5.3.3 Rural Communications

In order to resolve the bearing of a mobile source in a rural environment when there is a coherent multipath present, spatial smoothing must be employed. This was clearly illustrated in figure 5.20 for the static case. However, when mutual coupling is present between the antenna elements there is a severe degradation in the performance of the algorithms as shown in figure 5.21. Therefore, if the direction finding process is to be effective in a rural environment, alternative techniques may have to be found, e.g. the approach proposed by Yeh *et al* [7].

5.4 SIMULATION OF AN FDMA SCHEME

In section 4.4, the incorporation of the DF process into a cellular communications network was briefly discussed, and in particular, the application in a multiple access scheme such as frequency division (FDMA) or time division (TDMA). The general principle is that each active mobile is assigned a unique channel and, whether this is a frequency allocation or time slot, the task of the DF processor is now greatly simplified since it need only search within each channel for a single mobile. In this section an FDMA type scheme will be simulated to demonstrate how such an access technique could be accommodated within the proposed base-station antenna system.

The results presented thus far have only considered operation with a single frequency and are therefore restricted to narrowband sources with the same centre frequency. Wax *et al* [15] have proposed a 2D spectral estimation algorithm for simultaneous estimation of both the source AOA and centre frequency. The approach employs a tapped delay line behind each element in the antenna array and, in a similar way to the MUSIC algorithm, exploits the properties of the special eigenstructure of the array covariance matrix. The steering vector **u** in this case though is modified to search in the frequency domain as well as the spatial domain. Further details are given in Appendix H. It is also worth noting briefly that tapped delay lines have also been considered as a means of reducing the effect of mutual coupling in adaptive arrays [16], although this will not be considered in any more detail at this stage.

In order to represent an FDMA type scheme, the mobile sources must be assigned a unique frequency channel and so the signal model described in Appendix H accommodates M signal sources centred at frequencies $w_1,\cdots,w_M$. These frequency channels are separated by a value B_c Hz, which is often referred to as the channel spacing, and are ranged either side of a centre frequency w_o. Hence, the channel frequencies can be written as

$$w_m = w_o \pm \Omega(2\pi B_c)$$

$$= w_o\left(1 \pm \Omega \frac{B_c}{f_o}\right) \qquad (5.26)$$

where Ω is the channel number. Consider then, as before, a four element linear array with the inter element spacing d equal to $0.5\lambda_o$, and incorporate a three tap delay line behind each element. This enables up to eleven mobile sources to be estimated and so eleven frequency channels were defined, i.e. $\Omega = -5,\cdots,0,\cdots,+5$, with the ratio of the channel spacing B_c to centre frequency f_o set to 0.01. Since the purpose of this simulation is to simply demonstrate the feasibility of DF in a multiple signal/frequency environment, only seven mobiles were considered and their channel allocations and movements are defined in table 5.14 and illustrated in figure 5.31. A cluster of three mobiles has been included to simulate a traffic jam situation. The cell where the mobiles operated was a 180° sector and the simulation run was for 21 iterations. Only two types of signal environment were considered at this stage, and these were

(i) An urban type environment as defined in table 5.1 but with multiple mobile sources.

(ii) As for the urban environment but with no local scatterers. Hence, each mobile is represented as a point source with a Rayleigh fading envelope and a uniformly distributed phase.

The second environment was included to provide a comparison for the urban set-up and the error statistics (standard deviation only) for each of the mobiles are given in table 5.15 for both signal environments. Note that an ideal receiving array was assumed for this demonstration, i.e. the effects of mutual coupling and receiver mismatches were not considered.

Mobile ID	Freq. Channel (Ω)	Mobile Movements		
		Start	Step	End
A	-5	-30°	0°	-30°
B	-4	0°	+3°	+60°
C	-2	-35°	0°	-35°
D	-1	+60°	-2°	+20°
E	1	-60°	+3°	0°
F	3	-40°	0°	-40°
G	5	+35°	-3°	-25°

Table 5.14: Setup for mobile sources in simulated FDMA scheme.

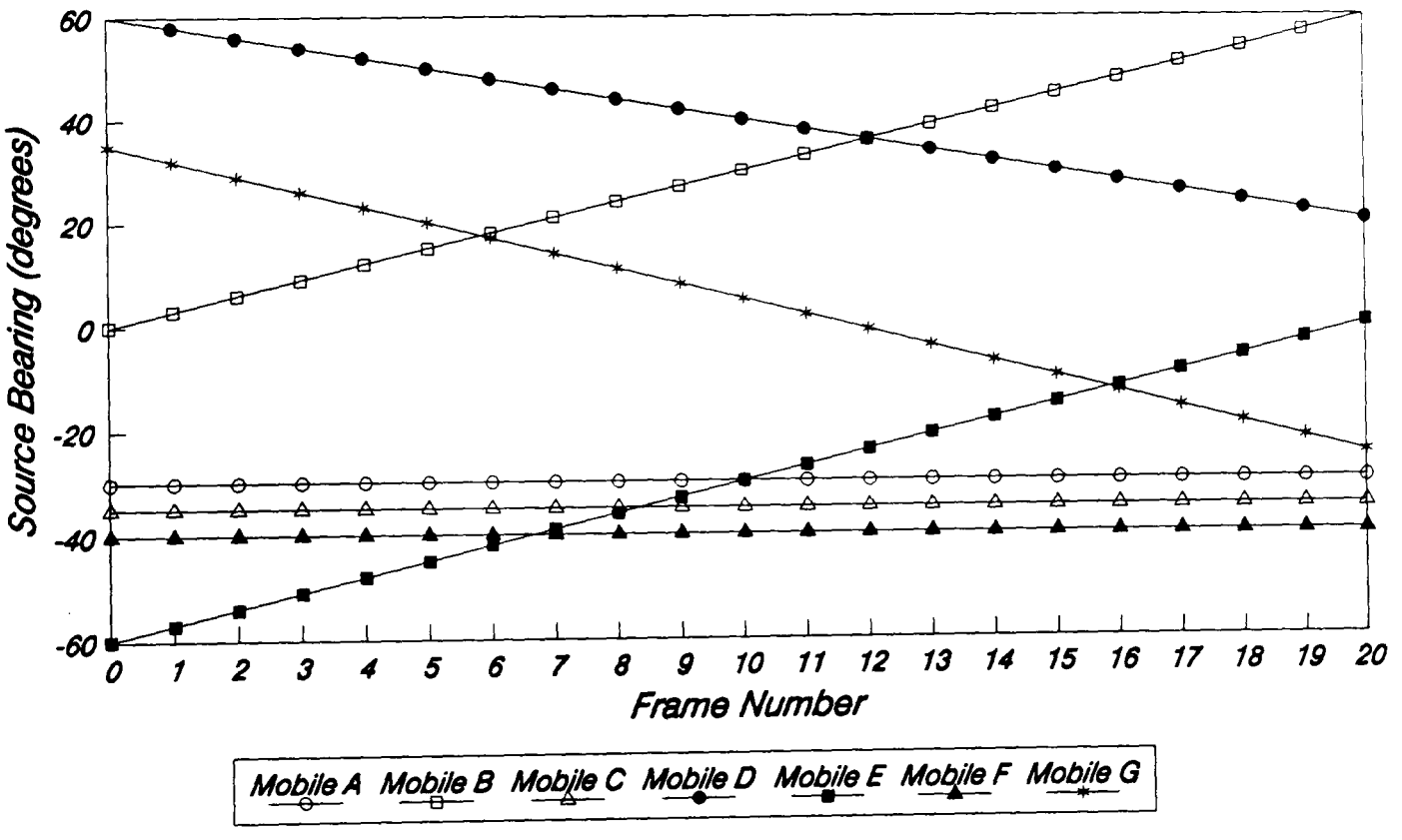

Figure 5.31: Movement of mobiles in a simulated FDMA scheme.

Note the reduced spread of the AOA error in the non-urban environment as expected, although mobile E still has the largest spread. This is to be expected since it moves across the path of four of the other mobiles. The increase in the error spread with mobile F however is not consistent with the others and this can be attributed to a single gross error of 18°. When this error is discounted, the standard deviation becomes only 2.0°. The spread of the errors with the urban environment compares very well with the results of the MUSIC algorithm with the single mobile scenario considered in section 5.3.1. Hence, the algorithm developed by Wax *et al* [15] for multi-dimensional AOA estimation could potentially be employed in a cellular FDMA scheme, although the approach requires considerably more investigation than the brief study presented here. In chapter 7, the implementation of the proposed base-station antenna architecture within an existing cellular framework is discussed further.

Mobile ID	Error Standard Dev. σ	
	URBAN	NON-URBAN
A	3.2°	1.1°
B	1.7°	1.0°
C	4.7°	2.8°
D	3.9°	1.9°
E	7.4°	4.3°
F	2.9°	4.1°
G	1.2°	0.5°

Table 5.15: Error statistics for urban and non-urban environments in an FDMA scheme.

REFERENCES

[1]: W.C. Jakes, *"Microwave Mobile Communications"*, John Wiley & Son, 1974.

[2]: W.C.Y. Lee, *"Mobile Communications Engineering"*, McGraw-Hill 1982.

[3]: *"Special Issue on Mobile Radio Propagation"*, IEEE Transactions on Vehicular Technology, Vol.VT-37, No.1, Feb. 1988, pp.3-71.

[4]: I.J. Gupta and A.A. Ksienski, *"Effect of Mutual Coupling on the Performance of Adaptive Arrays"*, IEEE Transactions on Antennas & Propagation, Vol.AP-31, No.5, Sept. 1983, pp.785-791.

[5]: A.J. Weiss and B. Friedlander, *"Direction finding in the Presence of Mutual Coupling"*, Proceedings of 22nd Asilomar Conference on Signals, Systems and Computers, USA, 1988, pp.598-602.

[6]: C.C. Yeh and M.L. Leou, *"Estimating Angles of Arrival in the Presence of Mutual Coupling"*, 1987 International Symposium on Antennas & Propagation, AP-S 1987, USA, 15th - 19th June 1987, Vol.II, pp.862-865.

[7]: C.C Yeh, M.L. Leou and D.R. Ucci, *"Bearing Estimation with Mutual Coupling Present"*, IEEE Transactions on Antennas & Propagation, Vol.AP-37, No.10, Oct. 1989, pp.1332-1335.

[8]: N.S. Hoult, C.A. Dace and A.P. Cheer, *"Implementation of an Equaliser for the GSM System"*, IEE Fifth International Conference on Radio Receivers & Associated Systems, Cambridge University, 24th - 26th July 1990, pp.182-186.

[9]: M. Wax and T. Kailath, *"Detection of Signals by Information Theoretic Criteria"*, IEEE Transactions on Acoustics, Speech & Signal Processing, Vol.ASSP-33, No.2, April 1985, pp.387-392.

[10]: A.W. Rudge, K. Milne, A.D. Olver and P. Knight, *"The Handbook of Antenna Design - Volume 2"*, Peter Peregrinus Ltd.,1983.

[11]: T.J. Shan, M.W. Wax and T. Kailath, *"On Spatial Smoothing for Direction-of-Arrival Estimation of Coherent Signals"*, IEEE Transactions on Acoustics, Speech & Signal Processing, Vol.ASSP-33, No.4, Aug. 1985, pp.806-811.

[12]: S.U. Pillai and B.H. Kwon, *"Forward/Backward Smoothing Techniques for Coherent Signal Identification"*, IEEE Transactions on Acoustics, Speech & Signal Processing, Vol.ASSP-37, No.1, Jan. 1989, pp.8-14.

[13]: B.H. Kwon and S.U. Pillai, *"A Self Inversive Array Processing Scheme for Angle-of-Arrival Estimation"*, Signal Processing (Netherlands), Vol.17, No.3, July 1989, pp.259-277.

[14]: R.T. Williams, S. Prasad, A.K. Mahalanabis and L.H. Sibul, *"An Improved Spatial Smoothing Technique for Bearing Estimation in a Multipath Environment"*, IEEE Transactions on Acoustics, Speech & Signal Processing, Vol.ASSP-36, No.4, April. 1988, pp.425-431.

[15]: M. Wax, T.J. Shan and T. Kailath, *"Spatio-Temporal Spectral Analysis by Eigenstructure Methods"*, IEEE Transactions on Acoustics, Speech & Signal Processing, Vol.ASSP-32, No.4, Aug. 1984, pp.817-827.

[16]: H.M. Bayri, D.R. Ucci, J.C. Hantgan and C.C. Yeh, *"A Technique for Reducing the Effect of Mutual Coupling in Adaptive Arrays"*, 1987 IEEE Military Communications Conference, MILCOM 87, USA, Vol.1, 19th - 22nd Oct. 1987, pp.285-288.

CHAPTER 6

DIRECTION FINDING IN THE CELLULAR LMR ENVIRONMENT: AN EXPERIMENTAL SYSTEM

In the last chapter, the operation of the source estimation process of the proposed base-station antenna system was modelled in a variety of signal conditions. The results clearly demonstrated the feasibility of a direction finding (DF) process, and several observations were made regarding the most suitable choice of DF algorithm for each of the environments considered. In order to take the work one stage closer to an operational system, an experimental DF receiver was constructed to verify the findings from the computer simulations. This chapter includes a description of a four channel DF receiver architecture which operates at 1529.625 MHz.

The computer simulations described in chapter 5 also demonstrate the degradation in the performance of the various DF algorithms caused by mutual coupling and receiver channel mismatch. The results of an array calibration process presented here, clearly underline the importance of the array manifold if the receiver is to be reliably employed in the field. Extensive field trials have been carried out in predominantly urban surroundings, and the results from some of the trials are presented and discussed in detail. Finally, some attention is given to the practical realisation of a DF receiver for land mobile radio operation.

The operating frequency of the experimental system was chosen in the range 1.5 GHz to 2.0 GHz even though the second generation Pan European GSM system, due to come into operation in 1992, operates around 900 MHz. The main reason for this is that the current trend for future mobile radio communications is moving towards the higher frequency bands, especially with the recent frequency allocations for the future Personal Communication Networks (PCN's). A test license was granted for operation at 1529.625 MHz and although only a CW transmission format was permitted, this was sufficient for the requirements of the work since the aim here is to only demonstrate the principles of operation.

6.1 FOUR CHANNEL DF RECEIVER

To date, most of the published research on AOA estimation using antenna arrays has primarily employed computer simulations to compare and investigate new algorithms. Exceptions to this include Evans *et al* [1] who have carried out field trials at L and C bands in order to analyse the effects of coherent multipath. Schmidt [2] has also constructed an experimental eight channel receiver operating at 1.8 GHz to validate the performance of the MUSIC algorithm, and Scott [3] has carried out similar trials at 15 MHz and 70 MHz. Each of these systems comprised of an N element antenna array with N receiving channels to simultaneously downconvert the signals received at each element to a frequency suitable for digitising and subsequent processing. This was the approach adopted here and a schematic of the receiver architecture is illustrated in figure 6.1. Based on the results of the simulation work and the fact that the field trials would initially only employ a single mobile source, the receiving array structure was chosen to be a linear array of four antenna elements with half wavelength spacing. This would ensure that there was sufficient resolution to study the angular spread due to scattering in an urban locality, without placing too significant a burden on the hardware requirements and the time available to construct the receiver. Also there are sufficient degrees of freedom to extend the single source scenario to consider multiple mobiles with either a different frequency allocation or time slot in subsequent studies. In the following sections each subsystem of the receiver is addressed separately.

6.1.1 Antenna Array

Two different types of antenna element were employed in the experimental system, and these were a centre fed half wavelength dipole and a microstrip patch. Each array consisted of four elements with half wavelength spacing (9.8cm at 1529.625 MHz), and photographs of the complete array structures are shown in figures 6.2. The dipole array was chosen initially since it is very straight forward to fabricate and, with a ground plane at a distance of $\lambda/4$ behind each element, the forward gain can be increased as well as reducing ambiguities caused by reflections from behind the array. Without the ground plane, each dipole has a nominal gain of 2.1 dB in free space, increasing to 7.6 dB over a ground plane [4][5]. The azimuth radiation patterns for each element in the array were measured in an anechoic Chamber (3m $\times$ 6m) using the

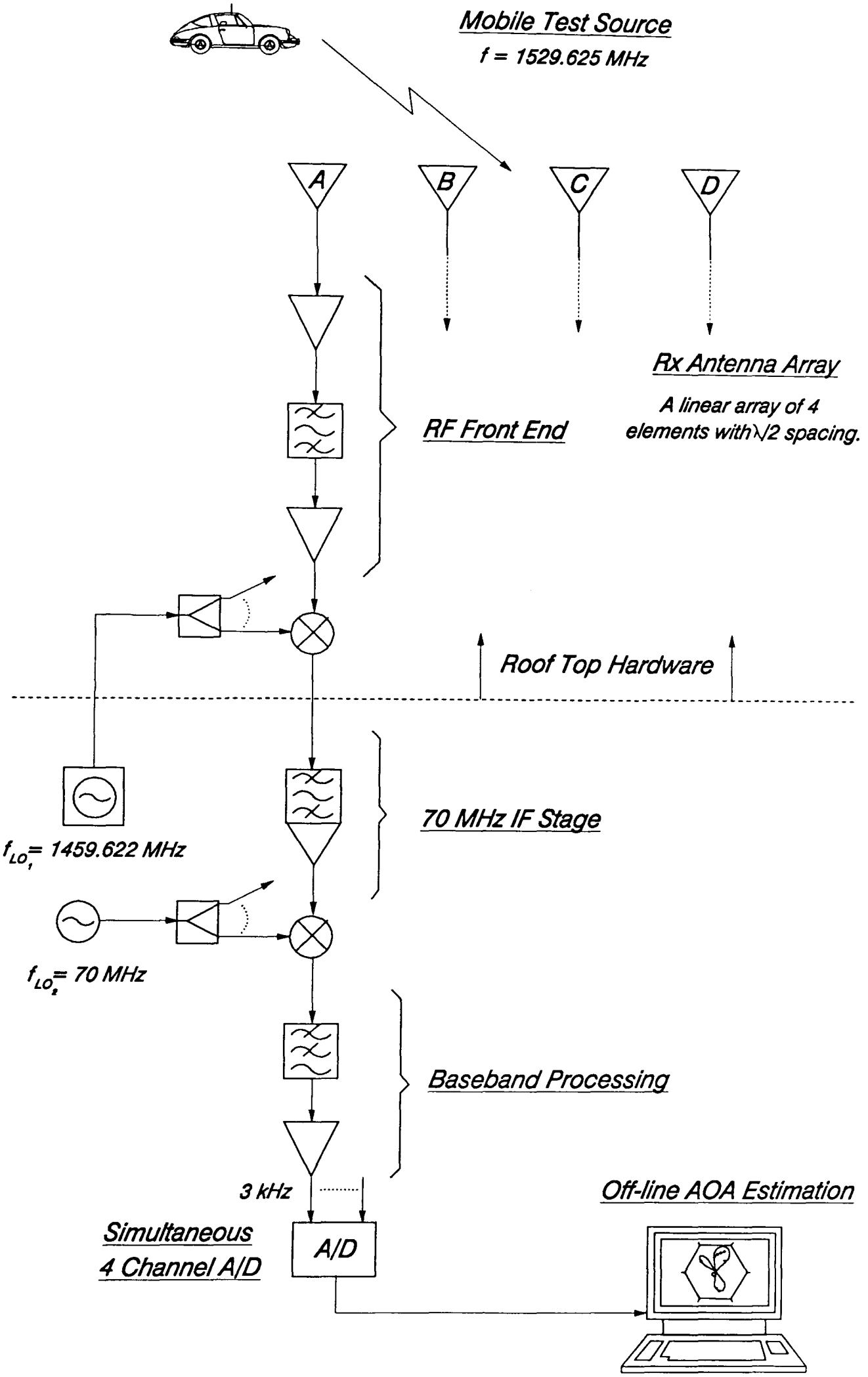

Figure 6.1: Four channel DF receiver architecture.

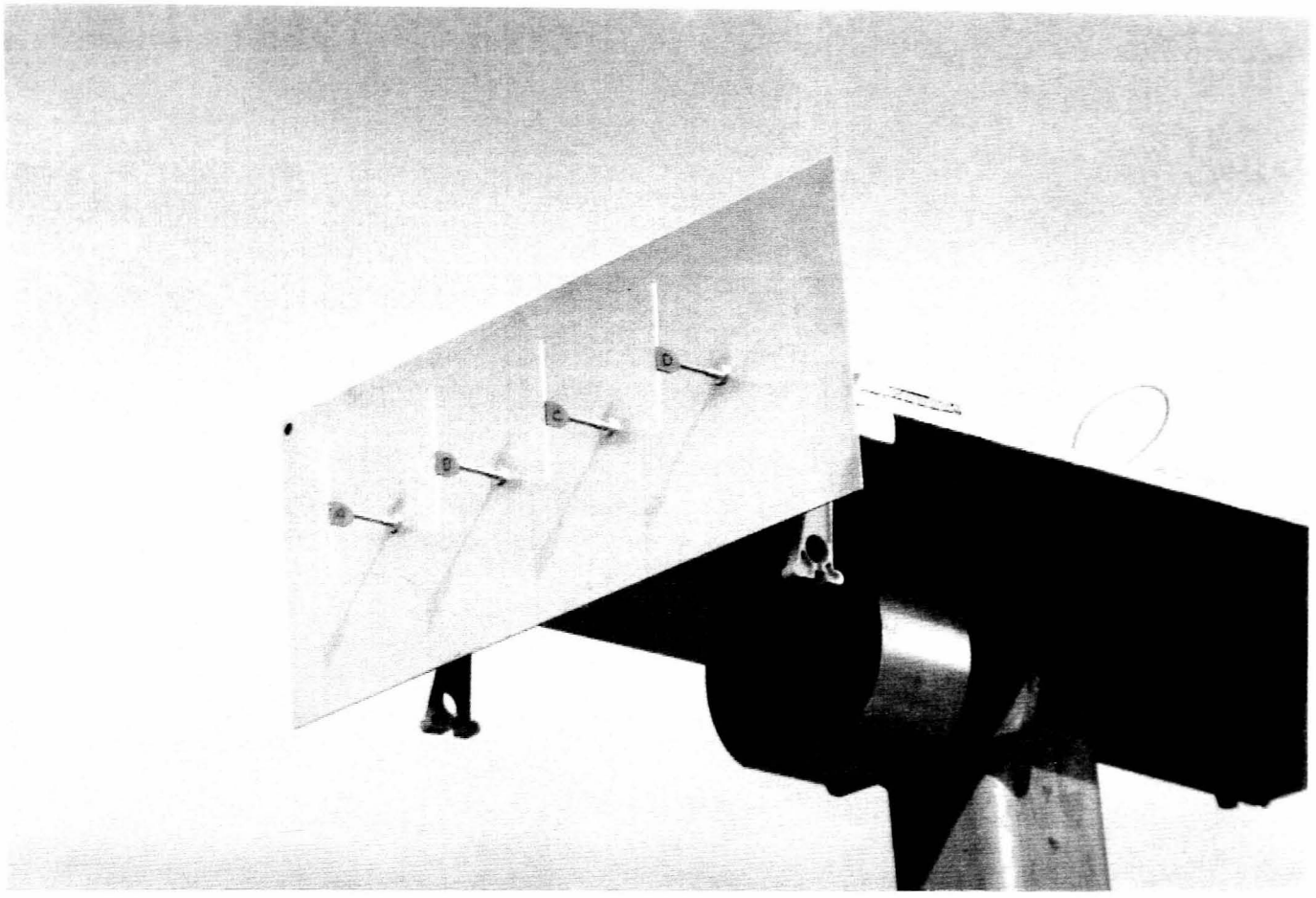

(a)

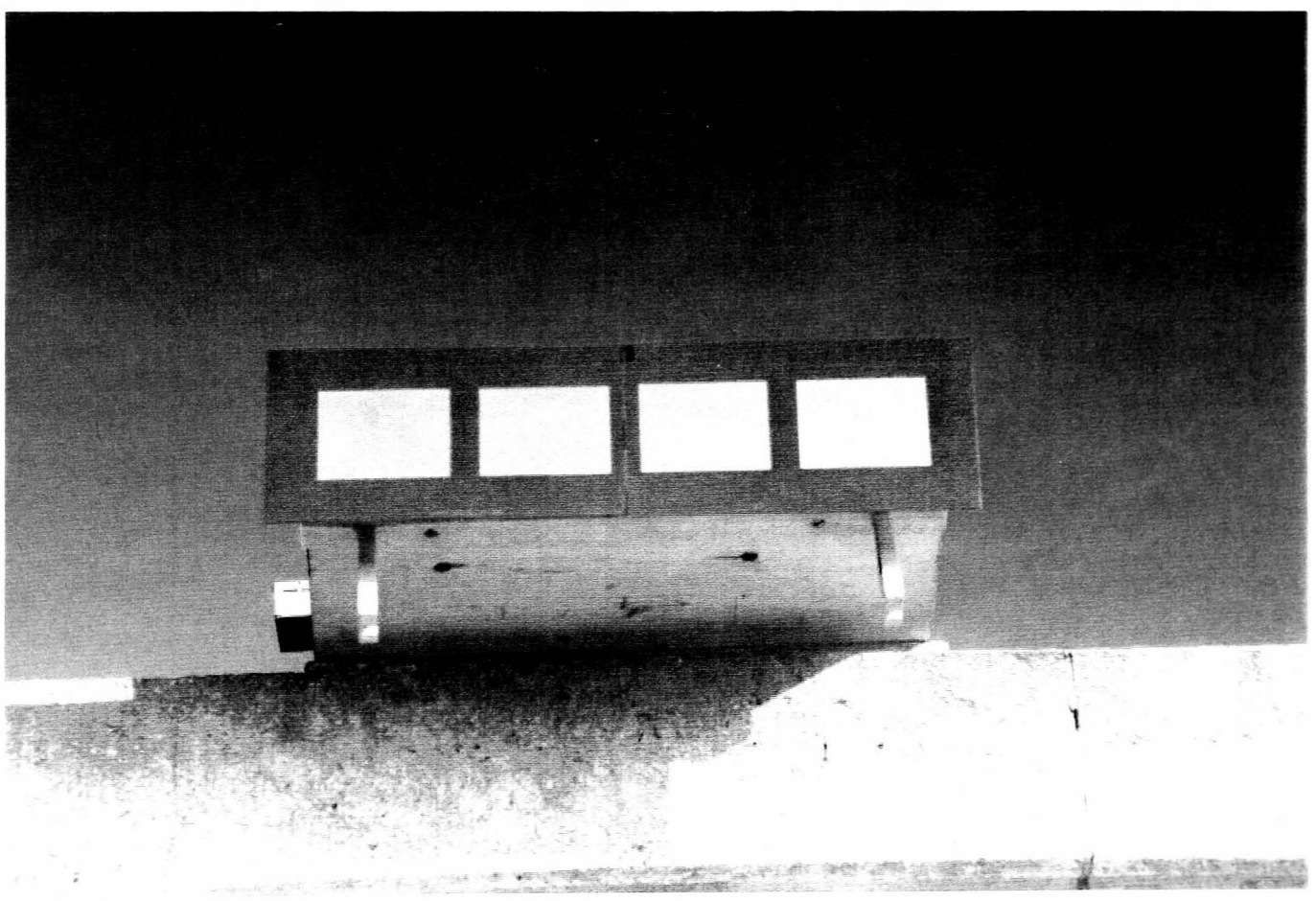

(b)

Figure 6.2: Four element antenna arrays for DF receiver: (a) the dipole array; (b) the patch array.

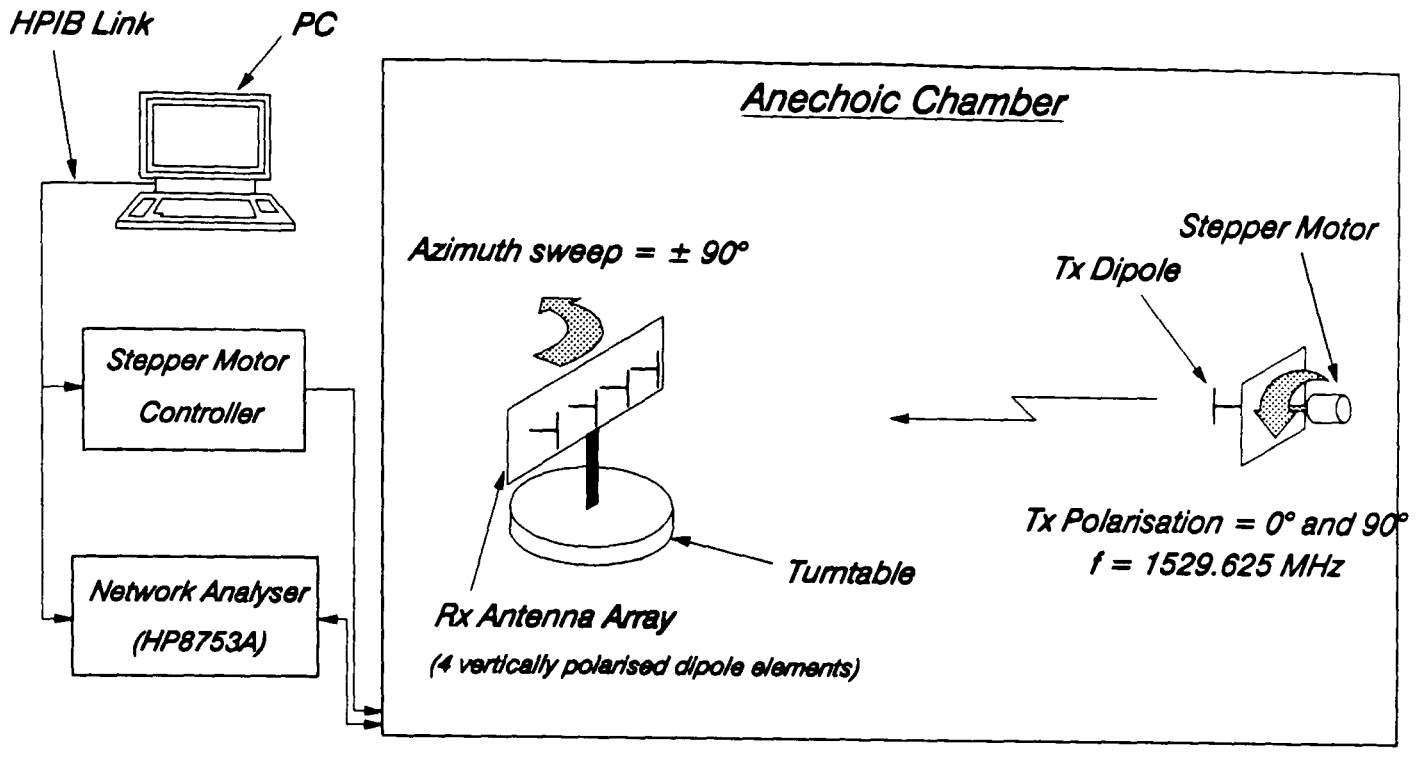

Figure 6.3: Antenna pattern measurement.

set-up shown in figure 6.3, and the results are given in figure 6.4. (Note that when measuring the response of each element all the other elements were terminated in a 50Ω load.) The co-polar response for each element clearly illustrates the strong effect of neighbouring elements on the overall shape of the pattern and this is attributed to mutual coupling effects.

Microstrip patch antennas have received widespread interest over the past decade and, more recently, have been considered for application in mobile radio [6]. Therefore it was decided to design and fabricate a four element patch array as shown in figure 6.2b. The microstrip patches were etched on RT/duroid® substrate, and the relevant substrate parameters are:

- Substrate thickness, h = 0.0625″ (1.5878mm)
- Dielectric constant, ε_r = 2.2
- Conductor thickness, t = 0.0014″ (0.03556mm)

The dimensions of a single patch are shown in figure 6.5a, and figure 6.5b illustrates how each patch was back fed using a standard SMA socket. A single patch has a nominal gain of approximately 5 dB, and the measured antenna patterns for each element are given in figure 6.6. Note the more uniform response of the co-polar patterns which is the result of reduced mutual coupling between elements. The design procedure for microstrip patch antennas is not within the scope of this study, and further details can be found in the text of James and Hall [6].

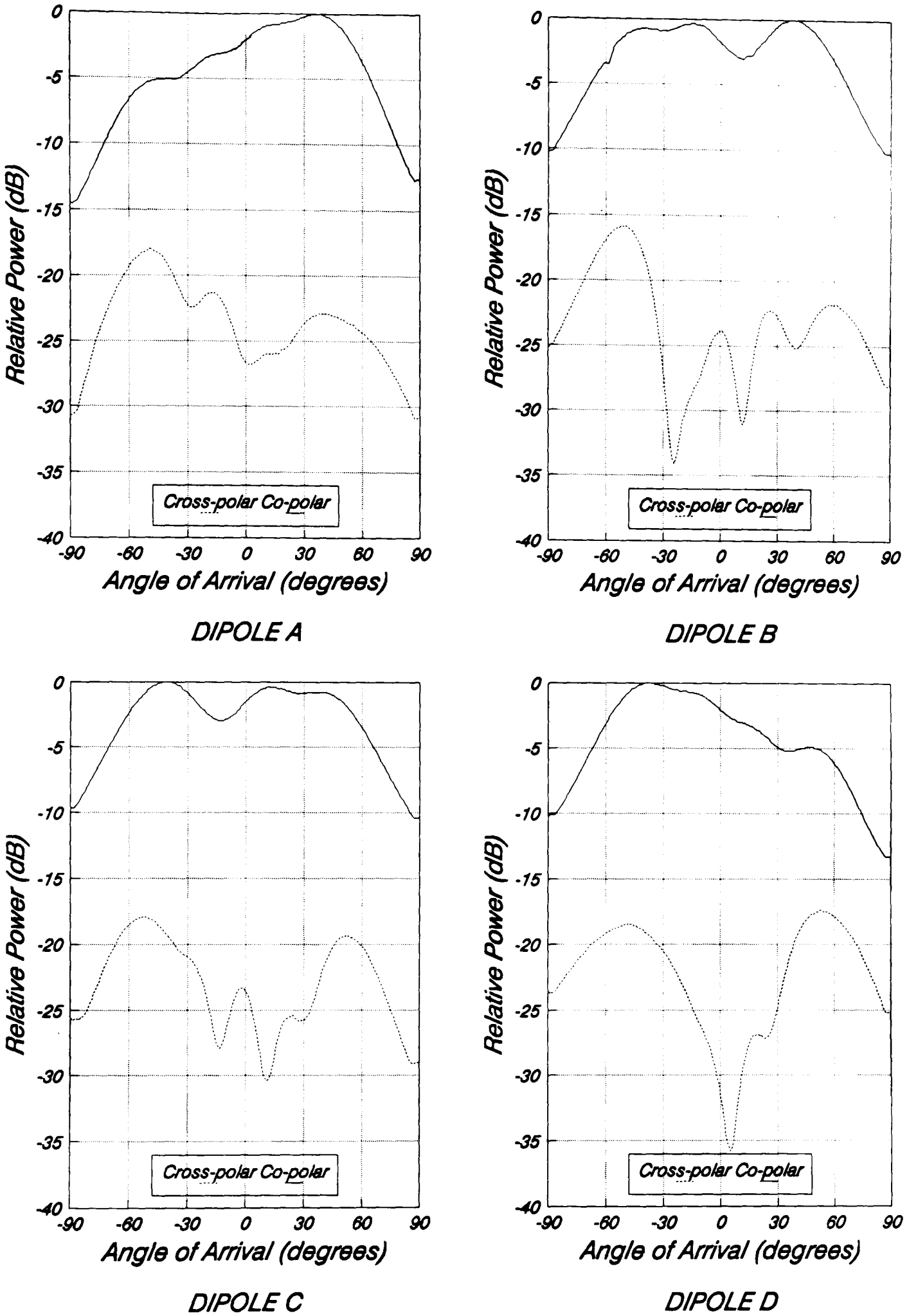

Figure 6.4: Azimuth radiation patterns for each element of the dipole array.

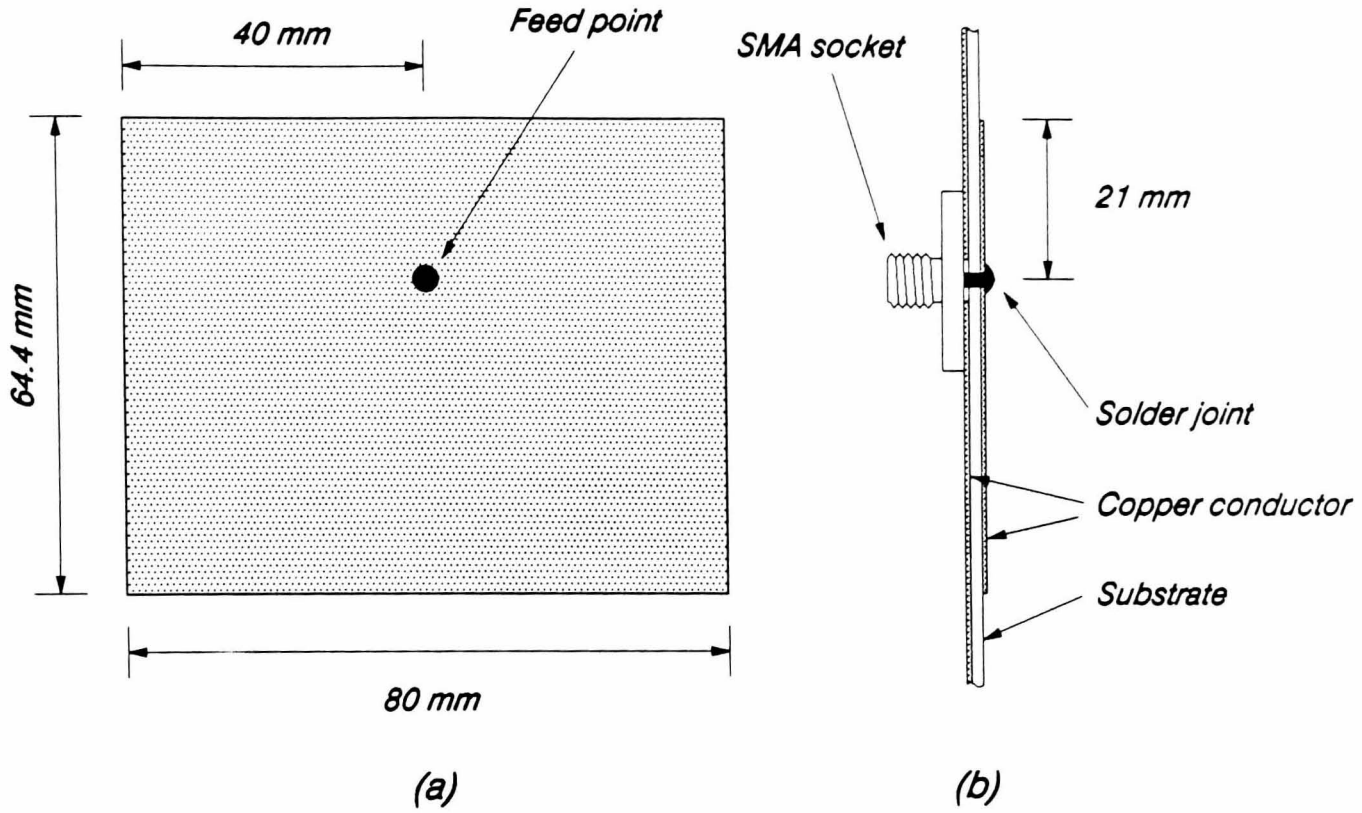

Figure 6.5: Dimensions of a single microstrip patch antenna element: (a) top view; (b) cross section.

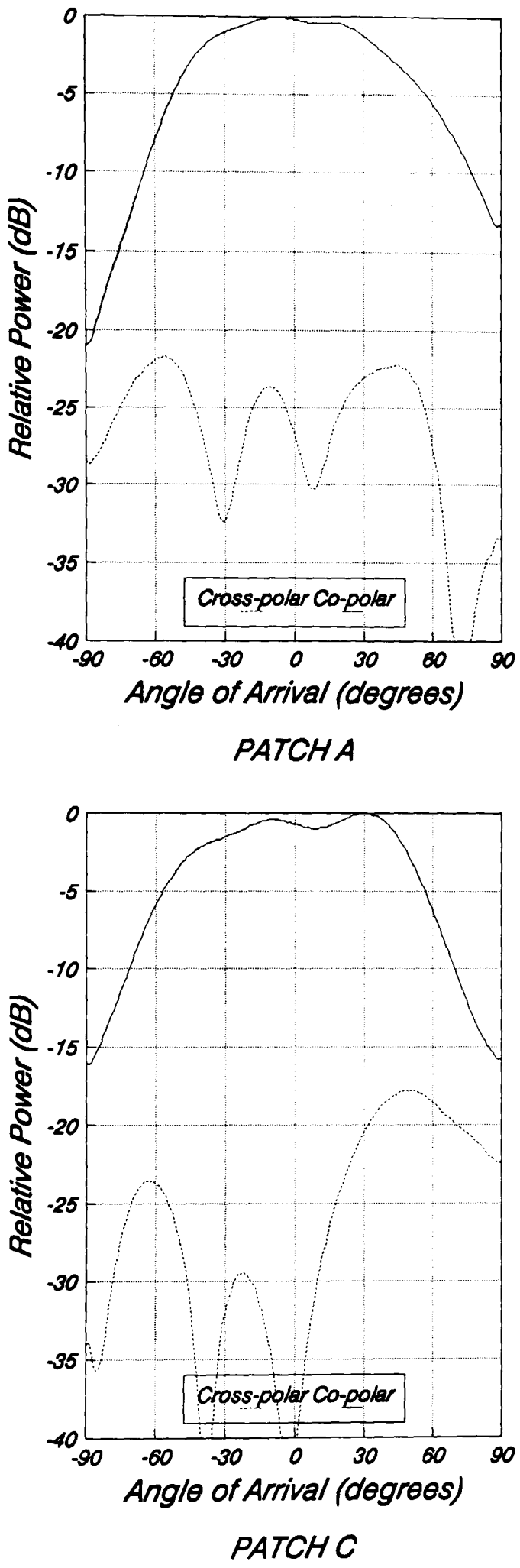

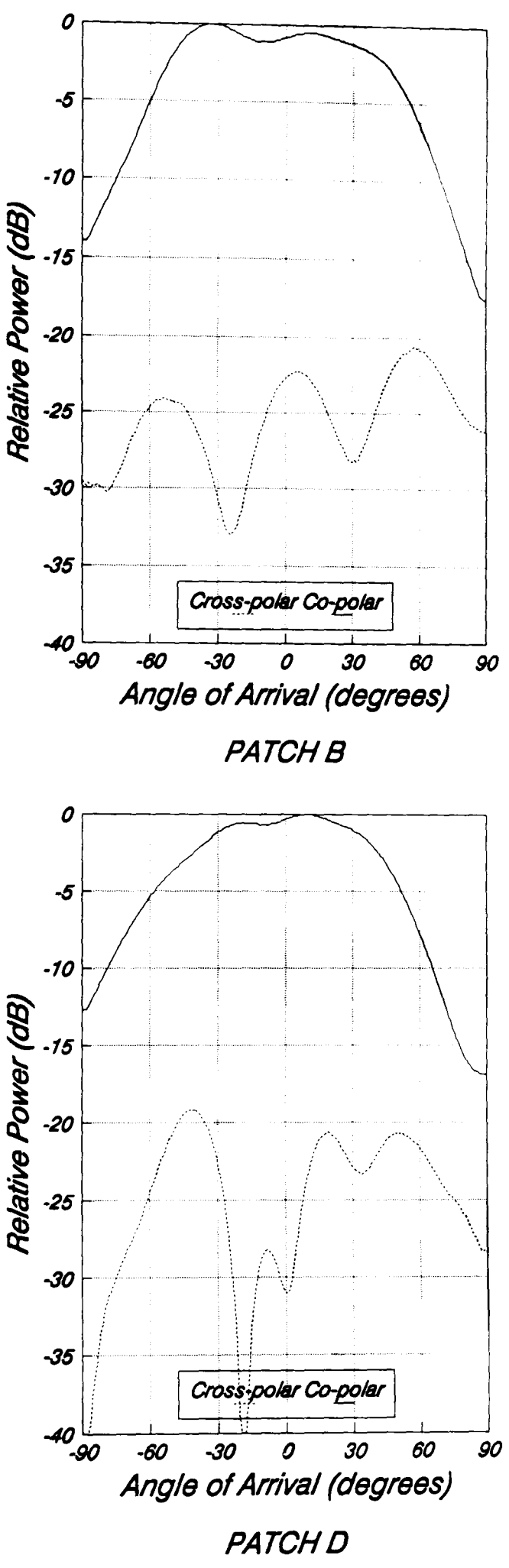

Figure 6.6: Azimuth radiation patterns for each element of the patch array.

6.1.2 RF Front End

The receiver front end consists of a low noise amplifier (LNA) followed by an interdigital bandpass filter and some additional RF gain. The LNA was based on a design already developed by Beach [7][8] for reception of an Inmarsat satellite communications channel for Land Mobile Satellite operation. The low noise performance is achieved using a balanced configuration of two GaAs FET devices (Avantek ATF-10135), employing a Wireline® hybrid coupler to provide the input and output match. The nominal specifications for this amplifier are as follows:

- Gain, $G \geq 15$ dB
- Noise Figure, $NF \leq 1.0$ dB

The interdigital bandpass filter was based on a microstrip design given in a Mullard Technical Note [9], and comprises of a number of parallel quarter wavelength coupled lines which, when grounded at one end, act as resonators at the required centre frequency. When implemented on microstrip, it is possible to produce very compact designs which are very straight forward to fabricate, although air spaced elements in a self supporting structure will minimise the dielectric loss associated with a microstrip substrate [10]. Following the design procedure in the Technical Note, the parameters for a seven element filter were simulated on the EESOF RF CAD package. The design was then optimised to have a insertion loss of less than 0.5 dB with a bandwidth of 150 MHz, before generating a mask and etching onto Ultralam™ 2000 microwave laminate (substrate thickness, h = 0.03″, dielectric constant, $\varepsilon_r = 2.45$, and thickness of copper conductor, t = 0.0014″). The simulation results turned out to be rather optimistic, with the response of the best filter measured as:

- Insertion Loss, L = 1.7 dB
- 3 dB Bandwidth, BW_{3dB} = 120 MHz

The two main factors causing the discrepancy between the measured and simulated responses, are the etching process and the method of grounding the filter elements. The etching process introduces errors of up to 0.1 mm and, as can be seen from the sketch of the filter mask in figure 6.7 (not to scale), this can be very significant. The RF CAD software was used to simulate the effects of these errors and demonstrated clearly the problems

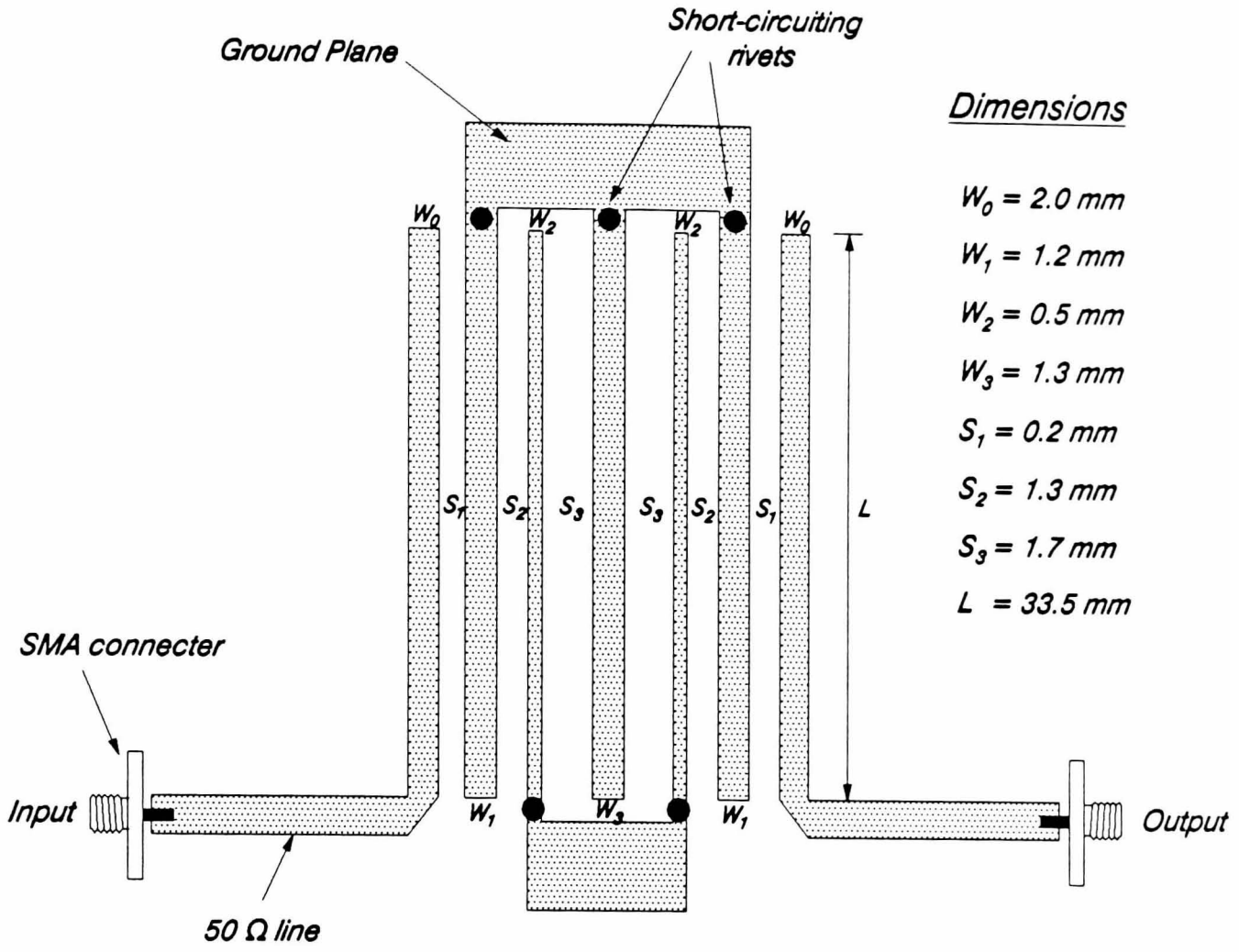

Figure 6.7: Dimensions of microstrip interdigital bandpass filter design.

caused by the etching process. The second problem with the design was the method of grounding the filter elements which was achieved in practice by drilling through the dielectric and using short-circuiting rivets to obtain a connection to the lower ground plane. This proved to be very unsatisfactory and difficult to model, however the best results were obtained with the design shown in figure 6.7 since, as well as the short-circuiting rivets shown, additional rivets placed in the ground plane ensured an adequate earth connection, minimising the inductance of the earthing pins. In spite of all these problems the response obtained was sufficient for the required task, although a more detailed model of the filter would probably produce a clearer insight into some of the problems associated with the implementation of this type of filter in microstrip.

Further RF amplification was provided using the Mini Circuits MAR-6 silicon bipolar monolithic microwave integrated circuit (MMIC) (equivalent to Avantek's MSA-0685), and provides RF amplification suitable for operation in a 50Ω system. At 1.5 GHz the device is specified to have a gain of 14.1 dB

with an input return loss of -13.6 dB (corresponding to an input VSWR[1] of 1.53). The device can also be cascaded, although in practice this was found to be limited to only two devices on the same piece substrate. Hence, a dual stage and a single stage amplifier were constructed, providing an overall RF gain of approximately 42 dB. Masks for the amplifiers were developed using the EESOF RF CAD package before etching onto Ultralam™ 2000 laminate.

Table 6.1 contains the measured gains and input VSWR of the individual RF blocks for each of the receiver channels, A, B, C and D. The noise figure for the LNA was measured using the EATON 2075 Noise Gain Analyser. This instrument was also used to measure the noise figure and gain of the complete RF front end for each of the four channels, and the values are given in the final column of the table.

	LNA			Filter		Single Amp.		Dual Amp.		Total Resp.	
	Gain*	NF†	VSWR	Gain*	VSWR	Gain*	VSWR	Gain*	VSWR	Gain*	NF†
A	14.5	1.05	1.3	-1.7	1.1	13.8	1.9	26.7	2.4	53.0	1.22
B	15.0	1.04	1.5	-1.8	1.3	13.8	1.9	26.5	2.4	53.7	1.15
C	15.2	1.15	1.2	-2.2	1.6	13.8	1.9	26.9	2.4	52.5	1.24
D	15.1	1.20	1.2	-1.8	1.3	13.7	1.9	26.4	2.3	53.7	1.51

* All signal gains are given in dB.
† The Noise Figure of the device in dB.

Table 6.1: Measured parameters RF front end.

6.1.3 70 MHz IF Stage

The RF signals were mixed down to a 70 MHz intermediate frequency (IF) using a Mini-Circuits SRA2000 double balanced mixer. The local oscillator was provided by a HP8341B Synthesised Sweeper which was split into four using a 4-way power divider implemented with Wireline®. The mixer LO ports were

---

1: Voltage Standing Wave Ratio.

driven with +4 dBm and, at this frequency, had a loss varying from 8 to 11 dB across all four devices selected. The four IF channels were now taken down from the antenna site on the roof using four 55 ft lengths of RG213/U coaxial cable (0.8 dB loss at 70 MHz) for further processing in the laboratory. This comprised of some additional filtering and gain at 70 MHz before finally mixing down to a 3 kHz baseband signal prior to digitising.

The initial approach employed a 70 MHz tuned amplifier stage, designed using a BFY90 transistor. This provided approximately 25 dB of gain with a 3 dB bandwidth of between 4 and 5 MHz, and was ideal for the task required. Unfortunately, such highly tuned active circuits are susceptible to environmental conditions causing variations in the passband characteristics, as well as non-linear phase variations as the input signal level fluctuates. This is a most undesirable phenomenon since it is the relative phase difference between the channels that defines the AOA of the incident signal. Ideally, the phase of this stage should not alter as the input drive varies and a more suitable device was the Plessey SL610C IF amplifier. A simple LC bandpass filter was designed to precede the amplifier, and the measured responses are given in table 6.2 below. The phase characteristics of this device were excellent as well as proving to be much more stable than the 70 MHz tuned amplifier stage.

	70MHz Amplifier	
	Gain (dB)	3dB BW (MHz)
A	25.4	3.7
B	25.7	3.8
C	25.9	4.3
D	25.2	3.6

Table 6.2: Measured response of IF filter and amplifier

An unfortunate drawback with the Plessey amplifier is apparent when the output is connected directly to the RF port of the mixer (Mini-Circuits TFM-2 double balanced mixer) for the final downconversion to baseband. As the

signal level is increased to the value required to provide sufficient drive for the A/D converters, the baseband signal is seen to distort. This is attributed to the inherent mismatch between the SL610C output and the TFM-2 mixer, and can be reduced by inserting a 3 dB pad. Although this decreases the available signal gain, additional amplification was provided at baseband to compensate.

6.1.4 Baseband Processing

As already mentioned, a Mini-Circuits TFM-2 double balanced mixer was employed for the final downconversion to baseband. The 70 MHz local oscillator was provided by a straight forward active crystal oscillator circuit, and was split into four using a Mini-Circuits 4-way power splitter (PSC-4-3). Normally at this stage, downconversion is achieved with a quadrature local oscillator to provide the inphase and quadrature (I & Q) components of the signal, thus maintaining full phase and amplitude information. However, this approach requires additional hardware and therefore it was decided to carry out the I & Q processing after digitising the channels with the use of the Hilbert Transform. Immediately after the mixer is a second order low pass Butterworth filter with a cut-off frequency of 5 kHz. This is followed by a standard inverting operational amplifier circuit with a variable voltage gain of between 25 and 33 to enable some compensation to be made for signal level fluctuations between the channels, as well as ensuring that there is sufficient drive available for the A/D converter (±4 volts for full scale conversion). At this stage it was not considered necessary to implement any kind of automatic gain control due to the added complexity and the nature of the mobile radio signal environment.

The complete receiver chain was initially tested in an anechoic chamber with the set-up shown in figure 6.8. From classic antenna theory the ratio of the received signal power to the transmitted signal power in free space is given by

$$\frac{P_R}{P_T} = G_T G_R \left(\frac{\lambda}{4\pi R}\right)^2 \qquad (6.1)$$

The power attenuation in decibels is $a_{dB} = 10\log_{10} P_T/P_R$, which can be expressed as

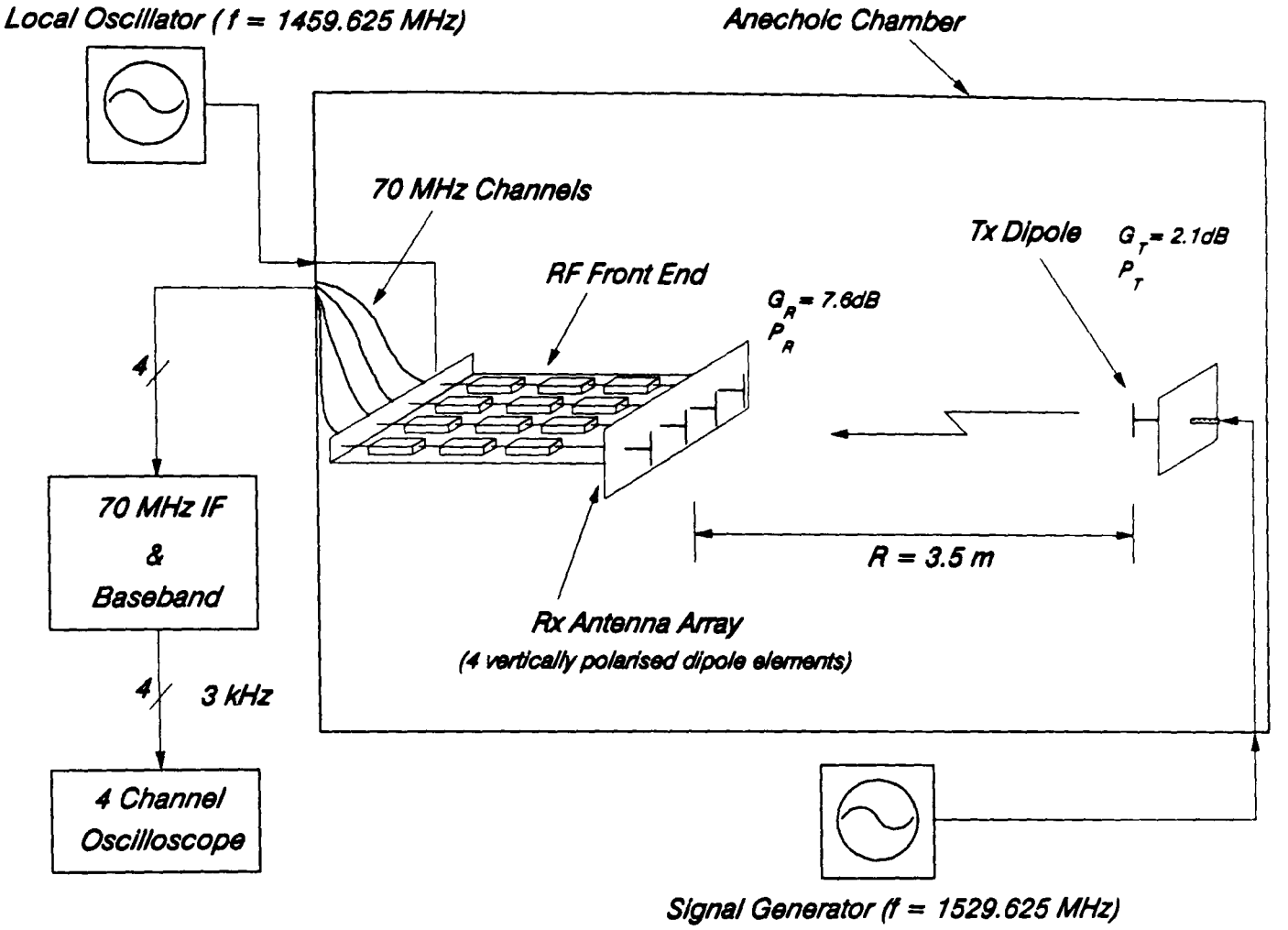

Figure 6.8: Testing the receiver chain in the anechoic chamber.

$$a_{dB} = 22 + 20log_{10}\left(\frac{R}{\lambda}\right) - G_T - G_R \qquad (6.2)$$

If the dipole array is used as the receiving antenna as shown in figure 6.8, then the the free space attenuation can be calculated from equation (6.2) as

$$\begin{aligned} a_{dB} &= 22 + 25 - 2.1 - 7.6 \\ &= 37.3 \text{ dB} \end{aligned} \qquad (6.3)$$

With the transmitter power adjusted to give a ±4 volt swing at baseband, P_T = -37 dBm giving the received signal power as

$$P_R = -37 - a_{dB} = -74.3 \text{ dBm} \qquad (6.4)$$

If channel A is considered, the signal level prior to the final downconversion can then be calculated as follows:

Power received, P_R	-74.3 dBm
Gain of RF front end	+53.0 dB
Mixer Losses	-8.0 dB
Cable losses	-0.8 dB
Gain at IF	+25.4 dB
3 dB pad	-2.8 dB
Signal power at 70 MHz	-7.5 dBm

This result compares very well with the measured response of the receiver. Photographs of the two main hardware blocks of the DF receiver, namely the RF front end and the IF to baseband downconversion stage, are shown in figure 6.9.

6.1.5 Analogue-to-Digital Conversion

As already discussed at some length, the crux to accurately estimating the AOA's of the incident signals is the determination of the inter element phase shift ϕ (Appendix C, equation (C.2)). In order to achieve this, all of the channels must be digitised simultaneously, thus requiring in this case a four channel parallel A/D conversion. The chosen device was the Maxim MAX150 8 bit A/D converter, offering a fast conversion time (1.34 μsec max.), a built in sample and hold function, and a straight forward microprocessor interface. For single channel operation, the maximum sampling frequency when operating in the WR-RD mode is approximately 588 kHz. This mode of operation allows all four converters to simultaneously sample the incoming channels and then hold the data, enabling each device to be read sequentially before initiating another conversion. With four channels operating, the maximum sampling frequency is governed by the speed of the external microprocessor controlling the converters, although with an input signal of 3 kHz, the chosen sampling frequency of 15 kHz was well within the capabilities of the device. This is also greater than the Nyquist sampling rate[2] but ensures that the signal can be reconstructed fully.

2: To ensure signal recovery, the sampling rate must be greater than twice the highest frequency component of the input signal.

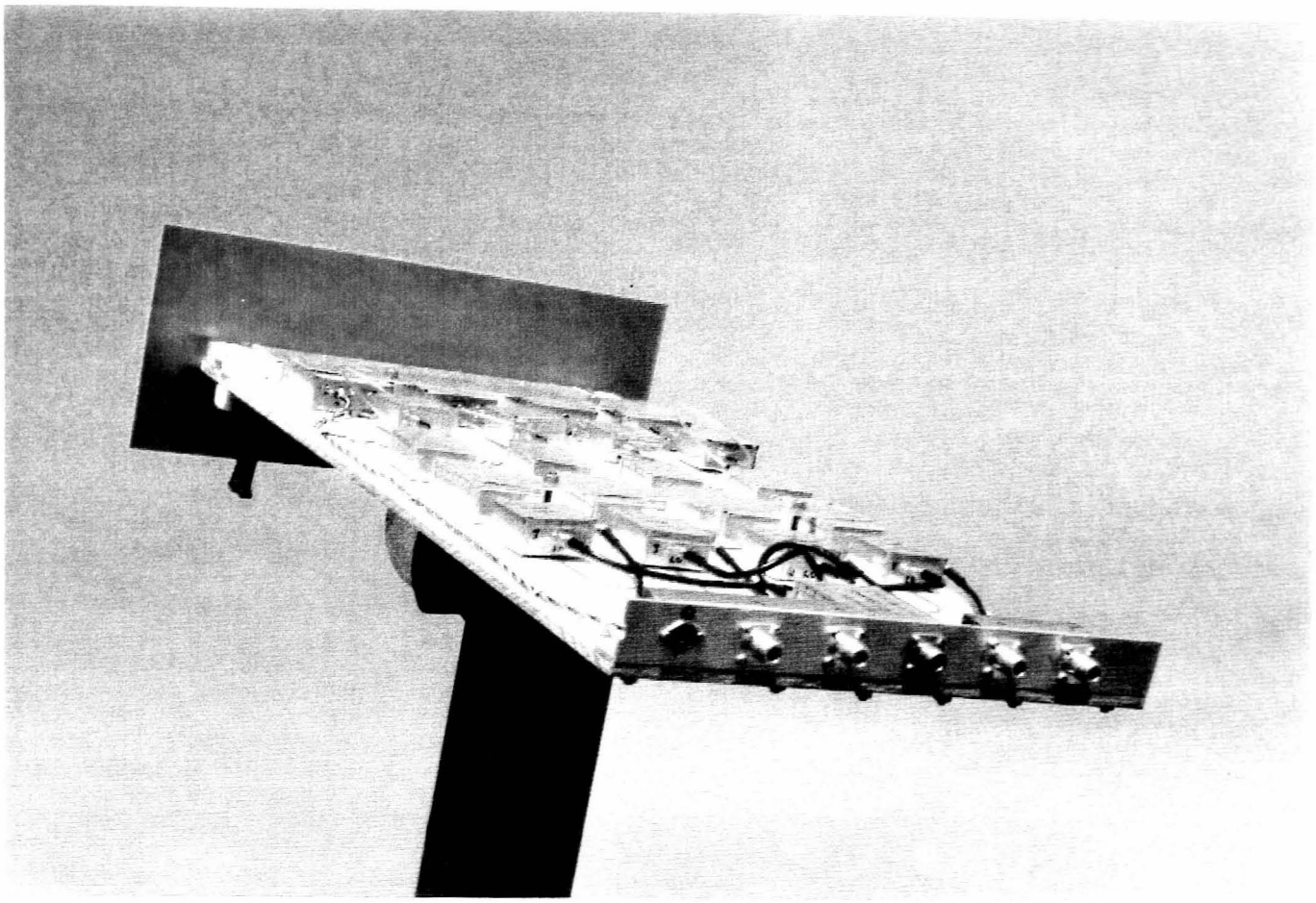

(a)

(b)

Figure 6.9: The complete DF receiver hardware: (a) RF front end; (b) IF to baseband downconversion unit.

The obvious choice for the microprocessor was one of the Texas Instruments TMS320 family since ready made general purpose boards had already been developed within the Communications Research Group. However, the project had recently received on loan from INMOS a B009 Transputer Evaluation Board [11] for installation in a Personal Computer (PC). This board is equipped with a T800 32 bit transputer, a T212 16 bit subsidiary transputer, as well as four A100 cascadable signal processors, and thus provides a very powerful processing tool[3]. A package called the Transputer Development System (TDS) [13] which runs on a PC was also provided, and this enables OCCAM code to be written, compiled, debugged, and finally run on the B009 board. Compilers also exist which would enable code written in Pascal, C or Fortran to be downloaded onto the transputer thus making the B009 a very attractive option. There is also an external interface available enabling extra transputers to be added, and so it was decided to utilise the B009 to control the A/D process and to then collect and process the data from the DF receiver. Initially, the board was only employed to file the received data for later off-line signal processing, although there is the potential for utilising the speed and versatility offered by parallel processing techniques to provide on-line AOA estimation at a later date.

The interface between the B009 board on the PC and the A/D converters was provided with a T222 16 bit transputer [12]. A board was designed to hold this chip, with a serial link running at 20 MHz connecting it directly to the T800 transputer on the B009 board. 32k $\times$ 16 bit of external RAM memory was also provided on the T222 board, and a PAL device was programmed to memory-map the A/D converters onto the T222 transputer. A schematic of the complete layout is shown in figure 6.10. A self-contained program written in OCCAM was downloaded onto the external T222 via the serial link using the TDS, and a program running on the T800 transputer was then employed to completely control the A/D process and to file the resulting data. Figure 6.11 illustrates the principle processes involved in this task, also demonstrating where some simple parallel processing techniques were employed to speed up the data throughput.

3: For further details on these transputers please refer to "The Transputer Data Book" [12].

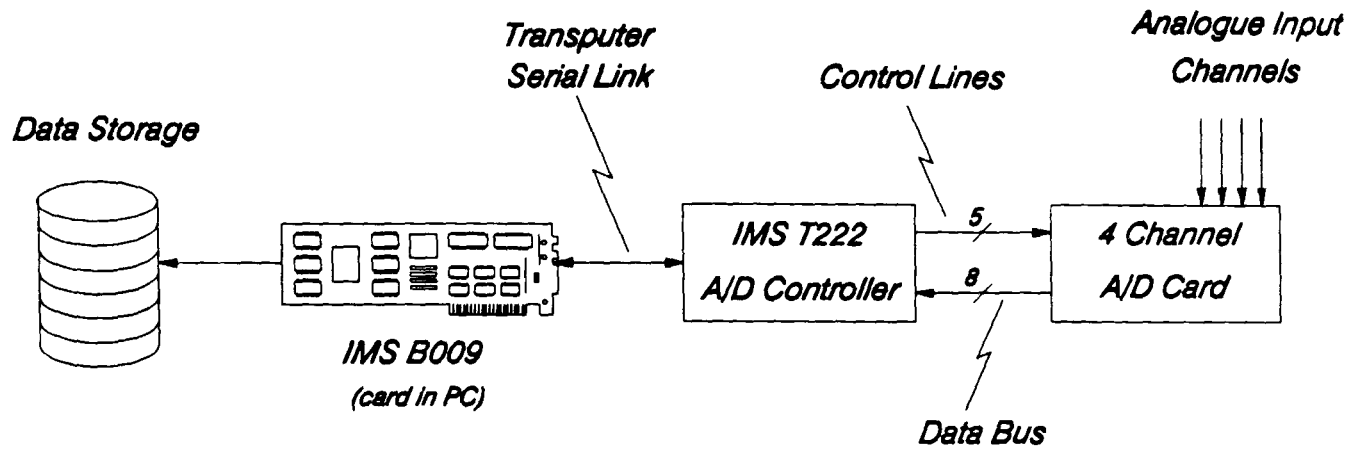

Figure 6.10: Schematic of data acquisition hardware.

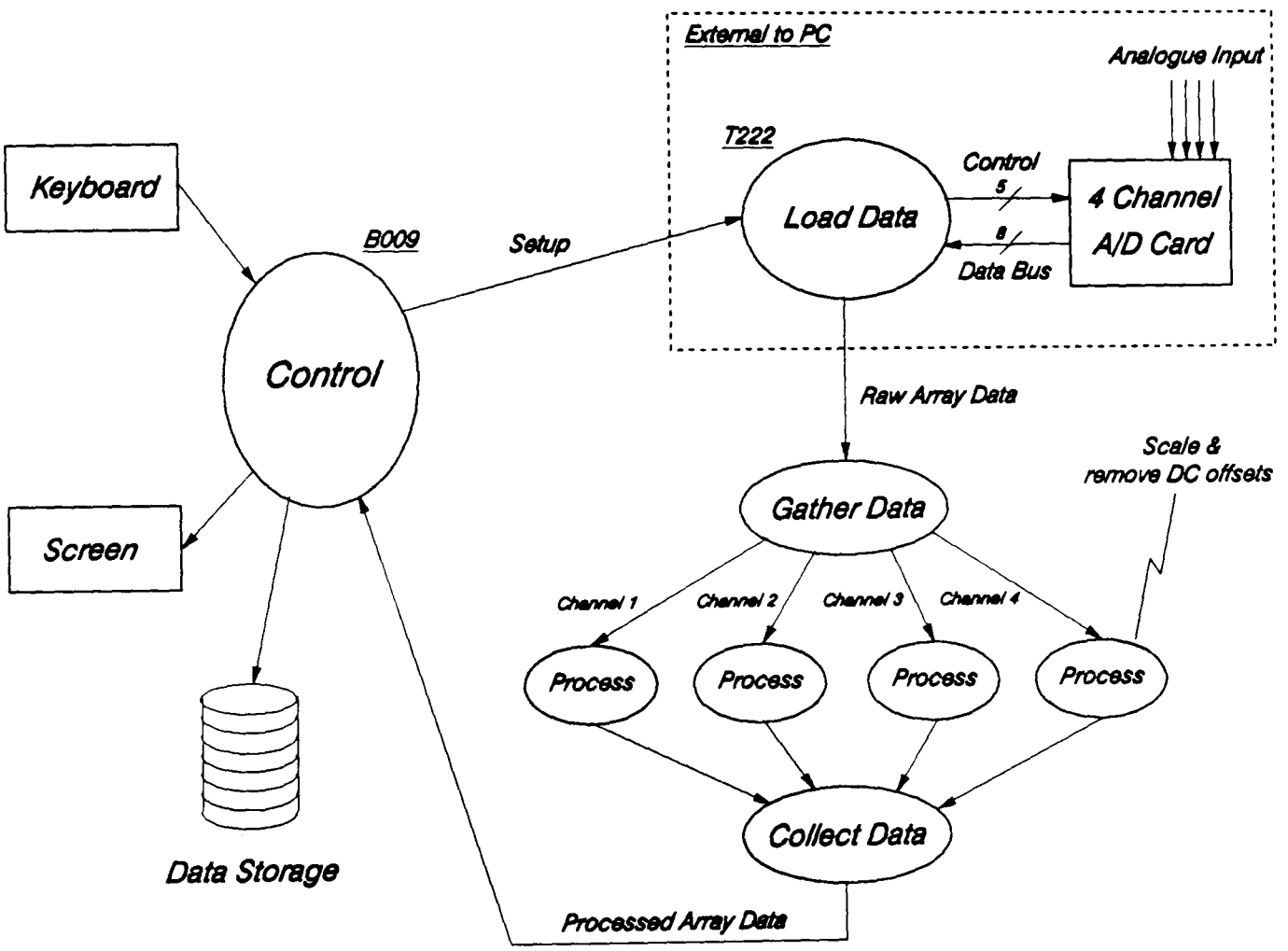

Figure 6.11: Processes involved in array data acquisition.

6.1.6 Off-line AOA Estimation

Estimation of the spatial spectrum from the stored array data was carried out using a software package called PC-MATLAB (developed by *The Math Works Inc.*). This package was chosen because, as well as providing a powerful programming language, it offers a complete library of routines for matrix computations, both real and complex. Antenna array processing inherently involves vector and matrix algebra and so, combined with an extensive graphics library (including three dimensional mesh plots), MATLAB provides an ideal environment for the processing of the received array data. A complete block diagram of the process, starting with the data acquisition, is given in figure 6.12. The Hilbert transform was implemented digitally with a 25 tap FIR filter designed using the *Digital Filter Design Package* (developed by Atlanta Signal Processors, Inc.).

6.1.7 Mobile Test Source

A mobile test source was required to transmit a CW tone at 1529.625 MHz, and a block diagram of the complete transmitter is shown in figure 6.13. The vehicle used was an Austin Montego Estate car which belongs to the Electronic Engineering Department and is equipped with a mains inverter to provide the necessary power for the transmitter circuits. A quarter wavelength monopole antenna over a ground plane was employed as the transmit antenna. The output of the signal generator after doubling (the maximum output frequency of the HP8656B is 990 MHz) provides the drive for a 100 mW preamplifier stage prior to a 1 W power amplifier. The 100 mW stage is a linear preamplifier, employing an Avantek AT42085 bipolar transistor followed by a MSA-0520 monolithic amplifier, and the 1 W stage is a Class C amplifier employing the Acrian ACR2001 device. The input and output matching networks for both amplifiers were designed using microstrip equivalents for lumped components. Further details of the design and performance of these amplifiers is included in [14]. Since no facility for power control was provided at the receiver, the transmit power level had to be controlled to avoid over-driving the digitisers. This was achieved with a switched attenuator block, enabling the transmit power to be varied within the range 0 dBm to 30 dBm (1 mW to 1 W).

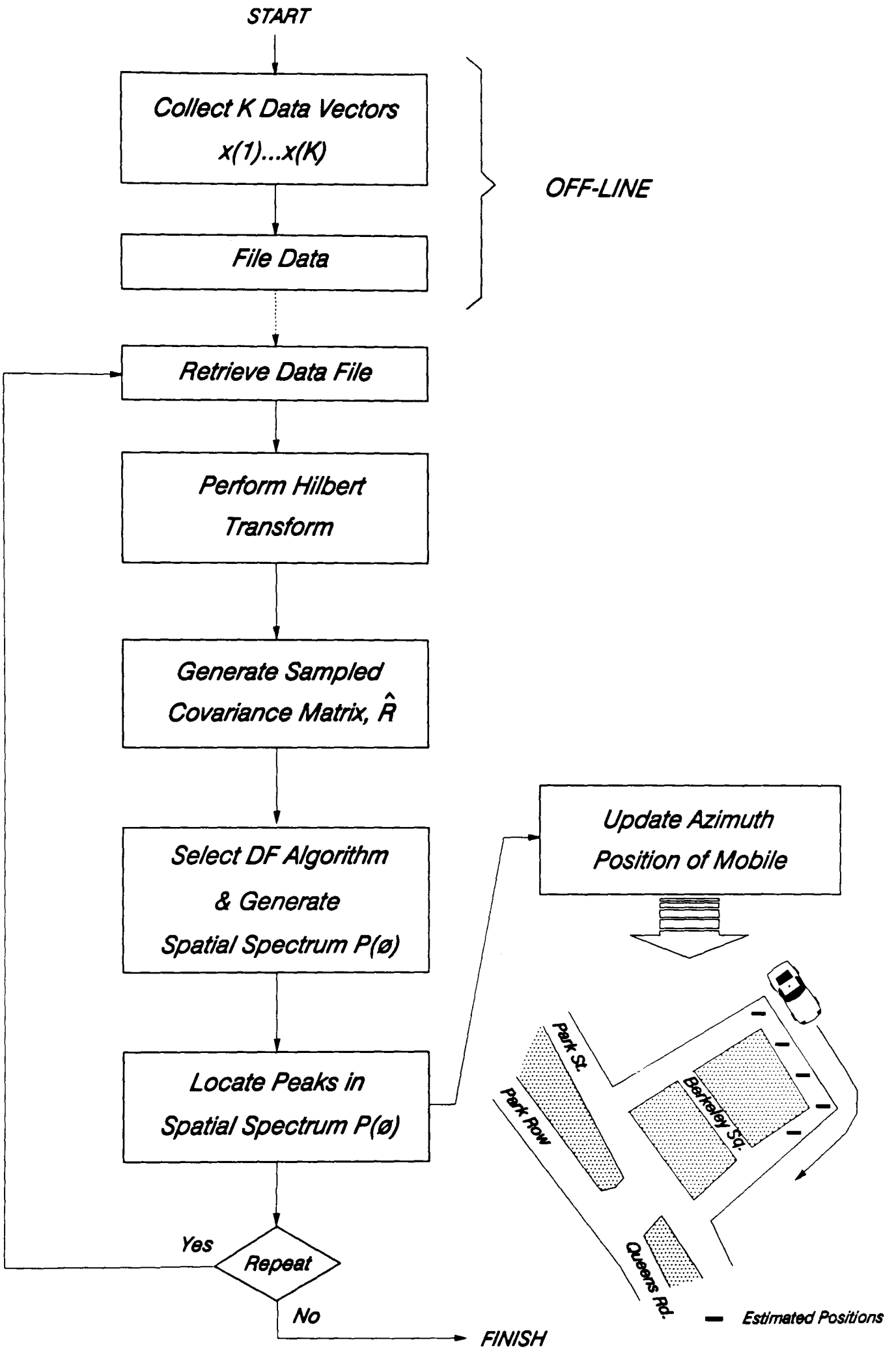

Figure 6.12: Block diagram of complete AOA estimation process.

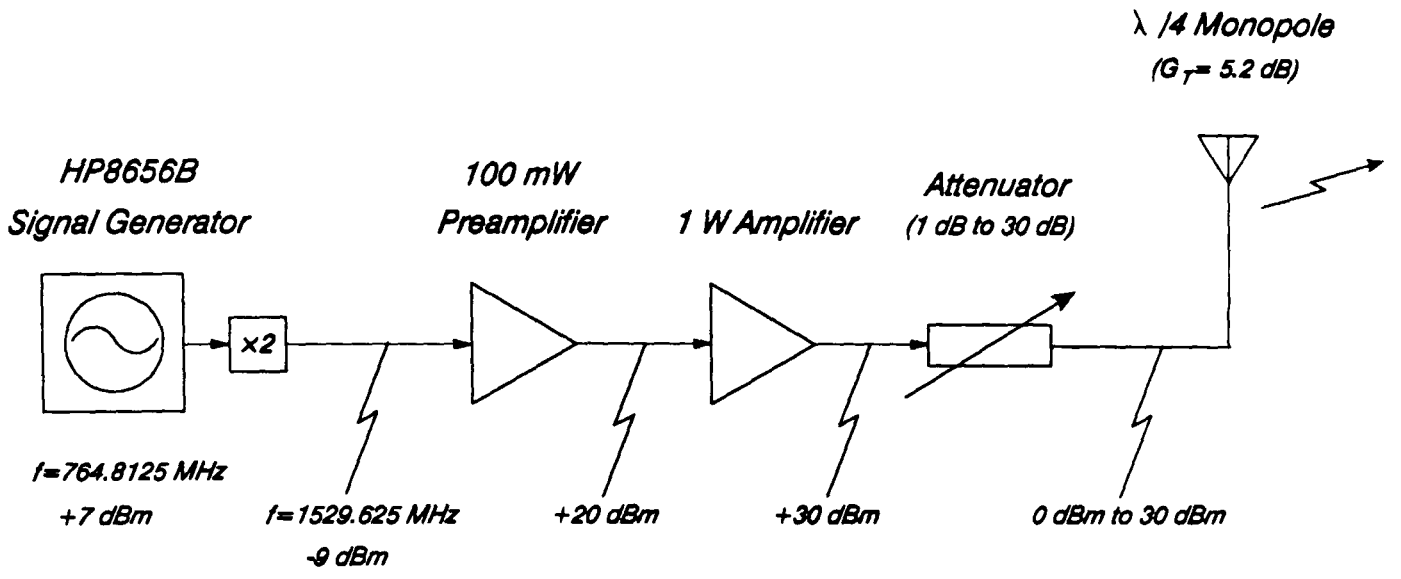

Figure 6.13: Mobile test source.

6.2 ARRAY MANIFOLD MEASUREMENT

In section 4.3, the concept of the array manifold was briefly introduced, and the computer simulations in chapter 5 demonstrated very clearly the errors that can occur in the AOA estimate when perfect reception of the signals with an ideal array is assumed. The main factors which must be taken into account are the mutual coupling that exists between the antenna elements and the amplitude/phase mismatch between the receiver channels. Both of these were included in a modified equation for the received signal vector **x** as follows:

$$\mathbf{x}(k) = \mathbf{C}\Gamma\mathbf{B}\mathbf{a}(k) + \mathbf{v}(k) \qquad (6.5)$$

where **C** is the coupling matrix for the antenna elements and Γ is a diagonal matrix containing the relative amplitude and phase of each channel in the receiver ($\mathbf{v}(k)$ is the additive sensor noise). Fortunately, the effects of these factors can be calibrated out by measuring the response of the system to a single source as a function of the AOA. The received signal vectors of (complex) voltages obtained from this calibration process collectively comprise the *array manifold*, and are filed away on a computer according to the source direction which can be in terms of the azimuth location as well as the elevation. The DF algorithms evaluate the spatial spectrum at each of the measured manifold points and, depending on the required accuracy, the correct AOA's are determined from the locations of the spectral peaks. Hence, in the completely general case with an antenna array comprising of elements with totally unknown characteristics, the array manifold unambiguously defines the response of the receiver. An experimental system developed by Schmidt [2] demonstrated this, with the measured array manifold enabling the accurate determination of the signal AOA's using the MUSIC algorithm.

Unfortunately, the measurement of the array manifold can be expensive and time consuming, especially if frequent re-calibration is required. An alternative would be to estimate the manifold on-line [15] or, if the characteristics of the array elements are known precisely enough, to generate it analytically. On-line estimation potentially offers the most attractive solution, especially as a means of updating the measured response which would then only have to be generated once. Hence, for a future working system this approach will have to be considered very seriously. In this section however, the procedure for measuring the array manifold will be discussed before presenting the results of the measurements for both the dipole and patch

arrays.

Initially, the receiver channels were matched as closely as possible in the anechoic chamber using the set-up shown in figure 6.8. Unfortunately, the anechoic chamber could not be employed for the measurement of the complete manifold response due to the large size of the RF front end hardware and the lack of a substantial turntable, although at this frequency the transmit source could be placed in the far field region of the receiving antenna[4]. Therefore, a suitable outdoor test range was required and, as part of the SERC CASE Award funding the work, the long test range at British Telecom Research Labs., Martlesham Heath was made available, providing an ideal opportunity to accurately calibrate the receiver system. The set-up is shown in figure 6.14, with the DF receiving array placed on the test range turntable at a height of 10.1 m above the ground. The transmitting source employed a vertically polarised horn antenna placed at the same level as the receiver on a portable tower 30 m away. The antenna gain was 11 dB at 1529.625 MHz and, assuming free space loss, the required transmit power to provide a full scale drive (±4 volts) for the A/D converters was approximately -28 dBm. A photograph of the complete set-up is given in figure 6.15, showing clearly the transmitter on the portable tower and the receiver mounted on the turntable. A close up view of the RF front end with the dipole array is shown in figure 6.16.

4: The frequently quoted boundary for far field operation is when the distance from the antenna R equals $2D^2/\lambda$, where D is the largest dimension of the antenna [16].

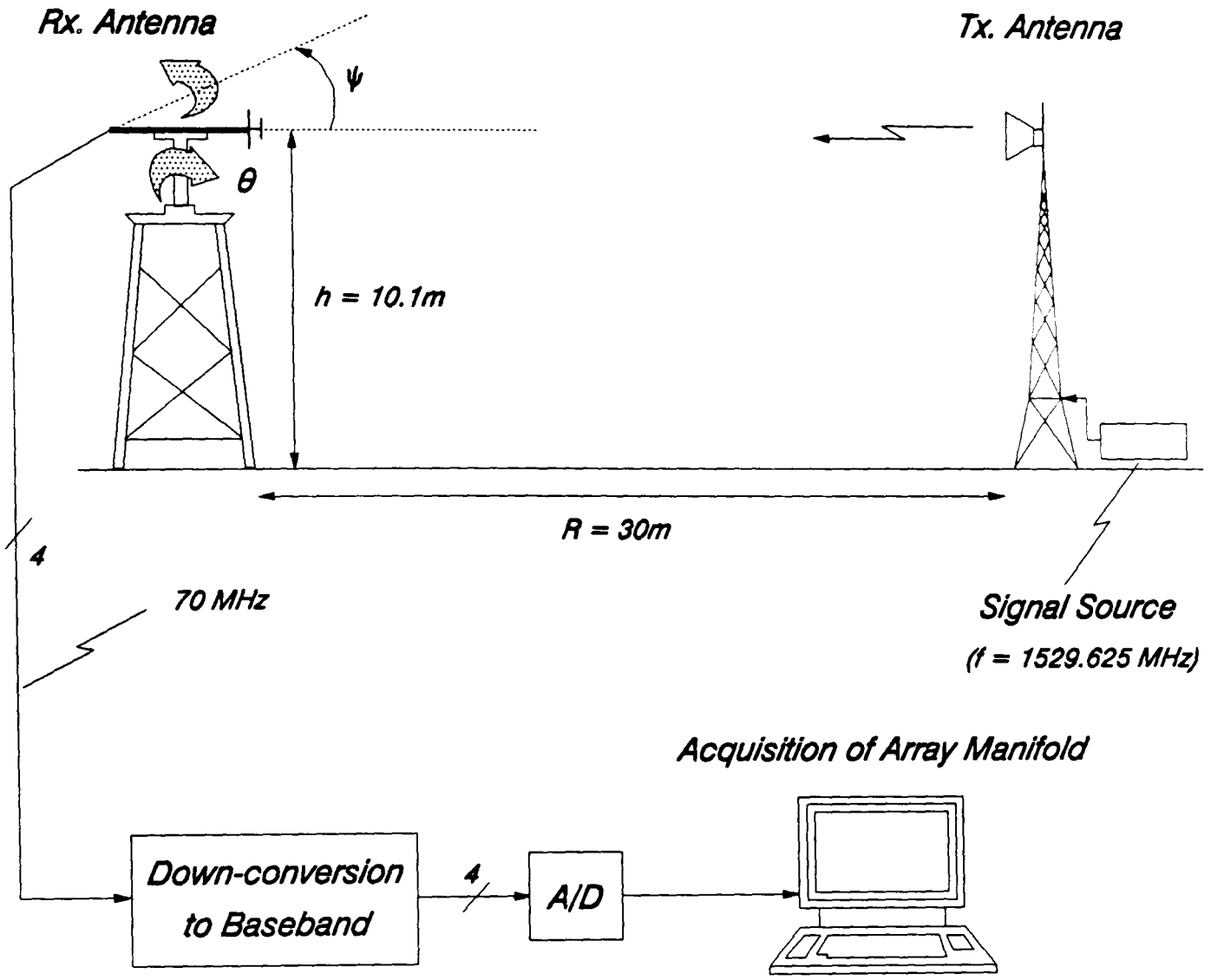

Figure 6.14: Measuring the array manifold.

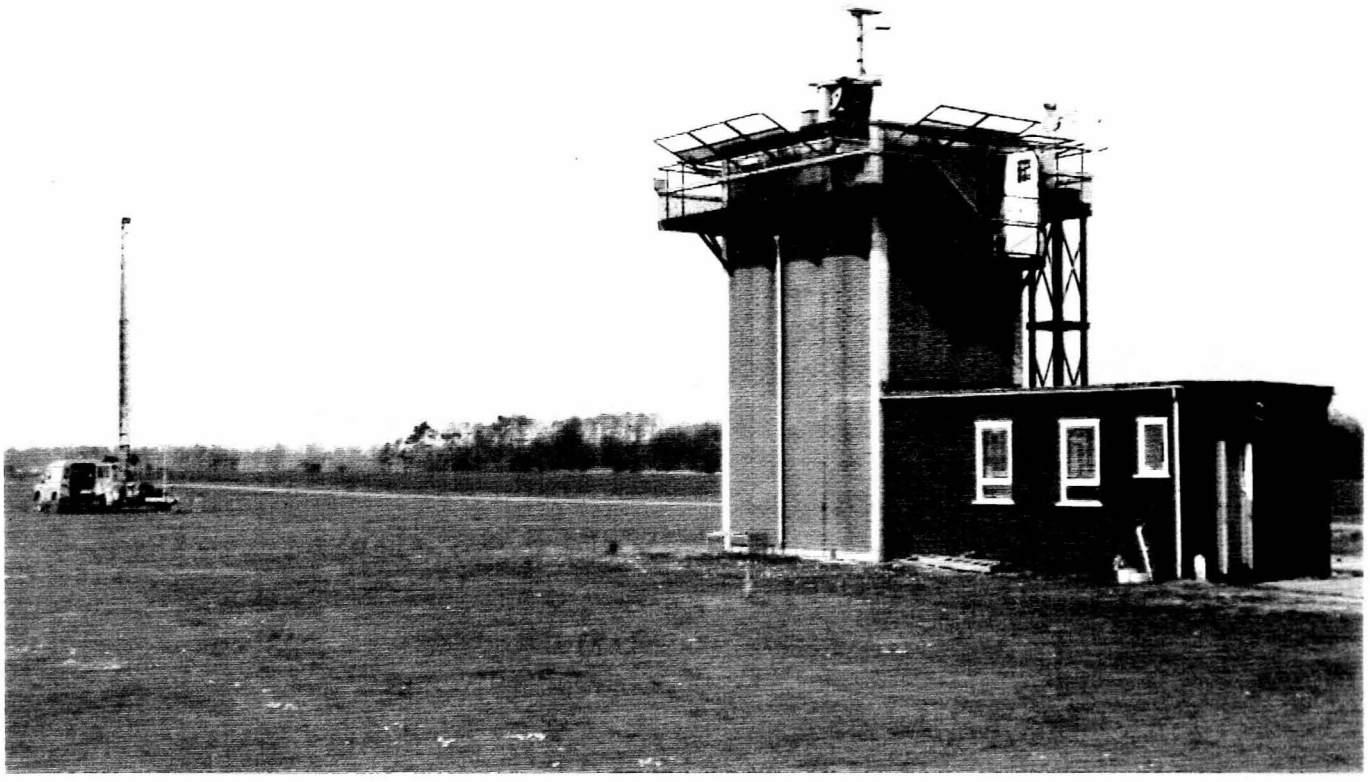

Figure 6.15: Set-up for measurement of array manifold.

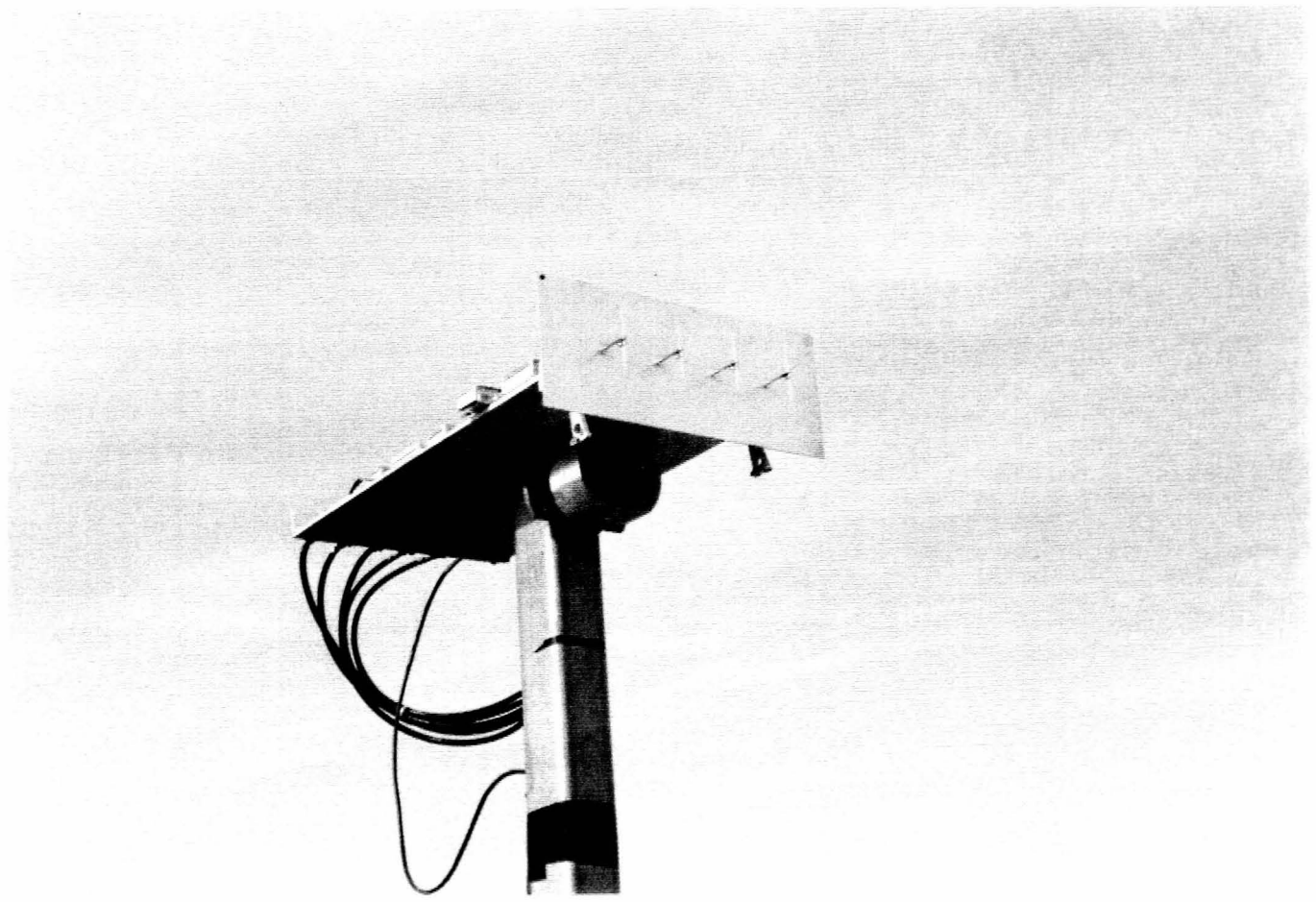

Figure 6.16: Dipole array and RF front end mounted on turntable.

The response for both of the arrays was measured at elevation angles of 0°, 5° and 10°, over the azimuth range $+110^\circ$ to -110° in 1 degree steps. Even though the range of elevation angles[5] for the planned test routes is between 0° and 15°, no further measurements were taken at this stage due to the lack of available time. At each manifold point 50 snapshots of data were recorded and filed on the computer for later processing. The first task was to apply the Hilbert Transform to the data, generating the inphase and quadrature components (I & Q), and enabling the full amplitude and phase response of each channel to be measured. Figure 6.17a contains the effective radiation patterns for each channel with the dipole array and, similarly, figure 6.17b contains the response with the patch array. The patterns are all relative to the peak value in channel A and are for an elevation of 0°. Note that the general shape of the responses ties up very closely with the measured azimuth radiation patterns of the antenna elements given in figure 6.4 and 6.6.

The received signal vector at each of the array manifold points includes both the effects of mutual coupling and receiver channel mismatch. Hence, if the amplitude and phase of each channel are referenced to channel A, the direction vector at each AOA can be expressed as

$$\mathbf{u}' = \begin{bmatrix} 1 \\ \alpha_{BA}\exp(j\phi_{BA}) \\ \alpha_{CA}\exp(j\phi_{CA}) \\ \alpha_{DA}\exp(j\phi_{DA}) \end{bmatrix} \qquad (6.6)$$

where ϕ_{iA} and α_{iA} are the phase and amplitude of the signal received in channel i with respect to channel A. For an ideal receiver, the direction vector of the received signal is given by equation (4.6), and for a four element linear array can be written as

---

5: The elevation angle is taken as the elevation of the base-station receiver from the mobile transmitter.

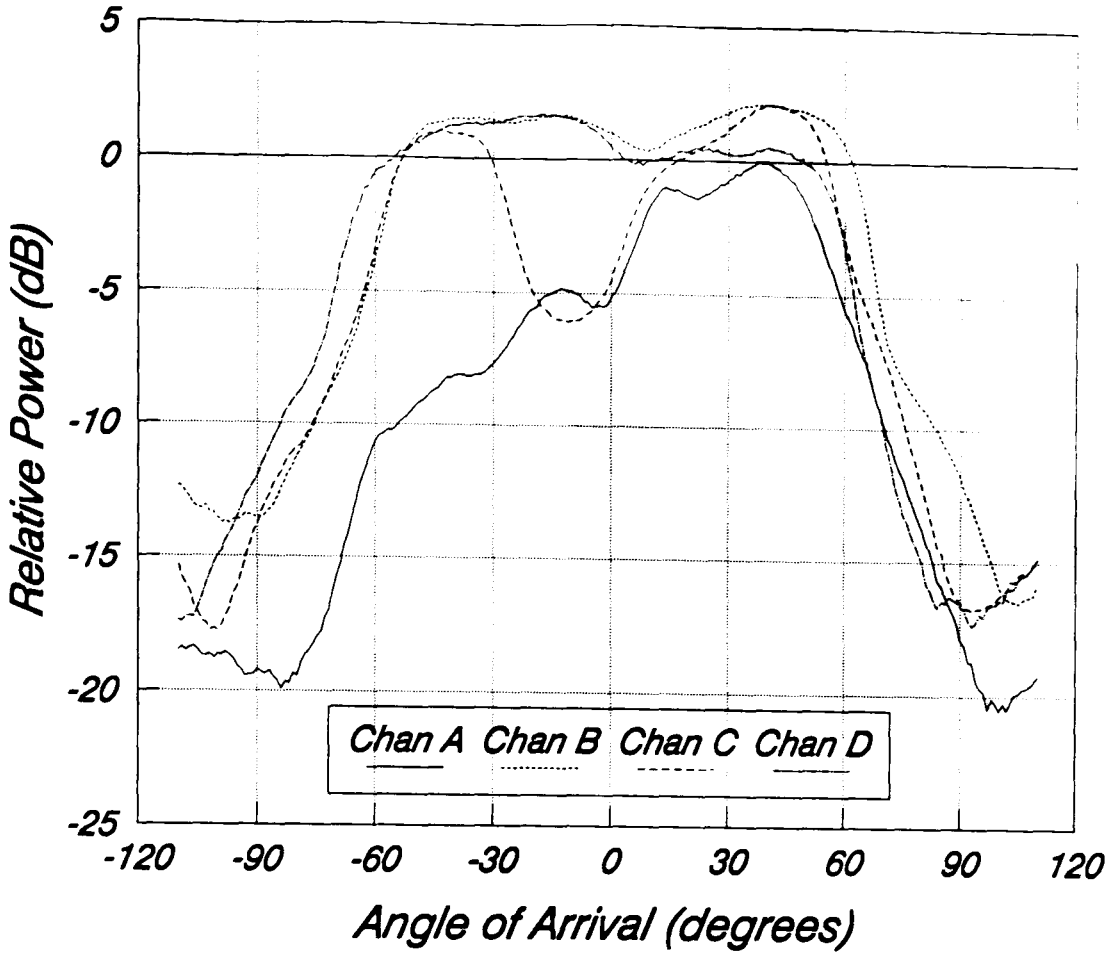

Figure 6.17: Effective radiation patterns for each channel with: (a) the dipole array; (b) the patch array.

$$\mathbf{u} = \begin{bmatrix} 1 \\ \exp(j\phi) \\ \exp(j2\phi) \\ \exp(j3\phi) \end{bmatrix} \tag{6.7}$$

where $\phi = (2\Pi d/\lambda)\sin\theta$ is the inter element phase shift associated with a signal incident at an angle θ off the array broadside. (Note that in order to account for a signal with an elevation of ψ down from the horizontal, the correct phase shift is given by $\phi = (2\Pi d/\lambda)\sin\theta\cos\psi$ [16].) Hence, the modified steering vector $\mathbf{u}'$ can be expressed in terms of the ideal steering vector $\mathbf{u}$ as

$$\mathbf{u}' = \begin{bmatrix} 1 & & & \cdots & 0 \\ & \alpha_{BA}\exp(j\varepsilon_{BA}) & & & \vdots \\ \vdots & & \alpha_{CA}\exp(j\varepsilon_{CA}) & & \\ 0 & \cdots & & & \alpha_{DA}\exp(j\varepsilon_{DA}) \end{bmatrix} \begin{bmatrix} 1 \\ \exp(j\phi) \\ \exp(j2\phi) \\ \exp(j3\phi) \end{bmatrix} = \begin{bmatrix} 1 \\ \alpha_{BA}\exp(j\phi_{BA}) \\ \alpha_{CA}\exp(j\phi_{CA}) \\ \alpha_{DA}\exp(j\phi_{DA}) \end{bmatrix} \tag{6.8}$$

where the phases ε_{iA} can be considered as the phase errors between the non-ideal and ideal situations and are given by

$$\begin{aligned} \varepsilon_{BA} &= \phi_{BA} - \phi \\ \varepsilon_{CA} &= \phi_{CA} - 2\phi \\ \varepsilon_{DA} &= \phi_{DA} - 3\phi \end{aligned} \tag{6.9}$$

Figure 6.18 contains plots of these phase errors with the dipole array, each of the three plots for a different elevation angle, i.e. $\psi = 0^\circ$, 5° and 10°. Figure 6.19 contains the same results but for the patch array. Note how the phase error associated with a particular channel depends on the elevation angle, clearly demonstrating the problem associated with array manifold measurement, where complete and unambiguous calibration would require the manifold to be measured at many more elevation angles.

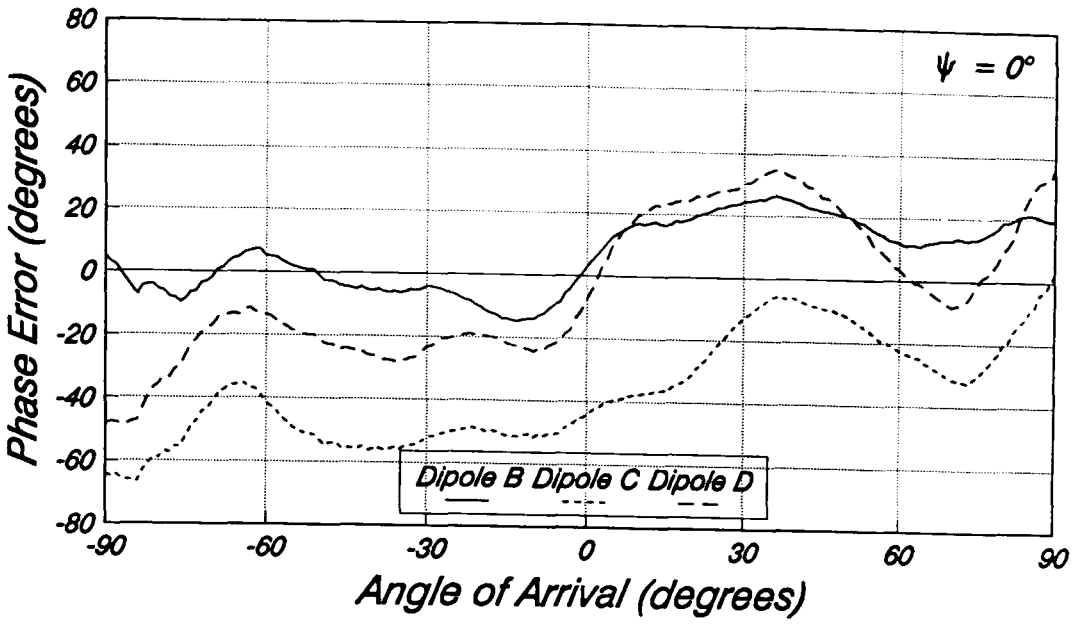

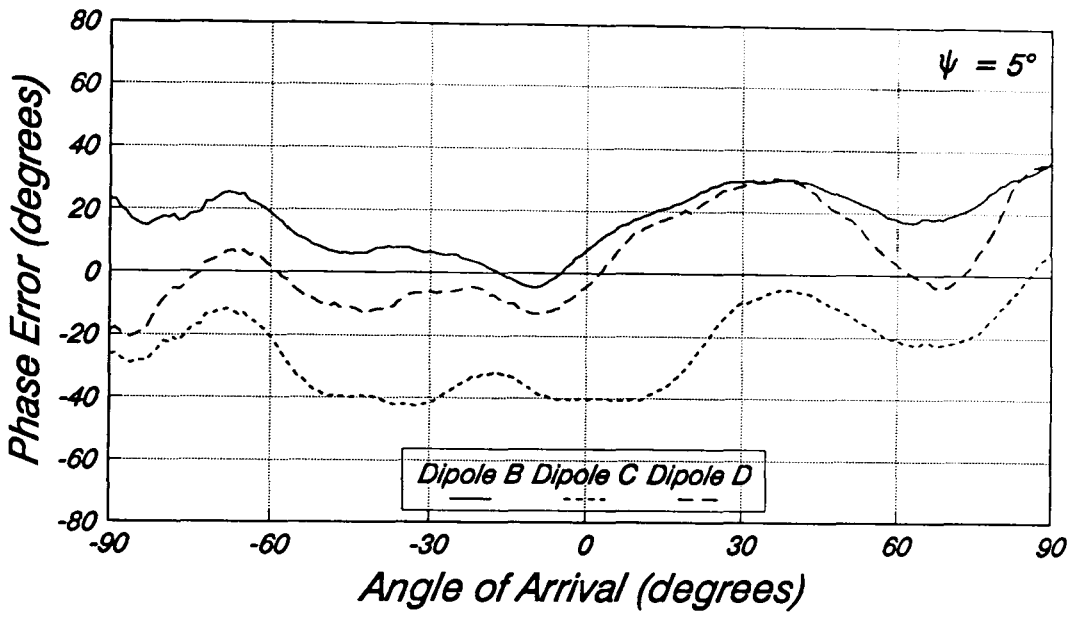

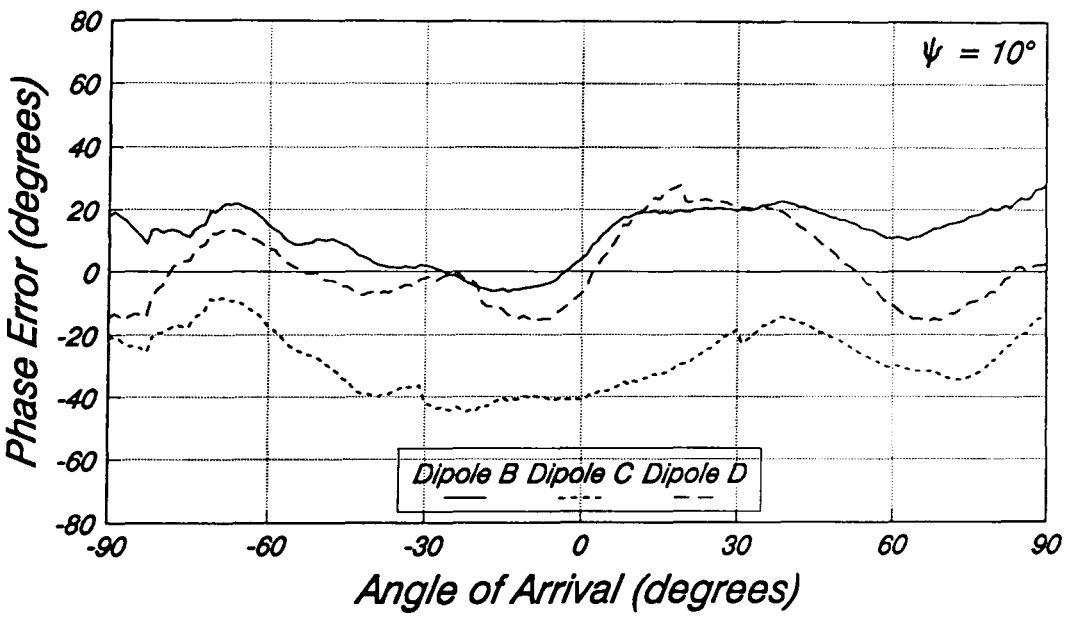

Figure 6.18: Phase errors across the dipole array for each channel at elevations of $\psi = 0^{\circ}$, 5° and 10°.

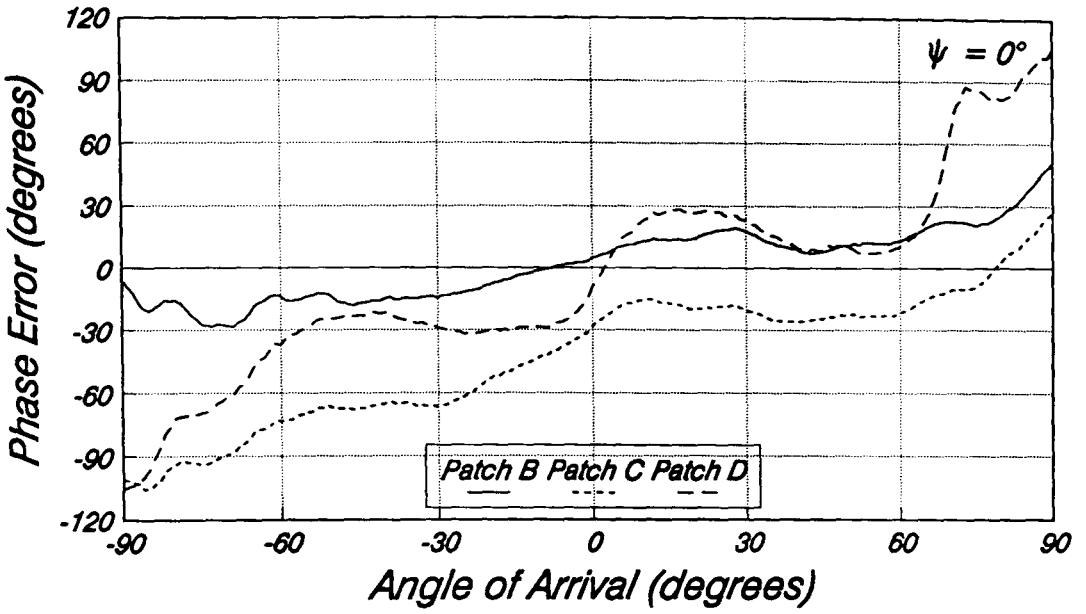

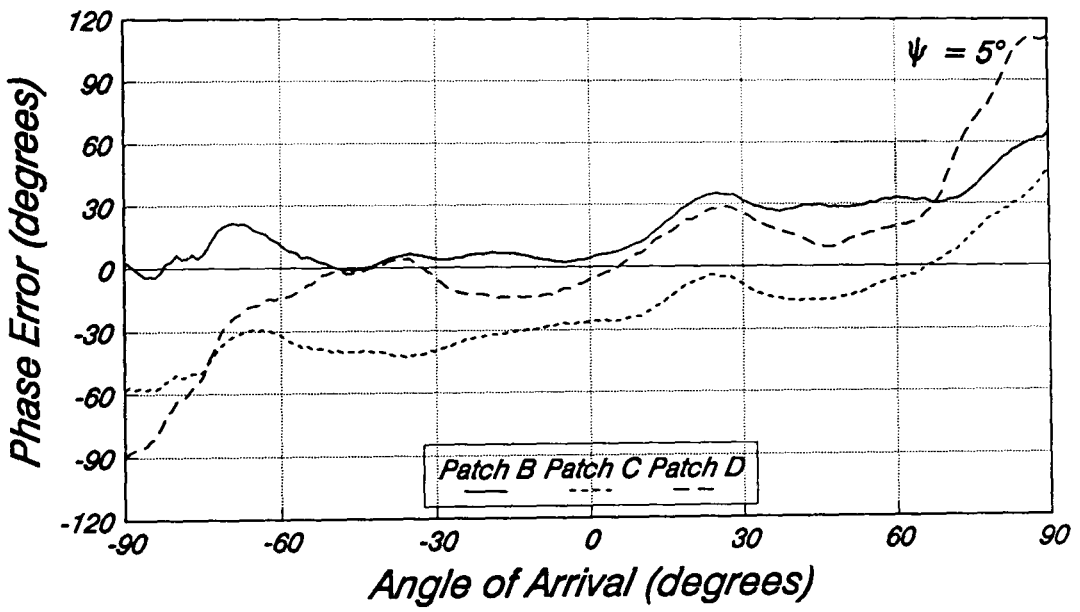

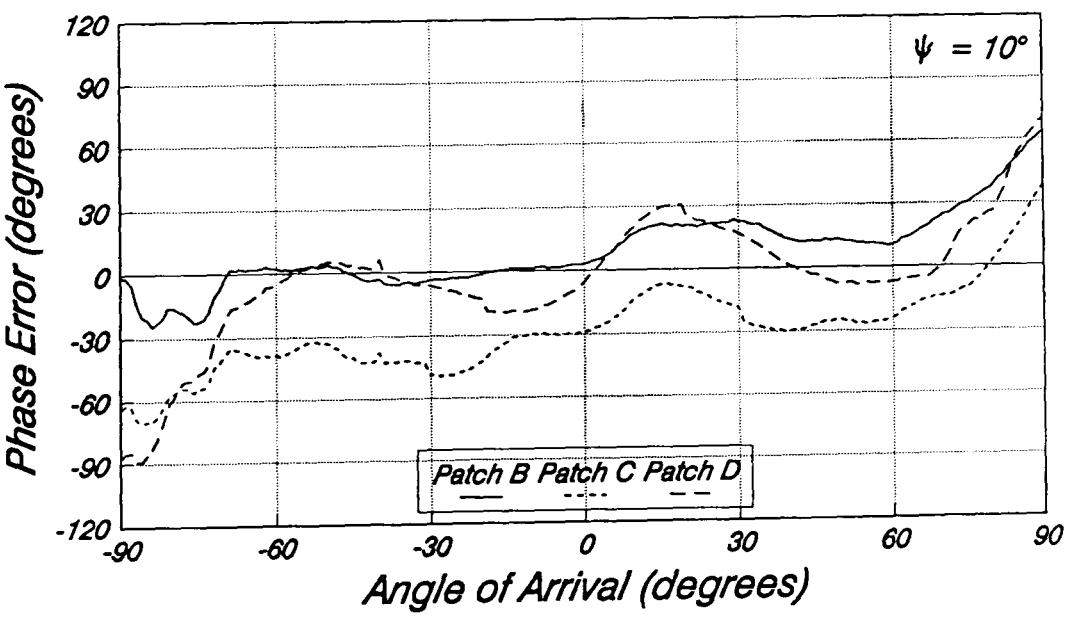

Figure 6.19: Phase errors across the patch array for each channel at elevations of $\psi = 0^{\circ}$, 5° and 10°.

Of particular interest at this stage would be the result of applying the various direction finding algorithms to the measured manifold data, and to then estimate the bearing of the source assuming an ideal array response, i.e the ideal steering vector **u** given in equation (6.7). By comparing the estimated AOA with the actual AOA, a number of objectives can then be achieved, namely

(i) The relative performance of the dipole and patch arrays.

(ii) The relative performance of all the DF algorithms in the presence of mutual coupling and receiver mismatches.

In order to compare the two types of array, the MUSIC algorithm was applied to the measured data from each antenna when at an elevation of 0°. Twenty snapshots of data were used per iteration ($K = 20$) and the results are presented in figure 6.20 in the form of a scatter plot. This illustrates very clearly the effects of assuming an ideal array manifold, although the trend over the range $\pm 45^\circ$ is moving towards the ideal response, with the number of ambiguities reduced. The gross variations outside the $\pm 45^\circ$ range can be partly attributed to the large reduction in signal gain in these directions as illustrated by the radiation patterns in figure 6.17. The error statistics over the $\pm 45^\circ$ range for both the dipole and patch arrays with the MUSIC algorithm are included in table 6.3. There is very little difference between the two antennas except maybe for the mean error which is substantially lower with the patch array.

ALGORITHM (antenna)	AOA Error Statistics ($\pm 45^\circ$)		
	MEAN	RMS	σ
MUSIC (patch)	2.6°	33.6°	33.5°
MUSIC (dipole)	10.5°	34.0°	32.3°
KuTu (dipole)	11.0°	34.3°	32.5°
JoDeG (dipole)	11.5°	34.8°	32.9°
MEM (dipole)	9.8°	37.6°	36.3°
MLM (dipole)	9.9°	27.2°	25.3°
FM (dipole)	-1.1°	2.8°	2.6°

Table 6.3: AOA error statistics for measured manifold data.

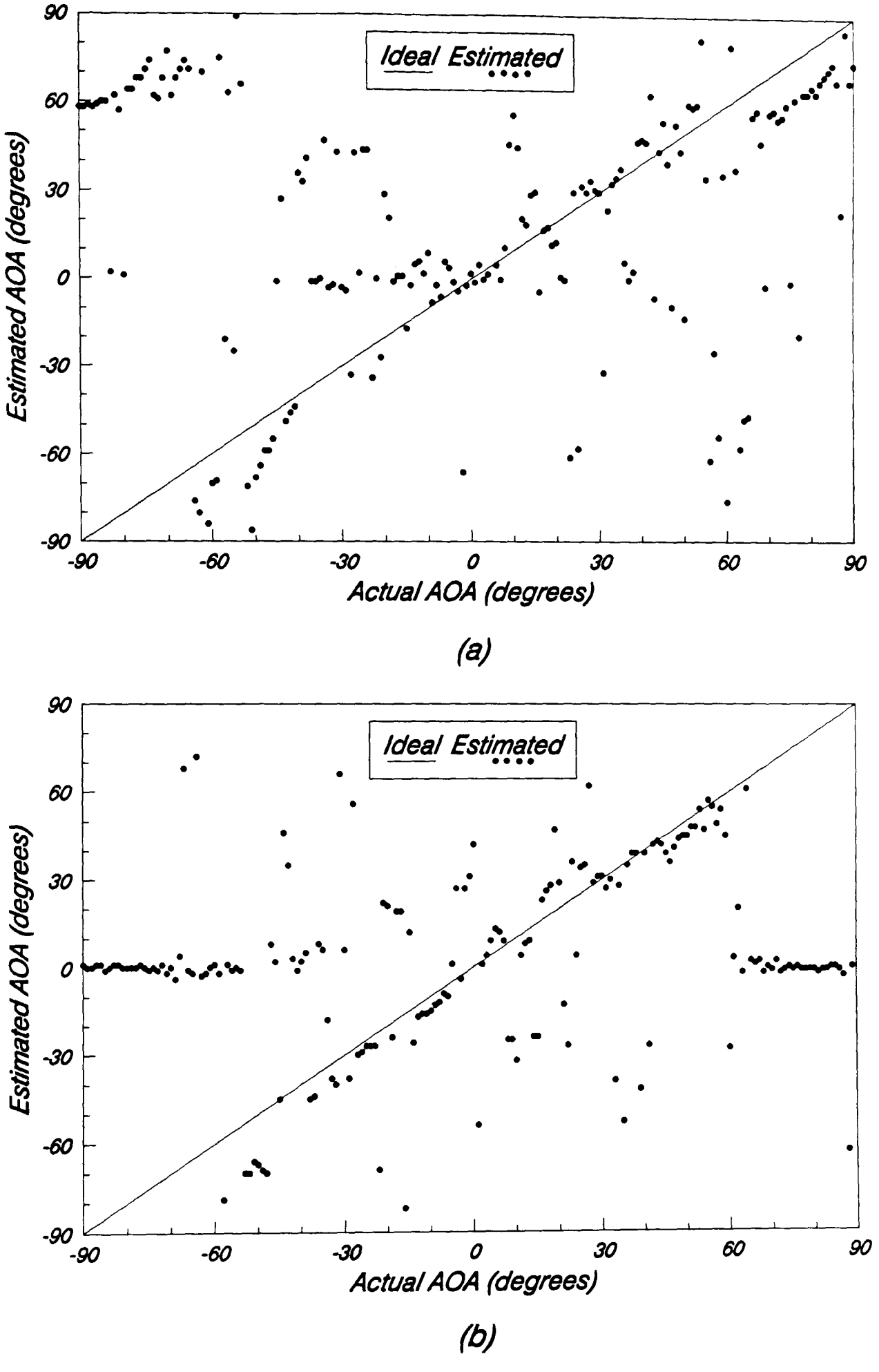

Figure 6.20: Estimated AOA's from manifold data (ψ=0°) with the MUSIC algorithm: (a) dipole array; (b) patch array.

Also included in table 6.3 are the error statistics obtained when the other DF algorithms are applied to the dipole data at an elevation of 0°, clearly showing the superior performance of the two lower resolution methods, especially the FM technique. The performance of the eigenstructure methods is very similar, and all are clearly very susceptible to mutual coupling effects and amplitude/phase uncertainties, with numerous ambiguous peaks occurring in the spectrum. This is reflected in the result of applying the MDL criteria, which always overestimated the number of sources, indicating two or even three. With the aid of computer simulations this effect could also be observed and highlights the problem of correctly estimating the number of sources incident onto the array, an essential task for the successful application of the eigenstructure techniques. The MEM technique is noticeably inferior to the other techniques, producing the largest spread of errors. This was demonstrated to some extent with the computer simulations of chapter 5, which showed that the MEM technique was strongly affected by mutual coupling, although was possibly more tolerant to amplitude and phase uncertainties.

DATA PROCESSING	MANIFOLD	AOA Error Statistics ($\pm 45^{\circ}$)		
		MEAN	RMS	σ
Amplitude & Phase	Ideal	10.5°	34.0°	32.3°
	Amp. & phase	2.0°	41.4°	41.4°
	Phase only	6.2°	33.8°	33.2°
Phase only	Ideal	0.0°	15.9°	15.9°
	Amp. & phase	-1.7°	46.7°	46.7°
	Phase only	0.0°	0.1°	0.1°

Table 6.4: AOA error statistics for different types of data processing with alternative manifolds.

Another important aspect to be considered at this stage, is how the measured manifold data is to be stored for later use during the field trials. The first option would be as a series of direction vectors as defined in equation (6.6) and therefore maintaining full amplitude and phase information. The alternative would be to only consider the relative phases between channels, ignoring any amplitude variations. Also, the received data

vectors can either be left unprocessed prior to estimation or have all amplitude information removed, leaving only the phase variations, i.e. an equalisation process. The various permutations of the above alternatives were implemented and the results of applying the MUSIC algorithm are summarised in table 6.4. With no data processing, the use of the measured manifold does not provide any appreciable benefits, with the full amplitude and phase manifold producing an even worse response. The same effect was also observed with the other algorithms. When the received data includes only the phase information however, the results with the ideal manifold are greatly improved but the full amplitude and phase manifold again produces a very poor response. Use of the phase only manifold though produces near perfect resolution, clearly demonstrating the best approach to applying the measured manifold response to the received array data.

6.3 FIELD TRIALS

The aims of these initial field trials were twofold:

(i) To demonstrate the ability to track the movements of a mobile source in an urban environment.

(ii) To investigate the effect of scattering objects local to the mobile on the angular spread of the signals received at a typical base-station site.

Also, the results obtained would provide a valuable insight to the signalling conditions in a built up area, thus enabling improved signal models to be developed.

The roof of the University's Engineering Building offered an excellent elevated site for the DF receiver away from any local scatterers, and provided good radio coverage of the Clifton area of Bristol. Clifton is a fairly typical urban environment, offering a wide variety of operating conditions, ranging from good line of sight to extremely cluttered surroundings which offer no direct path to the base-station. A view of Clifton from the base-station site is shown in figure 6.21. The height of the antenna above sea level was measured at 88 m, and this enabled the elevation angles of the chosen test routes to be estimated from the heights given on an Ordnance Survey map (Sheet ST 57 SE, scale 1:10 000). Figure 6.22 is an

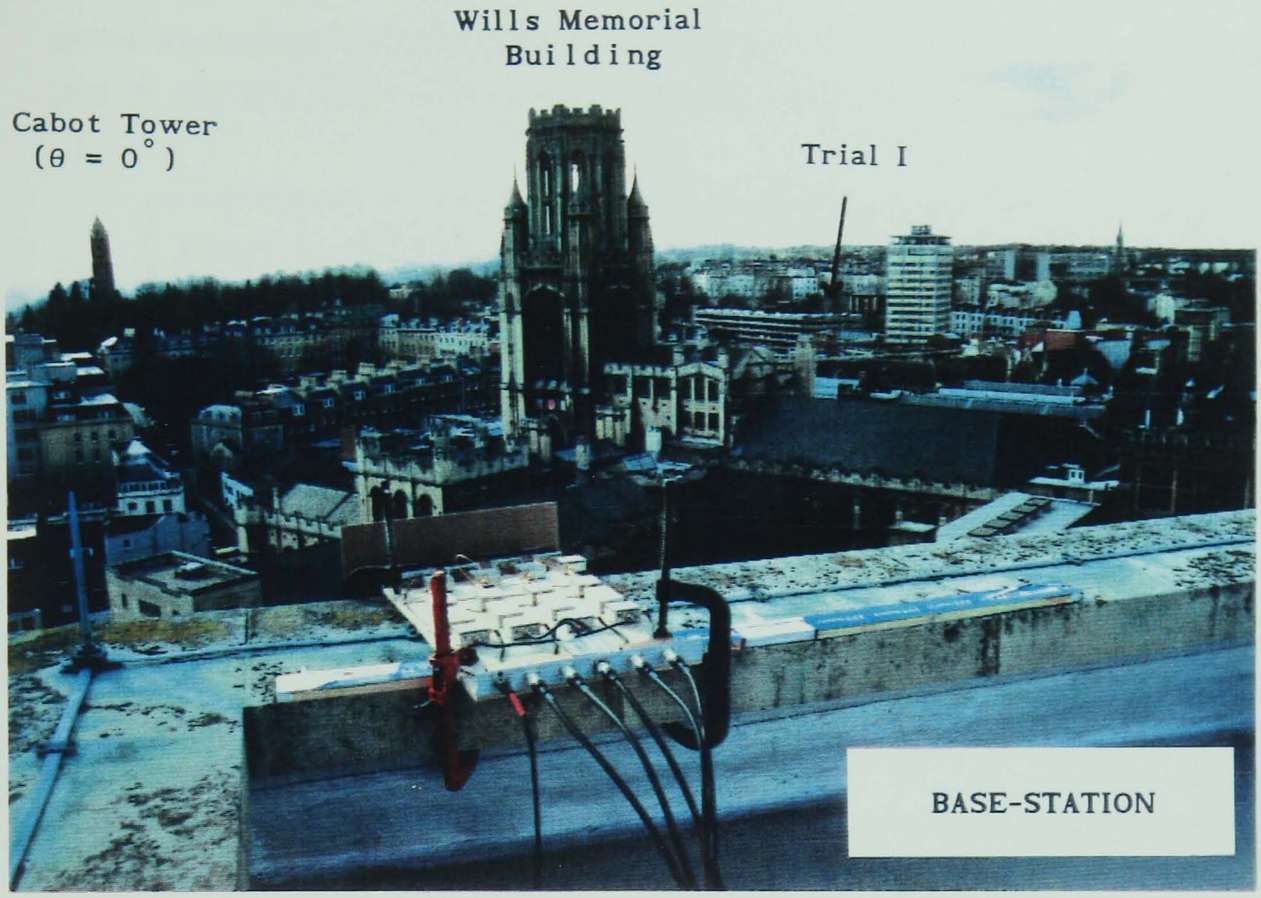

Figure 6.21: View of Clifton from the base-station site.

Figure 6.22: Aerial photograph of the test area (Clifton).

aerial photograph of part of the test area and figure 6.23 gives a detailed map of the area showing the test routes that were used.

Route	Range (m)		Elevation (ψ)		Bearing (θ)	
	Start	End	Start	End	Start	End
I	470	——	3°	——	37°	——
II	290	440	12°	5°	-37°	-20°
III	380	340	7°	5°	-23°	-9°
IV	250	170	13°	14°	-40°	5°
V	310	275	6°	7°	2°	27°

Table 6.5: Details of the test routes.

The selected routes provide a broad cross section of signal environments, and table 6.5 above provides details of the elevations, bearings and distances from the receiver. The elevation angles given were estimated from the contours on the Ordnance Survey map, and serve only to give some indication of the correct manifold response to employ during the processing. In practice, the spatial spectrum would have to be generated at each elevation angle, with the strongest peak defining the source location. The bearings were also measured using the map, with Cabot Tower (located on the left of the photograph in figure 6.21) providing the ideal landmark to define the broadside of the array ($\theta = 0^\circ$). Further efforts to obtain a more accurate measurement were not deemed necessary due to the nature of the trials.

In order to synchronise the movements of the mobile with the data acquisition, a VHF radio was employed to provide a voice link between the mobile and the base-station. Hence, with the mobile moving at a constant speed of approximately 10 mph ($\cong$ 5 m/sec), frames of data could be recorded at regular intervals along each route. The approximate distance between each frame could then be calculated, enabling the bearing of each location to be estimated from the map. Note that at a distance of 300 m, a ±5 m error in the

position of the mobile corresponds to approximately only a $\pm 1^{\circ}$ error in the actual source bearing. Hence, with only a one degree resolution in the AOA estimate, the chosen method of data acquisition is adequate.

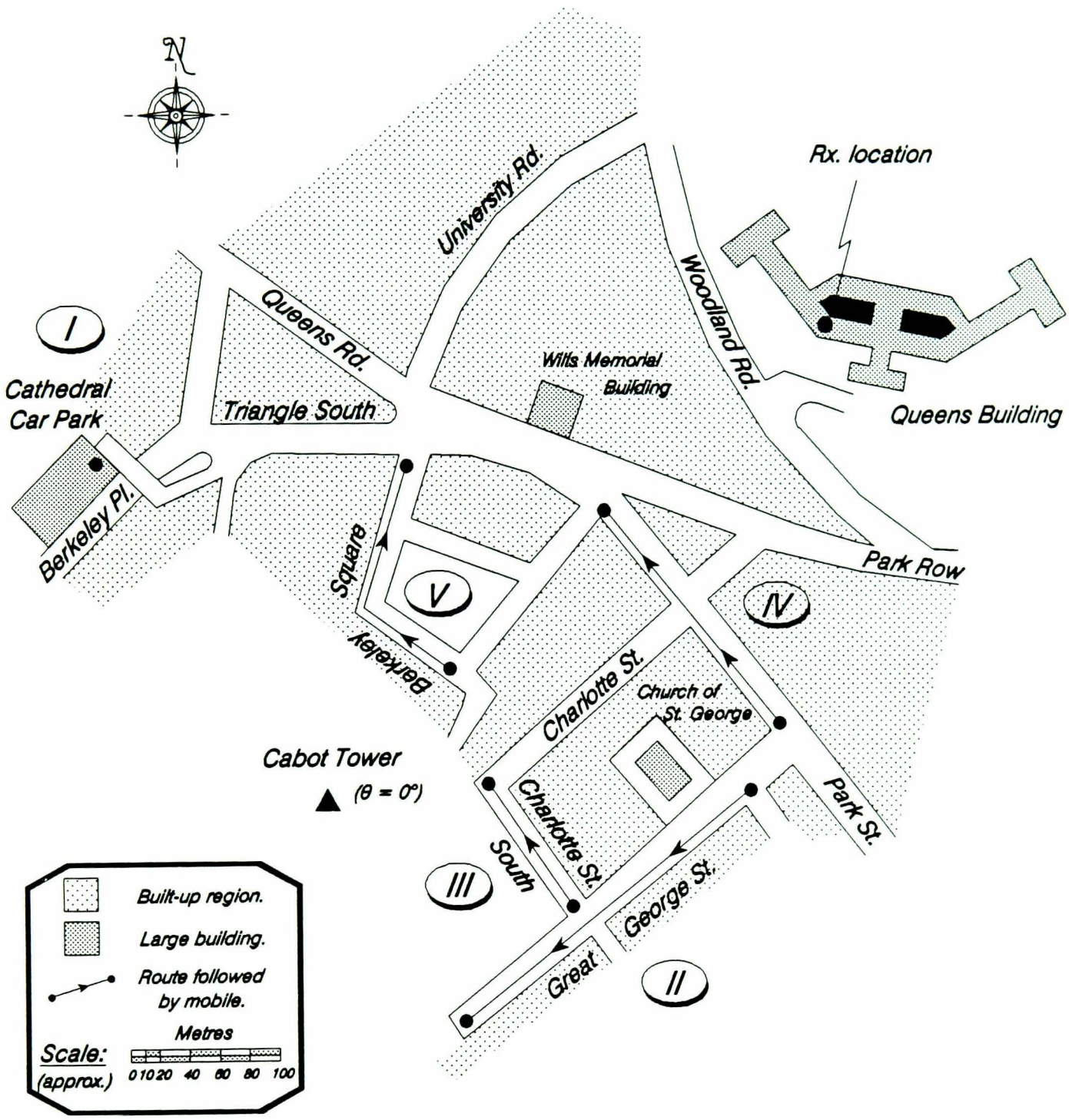

Figure 6.23: Map of Clifton showing test routes followed by mobile.

Each frame of data acquired during the trials consisted of 500 snapshots at a sampling frequency of 15 kHz. The frame period is then approximately 33.3 msec which, at a constant speed of 5 m/sec, corresponds to a distance travelled by the mobile of 0.17 m, or 0.87λ at the operating frequency. Figure 6.24 shows the received signal envelope in all four channels over a single frame period from one of the trials and, as can be seen, exhibits the characteristic fading envelope. Also note the similarity between the envelopes indicating, as expected, the high degree of correlation between the signals when the antenna elements are spaced half a wavelength apart. The following steps are a summary of the processing tasks that were carried out on each data frame acquired during the field trials:

(i) Perform the Hilbert transform to generate I & Q components (⇒ 476 snapshots remain).

(ii) Remove amplitude variations from each channel (⇒ only phase information considered).

(iii) Select phase only manifold at approximately correct elevation.

(iv) Generate the spatial spectrum with chosen DF algorithm.

(v) Estimate the azimuth bearing of the mobile source.

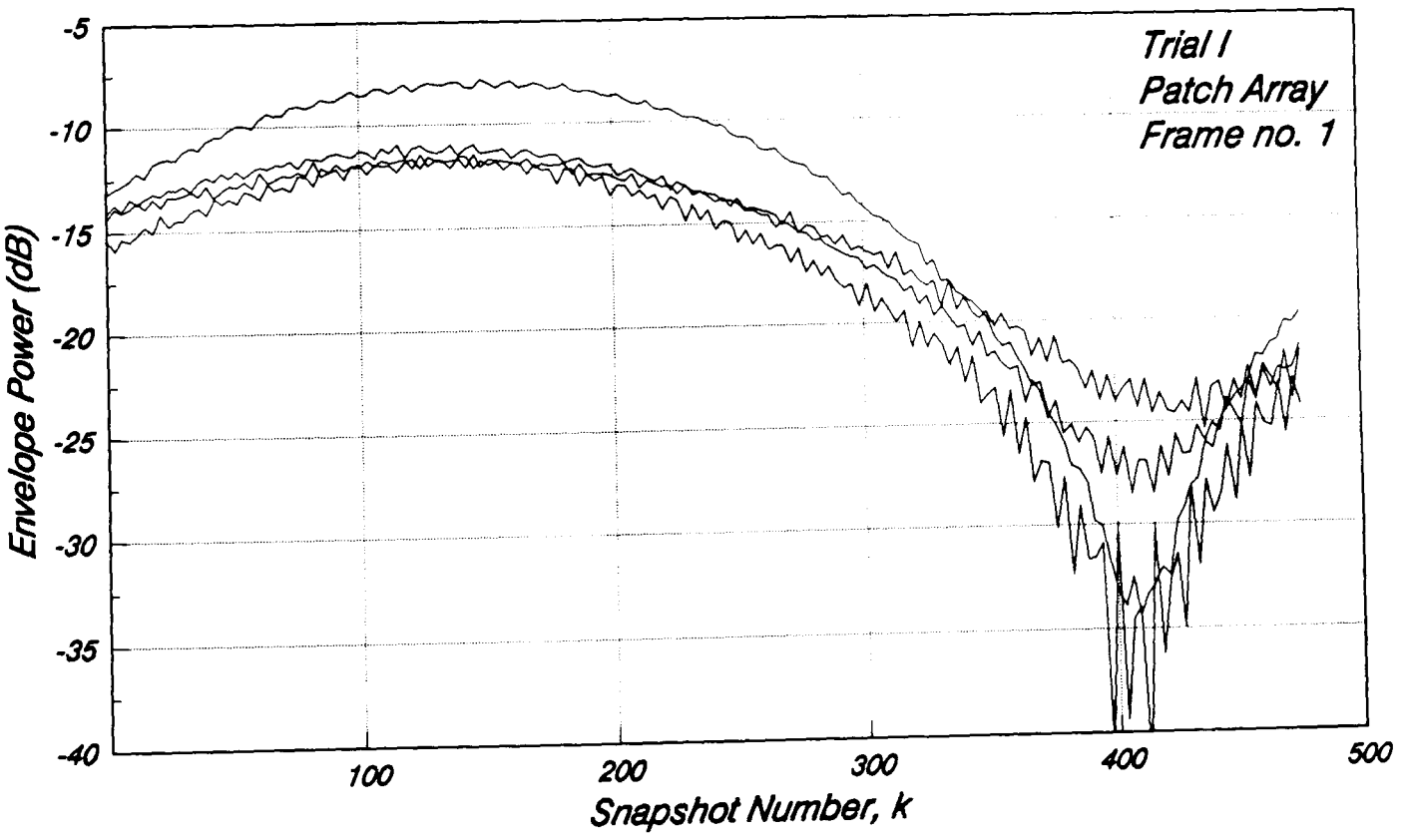

Figure 6.24: Measured fading signal in all four channels.

When generating the spatial spectrum using one of the eigenstructure techniques, the MDL criteria was employed to determine the number of signals present. This technique was also used in the computer simulations in chapter 5, and was discussed briefly in section 5.1.5.

In chapter 5, spatial smoothing techniques were employed to enable the resolution of coherent multipath signals. However, the results of the simulations showed that the presence of buildings and other scattering objects in the immediate vicinity of the mobile ensured that the mobile could still be successfully located even when discrete multipath reflections were present. For this reason, as well as the fact that the techniques considered are not directly applicable when there is mutual coupling between antenna elements (section 5.2.2), the results generated when spatial smoothing was employed are not presented here.

6.3.1 Trial I - Cathedral Car Park

Here the mobile was in a stationary position, with a clear line of sight path to the base-station antenna. Figure 6.21 shows the view from the base-station over the test area, with the mobile test site for trial I as labelled. The purpose of this initial trial was to establish a suitable reference point from a known bearing before carrying out the mobile tests, and then on subsequent trials to ensure that all the results were consistent. This location also provided a basis for the calculation of the received signal power to noise power spectral density which is included in Appendix I. The result gives a rather optimistic value of 97.5 dBHz.

All of the algorithms successfully estimated the bearing of the mobile source, although the accuracy was very dependent on the choice of manifold employed. Since the elevation from the site is approximately 3°, both the 0° and 5° manifolds ensured that the resulting spatial spectra gave the correct bearing. The 10° manifold and the ideal manifold (assuming perfect reception with an ideal array) on the other hand produced errors of 1° or 2° in the estimate and this is clearly illustrated in figure 6.25. Here the resulting spectra of applying the MLM algorithm to the dipole data with both the measured ($\psi = 5^\circ$) and ideal manifolds are given, with the ideal manifold producing an estimated bearing of $+39^\circ$.

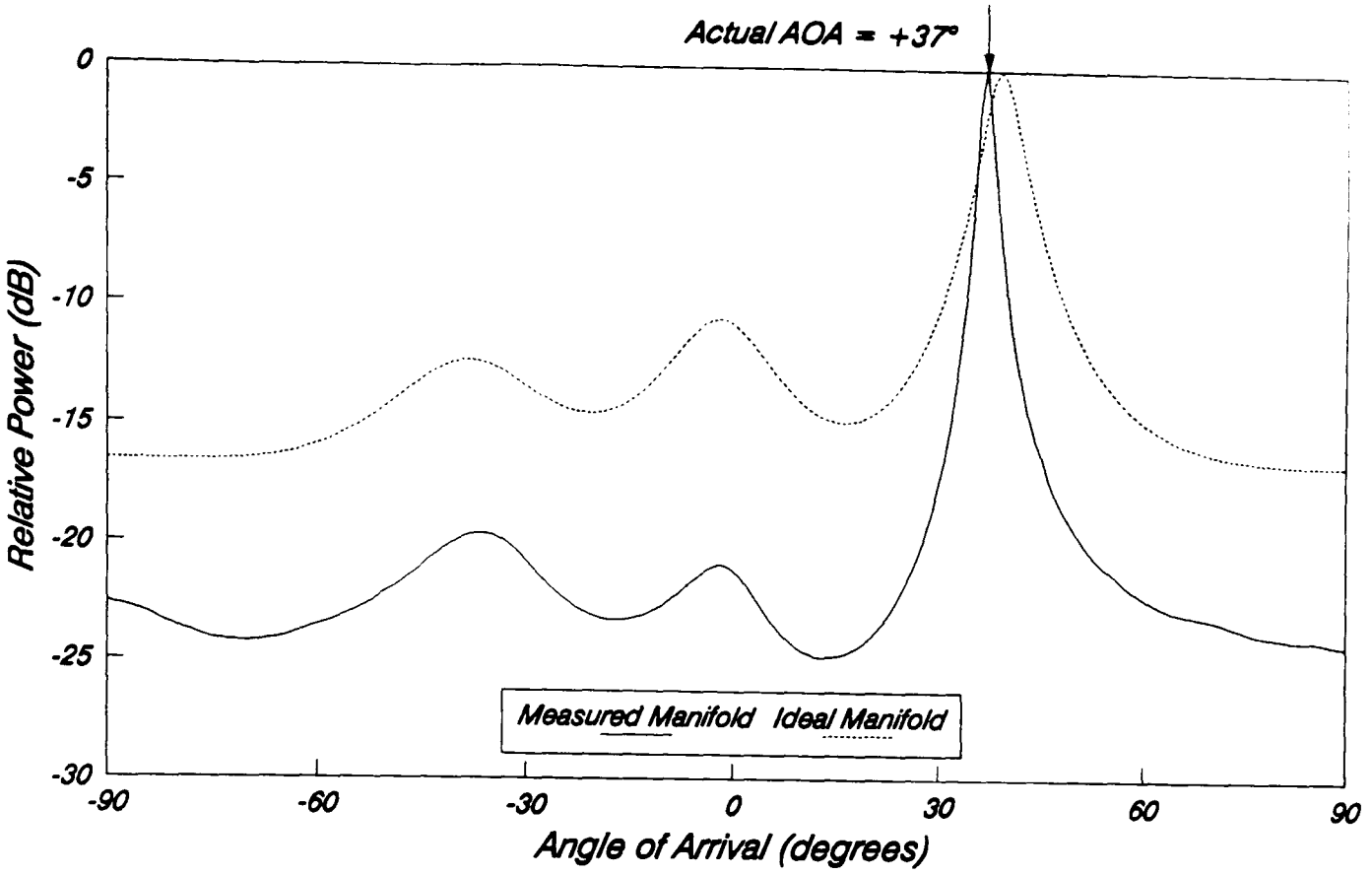

Figure 6.25: Spatial spectra for trial I with the dipole array and the MLM algorithm.

An interesting feature of the spatial spectra in figure 6.25 is the increased amount of ripple in the response, a particular characteristic not usually associated with the MLM algorithm (see discussion in section 4.3). In general, all the algorithms produced extra peaks as shown in figure 6.26a. These results were generated with the patch array and clearly show the presence of the mobile with a single strong peak, the sharpness of which depends on the algorithm employed. Notice the extra activity at bearings in the range $-10^{\circ} \rightarrow -40^{\circ}$. This can possibly be attributed to reflections from buildings, although the only obvious reflector is the large building (Wills Memorial Building) located at the centre of figure 6.21. The bearing however is approximately $+20^{\circ}$ and so the results of figure 6.26a are rather confusing and possibly misleading.

Computer simulations of this trial were very revealing, and the results are shown in figure 6.26b. The same algorithms were employed with a single signal source (SNR = 20 dB) at $+37^{\circ}$. No reflections were modelled, but the effects of mutual coupling with receiver mismatches (σ_{γ} = 0.1 and $\sigma_{\psi} = 10^{\circ}$) were included and the results were generated with the modified steering vector $\mathbf{u}'$, as described in chapter 5. Notice the very similar response with

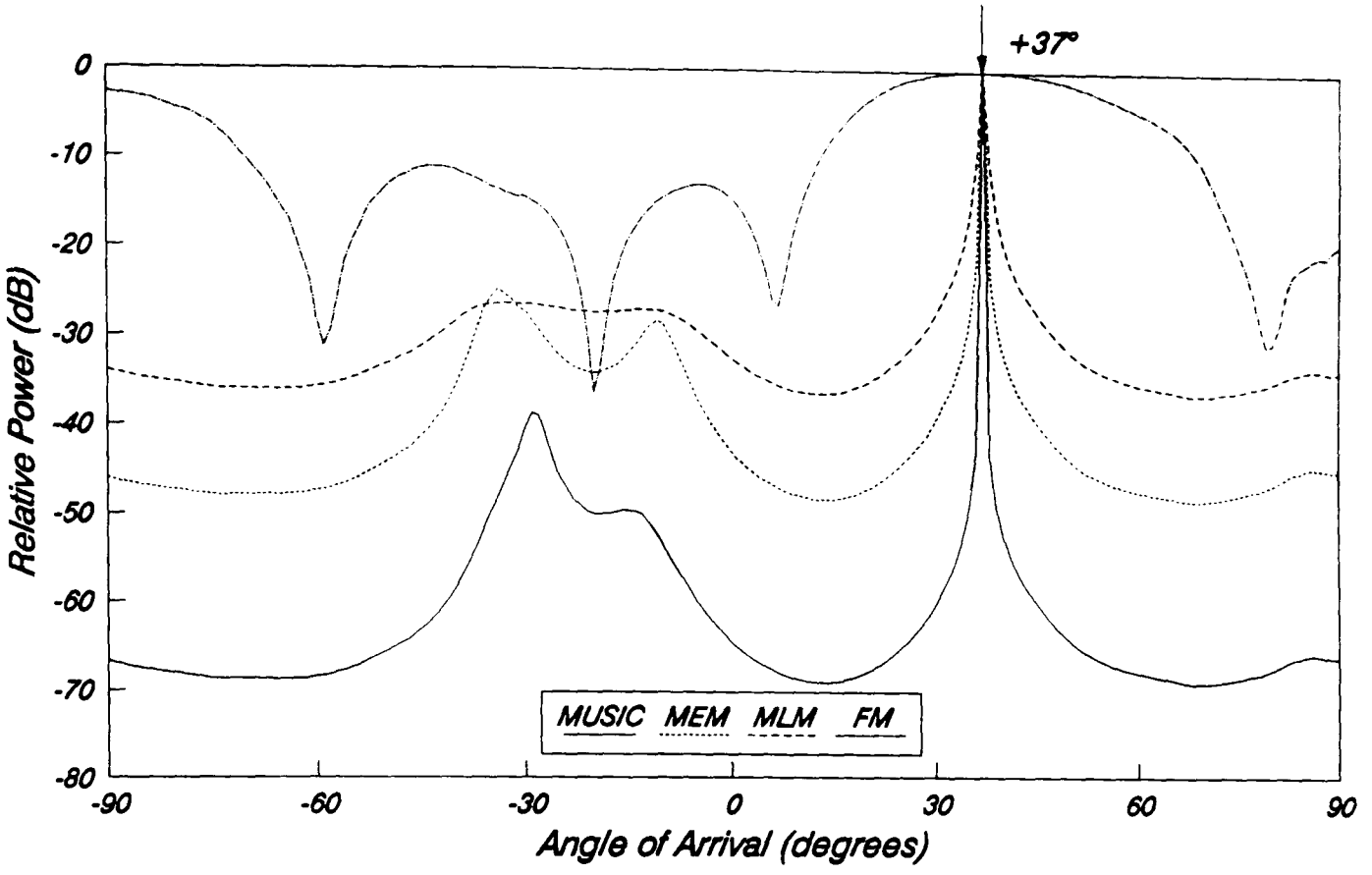

(a)

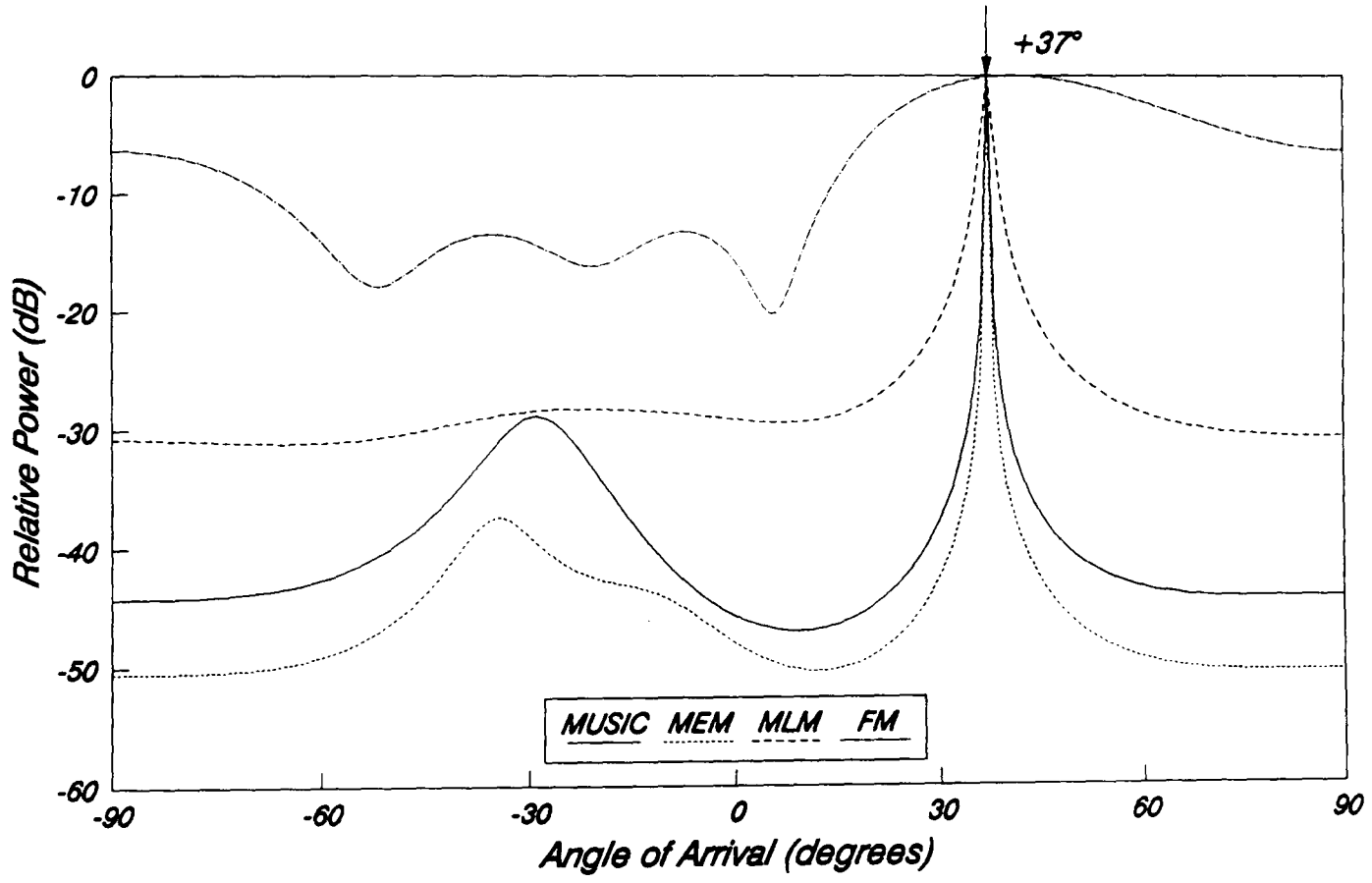

(b)

Figure 6.26: Spatial spectra for trial I with the patch array: (a) measured data; (b) simulated data.

the MEM and MUSIC algorithms to the measured results. The MDL criteria indicated that three sources were present with the measured data, but only one with the simulation which was to be expected. The result shown in figure 6.26b for the MUSIC algorithm assumes that the number of sources is equal to three. This clearly demonstrates that the higher resolution algorithms do have a tendency to produce spurious peaks which can not be attributed to actual signals. When discrete multipaths were introduced into the model (e.g. at a bearing of $+20^{\circ}$), the resulting spectra did not produce extra peaks to indicate their presence as expected. (The problem of coherent signal identification discussed in section 5.2.) However, the peaks/ripples in the $-10^{\circ} \rightarrow -40^{\circ}$ region were increased in height relative to the main signal peak.

The signal environment for trial I is difficult to model accurately without knowledge of the directions of the reflected signal energy, although the results presented have a high correlation with the measured results. Therefore, this provides evidence that the additional peaks in the measured spectra do not actually indicate the AOA of an extra source of signal energy, reflected or otherwise. If the photograph in figure 6.21 is considered there is in fact no obvious source for a reflection at this bearing.

6.3.2 Trial II - Great George St.

This was the first mobile trial undertaken, and a photograph of the route (as viewed from the start) is shown in figure 6.27. The street is fairly typical of an urban locality, with three to four storey town houses on each side, and parked cars in every available space along the road. The line of houses on the left-hand side is virtually continuous, while on the right-hand side the buildings vary as can be seen from the map in figure 6.25. The overall effect is that of an extremely cluttered signal environment. The large building of the Church of St. George[6] provides a significant obstruction to the signal energy, although just prior to the church there is a brief line of sight path to the base-station through the trees. (Note that the trees on the right-hand side of the street were not in full leaf during the period of the trials). Towards the end of the route, the houses on the right-hand side finish abruptly, and there is some open

---

6: Located at an approximate bearing of -30°.

Figure 6.27: The view of Great George St. from the start of trial II.

Figure 6.28: The view towards the base-station from the end of trial II.

parkland as shown in figure 6.28. This photograph was taken from the top of the street and shows the view towards the base-station antenna site. The base-station cannot be seen, since it is below the level of the rooftops, but the general direction is as indicated on the photograph.

The mobile was driven at an approximate speed of 5 m/sec along the route and frames of data were recorded at approximately 18 m intervals. Eleven frames were recorded in total, and the results of applying the FM, MLM, MEM and MUSIC[7] algorithms are presented in figure 6.29 for both the dipole and patch arrays. The phase only manifolds were employed for an elevation of 5°. The actual route followed by the mobile is given by the heavier line on the graph, and the results clearly show that all of the DF algorithms can successfully track the movements of the mobile, although with varying degrees of accuracy. In order to interpret these results, the route can be split up into four different sections as follows:

Frames 0 → 2 No LOS path, with buildings on both sides of the street.

Frame 3 Brief LOS path towards base-station between houses and church.

Frames 4 → 6 No LOS path, with buildings on both sides of the street. The church is also obstructing the path.

Frames 7 → 10 No LOS path but the street is now open on the right-hand side towards the base-station.

The estimated bearings for the first frame (**frame 0**) were generally too high for both antenna arrays, and the resulting spectra for the dipole array are given in figure 6.30. The MEM technique on this occasion produces the most accurate result, but notice the broad beam and clustering exhibited by the MLM algorithm, and the low shoulder/peak in the MUSIC spectrum indicates the presence of scattered signals at AOA's less than the actual bearing. The FM spectrum exhibits the characteristic broad main beam.

The dipole and patch results for **frames 1** and **2** are on either side of the actual bearing, indicating a definite spread with this scattering environment of the order of 12°. Some clustering in the spatial spectra for the patch array in **frame 2** confirms this also. Near the location of **frame 3**

7: The result for the MUSIC algorithm is representative of all the eigenstructure techniques.

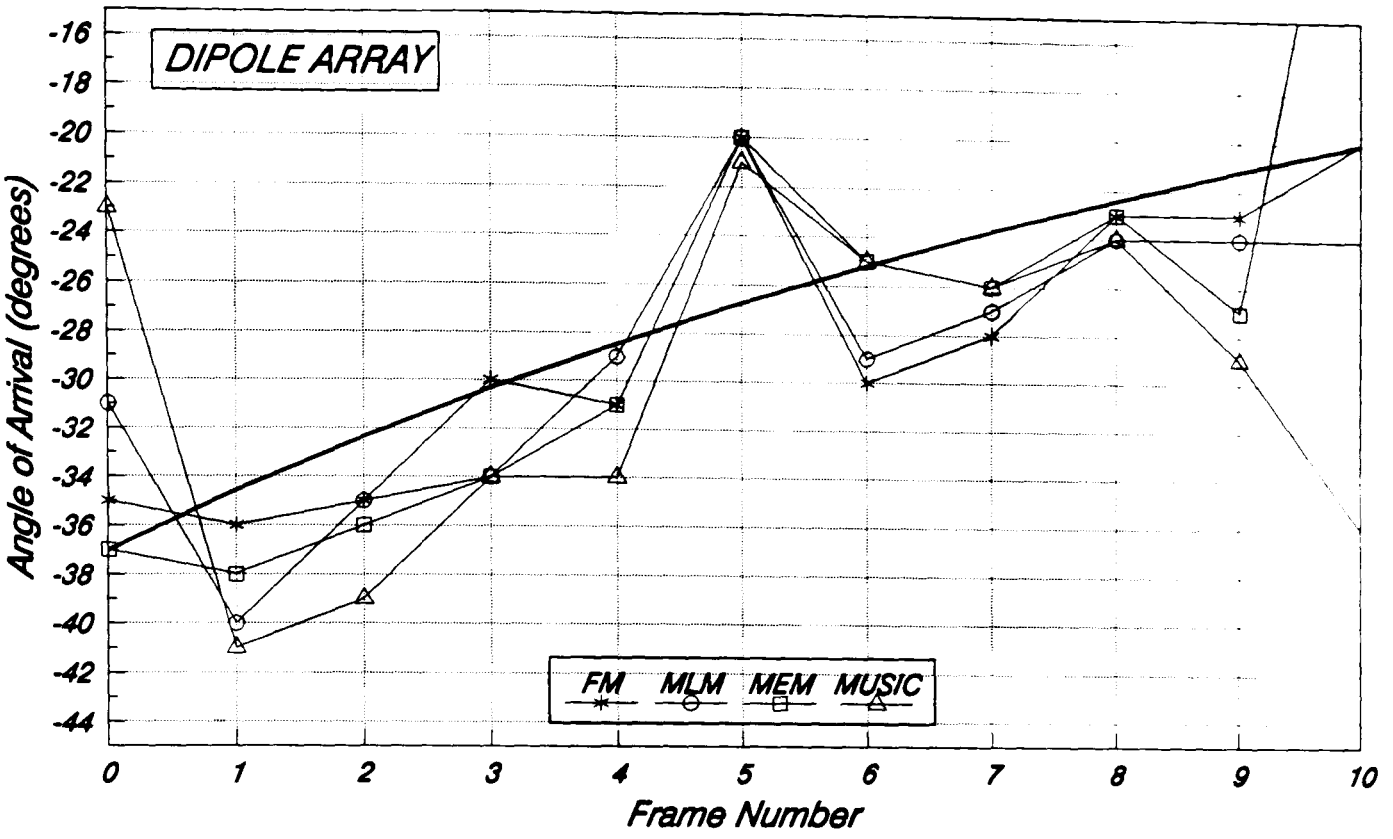

(a)

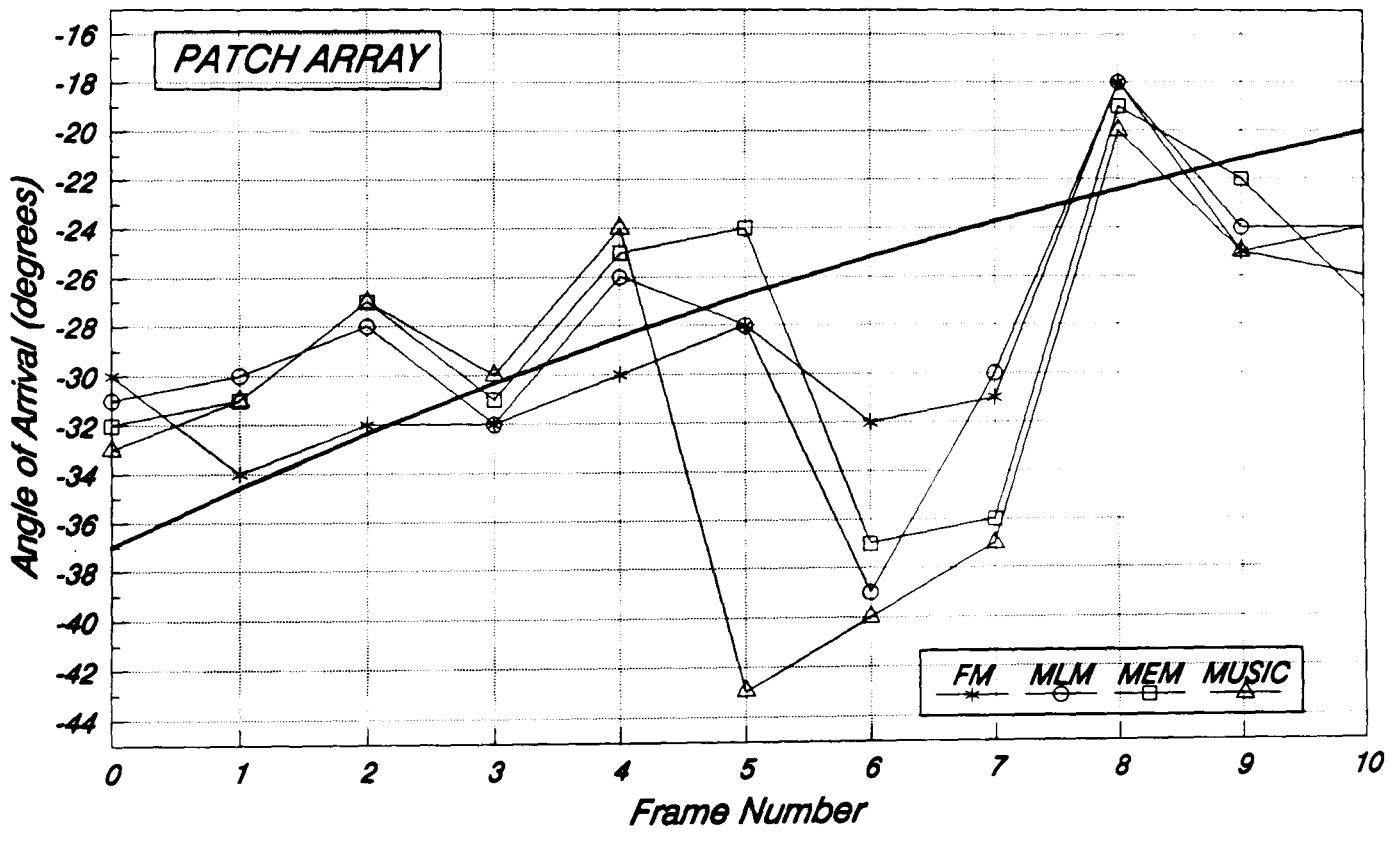

(b)

Figure 6.29: Estimated bearings for trial II with: (a) the dipole array; (b) the patch array.

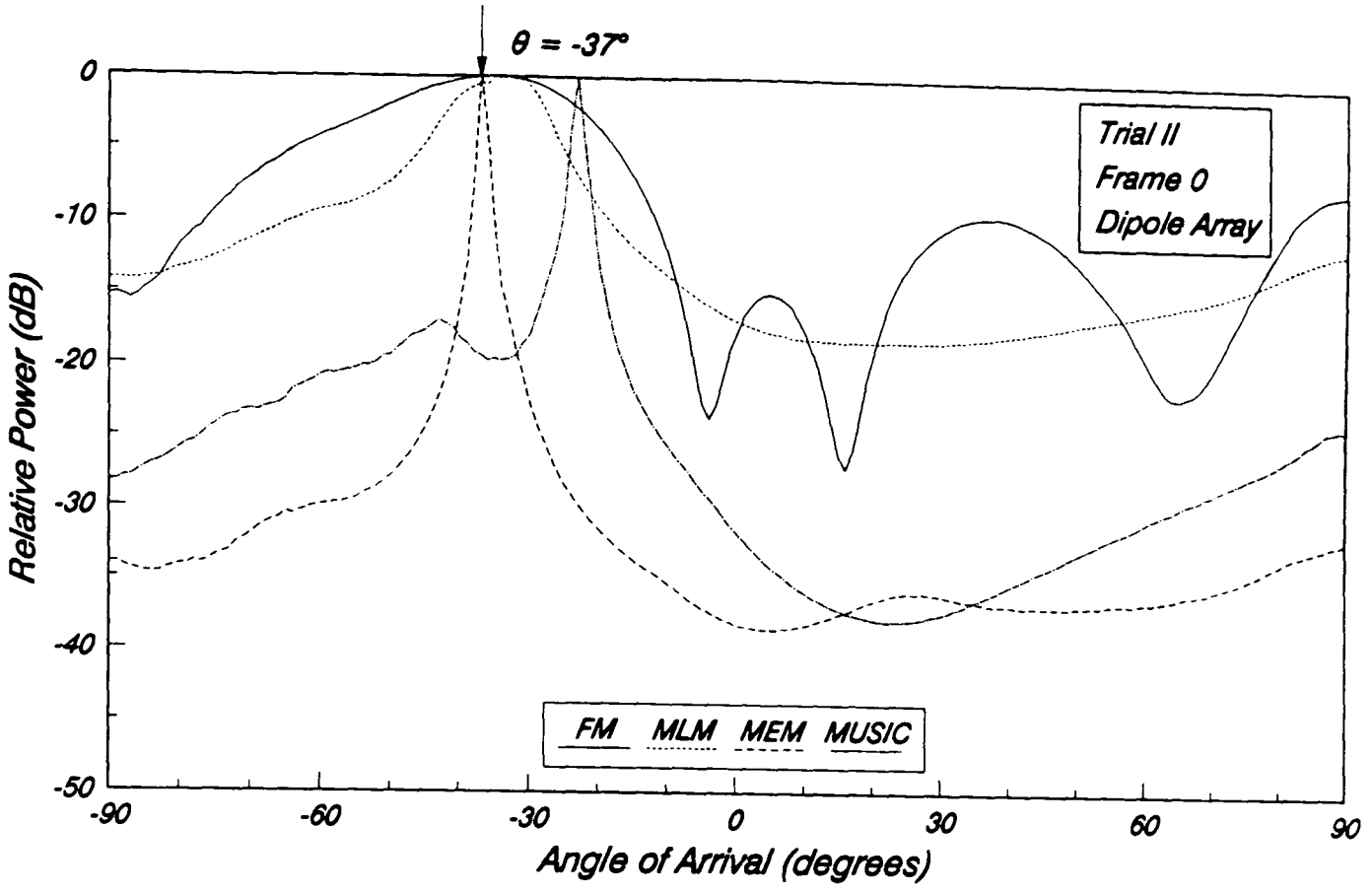

Figure 6.30: Spatial spectra for frame 0 of trial II with the dipole array.

there is a brief LOS path, and this is reflected in the results for the patch array, with all the algorithms producing strong, single peaks with a spread of only 2°. The peaks in the dipole results tended to be broader, indicating that the mobile was not quite at the LOS location, although the spread has still been significantly reduced to only 4°.

The results for **frame 4** are very interesting, with the estimated results for each antenna either side of the actual bearing. This can be attributed to some extent to the church obstructing the signal path and forcing the scattered signals to go either side. Figure 6.31 is a very good example of this phenomenon, and shows the resulting spatial spectra for the patch array, with the shoulders in the MUSIC and MLM responses indicating the presence of some scattering below the actual bearing. **Frames** 5 and 6 exhibit similar effects, with the patch array tending to produce peaks below the church, and the dipole above. Hence, the presence of a large building has increased the degree of scattering significantly, producing an angular spread of the order of 20° (particularly noticeable in **frame 5**).

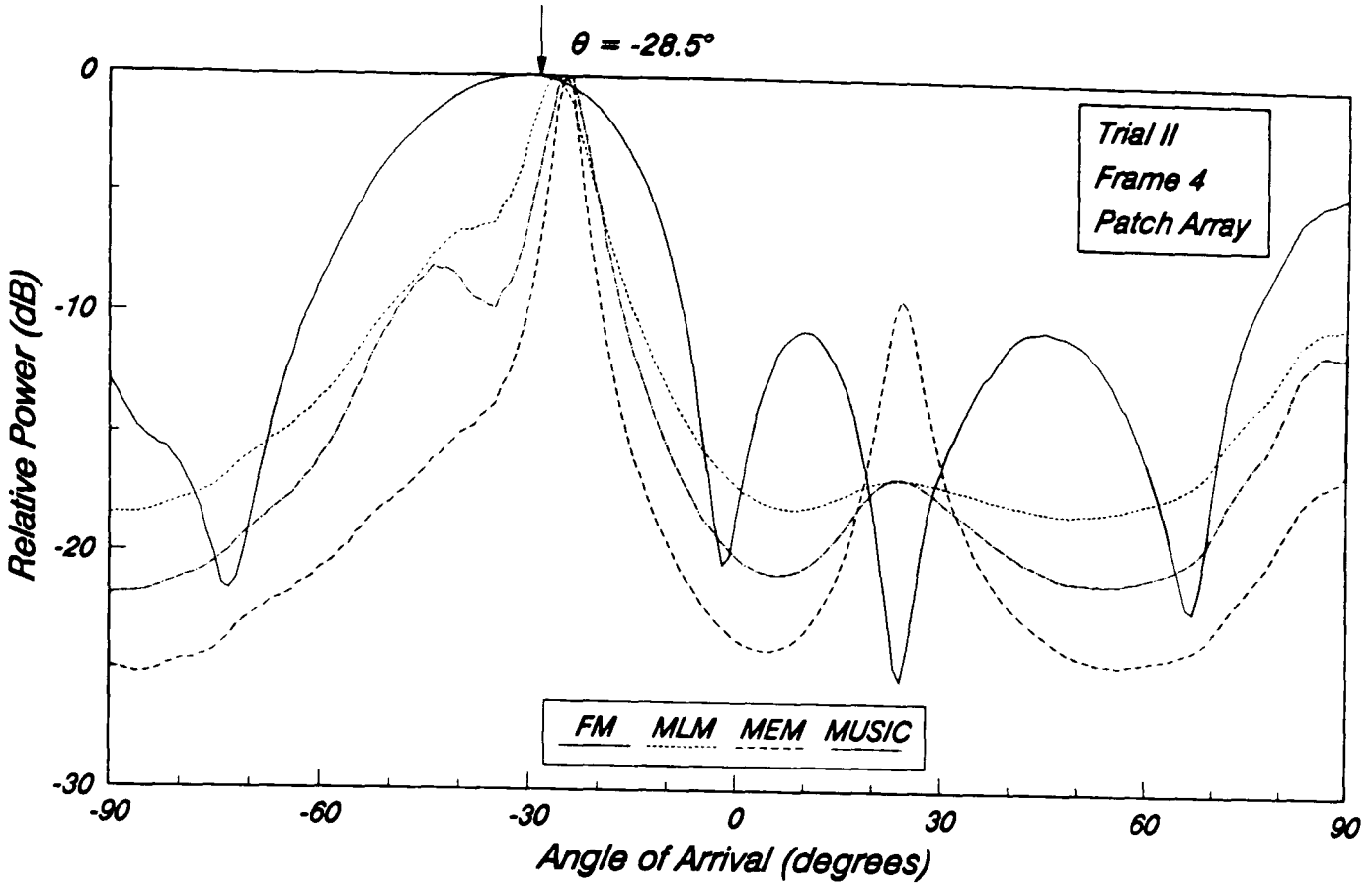

Figure 6.31: Spatial spectra for frame 4 of trial II with the patch array.

From **frame 7** onwards there are no houses on the right of the street and the scattering environment changes considerably. (The patch results for **frame 7** suggest that the mobile was possibly just before this point since the estimated bearings are more consistent with the previous frame.) This difference can be seen from the photograph in figure 6.28, with the reduced angular spread in **frame 8** ($\theta_s \cong 6^\circ$) attributed to a strong diffracted signal path over the rooftops. In general, all of the spectra exhibited some degree of clustering, and in **frames** 9 and 10 the tendency was to estimate the AOA below the actual bearing even though the actual spread is quite low.

The MUSIC and MEM results for **frame 10** with the dipole array were very interesting and are shown in figure 6.32. Notice the strong peaks in both the MUSIC (-36°) and MEM (-2°) responses on either side of the actual mobile bearing. The bearing errors are $+18^\circ$ and -16° respectively and clearly show the susceptibility of the higher resolution techniques to reflections other than the main wanted signal. The FM and MLM techniques on the other hand, gave estimates somewhere in between these two extremes, providing some confirmation of the simulation results presented in chapter 5. The tendency of the high resolution techniques to produce larger deviations in the

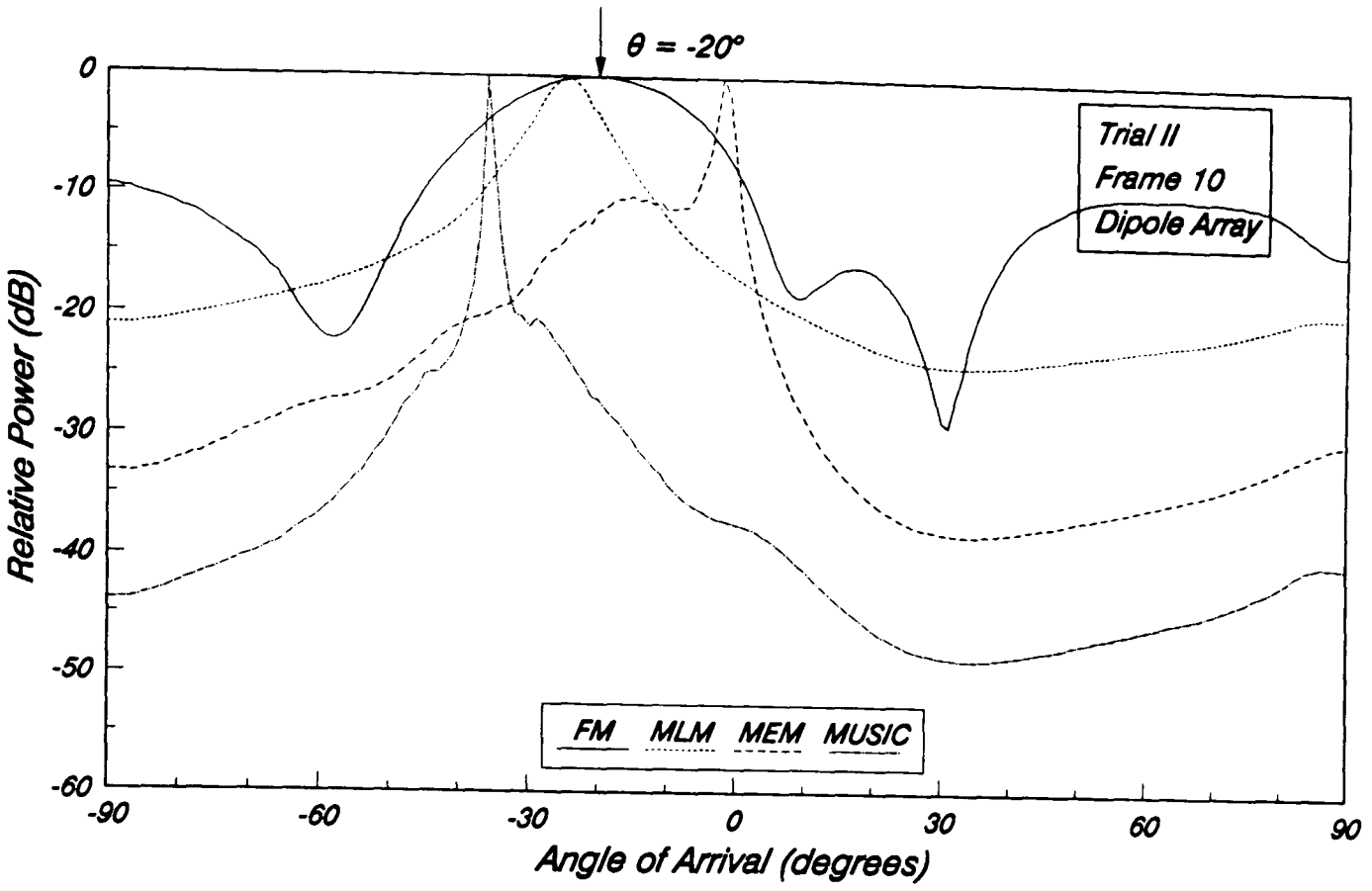

Figure 6.32: Spatial spectra for frame 10 of trial II with the dipole array.

estimated bearing was found to be generally true, and is particularly noticeable in the patch results for **frame 5** and **frame 7**.

6.3.3 Trial III - Charlotte St. South

This is the second mobile trial, and the route is shown in the photograph given in figure 6.28. The mobile starts at one end of Charlotte St. South (lower left-hand corner of figure 6.28), and moves across in front of the row of houses up to the corner with Charlotte St. (see also the map in figure 6.23). Frames of data were taken at approximately every 12 m and the total distance travelled by the mobile was 96 m. The photograph in figure 6.28 clearly shows that the signalling conditions for this route are very different from those found in Great George St. The row of houses ensures that there is no LOS propagation, although at the corner with Charlotte St. there is a clearer path towards the base-station as shown in figure 6.33. This is the view down Charlotte St. with the base-station situated just behind the rooftops of the row of houses on the left as indicated.

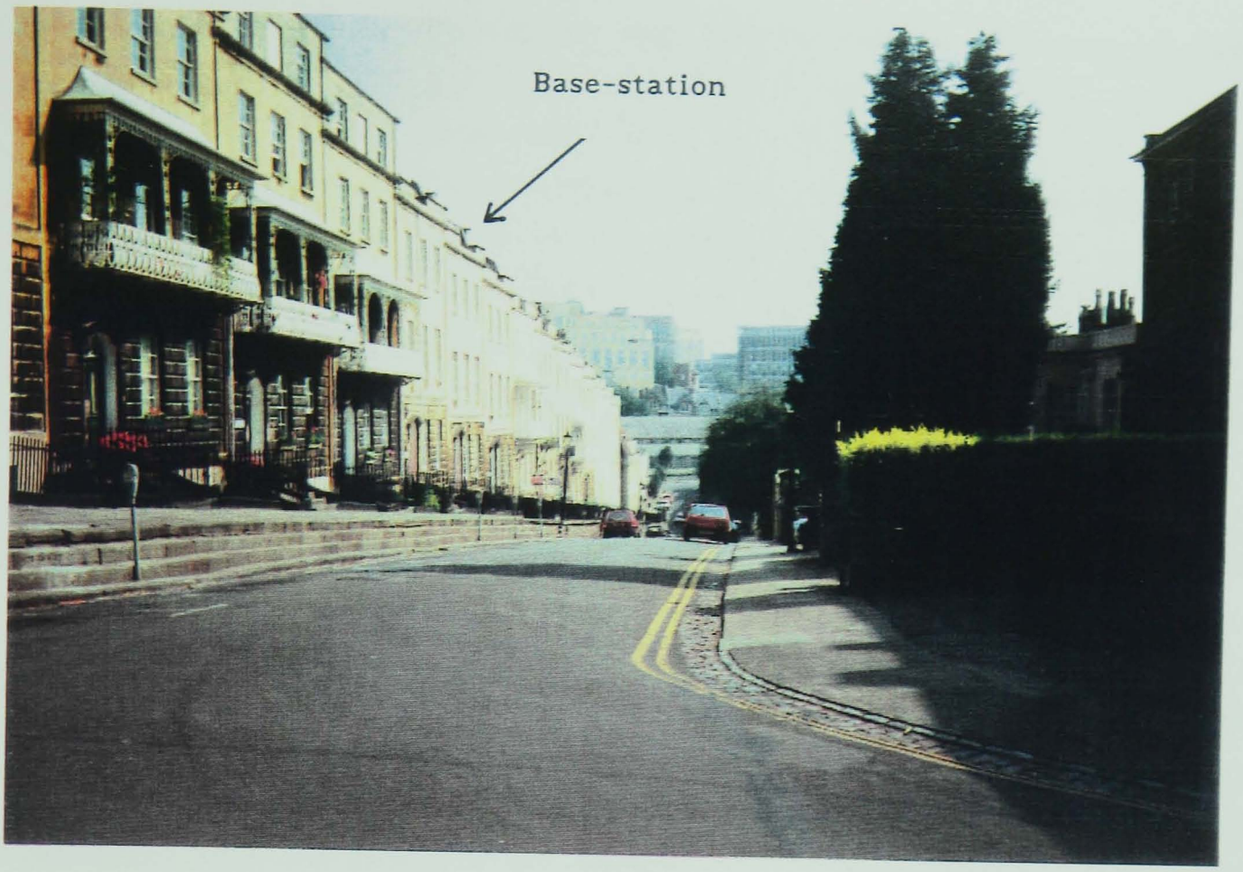

Figure 6.33: The view from the end of Charlotte St. South down Charlotte St.

Figure 6.34: The view of Park St. from the start of trial IV.

The results of applying the FM, MLM, MEM and MUSIC algorithms are given in figure 6.35 for both the dipole and patch arrays and, as with the Great George St. trial, the phase only manifolds at an elevation of 5° were employed. The most noticeable trend with the results is a reduction in the angular spread of the signals as the mobile moves towards the end of the route. This can be partly attributed to the closer proximity of buildings at the end of the route, as well as the fact that the parkland slopes up more steeply, thereby reducing the degree of scattering. Generally, the resulting spatial spectra for all the algorithms produced single peaks, although occasionally MUSIC and MEM produced responses which exhibited broad clusters of peaks. This was very noticeable with the MUSIC response for **frame 1** with the dipole array. The dominant peak was at -37° (an error of -16°) with a broad shoulder extending up to -20°, and indicating a spread of 17°. **Frame 3** with the dipole array was another example and the resulting spectra are shown in figure 6.36. Notice the broad clustering in the MUSIC response producing an angular spread of approximately 10°. This can be partly attributed to reflections from the Church of St. George.

The results for **frame 2** with the patch array show a similar effect, with both the MUSIC and MEM techniques producing responses with broad peaks as shown in figure 6.37. The MEM response in particular indicates a very large spread and again, it is very likely that this is the result of strong reflections from the Church of St. George. Note however, that when the degree of scattering is large, both the FM and MLM technique tend to produce only single peaks and so give the best estimates of the mobile's bearing. This phenomenon was one of the most significant findings from the computer simulations in chapter 5.

The general trend from the results up to and including **frame 6**, is to produce a lower AOA than the actual bearing, although in **frame 4** with the dipole array there is a very strong indication of signal energy from a bearing nearer to the end of the street. The FM result with the patch array in **frame 3** is at a similar bearing, although it is more likely that this is a result of low signal levels and a reduced SNR. Hence, in the early part of the route, the angular spread of the signals is quite large ($\theta_s > 15°$), and this is partly the result of the open parkland on one side of the street. From **frame 6** onwards however, there is a definite reduction in the spread of the signals as mentioned earlier, with all the DF algorithms producing single narrow peaks. An angular spread of only 6° would be a reasonable value.

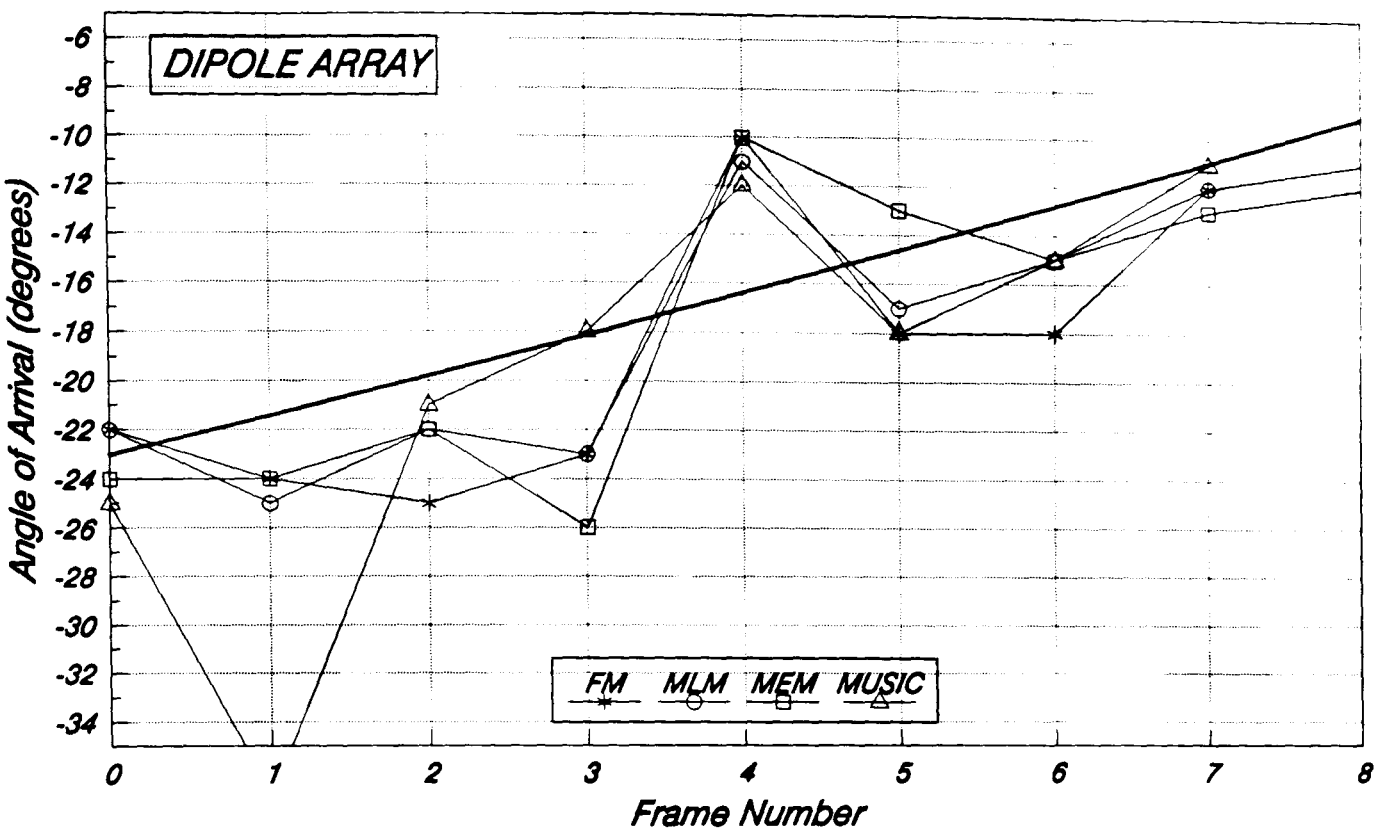

(a)

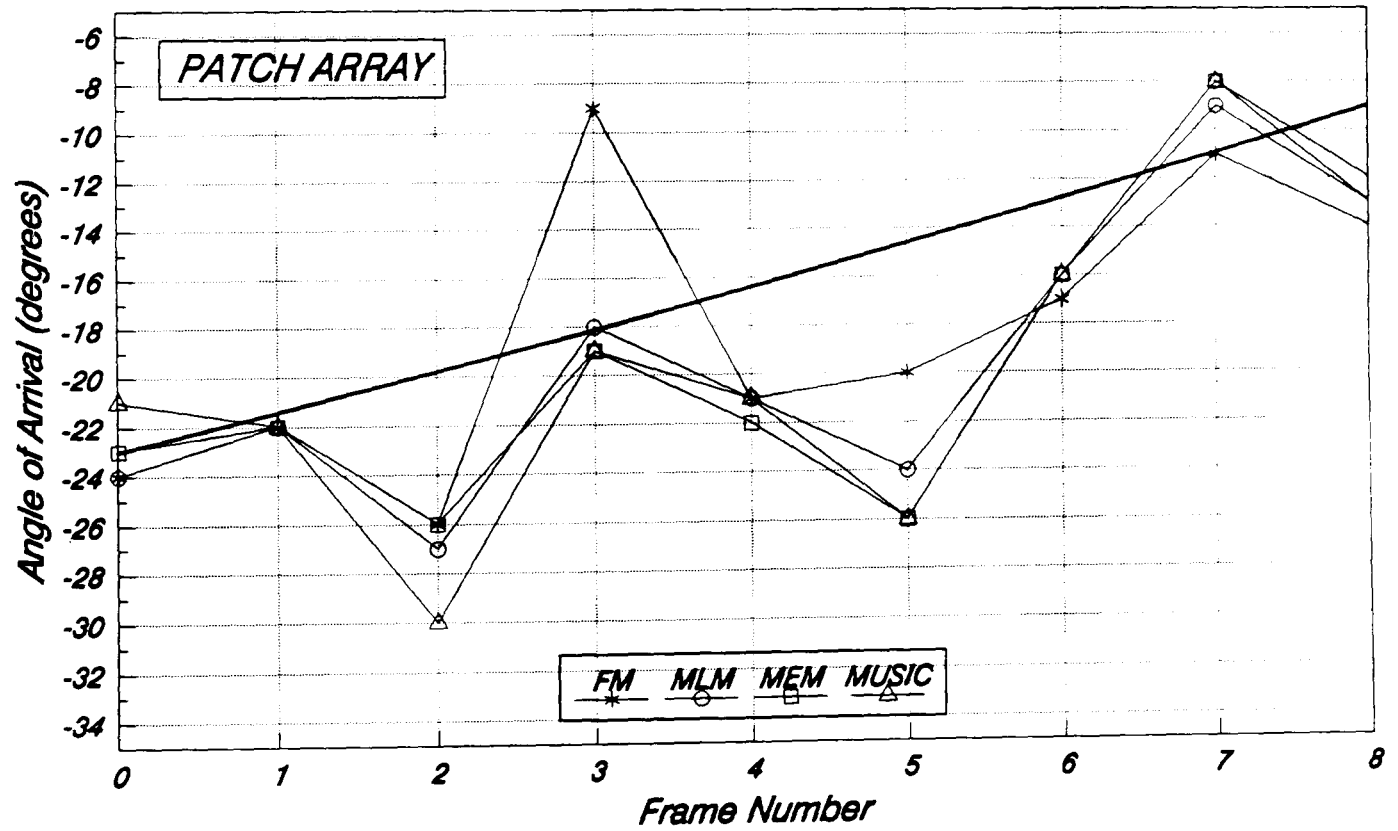

(b)

Figure 6.35: Estimated bearings for trial III with: (a) the dipole array; (b) the patch array.

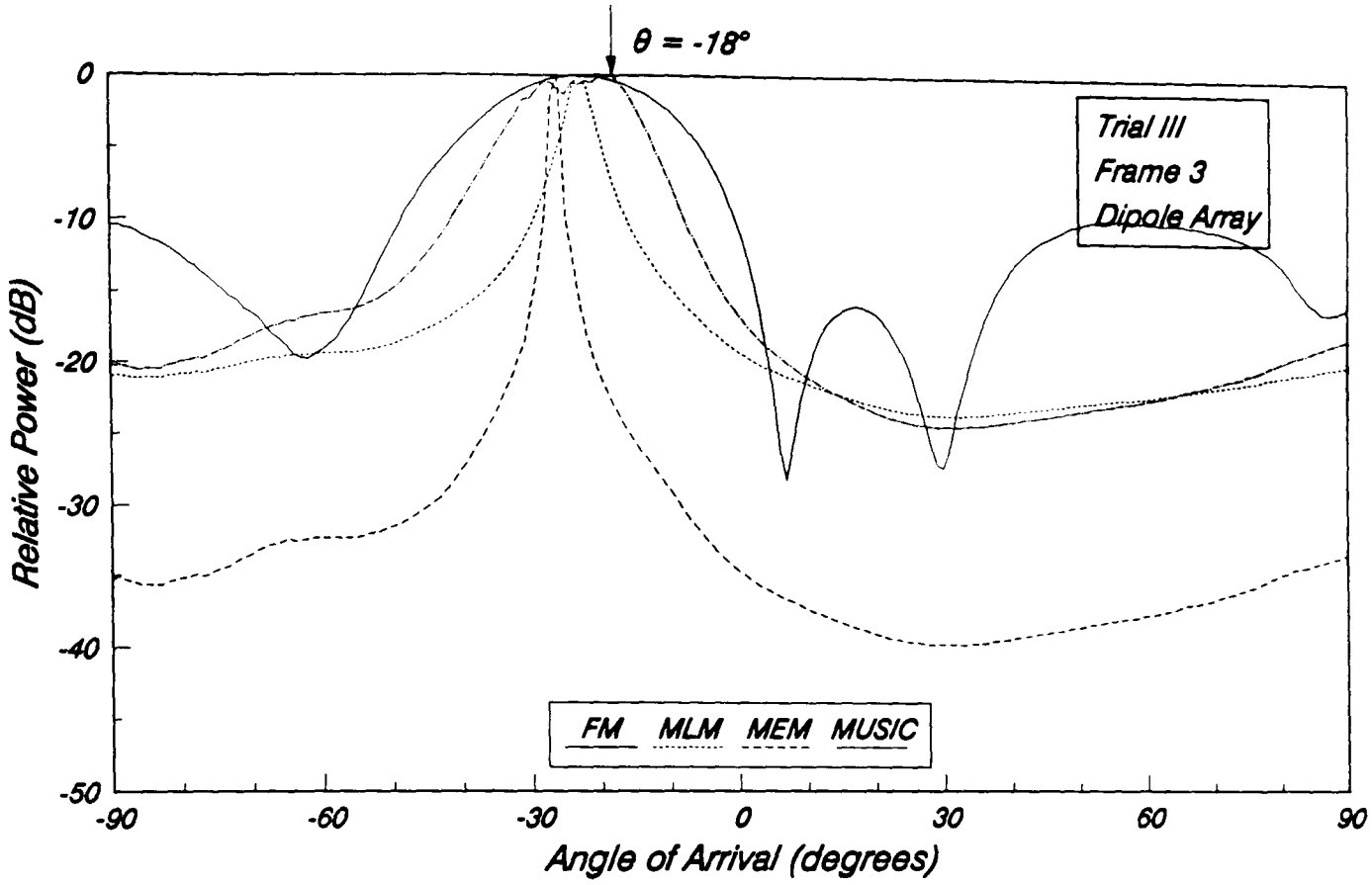

Figure 6.36: Spatial spectra for frame 3 of trial III with the dipole array.

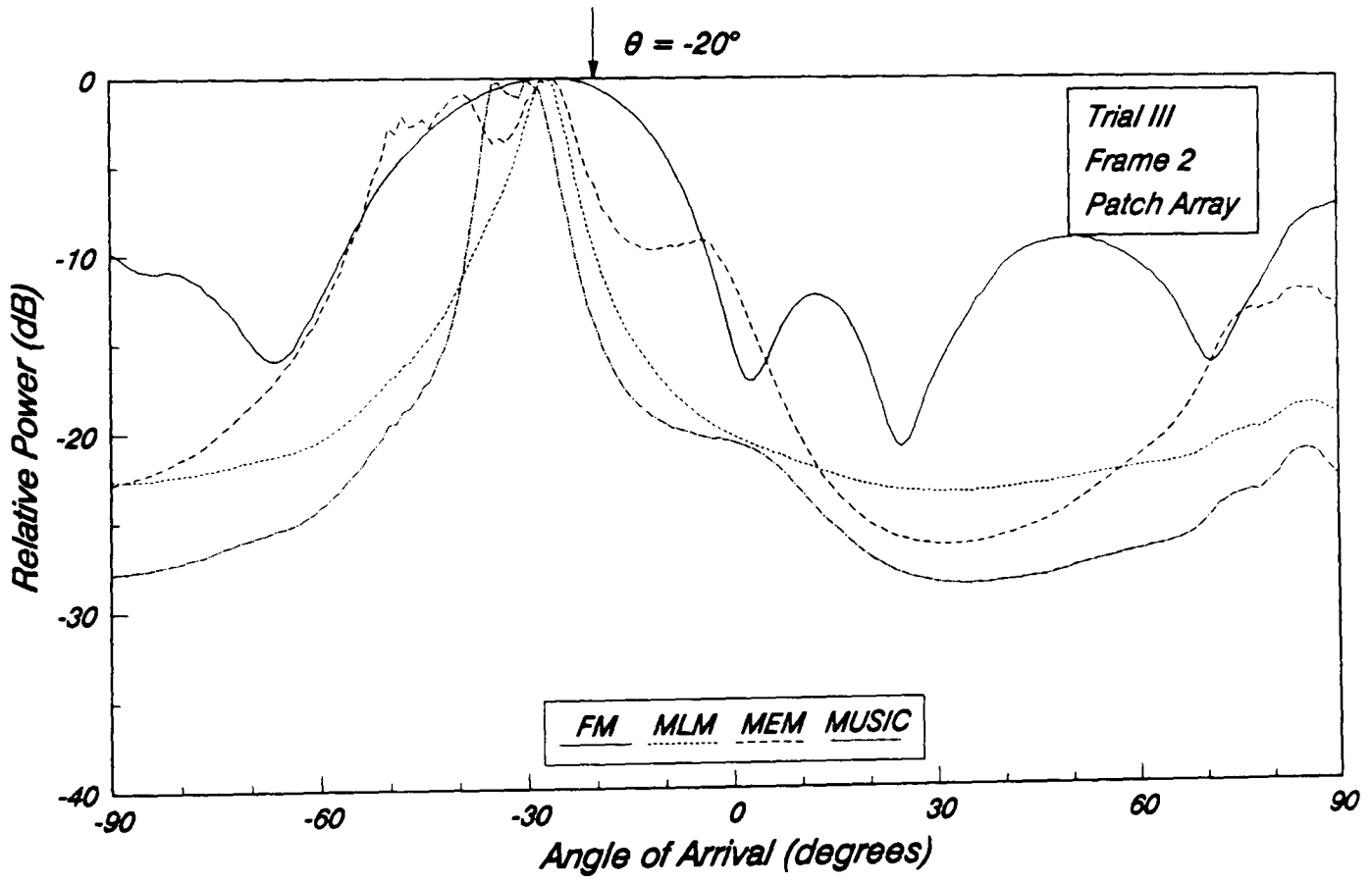

Figure 6.37: Spatial spectra for frame 2 of trial III with the patch array.

6.3.4 Trial IV - Park St.

Unlike the previous routes, Park Street is a busy main road and potentially offers the greatest challenge to the DF processing encountered so far. A view of Park St. from the starting point in the route is shown in figure 6.34, with the large building at the top of the street (Wills Memorial Building) providing an obvious source for a strong reflection. Consequently the results of the field trials were dominated by this structure, and some very interesting effects were noticed. As with the other mobile trials, the estimated bearings from the FM, MLM, MEM and MUSIC algorithms are shown in figure 6.38. The phase only manifolds were employed with an elevation of 10° and the distance between the frames was approximately 22.5 m.

The resulting spatial spectra for the first four frames (**frames 0** to 3) all exhibited two peaks as illustrated with the spectra in figure 6.39. These results were generated from the dipole array and correspond to **frame 1**. The additional peak is clearly as a direct result of a reflection from the Wills Memorial Building, with the centre of the tower at an approximate bearing of $+25^{\circ}$. In **frame 3** however, the peak associated with the mobile did not dominate as shown in figure 6.40, and hence underlines the problem of unambiguously determining the correct bearing of the mobile source. Closer inspection of **frame 3** is very revealing however, especially if a 100 snapshot window is moved across the total frame and the spatial spectra generated at 50 snapshot intervals. Over a 500 snapshot data frame, there are eight different sets of spectra and, generally, all contained the expected two peaks. However, the dominant peak changes as the 100 snapshot window moves across the total frame, with at first the reflection dominating and then the mobile. The result with the whole 500 snapshot frame clearly favours the reflected signal, but this exercise demonstrates that the signal environment is changing very rapidly. Hence in this situation either more snapshots of data are required to enable a confident prediction of the mobile's bearing, or knowledge of the previous estimate can be employed to discount any spurious peaks. Alternatively, if the base-station was armed with knowledge of the bearings of fixed reflectors like the Wills Memorial Building, such ambiguous estimates could be avoided. This problem is addressed in more detail in section 6.4.

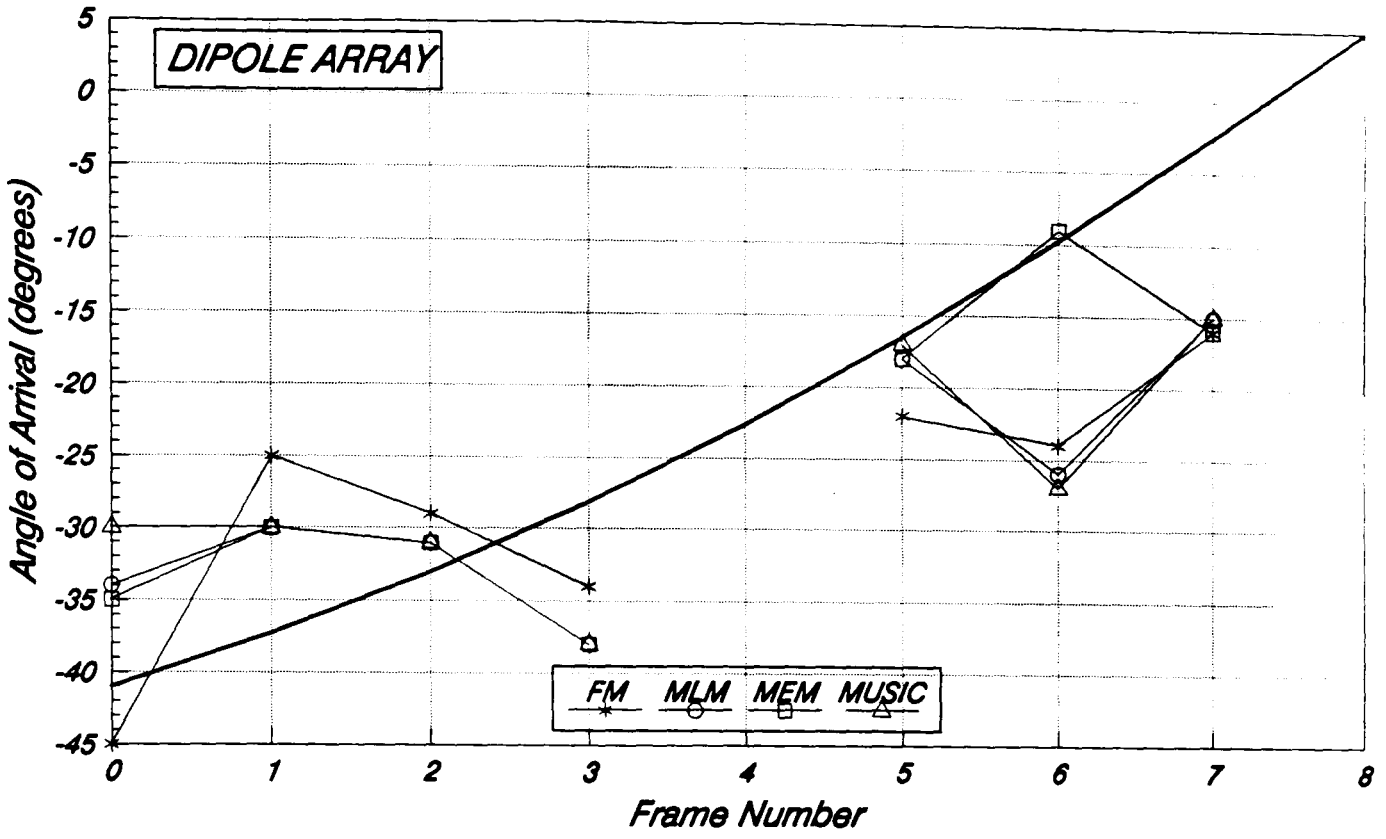

(a)

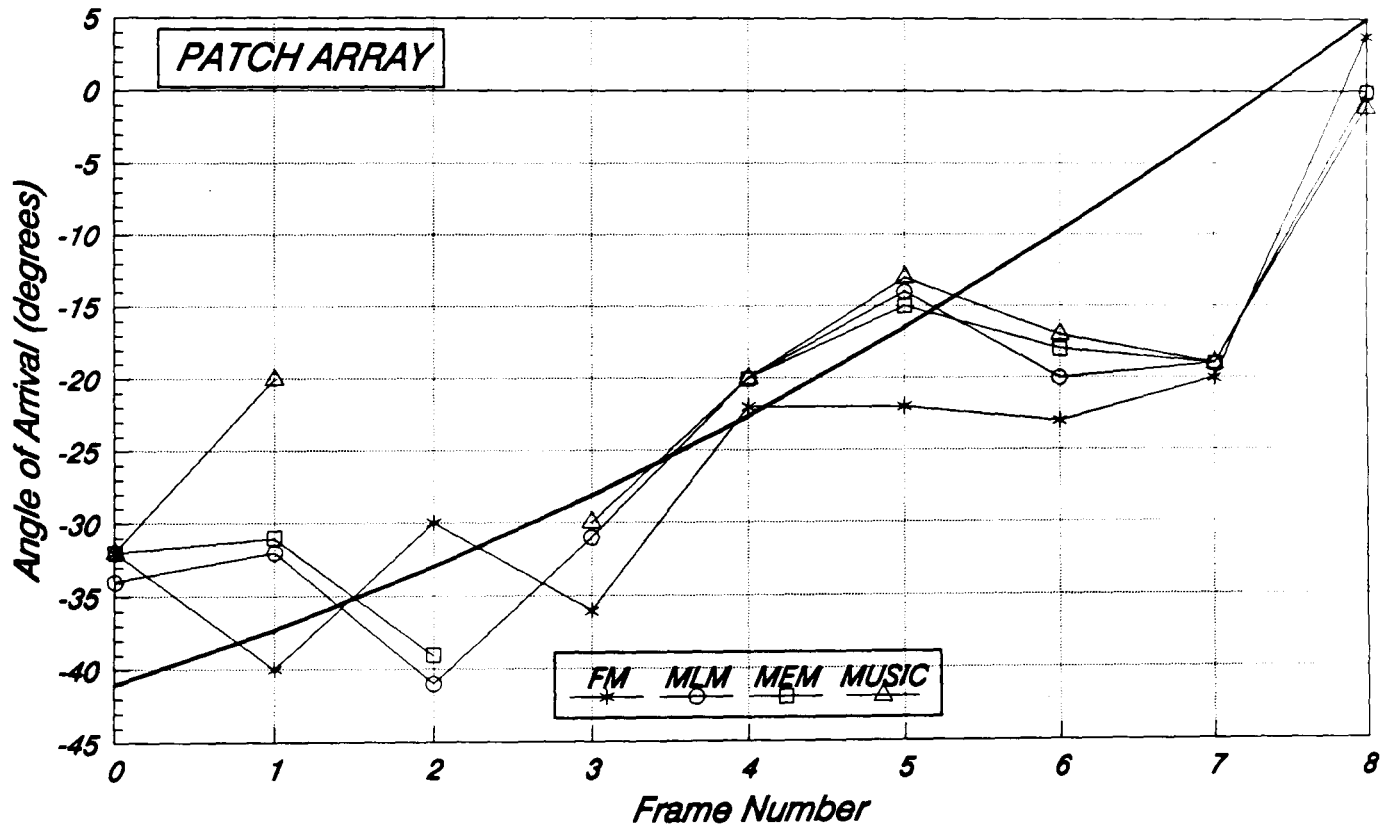

(b)

Figure 6.38: Estimated bearings for trial IV with: (a) the dipole array; (b) the patch array.

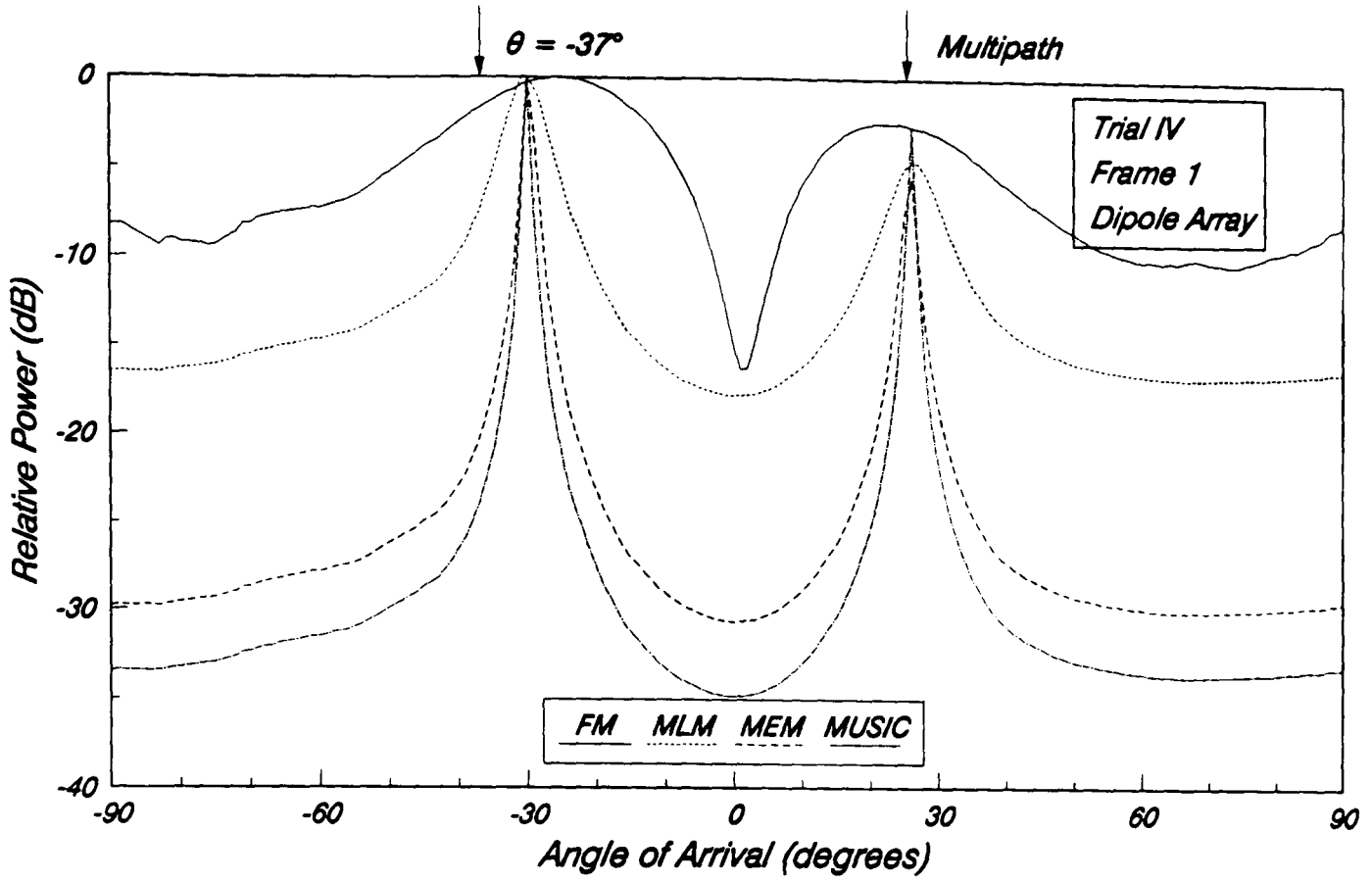

Figure 6.39: Spatial spectra for frame 1 of trial IV with the dipole array.

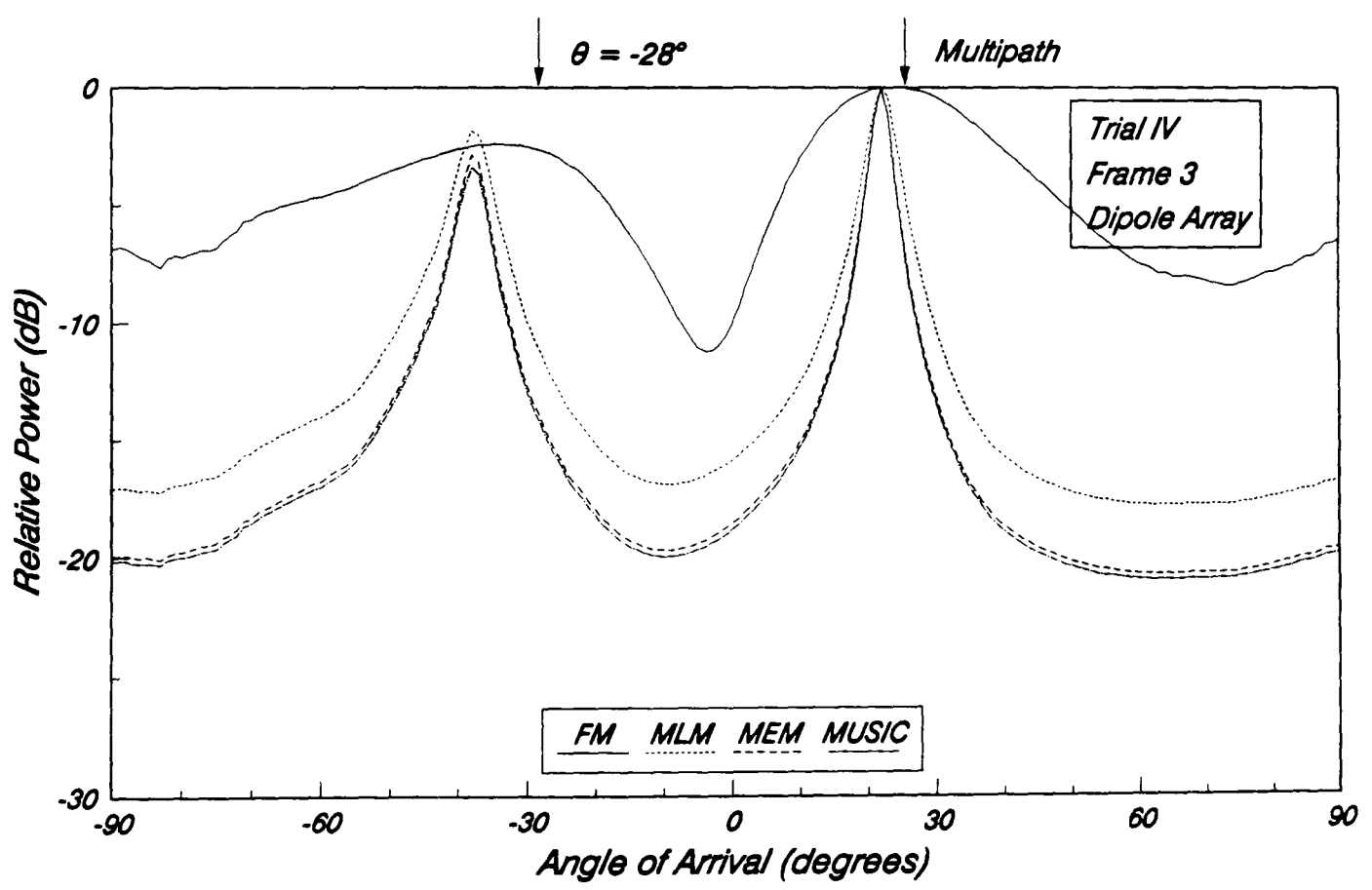

Figure 6.40: Spatial spectra for frame 3 of trial IV with the dipole array.

The results for **frames 0 to 3** with the patch array were very similar, with both MUSIC and MEM having a tendency to give the reflection off the Wills Memorial Building as the dominant signal source. In **frames 2** and **3** for example, MUSIC and MEM respectively failed to give any indication of the mobile source. The resulting spectra for the rest of the frames with the patch array tended to produce a single peak defining the mobile's position only, although the position of the peak is obviously strongly affected by the presence of a reflected signal.

In **frames 4** and **8**, with the dipole array, no usable information could be gleaned from the spatial spectra. In **frame 8** this can be attributed to the signal envelope being in a deep fade, and so a reliable position estimate would require further data frames. The results for **frame 4** require a different explanation, and this is where the experience gained in chapter 5 regarding two coherent signals incident on the array can be applied. At this point in the route, the mobile is very close to the junction with Charlotte St. (see figure 6.23). Hence there is a brief moment when there are no buildings on either side of the mobile, thus reducing the degree of local scattering and potentially resulting in only two coherent multipath signals incident onto the array. In fact, the application of spatial smoothing does provide evidence for this, with peaks in the MEM and MUSIC spectra indicating the position of the mobile and the strong reflection respectively. Hence, future work will have to consider the application of spatial smoothing techniques in more detail in order to resolve problems like this.

The large offsets in the estimates for **frames 6** and **7** can partly be attributed to a strong reflection at a bearing of approximately -25° from the small side street off to the right of Park St. (see figure 6.23). This effect can be confirmed by considering the resulting spectra from **frame 6** with the dipole array given in figure 6.41. Clearly the results for MUSIC and MEM show the characteristic clustering effect that was illustrated in the computer simulations of chapter 5. Hence an angular spread of 18° can be expected at this point in the route.

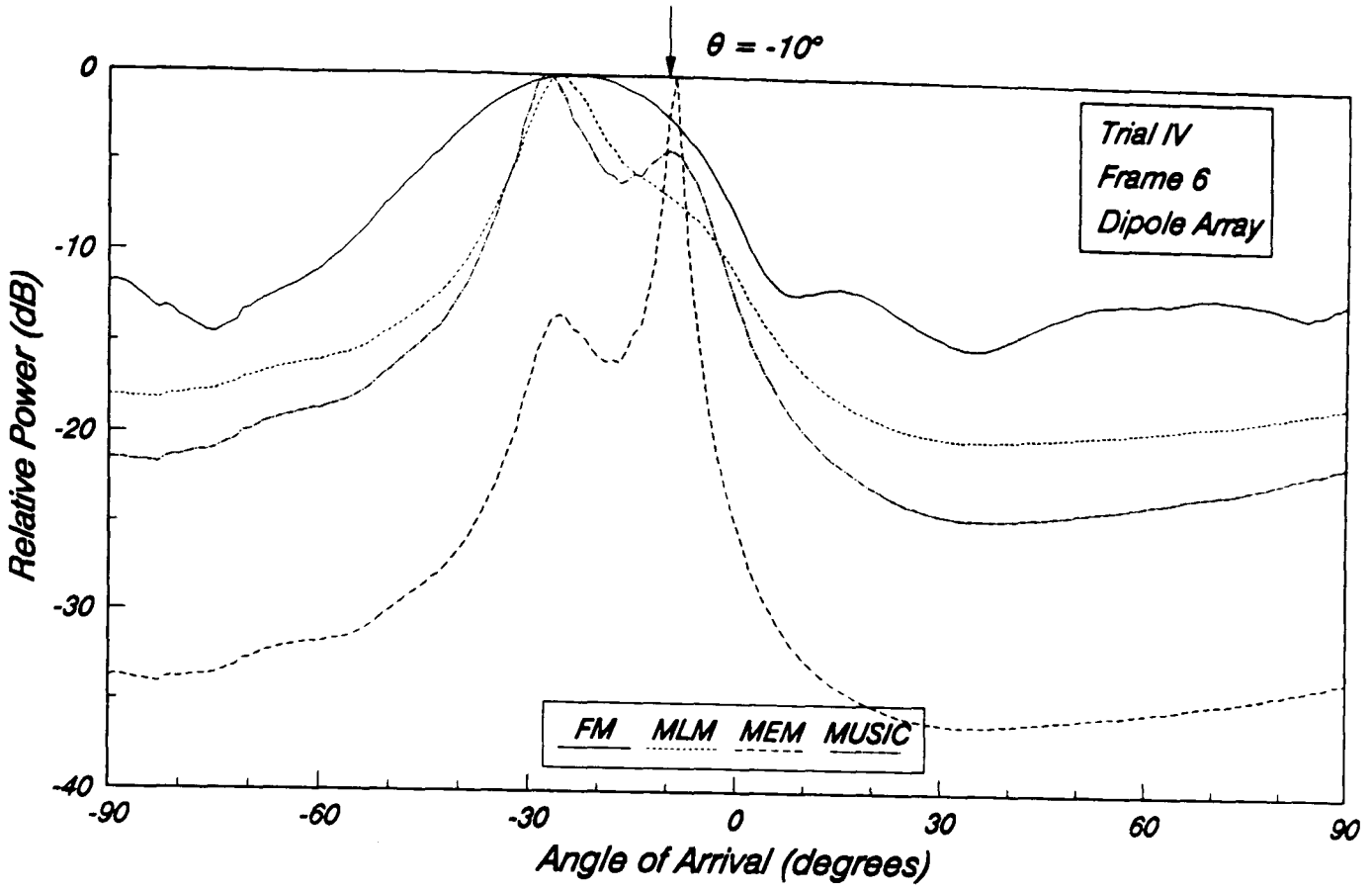

Figure 6.41: Spatial spectra for frame 6 of trial IV with the dipole array.

6.3.5 Trial V - Berkeley Square

This is the final mobile trial to be discussed here and a photograph of the route as seen from the base-station antenna is given in figure 6.42. Notice the RF front end hardware in the foreground, as well as Cabot Tower in the background which defines the broadside direction of the array. The starting point for the run is as indicated and the arrow shows the direction taken by the mobile around the square. (See also the map in figure 6.23.) Again the four main DF algorithms were employed (FM, MLM, MEM and MUSIC) and the results are presented in figure 6.44 in the usual manner. The phase only manifolds at an elevation of 5° were employed and the distance between frames was 15 m. Hence, the distance travelled along the first part of the route up to the corner of the square is approximately 70 m, followed by a 95 m stretch to the end of the run.

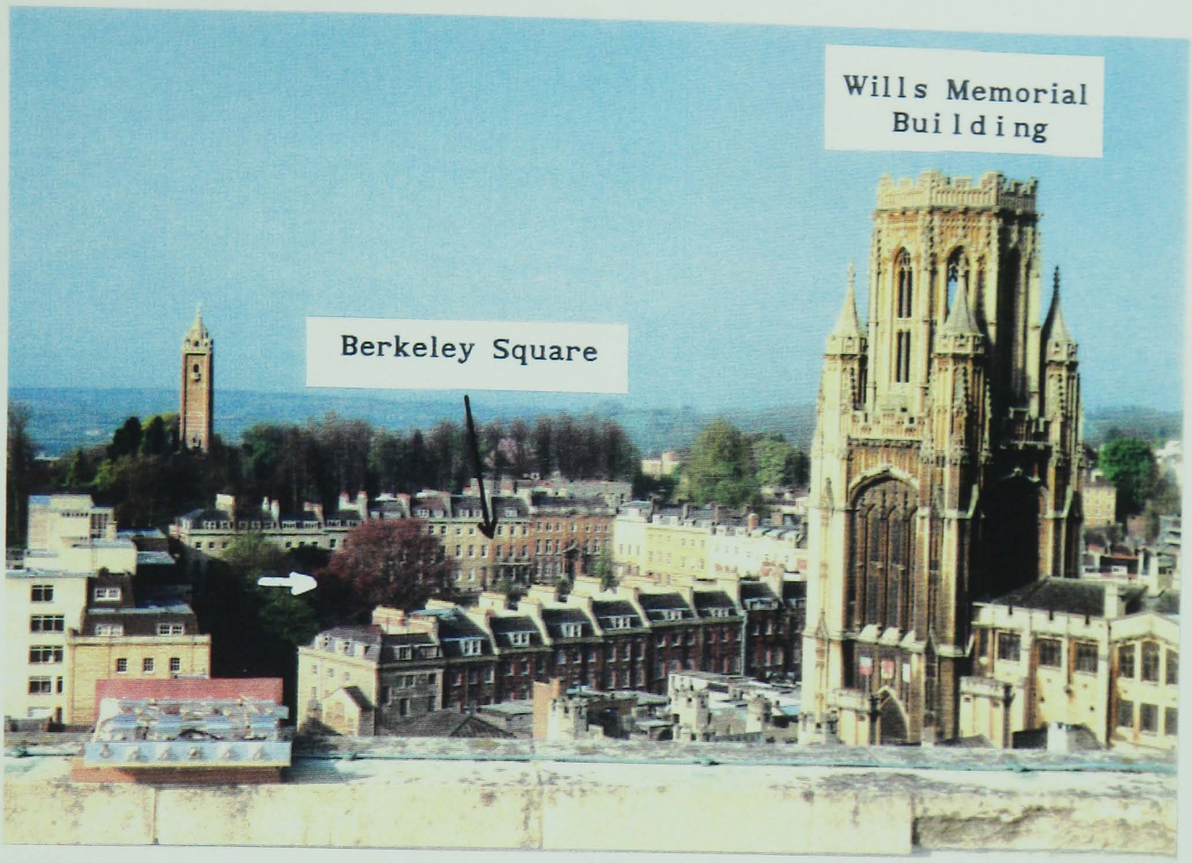

Figure 6.42: Berkeley Square (trial V) as viewed from the base-station site.

Figure 6.43: The view back from the end of trial V.

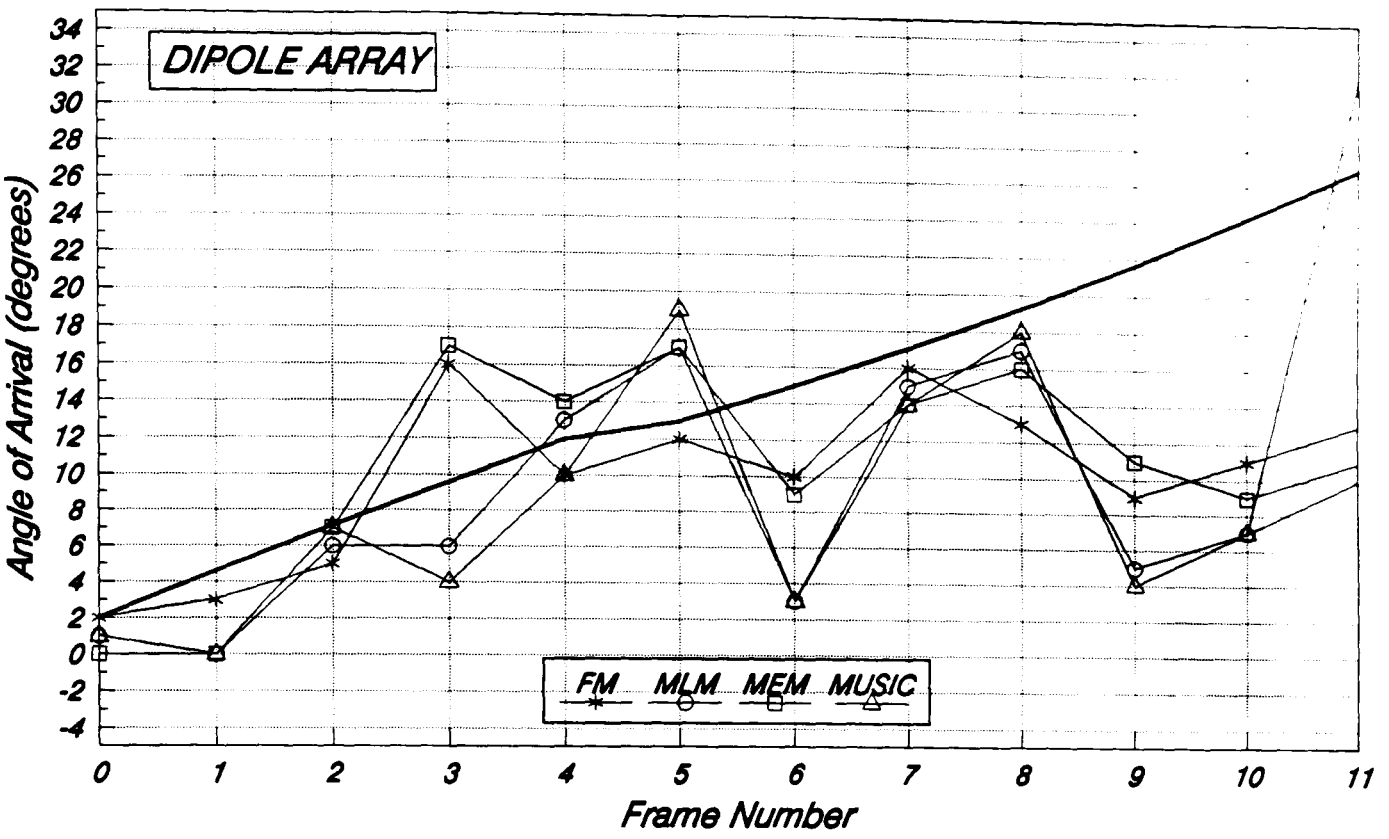

(a)

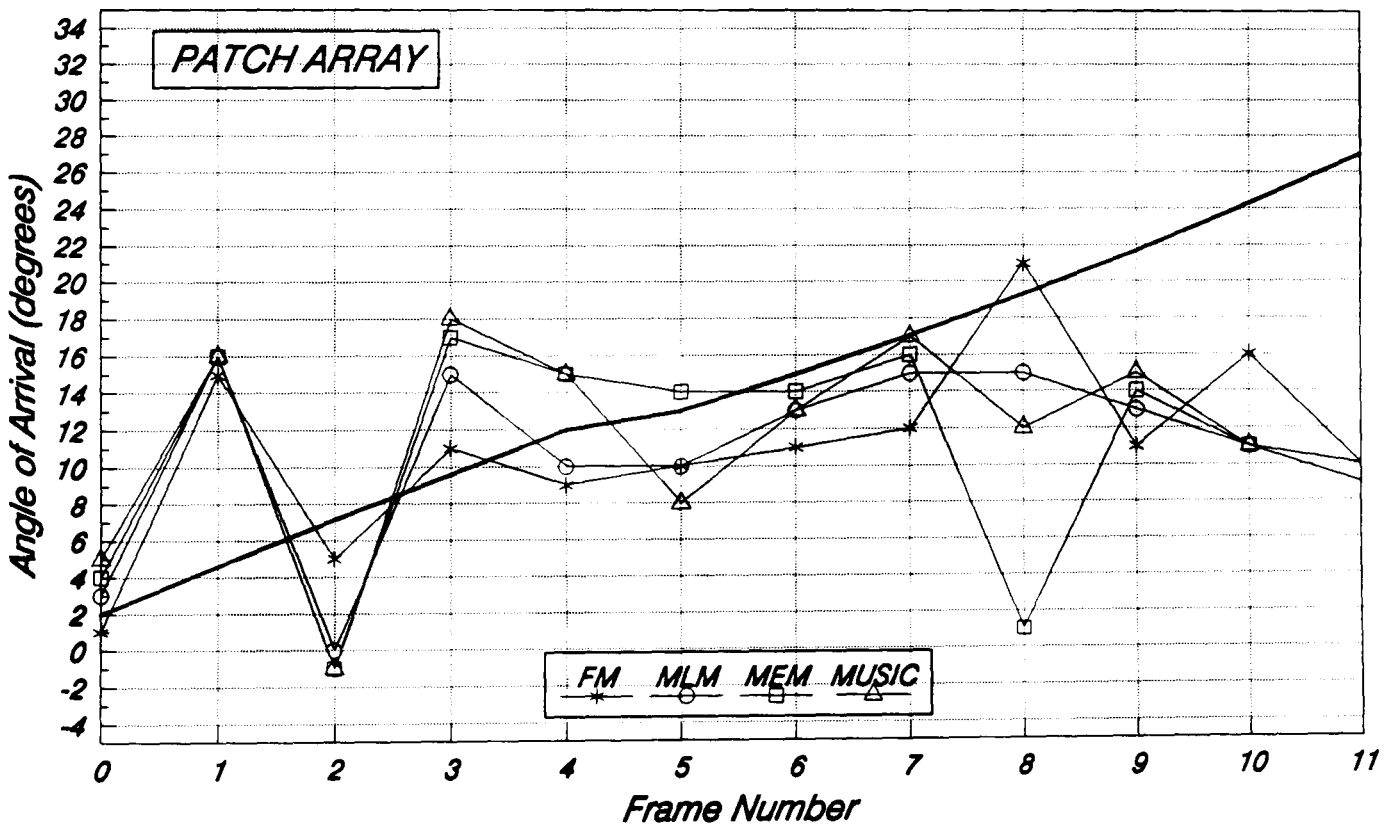

(b)

Figure 6.44: Estimated bearings for trial V with: (a) the dipole array; (b) the patch array.

The resulting spectra for **frames 0, 1** and **2** with the dipole array gave single narrow peaks which was to be expected since there is a LOS path to the base-station at the start of the run, although the trees present will introduce some shadowing. The patch results for the same frames were very interesting however, clearly showing that even though there is a LOS path, there are some strong reflections present. In **frame 1**, a single peak in all the spectra clearly indicates a strong reflection from the buildings on the right-hand side of the square (as viewed from the base-station). In **frame 2**, the single peak in the spectra again shows the presence of a strong reflection, but this time it is from the buildings on the left-hand side of the square, although the peaks are quite broad, indicating the presence of other scattered signals. Hence, the spread over this early part of the route is approximately 17°, with only the FM technique proving to be less susceptible to the scattered reflections. It is worth noting though, that over the short period of time in which data is acquired, only one scattered/reflected signal may dominate. The tendency for all the DF algorithms to produce very close estimates confirms this. If the run is repeated, a different set of signals/reflections dominates with each antenna array.

The resulting spectra for **frames 3, 4** and **5** (both antennas) show signs of an increase in the scattering of the signals with broader peaks and clusters in the spatial spectra. This is to be expected since the mobile is now starting to move below the line of houses on the opposite side of the square, and in frame 5 has just turned the corner of the square. The results for **frame 4** with the dipole array are fairly typical and are shown in figure 6.45. The response with each algorithm, especially MUSIC, clearly exhibits the characteristic shape when a tight cluster of signals is incident onto the array, and indicates a spread of only 6°. Hence, over this section of the route, the houses at the corner of the square clearly produce the dominant scattered signals and an overall angular spread of 12° is produced. The patch results for **frame 5** are given in figure 6.46, and again show the presence of a tight cluster of scattered signals ($\theta_s = 6^{\circ}$).

Once the mobile has turned the corner of the square it starts to move further below the level of houses on the opposite side of the square, and this is reflected in the results for **frames 6, 7** and **8**. With the dipole array, all three frames produced single peaks, and clearly in **frame 6** the strongest reflection is from the buildings nearer the start of the route.

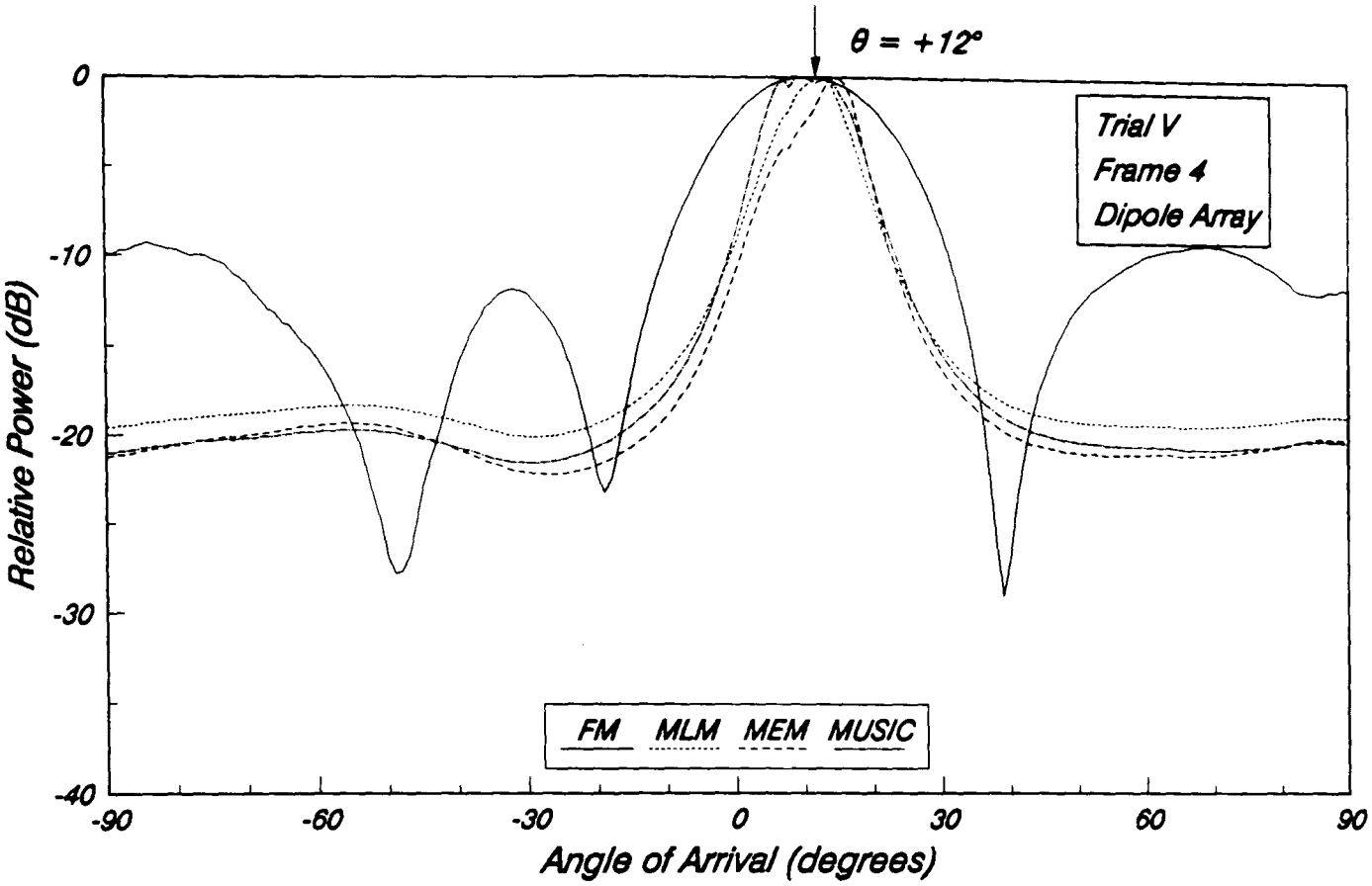

Figure 6.45: Spatial spectra for frame 4 of trial V with the dipole array.

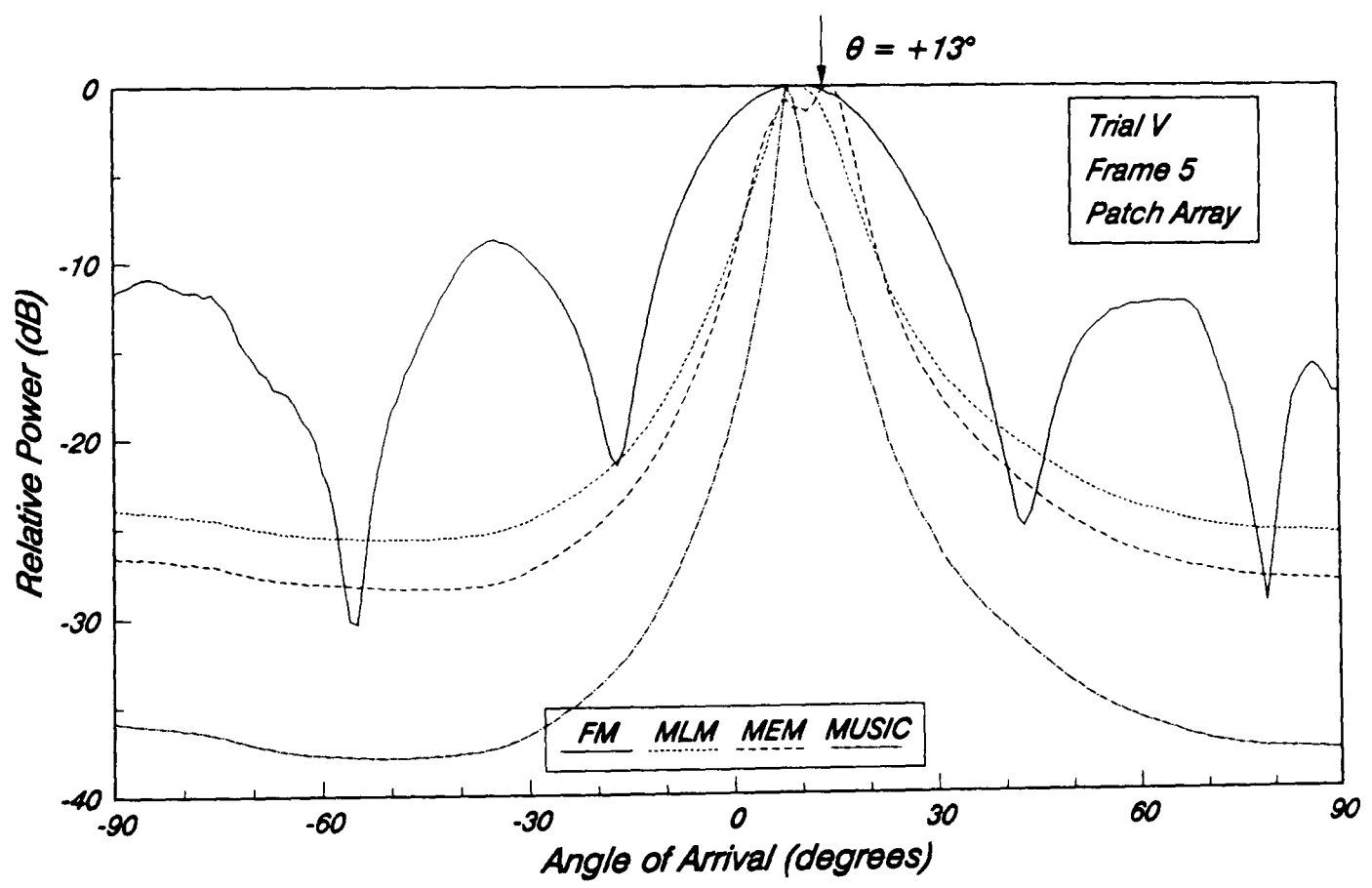

Figure 6.46: Spatial spectra for frame 5 of trial V with the patch array.

With the patch array this is also evident (e.g. **frame 8** with MEM), hence as the mobile moves away from the corner, the angle of incidence with the row of houses along the top of the square ensures strong reflected signals. Figure 6.43 shows a photograph taken from near the end of the route back towards the corner of the square, and plainly shows the row of houses facing the base-station which act as convenient reflectors.

The results for the final three frames of the run (**frames** 9, 10 and 11) also indicate the presence of a **strong** reflected signal from near the corner of the square, hence the errors in the bearing estimates are now quite large. This is to be expected since the large structure of the Wills Memorial Building (on the right of figure 6.42) effectively blocks a more direct signal path from the mobile. The results for the dipole array in **frame** 11 are given in figure 6.47, with the MUSIC response producing the strongest peak at a bearing of $+32^{\circ}$. This can be attributed to a strong reflection from the far side of the Wills Building, or possibly diffraction of the signal energy around the building.

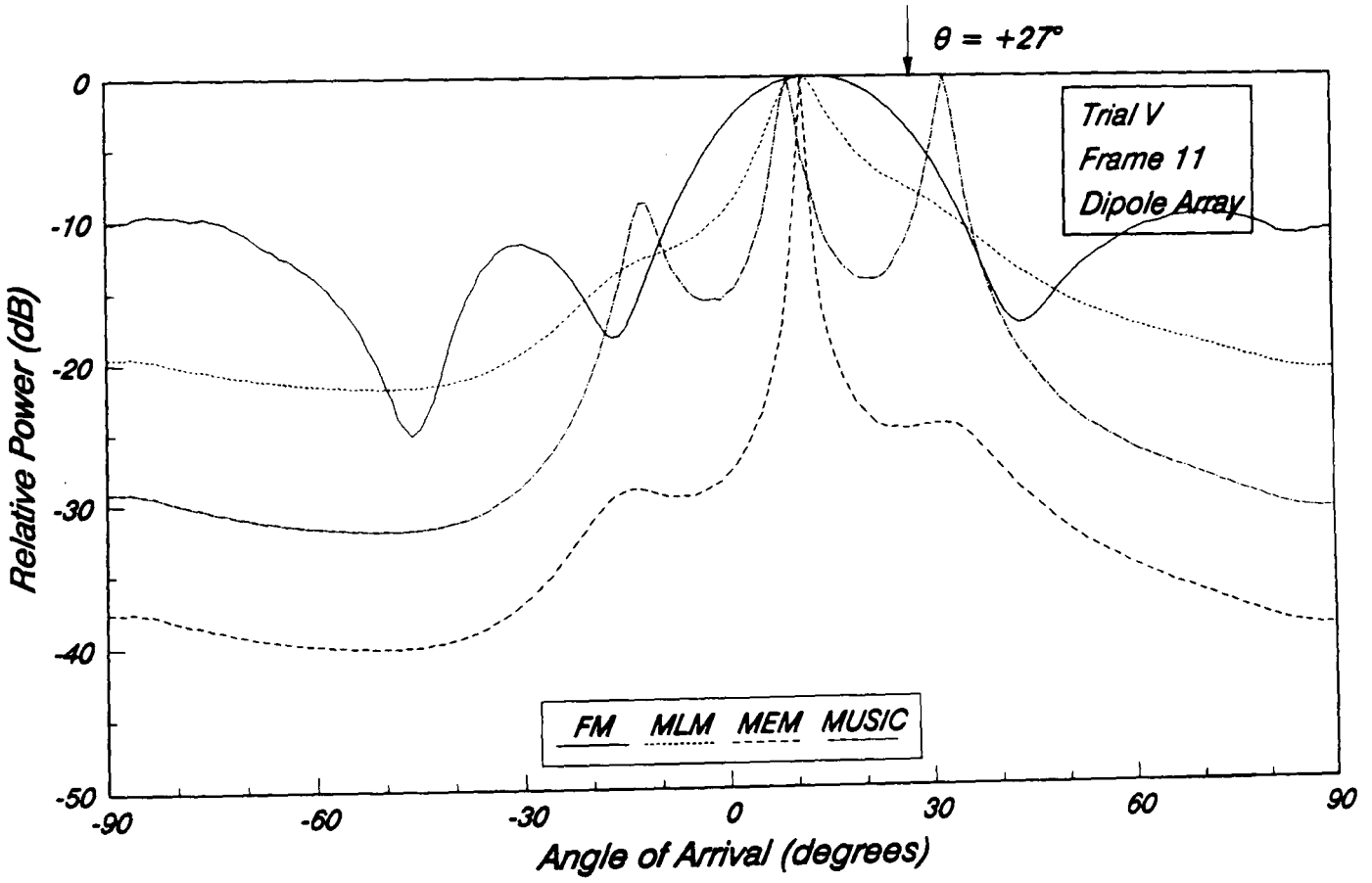

Figure 6.47: Spatial spectra for frame 11 of trial V with the dipole array.

6.4 CONCLUSIONS

6.4.1 Comparison of Simulation Results with Field Trials

The main conclusion to be made from these field trials is that a DF antenna system can track the movements of a single mobile source operating in an urban environment. The results also confirm many of the findings from the computer simulations, for example the clustering effect produced in the spatial spectrum due to the urban scattering environment. Also, they show the tendency for the lower resolution DF techniques (FM and MLM) to average out the effects of the scatterers and produce more accurate bearing estimates. This latter result was not as consistent as predicted by the computer simulations and this can be attributed to two factors:

- The limited sampling period of the received signal waveform in the field trials.
- The asymmetry and non-uniformity of the *scattering volume* associated with the mobile's position.

The sampling period used in the field trials was only a fraction of that employed in the simulations. This can be seen from figure 5.10, with the simulated mobile signal experiencing a large number of fades in a 100 snapshot data frame. In reality this would correspond to a distance of approximately 20λ travelled by the mobile[8] ($\cong$ 4 m at 1529.625 MHz). Consequently, in order to employ such a large sampling period in practice, the amount of data that would have to be recorded would be impractical. Therefore, a much shorter sampling period was employed as shown in figure 6.24. This corresponds approximately to a distance of 0.87λ travelled by the mobile (0.17 m at 1529.625 MHz).

The results from the field trials showed that during this short data frame, the signal environment changes, with one or more of the scattered reflections dominating. Consequently, the estimated bearings from all the algorithms varied considerably from one data frame to the next, although the variations with the lower resolution techniques (FM and MLM) were not so pronounced. This effect was also noticeable when a 100 snapshot window was moved across the total 500 snapshot data frame in 50 snapshot steps. The

---

8: This is based on the approximation that the signal experiences a fade every 0.5λ of distance travelled [17].

application of the DF algorithms revealed that over the short duration of a single data frame, the signal environment changes, with peaks produced at different AOA's. Unfortunately, the 500 snapshot data frame was not long enough to enable a full analysis to be made, and so the complete results of this study will not be presented here. It must be stressed that these trials were only intended as a preliminary study and obviously the above findings would provide a valuable insight into the signal conditions in a mobile radio environment. Hence a more detailed study into this particular aspect will form the basis for future trials.

In contrast to these findings, the computer simulations employed a data frame taken over a large number of signal fades. With a uniform distribution of scatterers around the mobile, the result was a symmetrical spatial spectrum, with the lower resolution techniques (FM and MLM) averaging the effects of each scatterer and producing the most accurate bearings. The higher resolution techniques (MUSIC, JoDeG, KuTu and MEM) on the other hand tended to produce one or two peaks, and the accuracy of the estimated bearing was more dependant on the spread of scatterers. This result was confirmed in some of the data frames, e.g. the spectra in figure 6.32.

The term *scattering volume* has been chosen here to describe the scattering effects when a mobile is in a typical urban street, with buildings on either side. In the computer simulations, a simple two dimensional model was employed, with the scattering objects placed uniformly around a circle centred on the mobile. The results from the field trials have confirmed that the angular spread of 10° ($\theta_s = 10^{\circ}$) employed in the simulations is not untypical of an urban environment. However, the results also show that a symmetrical ring of scatterers is unusual, with figure 6.37 typical of many of the results. This shows the scattering concentrated away from the actual location of the mobile. This would be very difficult to model though, since it is very dependant on a number of factors, e.g. the orientation of the street with respect to the base-station and the height of the buildings surrounding the mobile.

Another observation that can be made from the field trial results is that the distribution of scatterers is very non-uniform and varies with time. The uniform model employed in the simulations predicted a response similar to that shown in figure 6.45, with the FM and MLM algorithms producing single peaks within the scattering limits. The higher resolution techniques

(eigenstructure and MEM), on the other hand, produced the characteristic clustering effect, resulting in some uncertainty in the bearing estimate. A more typical response is shown in figure 6.41, with the lower resolution techniques producing quite large errors in the bearing estimate corresponding to the strongest concentration of signal energy. This type of effect could easily be incorporated into the simulation model by placing the scatterers randomly around the mobile.

So far in the presentation of the results from the field trials, little has been said about the performance of the other two eigenstructure algorithms, JoDeG and KuTu. The main reason for this is that their performance was generally very similar to MUSIC. This was also shown in the computer simulations, although the KuTu technique was found to occasionally produce spurious estimates (see for example figure 5.25). This phenomenon was apparent a few times during the trials, and the resulting spectra were similar to the MEM results. The results with the JoDeG algorithm also differed from the MUSIC results occasionally, and this was usually when the number of sources estimated by the MDL criterion was one or two. When this happened, the resulting spectra closely resembled those generated by the MLM technique, a characteristic mentioned briefly in section 4.3.

6.4.2 Characteristics of the Urban Environment

The results from the field trials show that the angular spread of the signals typically varies from 10° to 20° with the mobile at approximately 300 m from the base-station. At a distance of 1 km this translates to an angular spread of between 3° and 6° and would agree with previously reported values for angular spread, e.g. the 1° to 2° spread reported by Jakes [18] with the mobile greater than 1.5 miles from the base-station. The range of angular spreads above corresponds to a scattering volume with a cross section ranging from 50 m to 100 m. These values would seem to be fairly representative of the different localities encountered in the field trials.

6.4.3 Implementation Issues

The results of the field trials have confirmed that a DF antenna Array architecture is a feasible approach for determining the bearings of the

mobile sources in an urban environment. The most suitable algorithms in terms of bearing accuracy are the lower resolution techniques, FM and MLM. This result was also confirmed in the computer simulations, with the MLM algorithm producing the most consistent results (see for example section 5.3.1). Of the higher resolution techniques, the KuTu and MEM algorithms would not be very strong candidates since they have a tendency to produce spurious peaks which could lead to ambiguous estimates. This phenomenon was apparent in both the simulations and field trials and is predominantly the result of mutual coupling between the antenna elements.

The MUSIC and JoDeG algorithms produced very similar results, both demonstrating the susceptibility of all the higher resolution techniques to the scattering produced in an urban environment. However, the extra detail provided about the scattering conditions is very valuable to understanding mobile communications in different surroundings. Certainly in the less cluttered environment found in more rural areas, the higher resolution techniques would produce the most accurate estimates, as demonstrated in section 5.2.

As already mentioned above, the sampling period of the fading waveform would ideally be over a number of signal fades in order to produce the most accurate bearing estimates. In practice this may not be possible, and will ultimately depend on the sampling frequency and the modulation format (to be discussed in chapter 7). If only a fraction of the fading waveform is employed, the signal processing will have to ensure that the frame is not acquired during a deep signal fade.

Occasionally during the field trials, all of the algorithms failed to determine the location of the mobile. This was particularly true in trial IV and was due to the presence of a strong reflected signal. In order to overcome this problem, a certain amount of 'intelligence' can be employed by the processing. Firstly, algorithms could be employed which utilise the bearing estimates obtained from the DF process to track the movements of the mobile, a technique commonly employed in radar [19]. Consequently, the possibility of a completely erroneous estimate would be greatly reduced. Also, the system could 'teach' itself about the surroundings in which it is operating. For example, in trial IV, if the processor knew that there was a source of reflected signal energy, i.e. the Wills Memorial Building, then an estimate in that direction could be ignored. It is partly this ability to

'learn' about the signal environment that prompted the use of the title "smart" base-station antenna to describe the proposed antenna system.

Throughout the field trials both the dipole and patch arrays were employed. In presenting the results, no attempt was made to associate a particular characteristic with one or other of the arrays since a different set of results was produced each time a trial was repeated. The primary aim was to demonstrate the ability to track the movements of a single mobile source with both types of antenna array. Therefore, if a choice is to be made about the most suitable antenna, each trial would have to be repeated many times in order to provide a statistical basis for a comparison.

REFERENCES

[1]: J.E. Evans, J.R. Johnson and D.F. Sun, *High Resolution Angular Spectrum Estimation Techniques for Terrain Scattering Analysis and Angle of Arrival Estimation*", Proceedings of 1st Acoustics, Speech & Signal Processing (ASSP) Workshop on Spectral Estimation, Canada, 1981, pp.5·3·1-5·3·10.

[2]: R.O. Schmidt and R.E. Franks, *"Multiple Source DF Signal Processing: An Experimental System"*, IEEE Transactions on Antennas & Propagation, Vol.AP-34, No.3, March 1986, pp.281-290.

[3]: K.K. Scott, *"A Practical Implementation of Superresolution Algorithms for Direction Finding"*, Fifth IEE International Conference on Antennas & Propagation, ICAP87, 1987, pp.411-414.

[4]: T.S.M. MacLean, *"Principles of Antennas: Wire and Aperture"*, Cambridge University Press, 1986.

[5]: T.A. Milligan, *"Modern Antenna Design"*, McGraw Hill, 1985.

[6]: J.R. James and P.S. Hall, *"Handbook of Microstrip Antennas: Vols. I and II"*, Peter Peregrinus, 1989.

[7]: M.A. Beach, S.C. Swales, A. Bateman, D.J. Edwards and J.P. McGeehan, *"A Diversity Combining Antenna Array for Land Mobile Satellite Communications"*, 39th IEEE Vehicular Technology Conference, April 29th - May 3rd 1989, San Francisco, USA, pp.749-756.

[8]: M.A. Beach, S.C. Swales, J.P. McGeehan and D.J. Edwards , *"A Diversity Combining Antenna Array for A Land Mobile Satellite Terminal"*, Fifth IEE International Conference on Mobile Radio and Personal Communications, 11th - 14th Dec. 1989, Warwick University, UK, pp.177-181.

[9]: *"Interdigital Filters and Experimental Microstrip Filter Design at 470 MHz"*, Mullard Technical Communications, No.116, October 1972,

pp.188-192.

[10]: G.L. Matthaei, L. Young and E.M.T. Jones, *"Microwave Filters, Impedance-Matching Networks and Coupling Structures"*, McGraw-Hill, 1964.

[11]: *"IMS B009: IMS A100 DSP System Evaluation Board"*, INMOS Ltd., Product Overview, Document No.72 TRN 107 00.

[12]: *"The Transputer Databook"*, Bath Press Ltd., 1988.

[13]: *"Transputer Development System"*, Prentice Hall, 1988.

[14]: J. MacLeod, *"Microwave Amplifier Design"*, Internal Report, Centre for Communications Research, University of Bristol, 24th Jan. 1990.

[15]: A.J. Weiss and B. Friedlander, *"Direction Finding in the Presence of Mutual Coupling"*, Proceedings of 22nd Asilomar Conference on Signals, Systems & Computers, USA, 1988, pp.598-602.

[16]: A.W. Rudge, K. Milne, A.D. Olver and P. Knight, *The Handbook of Antenna Design - Volume 1 & 2"*, Peter Peregrinus Ltd., 1982.

[17]: W.C.Y. Lee, *"Mobile Communications Engineering"*, McGraw-Hill, 1982.

[18]: W.C. Jakes, *"Microwave Mobile Communications"*, John Wiley & Son, 1974.

[19]: V.C. Vannicola and J.A. Mineo, *"Applications of Knowledge Based Systems to Surveillance"*, Proceedings of 1988 IEEE National Radar Conference, USA, 20th - 21st April 1988, pp.157-164.

CHAPTER 7

IMPLEMENTATION ISSUES

The previous three chapters have considered in some detail the task of determining the location of the mobile sources within a cell of the communications network by utilising an antenna array at the base-station site. With the aid of computer simulations and an experimental test rig, it was demonstrated that the azimuth bearing of a single mobile transmitting a CW tone could be estimated using a four element linear array. The field trials were carried out in a fairly typical urban locality, and it was shown that the proximity of the nearby buildings had a pronounced effect on the accuracy of the estimated bearing. As a mobile user moves along a street, a scattering volume can be associated with its instantaneous location, which then defines the angular spread of the signals arriving at the base-station. From the results obtained in the field trials, it can be seen that the angular spread typically lies within the range 3° to 6° in the selected test environment. This corresponds to the mobile at a distance of 1 km from the base-station.

Having established the feasibility of the direction finding process, this chapter considers how the proposed antenna system could be incorporated into an existing cellular network, and further addresses some of the initial implementation issues. As a starting point for this discussion, the base-station hardware requirements are considered and therefore a brief description of first generation cellular base-station technology is included to provide some necessary background. The realisation of the source estimation or direction finding process is then considered, with particular reference to the modulation and access techniques employed. It is recognised that many additional overheads would be incurred in order to successfully accommodate this process and therefore some of the most critical factors are addressed.

Finally, the the task of effectively utilising the knowledge of the mobile locations to generate a beam set to provide complete coverage of the

cell is considered. The example depicted in figure 2.3 illustrates this, with the different beams tailored precisely to fit the distribution of mobiles in an optimum manner. The criteria in this case is to minimise the directions in which co-channel interference can be transmitted or received, thereby maximising the spectrum efficiency advantage. In this chapter a number of different beamforming options are considered which can either provide an optimum coverage of the cell using agile beams, or a fixed coverage using static beams.

7.1 BASE-STATION HARDWARE

A description of the base-station hardware requirements for the early American Advanced Mobile Phone Service (AMPS) is given by Ehrlich *et al* [1], and a simplified block diagram of the system architecture is illustrated in figure 7.1. Voice and data is transferred between the cell site controller and the Public Switched Telephone Network (PSTN) via a Mobile-Services Switching Centre as shown. Once assigned a frequency channel, the cell site controller then supervises the transmission and reception of the signals to and from the mobile. The two transmission paths are referred to as the *uplink* and *downlink* respectively. The UK Total Access Communications System (TACS)[1] is based on the American AMPS standard, and the main system parameters for both networks are summarised in table 7.1 below. A frequency division multiple access (FDMA) scheme is employed and consequently requires the combination of a number of different frequency channels as shown in figure 7.1. The proposed 2nd generation Pan European system will employ a narrowband multi-carrier time division multiple access (TDMA) scheme, and so will still require the multiplexing of different carrier frequencies on both transmission and reception. Note also that the system depicted in figure 7.1 is primarily for analogue operation and therefore, with the introduction of digital modulation schemes for the next generation of networks, the necessary digital interface must be included.

1: Currently the extended TACS system (E-TACS) is in operation, providing additional frequency channels.

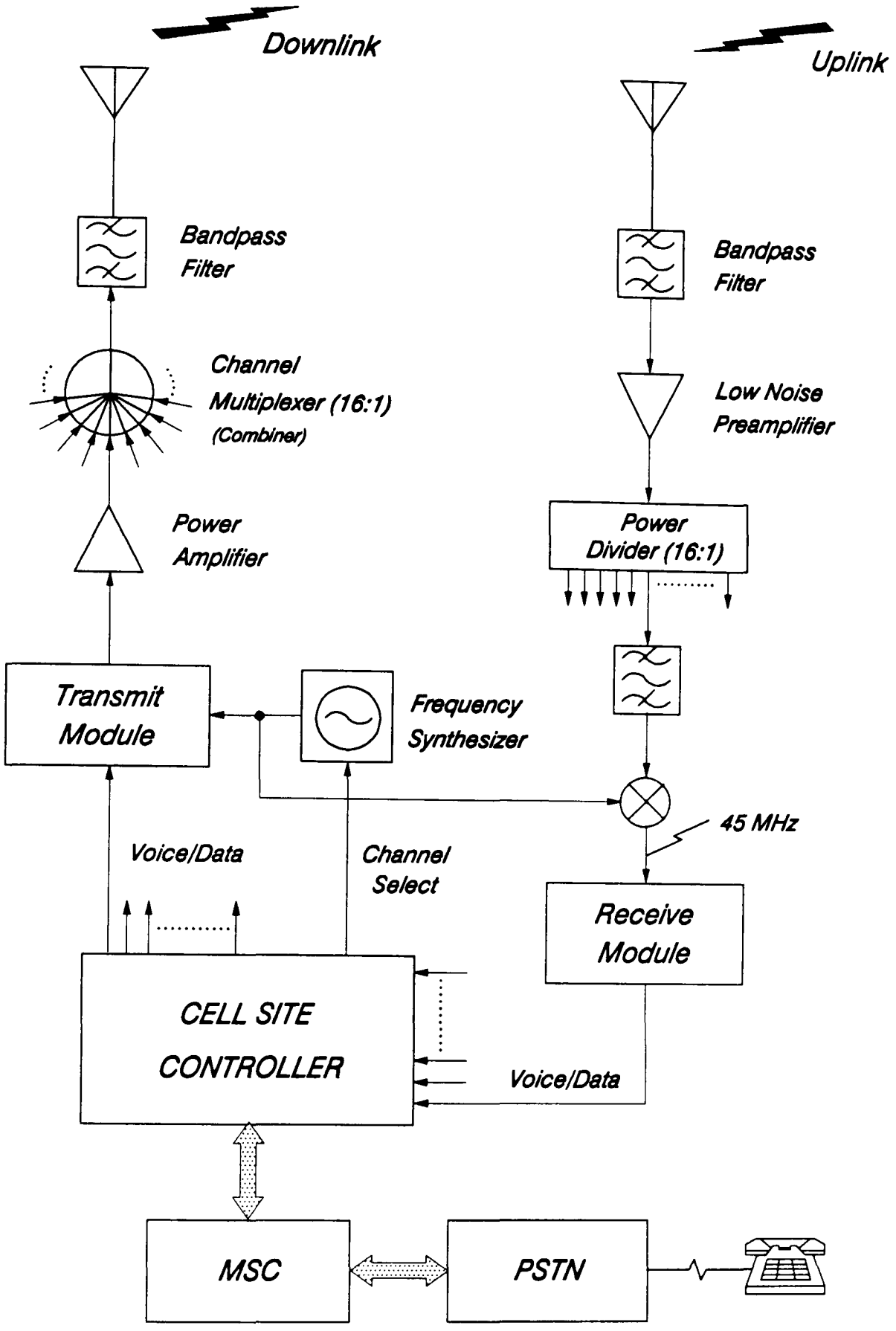

Figure 7.1: Simplified block diagram of base-station hardware for the American AMPS system.

		TACS	AMPS
RF Carrier Frequencies	Uplink	890-915 MHz	825-845 MHz
	Downlink	935-960 MHz	870-890 MHz
Spacing between Up & Downlink Frequencies		45 MHz	45 MHz
Channel Spacing		25 kHz	30 kHz
Number of Channels		1000	666
Voice Channel		9.5 kHz FM	12 kHz FM

Table 7.1: System parameters for 1st generation UK and USA networks.

Due to the high power levels transmitted from the downlink antenna (100 W maximum) and the low powered signals received from the mobile on the uplink (> -100 dBm), the two antennas must be sufficiently far apart to ensure adequate signal isolation. Normally with omni-directional antennas this is achieved with vertical separation on the same support tower. With directional antennas, this restriction can be relaxed, and the antennas can often be placed in the same horizontal plane. The AMPS specification also provides for space diversity reception with two receiving antennas. Space diversity at the base-station site has already been discussed in chapter 2, and the benefits in terms of reducing the effects of Rayleigh fading can be very significant. Unfortunately for effective diversity action, large antenna separations are required and this is not always a practical option.

The main limitations with present generation systems is the method employed to combine the signals prior to transmission. Currently, this is accomplished using cavity resonators which act as narrowband filters feeding a common load. In order to reduce the losses to 3 dB per channel, the channels to be combined must be separated by at least 630 kHz. This also ensures that the minimum channel-to-channel isolation is 18 dB. Intermodulation is controlled using ferrite isolators which provide a 30 dB reverse loss. Combiners of this type for cellular base-stations are specified for a capacity of 16 channels, and so a separate transmit antenna is required

for each subset of 16 channels provided at the base-station. A ring combiner [2] can be used to combine two or more channel subsets onto a single antenna, although the number is limited by the total amount of transmit power. (Some combiners have a 600W power limitation.)

It is apparent from this discussion that each combiner must be mechanically tuned to a specific set of channels. Hence the frequency assignments cannot be easily altered, severely degrading the performance of the proposed multiple beam base-station antenna system. If a set of fixed multiple beams were employed, this would reduce to the equivalent of fixed sector directional antennas. Recent developments however, will enable the combining to be implemented using broadband stripline combiners at lower powers where the losses can be tolerated. A single broadband linear power amplifier can then be employed to bring the signals up to the required transmit power level [3]. This arrangement is illustrated in figure 7.2 and essentially removes the rigid frequency restrictions, enabling the channels to be assigned as required. Also, the limits on the channel spacing can be relaxed and the total number of signals which can be transmitted from a single antenna is now only limited by the total power considerations. Not only can dynamic channel assignment schemes be employed along with many other techniques to increase the spectrum efficiency, but the proposed base-station antenna system can achieve its full potential.

On reception, the uplink signals are first of all filtered and amplified before splitting using a broadband hybrid power splitter. The required channel can then be selected and downconverted in the usual manner without any restrictions on the channel assignment. Hence, the future base-station site hardware will be an integral part of the proposed multiple beam antenna system.

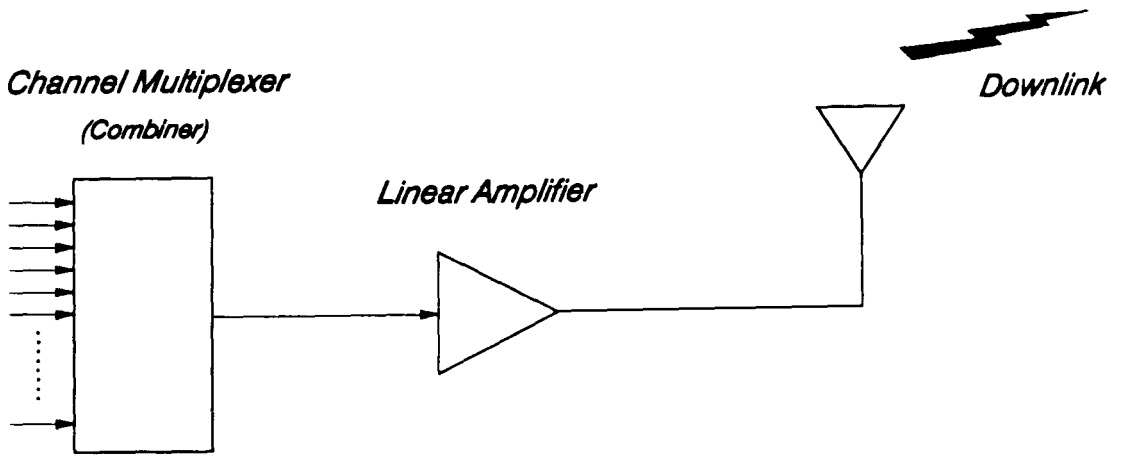

Figure 7.2: Broadband linear power amplifier.

7.2 MODULATION FORMAT

Throughout the study so far, no particular modulation scheme or access technique has been considered in conjunction with the proposed base-station antenna system, even though some well established trends are becoming apparent in the quest towards higher spectrum efficiency. The dominant choice with the first and second generation systems has been narrowband modulation, therefore a CW transmission format was chosen initially for the computer simulations and field trials. This does however, exclude wideband modulation schemes from the study, although with recent interest in a code division multiple access (CDMA) scheme employing wideband spread spectrum communications, the format for the future is by no means settled. Therefore, a brief discussion is also included on a co-channel interference reduction technique for wideband spread spectrum communications employing an adaptive antenna array.

7.2.1 Narrowband Modulation

Narrowband modulation has dominated the first generation of cellular networks, and in particular narrowband FM, e.g. the UK TACS network employs 9.5 kHz FM with a 25 kHz channel spacing. This trend is set to continue, for the next generation at least, with narrowband digital modulation schemes proposed in Europe and the USA, e.g. the Pan European system will adopt 200 kHz channels in a multi-carrier time division multiple access (TDMA) scheme. As a result of this, the emphasis of the work was placed on the narrowband approach although to date, only a CW signal has been employed with no modulation. If the work was to continue, then a target scheme like the Pan European digital network could be selected, and the DF receiver architecture adapted accordingly.

In order to provide an accurate bearing estimate for all the mobile users within a cell, high performance digital processors will be required, although it is not envisaged that the position of each mobile would have to be updated continuously due to the relatively slow movement of the traffic. (The receiver would not have to resolve and track a fast moving jet plane for example.) If a vehicle was moving across the field of view of the array at an average speed of 50 km/h ($\approx$ 14 m/sec), then at a distance of 1 km the change in bearing would be less than 1° per second. At this range, the angular

spread would be between 3° and 6° and therefore an update rate of 1 second would not reduce the accuracy of the bearing estimates. As the mobile moves throughout the cell the angular velocity will vary depending on the range, direction of travel and speed. The range and speed of the mobile can be estimated from the knowledge of the mean received signal and the level crossing rate[2] [4]. Therefore, the rate at which the bearing is updated can be varied to minimise the processing overheads.

Some additional savings could be made by exploiting the knowledge of the mobile's location to constrain the range of the angular search carried out by the DF processor. The limits of the search would again depend on the position and speed of the mobile, but would help to reduce the number of computations required to estimate the bearing. (The bearing of the mobile at the start of the call could be determined from the control channel used to initiate a call.) However, the combination of large numbers of snapshots required for each data frame, and the potential for large numbers of users requiring simultaneous access to the network, would necessitate the use of very fast and efficient parallel processing techniques. The INMOS Transputer would be a potential candidate, and has already been employed to successfully acquire the data in the field trials described in chapter 6. The next stage of the work would be to implement both the data acquisition and the bearing estimation process on a network of transputers. Alternatively, the parallel processing capabilities of the transputer could be employed in conjunction with the INMOS high speed IMS A100 digital signal processor [5] capable of a 10 MHz data throughput. The IMS A100 can also be cascaded, and has been employed to perform digital filtering [6], complex (I&Q) processing [7], as well as the discrete fourier transform [8].

The cell site hardware described in the previous section was for frequency division multiple access (FDMA) operation. Therefore, on reception, the signals received at each antenna are first of all divided into the constituent number of channels prior to downconversion and demodulation. In order to perform the spatial estimation process, the signal received in each element in the array can be downconverted in a similar fashion. Each channel would then be isolated using narrowband crystal filters, for example, and then digitised. The DF processor can then estimate the bearing of each source

---

2: The level crossing rate is defined as the average number of times per second that the signal envelope crosses a specified signal level in a positive going direction.

in parallel. An alternative technique was considered in section 5.4 of chapter 5, which employed a tapped delay line behind each element in the array to enable a two dimensional estimation process [9]. If there were 100 channels, a four element array would require at least 26 delay taps behind each element. The added hardware complexity that would be incurred would therefore prohibit this approach. A multi-carrier TDMA scheme could also be accommodated, with parallel processing of all the frequency channels as well as the synchronised processing of the individual time slots within each channel.

7.2.2 Wideband Modulation

The wideband modulation format which is currently receiving the most attention is spread spectrum. By assigning each mobile user with a unique quasi-orthogonal code, a code division multiple access scheme (CDMA) is implemented providing each user with access to the entire system bandwidth. If there are M wideband sources occupying the same bandwidth, the approach considered by Wax *et al* [9] could be employed to determine the source angles of arrival. This requires that the number of sources is less than the number of elements N (i.e. $M \leq N-1$), and since there would be a large number of sources, the hardware costs would be increased dramatically. Hence, the proposed multiple beam base-station antenna system would not be a cost effective option with a wideband modulation format.

An alternative approach would be to exploit the long association between spread spectrum techniques and the adaptive antenna array. In chapter 2, Winters [10] proposed an optimum combining scheme using an adaptive antenna array to reduce the levels of co-channel interference in a cellular communications environment. It was proposed that the optimum combining (or adaptive beamforming as it is sometimes referred to) could be achieved using the LMS algorithm, and therefore would be best suited to a spread spectrum communications format since a suitable reference signal is readily available to generate the error signal in the feedback loop. The results demonstrated that this approach was effective in reducing the levels of co-channel interference, and therefore would be a suitable option for increasing spectrum efficiency with wideband spread spectrum communications.

In a more recent study by Kohno *et al* [11], the optimum combining

principles discussed by Winters have been applied directly to a CDMA scheme employing spread spectrum. The co-channel interference problem is slightly different from that experienced in an FDMA or TDMA scheme since all the users could potentially be assigned a unique code or channel. In this case, the source of interference stems from the degree of cross correlation that exists between the pseudo-noise sequences which are employed as the user codes. Ideally the codes are designed to have a low cross correlation, enabling the receiver to acquire and track the incoming codes from each user. Unfortunately, the large numbers of users requiring simultaneous access in cellular radio will increase the received level of interference power (the combined signal powers from all users other than the desired user). This results in an increase in the cross correlations between codes, reducing the processing gain of the system, and limiting the total number of users that can have simultaneous access to the network. This co-channel interference can be effectively reduced through the use of the adaptive antenna array since radiation pattern nulls can be placed in the directions of the interferers. The problem of interference emanating from the same direction as the wanted source is also addressed by Kohno *et al*, and an adaptive canceller is proposed. Further details of this and the other techniques can be found in the referenced work [11]. The simulation results indicate that a very significant reduction in the received data error rate can be achieved, and therefore would increase the potential capacity advantage of the system.

7.3 BEAMFORMING

In chapter 2, the antenna array was introduced as an adaptive beamformer capable of adjusting its radiation pattern in an optimum manner depending on the requirements of the system, e.g. the nulling of interference sources or jammers. One of the main drawbacks of this approach is the high computational load and therefore, in direct contrast to steering nulls, the ability of the adaptive array to steer radiation pattern maxima towards the mobiles is considered. This involves generating a number of independent beams and using the knowledge of the mobile locations to confine the signal energy associated with each mobile to a beam in the required direction. Communications satellites perform a very similar task but on a very much larger scale, employing multiple beam antennas to restrict coverage to certain areas of the earth's surface. In this way, the beam patterns can be adjusted to

accommodate changing requirements, as well as reducing the effects of interference.

An example of a multiple beamforming antenna is given in figure 7.3 for an N element array with four independent beams ($N_b = 4$). There are three main functional blocks: an antenna array, a beamforming network and a processor to adjust the operation of the beamformer. Each beam is generated by weighting and combining the elements of the array, as shown in figure 7.4 for the formation of a single beam. The set of complex weights are chosen to give a specified response in terms of the direction of the beam, the sidelobe levels and the overall beam shape. Obviously the larger the number of elements the greater the degrees of freedom available to the designer. Further details on pattern synthesis can be found in most of the literature on antenna arrays

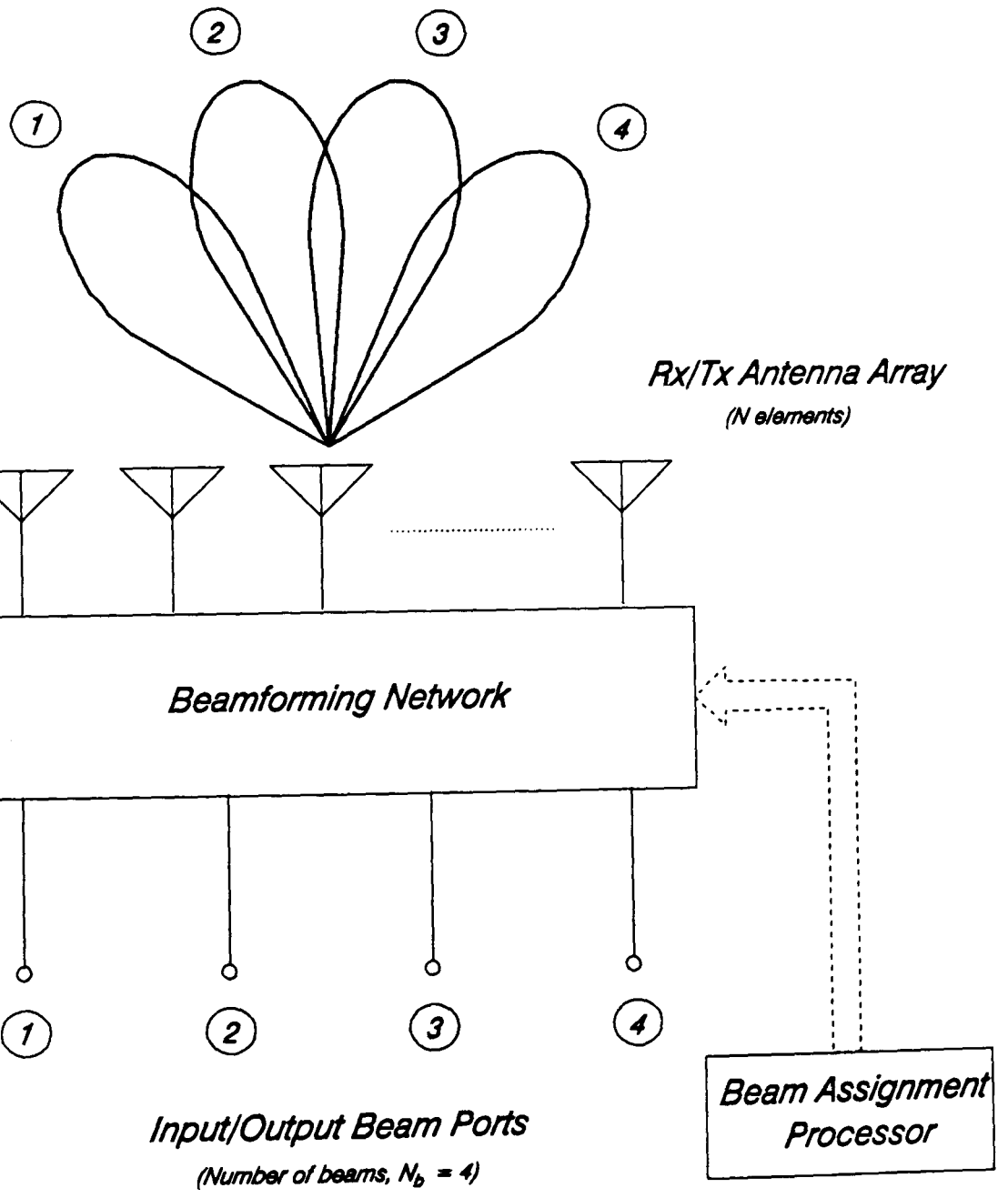

Figure 7.3: Multiple beam antenna array.

[12]. When implementing multiple independent beams there are however some restrictions on the performance of the array as discussed by Hansen [13]. In order for the beamformer to be lossless, the multiple beams must be orthogonal. This places a limit on the cross over level for adjacent beams, and in some instances this may be too low. Therefore, to specify a particular beam set, the orthogonality rule must be broken resulting in a lossy beamformer. Since this loss can be calculated, the correct level of amplification can then be applied prior to the beamformer to compensate.

In the following sections, a number of different multiple beamforming techniques will be presented, and their suitability for application in the proposed multiple beam base-station antenna system discussed. As a precursor to this discussion however, some attention will be given to the beamforming requirements of the proposed antenna system and how it could be incorporated within a cellular network.

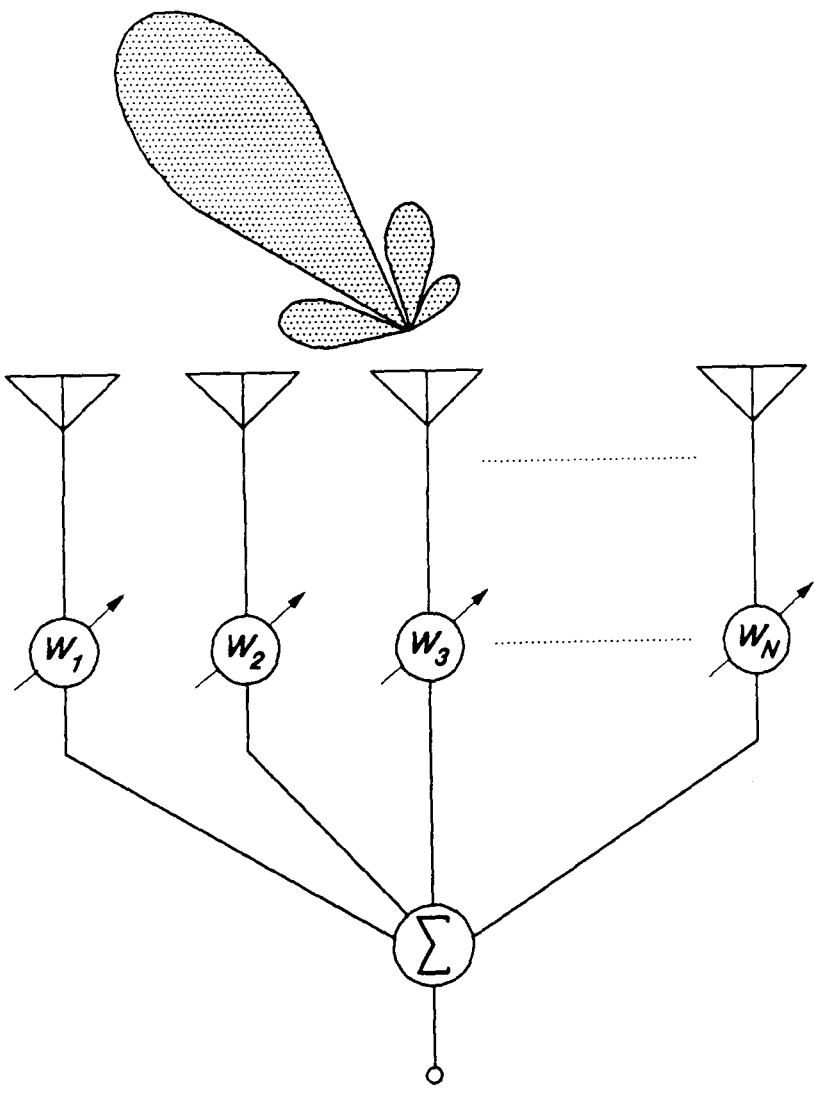

Figure 7.4: Beamforming network for single beam operation.

7.3.1 Potential Antenna Configuration

It has already been established that sufficient angular resolution of the mobile sources in a 180° sector can be achieved with a linear array containing at least four elements ($N \geq 4$). In order to provide full omni-directional coverage, an alternative array configuration would be required, e.g. a circular array of dipoles or a conformal array of microstrip patches. Unfortunately, in order to obtain the best possible coverage with an omni-directional array, the antenna must be located in an elevated position away from local scatterers. This is especially important in an urban/suburban environment, and can often only be achieved with a purpose built tower. In many situations this is not a very practical or economical solution due to the increased installation costs and the limited number of suitable antenna sites that would be available. The deployment of fixed sector directional antennas has overcome this problem to some degree since the antennas can often be placed on the corners of a large building.

With this in mind, the most suitable antenna design for the proposed base-station would employ a number of linear arrays, each providing coverage of specified sector or *zone*. Full 360° coverage of a cell can then be provided by dividing the cell up into a number of zones, and two possible configurations are shown in figure 7.5. If the number of elements in each

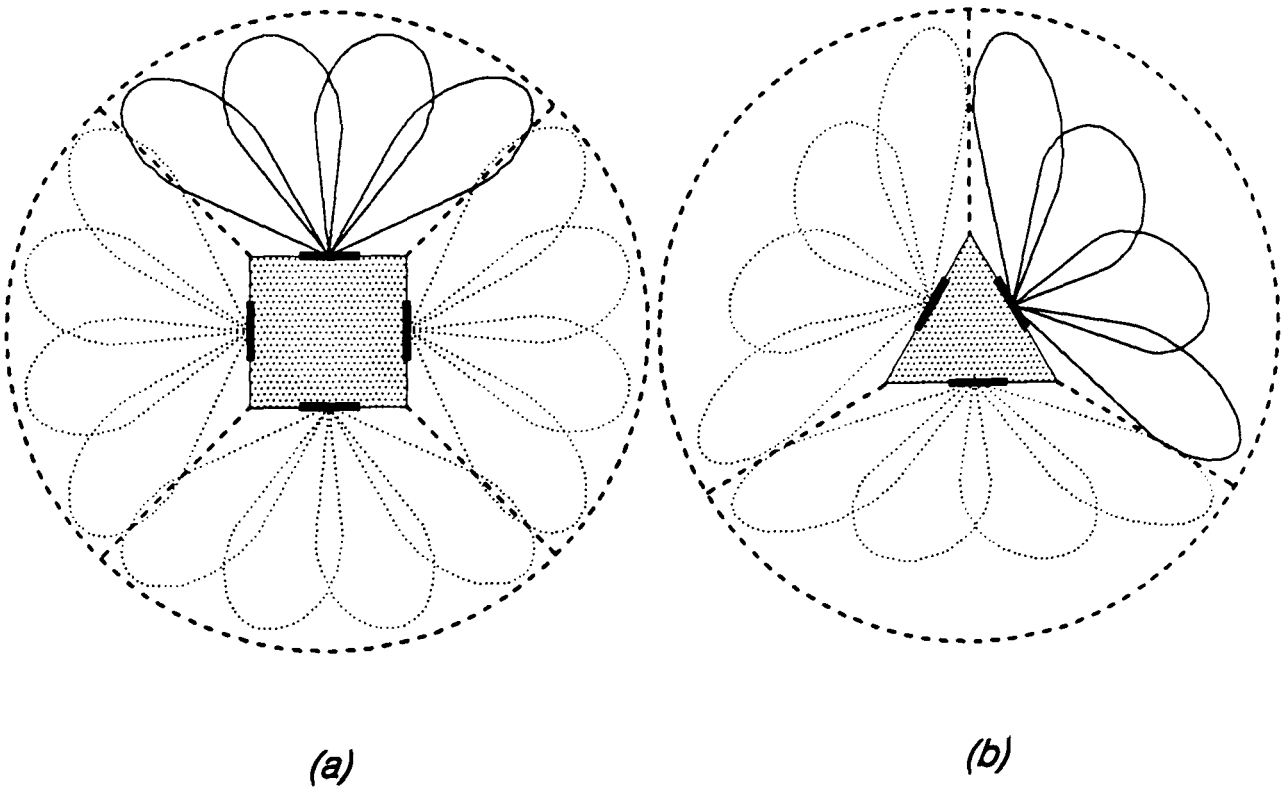

Figure 7.5: Potential antenna configurations:
(a) 16 beams in 4 zones; (b) 12 beams in 3 zones.

array is initially limited to four, then each zone can be covered by up to four independent beams. The total number of beams covering each cell would then be 16 or 12 respectively, providing a potential capacity advantage of at least five (see figure 3.5 in chapter 3).

In order to provide a facility to tilt the beam patterns downwards and further reduce the levels of co-channel interference, a vertical array of elements could also be included [14]. The required tilt angle is then determined by the feed arrangement, and a potential design comprising of a 4×8 planar array of vertical polarised microstrip patch elements is illustrated in figure 7.6. The patches are a very attractive option since the

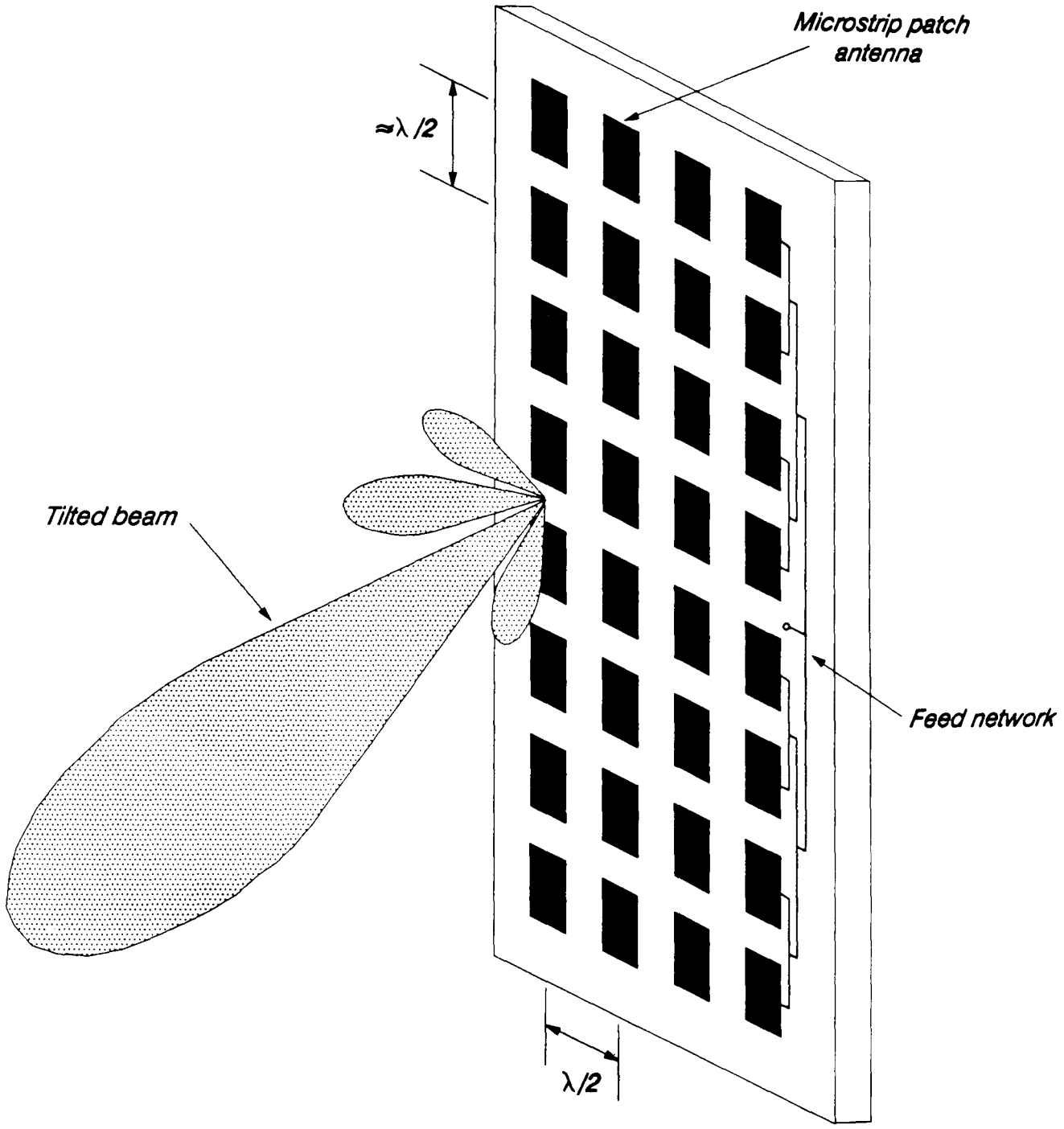

Figure 7.6: 4×8 patch array for proposed base-station antenna.

complete array structure could easily be mounted on the side of a building. Rooftops cluttered with a variety of antennas are becoming an increasingly common sight in cities and large towns, and therefore an antenna system that could be easily disguised would have a certain aesthetic value at least. The four zone system depicted in figure 7.5a could be envisaged mounted on the four sides of a high office tower block. Alternatively, the antenna arrays could be co-located on a support tower, e.g. at a rural base-station site. The versatility offered by microstrip antennas could also be exploited to provide conformal array structures which are customised to the requirements of the site. Another advantage with microstrip is that all the necessary feed networks can be placed on the same surface, or in a multi-layer structure, providing a very compact and economical design.

The main drawbacks with using microstrip patch antennas in the past have been their inherent narrow bandwidth and limited power handling. However, the rapid advances made over the last few years have alleviated these problems to some degree, with sophisticated antenna designs and many new substrate materials [15], making microstrip antennas a very strong contender for future cellular base-stations.

7.3.2 Fixed Multiple Beams

Two of the most commonly used feed techniques for producing a set of multiple independent beams at RF frequencies are briefly described below.

Rotman Lens [16]

In its simplest form, the lens consists of a pair of parallel plates with either waveguides or probes as inputs and outputs. Each of the array probes is connected to an array element with a specified length of line designed to provide perfect focusing at three points along the circular focal arc. This corresponds to beam ports 1, 3 and 7 for the ten element, 7 beam array shown in figure 7.7. However, the departure from perfect focusing is negligibly small across all the beam ports for most practical designs. The electrical lengths from each beam port to the corresponding radiating wavefront are equal for all the elements in the array, resulting in a true time delay beamformer with fixed beams that do not scan with frequency. The orthogonality condition however, is only met at one frequency, although reasonable operating bandwidths can be obtained (3:1).

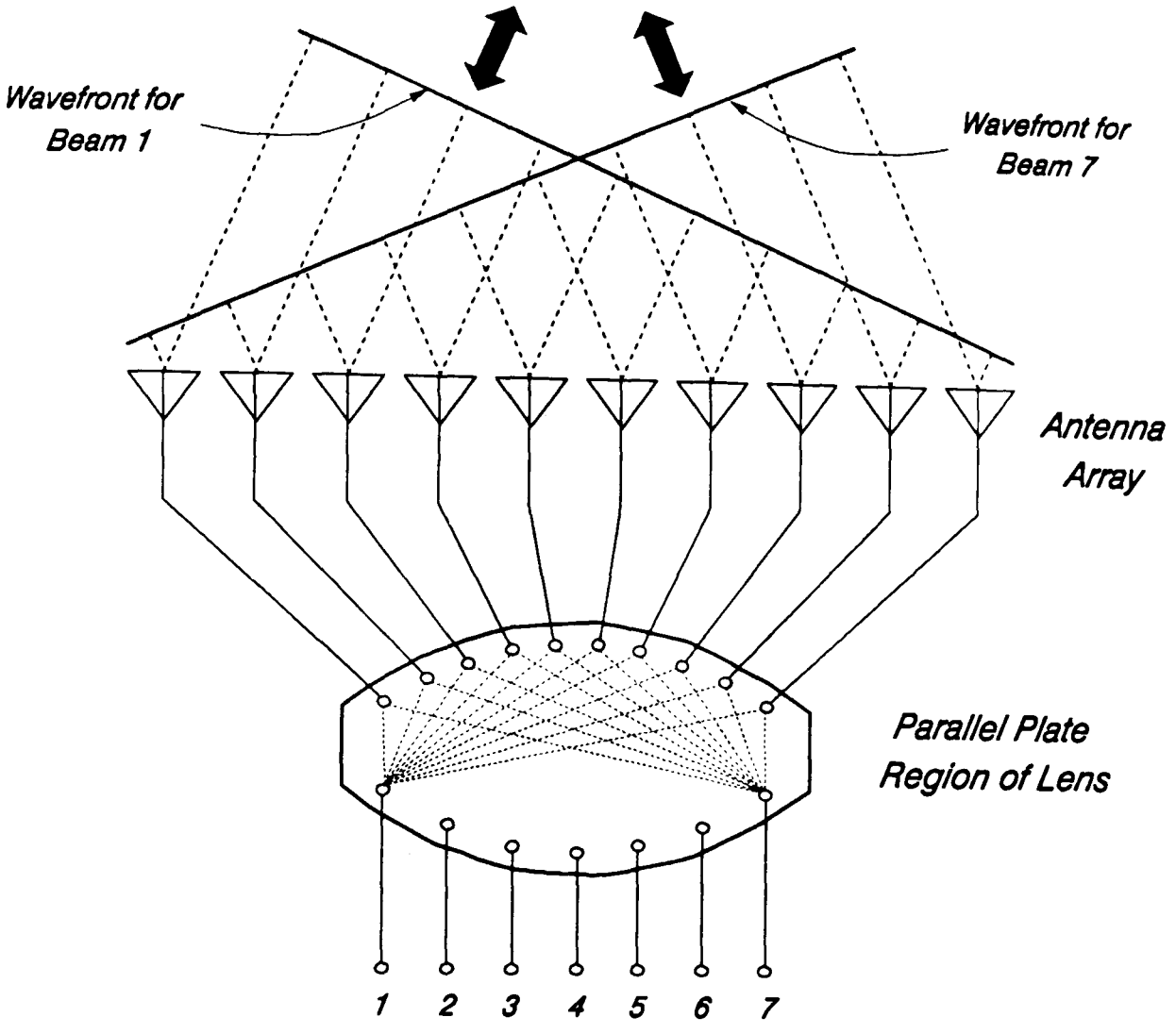

Figure 7.7: The Rotman lens feeding a linear array.

Butler Matrix [17]

The Butler Matrix beamformer consists of a network of interconnected hybrid couplers and phase shifters, which produce constant phase ramps across the array defining the beam directions. The standard Butler Matrix comprises of an N×N network where N defines the number of input and output ports, and is an integer power of two, i.e. $N = 2^n$. A total number of N×n/2 hybrid couplers are required, in addition to a large number of phase shifters. Consequently the hardware complexity increases rapidly as the number of elements in the array rises and, for many applications, this can be unacceptable. The feed network can be implemented using either 90° or 180° hybrids [17], enabling the beams to be either symmetrically placed about the array broadside, or with one of the beams at the broadside position. An example of a lossless Butler Matrix feed is given in figure 7.8 for an eight element, eight beam array. Since the network produces constant phase ramps, the beams will scan with frequency, although the 20 MHz transmit and receive

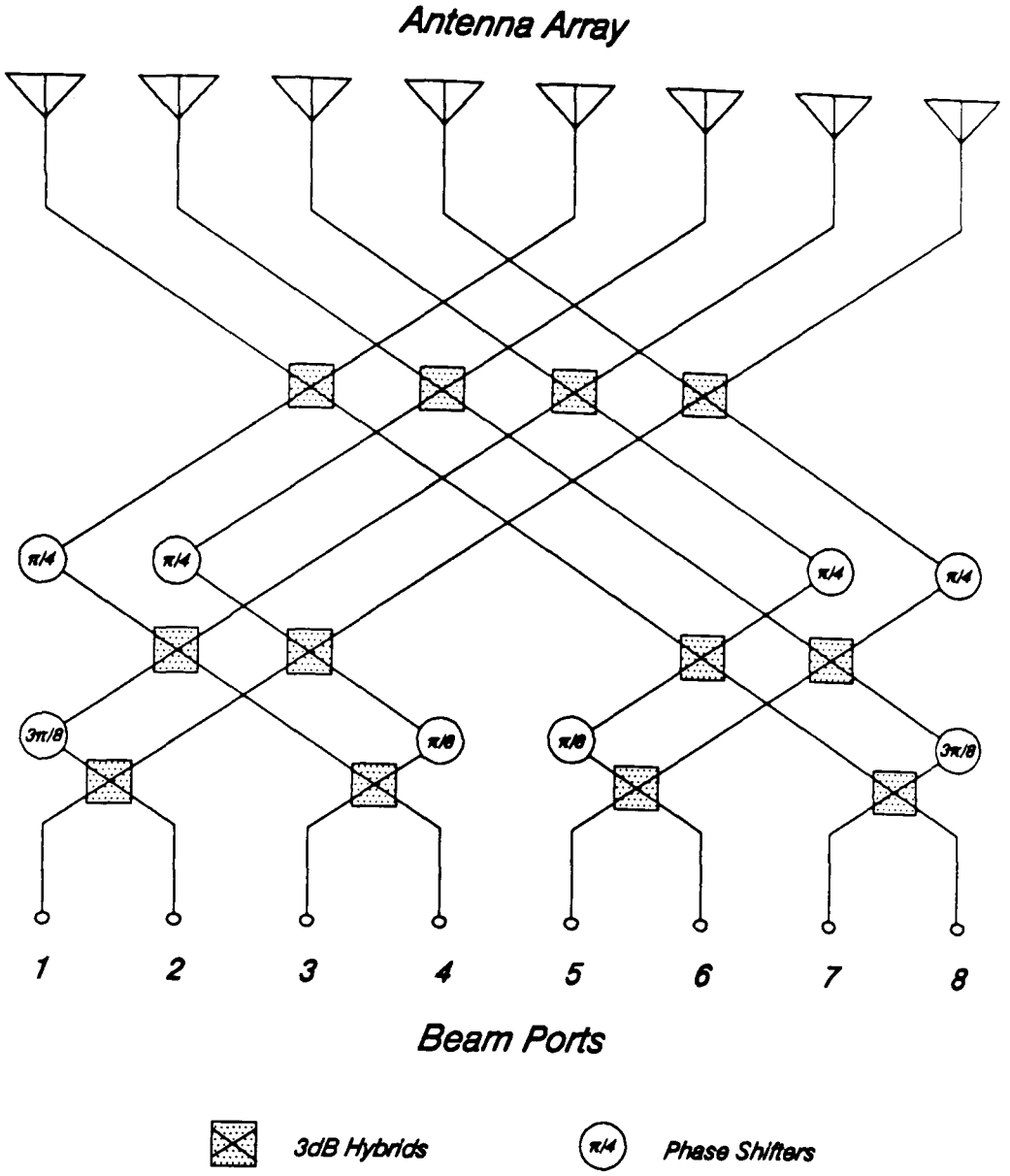

Figure 7.8: Lossless 8 element, 8 beam Butler matrix beamforming network.

bandwidths at the 900 MHz RF carrier for cellular radio would not cause any significant variations in the beam directions. (This assumes that separate beamformers would be designed for the uplink and downlink respectively.)

A possible drawback of the Rotman lens is that it can only give a limited scan in azimuth, although Archer [16] discusses some alternative designs which could even provide full 360° coverage. In many applications only a limited scan would be required as shown in figure 7.5, and therefore the Rotman lens could be employed as the beamforming network for a linear array. The main drawback of the Butler matrix beamformer is the complexity of the hardware, although again this would depend on the requirements of the system. The four element, four beam architecture described in the previous section would not introduce a significant penalty. One very attractive feature offered by both beamformers is that they can be fabricated in

microstrip [18][19] and maybe used in conjunction with microstrip antennas. In fact, an 8×8 microstrip patch array with a Butler matrix feed has already been considered in Japan for operation at a cellular base-station [15]. The system provides eight independent beams covering a 120° sector and, with the antennas and feed network etched onto the same surface, offers a very low cost and compact alternative to current generation base-station antennas. This is very similar to the proposed antenna design discussed earlier.

Figure 7.9 shows a schematic of how the Rotman lens or Butler matrix RF beamformer could be incorporated with existing cellular base-station hardware. Both the transmit and receive antennas contain only four elements and can therefore generate up to four beams. This would be suitable for

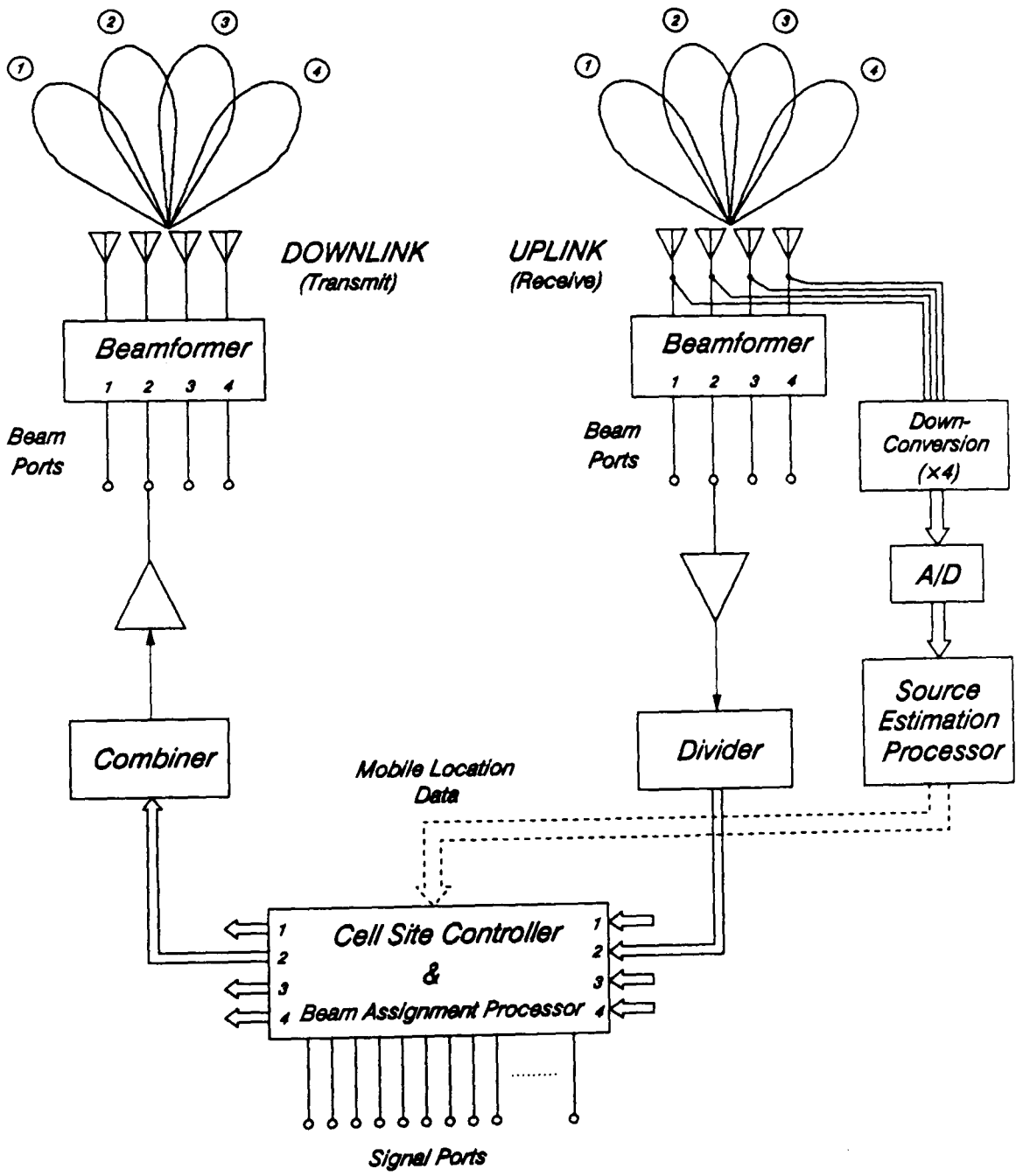

Figure 7.9: Schematic of the "smart" base-station antenna employing RF beamforming.

inclusion in either the four or three zone network depicted in figure 7.5. If the orthogonality condition must be broken in order to provide sufficient coverage of the zones, then additional antenna elements may be required. Note that the linear broadband amplifier discussed in section 7.1 is included for the downlink (transmit) in order to enable the channels to be dynamically assigned to the specified beam port. One of the drawbacks of RF beamforming is the requirement for a separate downconversion chain to enable the DF processor to estimate the azimuth bearings of the mobiles, although spatial estimation can be carried out in beam space as opposed to antenna space [20]. Here the DF processing is carried out on the beam outputs and therefore would require no additional hardware. Unfortunately, the large number of beams required to cover the field of view would make this approach uneconomical. An alternative approach which will enable both the beamforming and direction finding to be carried out digitally is described in section 7.3.4.

7.3.3 Active Multiple Beams

In a typical cellular environment, the distribution of mobiles within each cell is very non-uniform, with most of the traffic concentrated along the major highways. Consequently the fixed beam solutions cannot provide the optimum coverage of a cell. In order to achieve full control over the individual beam patterns, active phase shifters are required behind each element in the array, as illustrated in figure 7.10 for an N element array with four independent beams. Once the distribution of mobiles is known, the beam assignment processor is now able to control the beam patterns to cover the mobiles in an optimum manner. The criteria for assigning beams is to minimise the directions in which co-channel interference can be transmitted or received. Additional control over the beam patterns can be achieved if active amplifiers (or attenuators) are also included.

If the number of elements in the array is low (e.g. $N = 4$), the benefits of active beamforming over fixed beamforming would not be very significant since only a limited amount of control can be achieved. Ideally, if only four independent beams are required, the number of elements in the array would be much higher (e.g. $N \geq 8$). In this way pattern synthesis techniques could achieve a greater degree of spatial filtering, producing the most significant increases in spectrum efficiency. The phase shifters could be implemented using PIN diodes operating as single-pole single-throw (SPST) switches. These

can be digitally controlled to switch in different lengths of line and introduce the required phase shift onto the signal. If microstrip design techniques are employed, the phase shifters and power combiners/dividers could all be placed on one microwave integrated circuit (MIC) [15]. If a microstrip antenna array is also employed, the result would be a very compact and economical design. Phased array antennas of this type have already been considered for vehicle mounting in mobile satellite communications since a very low cost and low profile structure can be obtained [21].

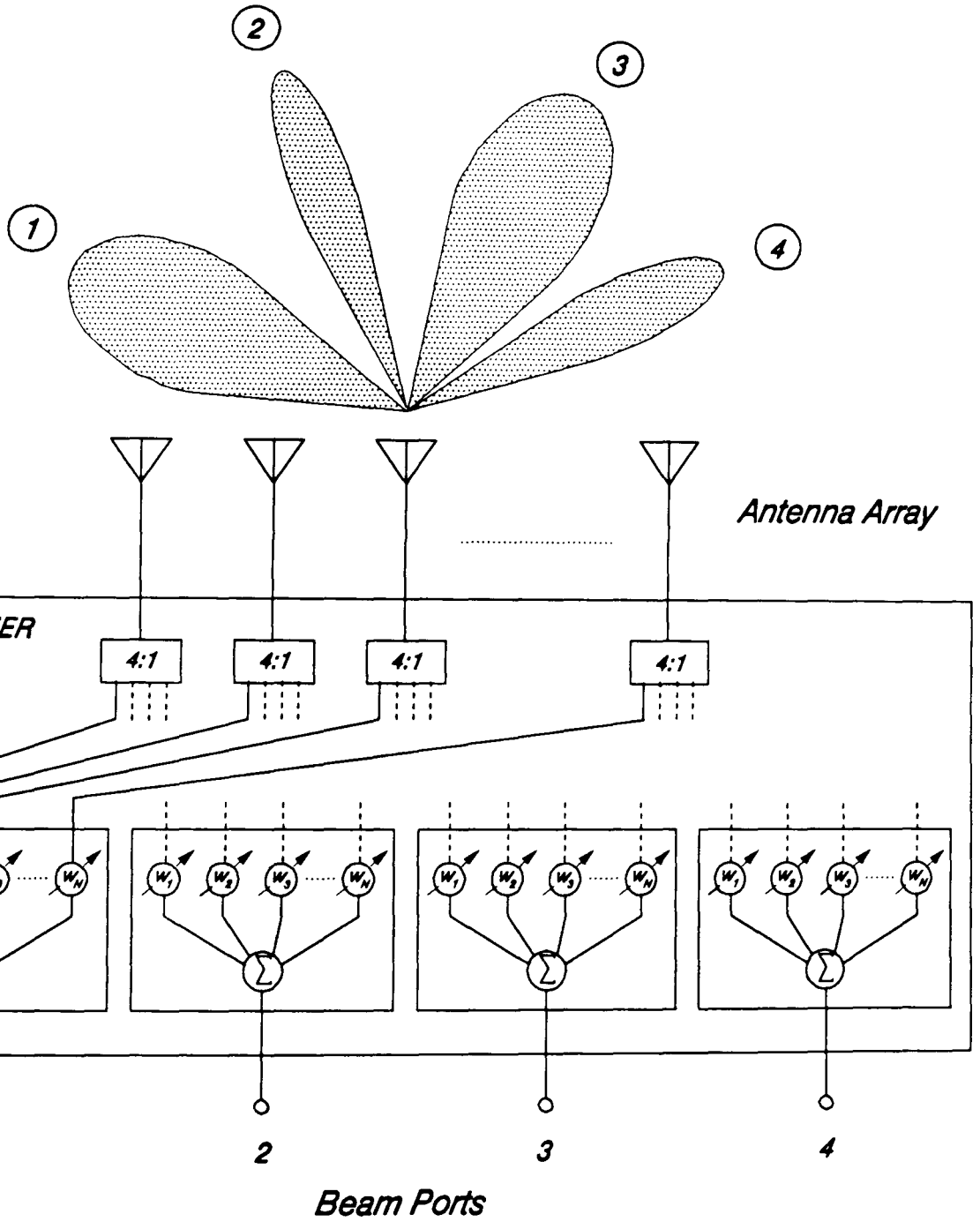

Figure 7.10: Active beamforming network.

7.3.4 Digital Beamforming

Digital beamforming is a very powerful technique and is currently receiving a lot of interest, in particular for radar systems [22]. With the advent of digital technology for the next generation of cellular networks, this approach is very attractive since it would enable both the direction finding and beamforming tasks to be carried out by a digital processor. A simplified block diagram showing the main functional blocks of a possible implementation is illustrated in figure 7.11. The signals received at each element in the array are downconverted in the usual way to a suitable IF frequency before being digitised. At this stage, the source estimation processor determines the bearing of each mobile source enabling the beam assignment processor to calculate the appropriate beamforming weights for both reception and transmission.

One important requirement is for very close amplitude and phase matching between channels, although if the *array manifold*[3] was known already, any mismatches could be compensated for digitally. The array manifold was measured for the experimental DF receiver in chapter 6 using an external source in the far field of the antenna. The received signal vector across the array could then be measured for different azimuth and elevation angles. This would be a very expensive technique in practice, especially if the receiver required frequent recalibration. An alternative approach was proposed by Steyskal [22] and employed a self calibration scheme in which precise RF pilots were injected at the receiver front ends. Any antenna effects such as mutual coupling would not be included, although these could be calculated analytically. An alternative on line calibration scheme was also discussed in chapter 6.

Hence, in principle, a digital beamforming base-station antenna system could be realised although the complexity of the hardware and the large processing overheads would probably make it an uneconomical option. A possible hybrid scheme could be considered as a compromise, with a fully digital receiver to combine the beamforming and direction finding, and an RF beamformer for the downlink.

3: The array manifold is defined as the response of the receiver to a single source as a function of the angle of arrival.

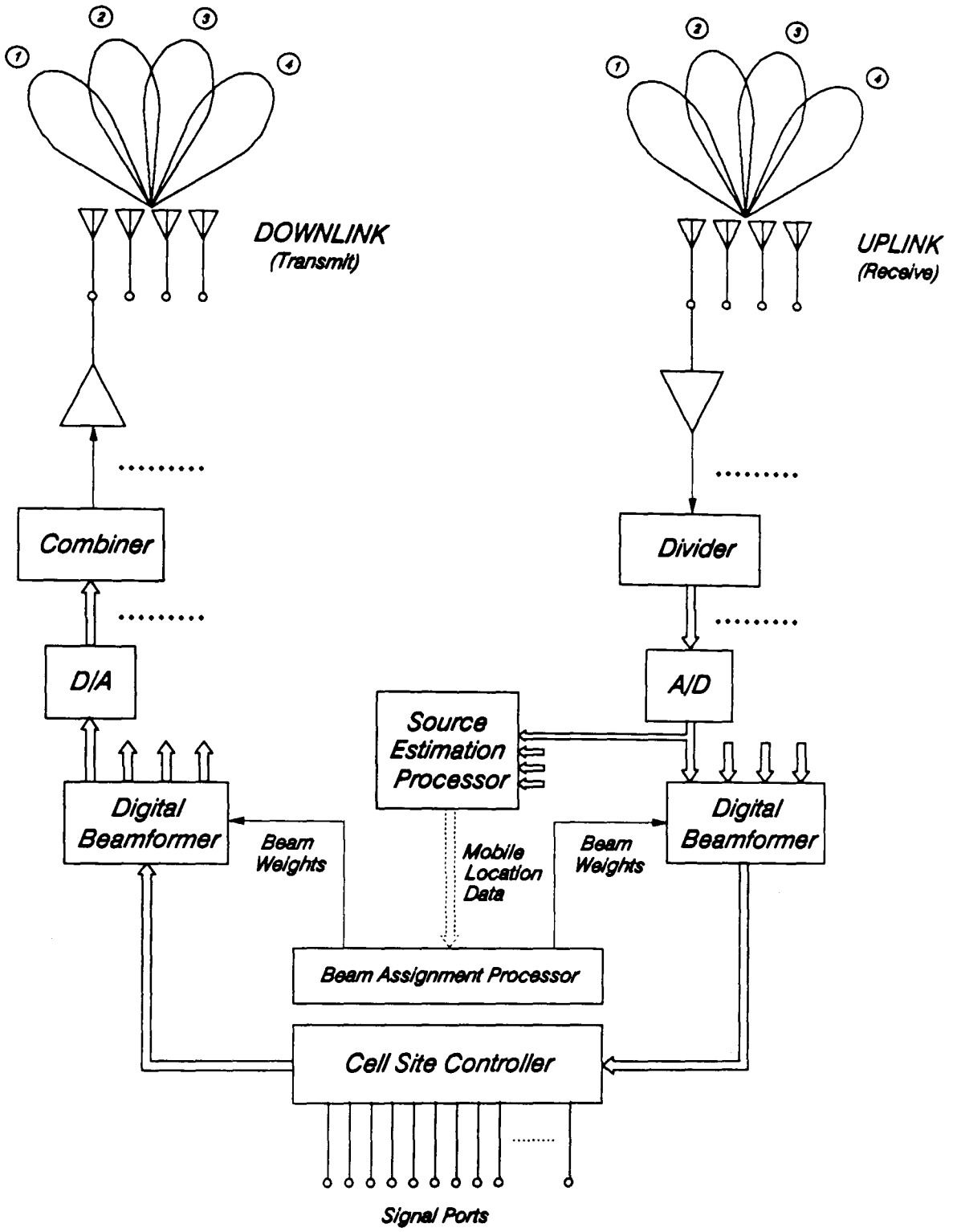

Figure 7.11: Schematic of full digital implementation of proposed base-station antenna system.

REFERENCES

[1]: N. Ehrlich, R.E. Fisher and T.K. Wingard, *"Cell-Site Hardware"*, The Bell System Technical Journal, Vol.58, No.1, Jan. 1979, pp.153-199.

[2]: W.C.Y. Lee, *"Mobile Telecommunication Systems"*, McGraw-Hill, 1989.

[3]: A.K. Johnson, *"Linear Amplifier Combiner"*, 37th IEEE Vehicular Technology Conference, Tampa, USA, 1st - 3rd June 1987, pp.421-423.

[4]: J.D. Parsons and J.G. Gardiner, *"Mobile Communication Systems"*, Blackie & Son Ltd., 1989.

[5]: *"IMS A100 Cascadable Signal Processor"*, INMOS Data Sheet, 72TRN10002, April 1987.

[6]: H. Yassaie, *"Digital Filtering with the IMS A100"*, INMOS Application Note 1, 72APP00101, July 1987.

[7]: H. Yassaie, *"Complex (I&Q) Processing with the IMS A100"*, INMOS Application Note 4, 72APP00401, July 1987.

[8]: H. Yassaie, *"Discrete Fourier Transform with the IMS A100"*, INMOS Application Note 2, 72APP00201, July 1987.

[9]: M.W. Wax, T.J. Shan and T. Kailath, *"Spatio-Temporal Spectral Analysis by Eigenstructure Methods"*, IEEE Transactions on Acoustics, Speech & Signal processing, Vol.ASSP-32, No.4, Aug. 1984, pp.817-827.

[10]: J.H. Winters, *"Optimum Combining in Digital Mobile Radio with Co-channel Interference"*, IEEE Transactions on Vehicular Technology, Vol.VT33, No.3, Aug. 1984, pp.144-155.

[11]: R. Kohno, H. Imai, M. Hatori and S. Pasupathy, *"Combination of an Adaptive Array Antenna and Canceller of Interference for Direct-Sequence Spread-Spectrum Multiple-Access System"*, IEEE Journal on Selected Areas in Communications, Vol.8, No.4, May 1990, pp.675-681.

[12]: A.W. Rudge, K. Milne, A.D. Olver and P. Knight, *"The Handbook of Antenna Design - Vol.I"*, Peter Peregrinus Ltd., 1982.

[13]: R.C. Hansen, *"Microwave Scanning Antennas: Vol.III, Array Systems"*, Academic Press Inc., 1966.

[14]: Y. Yamada and M. Kijima, *"Low Sidelobe and Tilted Beam Base-Station Antennas for Smaller Cell Systems"*, 1989 International Symposium on Antennas & Propagation, APS89, pp.138-141.

[15]: J.R. James and P.S. Hall, *"Handbook of Microstrip Antennas: Vol.2"*, Peter Peregrinus Ltd., 1989.

[16]: D.H. Archer, *"Lens-Fed Multiple Beam Arrays"*, Microwave Journal, Sept. 1984, pp.171-195.

[17]: T. Macnamara, *"Simplified Design Procedures for Butler Matrices Incorporating 90° Hybrids or 180° Hybrids"*, IEE Proceedings, Vol.134, Pt.H, No.1, Feb. 1987, pp.50-54.

[18]: L. Musa and M.S. Smith, *"Microstrip Port Design and Sidewall Absorption for Printed Rotman Lens"*, IEE Proceedings, Vol.136, Pt.H, No.1, Feb. 1989, pp.53-58.

[19]: S.J. Foti and T. Macnamara, *"Design of Wideband Butler Matrices Using Schiffman Lines"*, IEE Colloquium on Multiple Beam Antennas & Beamformers, Digest No.1989/136, 21st Nov. 1989, pp.5·1-5·8.

[20]: J.T. Mayhan and L. Niro, *"Spatial Estimation Using Multiple Beam Antennas"*, IEEE Transactions on Antennas & Propagation, Vol.AP-35, No.8, Aug. 1987, pp.897-906.

[21]: G. Schaffner, *"Low Cost Phased Array Steering"*, 1987 IEEE MTTS International Microwave Symposium Digest, Vol.2, June 1987, pp.949-952.

[22]: H. Steyskal and J.F. Rose, *"Digital Beamforming for Radar Systems"*, Microwave Journal, Jan. 1989, pp.121-136.

CHAPTER 8

DISCUSSION

8.1 SUMMARY

Increasingly over recent years, competition for the use of the radio spectrum has highlighted the need for spectrum efficiency in cellular Land Mobile Radio (LMR) systems. Consequently we have seen the emergence of such techniques as *cell splitting* and *cell sectorisation*, as well as the development of more spectrum efficient modulation schemes. Research activity in recent years has focused primarily on the modulation format and consequently this area has witnessed some of the most significant advances, especially with the advent of digital technology. The base-station antenna, or more importantly the base-station antenna operating system, has not experienced the same level of interest, although there has been some noteworthy research into the potential application of antenna arrays.

Antenna array technology has been employed extensively in military communications, radar, sonar and, more recently, in satellite communication systems. Their application in civil, or cellular, communications has not been so widespread, and some potential schemes were discussed in chapter 2. One of the most notable proposed the use of an antenna array as an adaptive beamformer, or optimum combiner, which could steer radiation pattern nulls in such a way as to reduce the level of co-channel interference. This approach exploits one of the better known properties of adaptive antenna arrays, namely the anti-jamming capability. The maximum number of nulls that can be generated is governed by the number of elements in the array. Therefore, if the number of interferers exceeds the degrees of freedom of the array, they cannot all be cancelled. Also, if the interference emanates from the same direction as the wanted signal energy, the array cannot perform as effectively. Instead of trying to cancel out the interferers, a conceptually simpler approach would be to steer a radiation pattern maxima, or beam, towards the wanted user or mobile. This would achieve the following objectives:

- For the **uplink** (mobile-to-base) the level of interference received at the base-station antenna from co-channel mobiles would be governed only by the sidelobes of the beam.

- For the **downlink** (base-to-mobile) the signal energy is constrained towards the wanted mobile only, greatly reducing the level of interference that would be experienced by mobiles in neighbouring co-channel cells.

The problem of interference from the same direction as the wanted mobile could be removed by changing the channel allocation to one experiencing less interference. Since the signal energy is constrained to a single beam, the benefits would be experienced on both the uplink and the downlink.

The realisation of this base-station antenna system requires that the following two tasks are fulfilled:

- **Source Location:** The estimation of the current mobile user distribution within a cell, i.e. the azimuth bearing and possibly the range.

- **Beamforming:** The generation of an optimum set of beams to cover the cell using the knowledge of the user distribution.

This concept was introduced in chapter 2 and the term "smart" was first used to describe the proposed base-station antenna due to the ability of the system to acquire knowledge of the signalling environment and apply it in an intelligent manner. In subsequent chapters the realisation of the "smart" base-station antenna was addressed and some of the work has been included in a number of publications (listed in Appendix J). The achievements can be summarised as follows:

- **Figure of Merit**

  In chapter 3, a figure of merit was established for the "smart" base-station antenna with respect to a conventional omni-directional antenna system. The calculation was based on the ability to reduce the level of co-channel interference in a typical mobile radio environment. Statistical propagation models were employed with up to six co-channel interferers. The figure of merit is measured as the relative increase in spectral efficiency and the results are summarised in figure 3.5. An ideal eight beam antenna system, for example, could provide a three fold increase in capacity for the same traffic load in each cell.

- **Direction Finding**

  The task of determining the location of the mobile within a cell using an antenna array was addressed in chapter 4. A number of direction finding (DF) algorithms which are employed extensively in radar were outlined, and their suitability for operation in a cellular radio environment discussed. Finally, a number of key factors which could affect the performance of the DF algorithms were introduced.

- **Computer Simulations**

  A computer simulation suite was developed in chapter 5 in order to assess the performance of the DF techniques in a variety of mobile radio environments, e.g. urban, suburban and rural. The results clearly show that in the scattering environment found in urban and suburban areas, the lower resolution algorithms provide the most accurate bearing estimate. In rural areas the higher resolution techniques offer the superior resolution, although the problem of coherent multipath reflections will have to be overcome.

- **Field Trials**

  In chapter 6, the construction of a DF receiver employing a four element linear array was described. Field trials were carried out to assess the performance of the DF algorithms in typical urban surroundings. The results clearly demonstrate the ability of the receiver to track the movements of a single mobile transmitting a CW tone, and confirm many of the findings from the computer simulations. In particular, the concept of a scattering volume associated with the position of the mobile due to the presence of buildings and other local scatterers in the immediate vicinity. The results also provide a unique insight into the scattering conditions which prevail in an urban locality. With the mobile at a distance of 1 km from the base-station antenna, the angular spread of the signals received at the base would typically be in the range of 3° to 6°.

- **Implementation Issues**

  Having established the ability to locate the position of a mobile source, chapter 6 addresses a number of implementation issues

which will affect the ultimate realisation of the "smart" base-station antenna system, e.g. the base-station hardware currently available and the signal modulation format employed. In particular, the beamforming aspect of the proposed antenna system is discussed. A number of solutions were considered employing either fixed or agile beams, and potential system architectures were presented.

In conclusion then, the study presented here has demonstrated the feasibility of a multiple beam (or "smart") base-station antenna system for future high capacity cellular networks. The work has primarily been targeted at a narrowband modulation format operating within either an FDMA or TDMA scheme, although an alternative system for a wideband format is discussed in chapter 7. In contrast to current methods of meeting growing public demand for service, the proposed system could adapt gracefully with the provision of additional beams at each base-station site. This would dramatically reduce the infrastructure costs associated with the acquisition of new base-station sites, as well as ensuring that the trunking efficiency of the network is not impaired (a result of an increased handover rate with the current methods of cell splitting and cell sectorisation). It must be recognised that the initial installation costs would be very high in comparison, although the investment would be more than repaid as the network expanded and the number of users grew.

8.2 FUTURE WORK

The development work so far has only concentrated on the ability to locate the position of a single mobile source. Therefore the next stage would be to synthesize a single beam to track the movements of the mobile, thereby closing the loop. A comparison can then be made between the adaptive base-station and a conventional omni-directional base-station by measuring the ability of the array to reduce the level of co-channel interference. A schematic of the modified receiver architecture is shown in figure 8.1. The signals received at each element in the array are split equally between the direction finding and beamforming processes, the DF process employing the receiver hardware that has already been developed. On-line estimation of the source bearing could be carried out on the existing transputer network

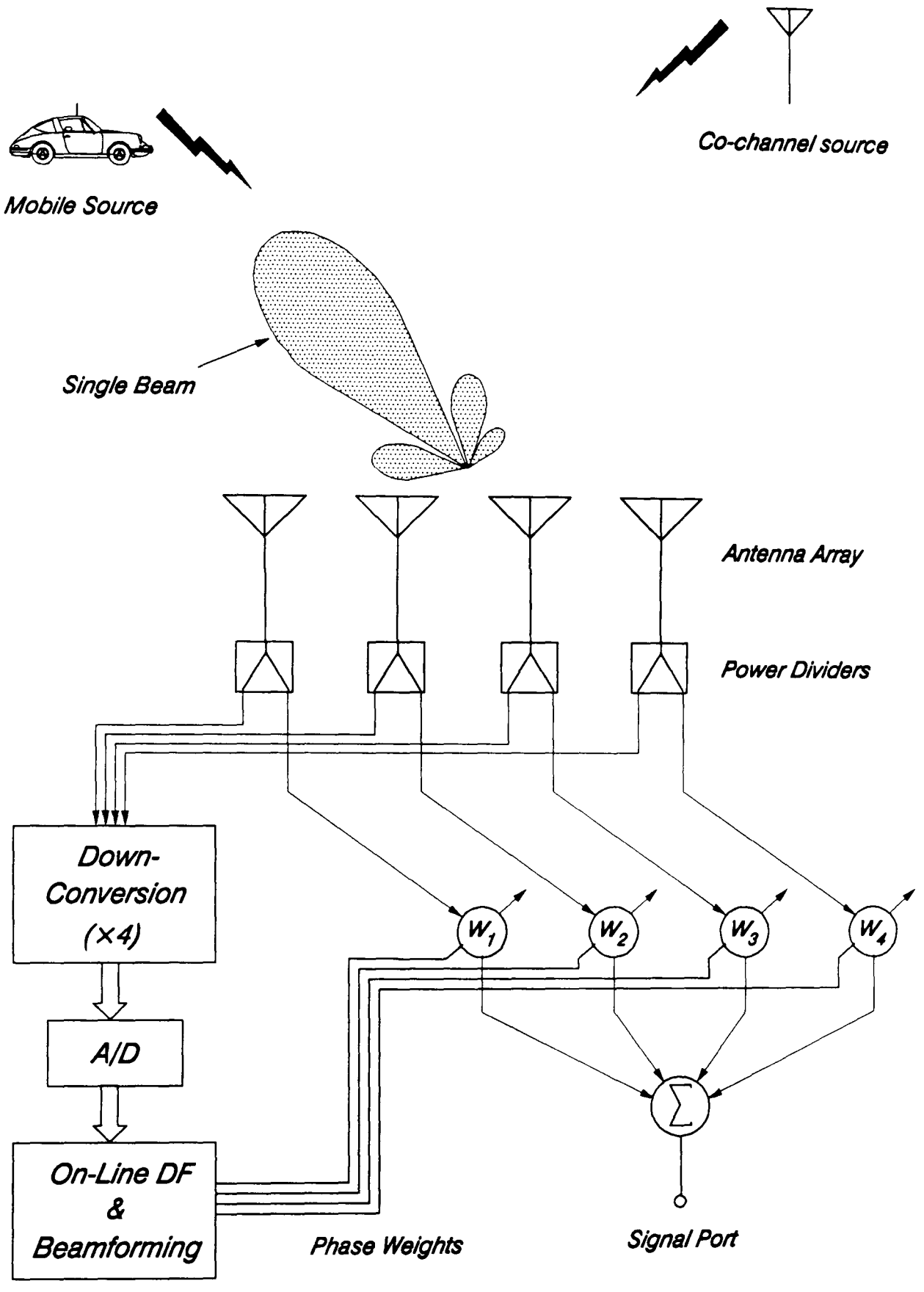

Figure 8.1: Closing the loop.

installed in a PC, and a digital interface provided to control the values of the element weights. Initially only phase weights would be employed, although PIN diode attenuators could be included to enable lower sidelobe beams to be generated. In order to achieve the necessary azimuth scan of the beam, digital phase shifters employing hybrid couplers, PIN diode switches and different line lengths would be constructed. By measuring the received signal levels from the wanted mobile source and co-channel source independently the reduction in the interference level can then be determined.

Once the beamforming principle has been established, the next stage would be to target the system for a particular network, e.g. the Pan European proposal, and develop full duplex voice channel operation. In parallel with this, the direction finding ability of the system could be developed and various value added services investigated. This particular aspect is discussed in the following section. At this stage however, the full potential of the proposed antenna system has yet to be realised, and the role it could play in the development of the personal communications dream discussed in chapter 1. The goal is to provide universal pocket sized communications by the end of the century. This implies first of all that the system must make very efficient use of the radio spectrum if it is to be made available to a large consumer base. It is also highly desirable that the portable communicator has a long duty cycle between battery recharging thus implying power efficient hardware and modulation [1]. The role of the adaptive antenna has already been discussed in terms of the former requirement, however the potential enhancement in the power efficiency obtainable using spatial filtering has not been fully assessed to date. The merits of the proposed multiple beam base-station antenna system in a rural service area are of particular interest. Here cell sizes can be of the order of 30km with greatly reduced user densities when compared with suburban and urban service areas. The antenna array at a rural base-station site could then be employed to constrain the signal energy (in both transmit and receive modes of operation) to a narrow beam directed towards a distant user, thereby reducing the required transmitted RF energy from the handheld transceiver. It is thus envisaged that this technique would yield significant benefits in terms of power consumption of the portable communicator, and would make a significant contribution towards the realisation of the truly universal personal communications network.

8.3 VALUE ADDED SERVICES

There is currently a lot of interest within Europe in providing extra services for mobile users, and three programmes of work have recently been undertaken. These are Prometheus, Autoguide and DRIVE [2]. The aim is to make driving in Europe safer, more economical and more comfortable through the exchange of information between vehicles and between vehicles and roadside equipment. Within the European community it has recently been estimated [3] that the losses to the economy resulting from traffic congestion, difficult routing of vehicles and lost drivers amounted to a staggering $22 billion every year. Therefore, in addition to providing drivers with a navigation service, the Prometheus project plans to warn drivers of traffic jams and possible holdups as well as providing alternative routing information. The project is very ambitious and is still in the planning stage, but with substantial financial backing throughout Europe, is set to revolutionise motoring in the near future.

The proposed base-station antenna system could provide a facility for determining the location of the mobile users within a network. This would be in terms of an azimuth bearing and a range, and a number of value added services could be provided as follows:

- User location and navigation aid.
- Provide traffic information/control.
- Location of distress calls for the Emergency services.

The users could request these services in the same manner as a normal request to set up a call. The voice channel, or a dedicated set of channels, would then be employed to enable a position fix of the user to be made and allow the exchange of information. From the results of the trials a 3° to 6° angular spread of signals can be expected in an urban environment at a distance of 1 km. This corresponds to a position uncertainty of between 50 m and 100 m and, combined with a range uncertainty, the position of the user can only be estimated as shown in figure 8.2. The provision of an additional base-station would remove some of the ambiguity as illustrated.

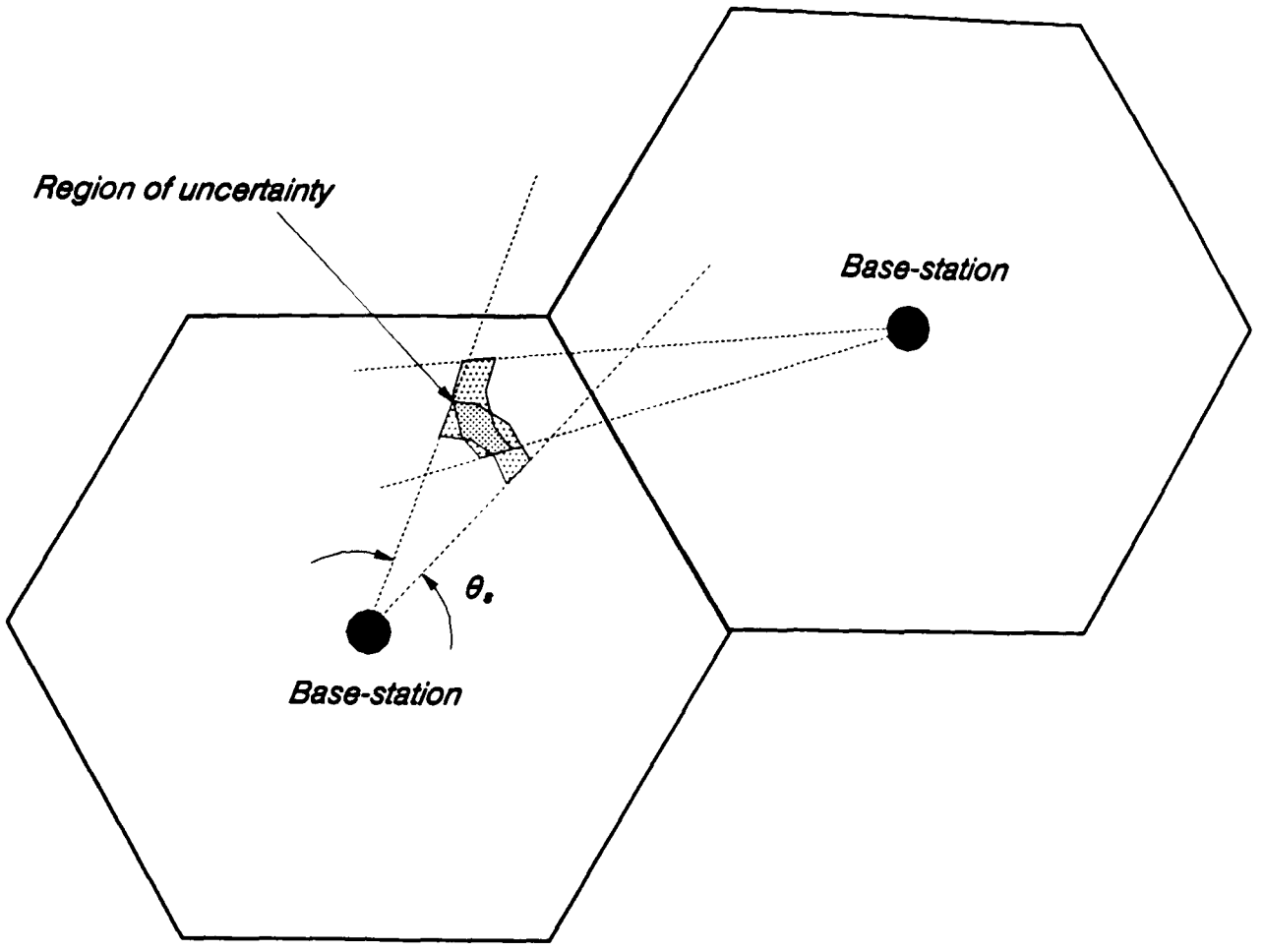

Figure 8.2: User location with two base-station antennas.

It remains to be seen whether the accuracy of the estimate would be sufficient to provide a reliable service. However, a rough estimate of the users location during a call would be an extremely valuable piece of information for network operators. In conjunction with the proposed base-station antenna system, a number of additional benefits could be envisaged as follows:

- Elegant handover mechanism.
- Dynamic cell boundaries.
- Dynamic channel assignment.

The handover mechanism and dynamic cell boundaries would utilise the ability to steer multiple independent beams to increase the effective coverage area of each cell. This will create regions of overlap as shown in figure 8.3, and the knowledge of the active mobile locations would enable two modes of operation. The first is when an active mobile is about to handover to an adjacent cell. Normally if there is no new channel available, there is a

possibility that the call would be dropped. However, with the proposed scheme, the current base-station could extend its coverage area to the active mobile, only handing over when a new channel has been made available. Hence the base-station effectively adapts the cell boundaries to accommodate handovers, thus reducing the number of dropped calls. In the second case, all the base-stations could adapt their coverage area according to the loading of the network, and the local terrain. Hence the term *dynamic cell boundaries*.

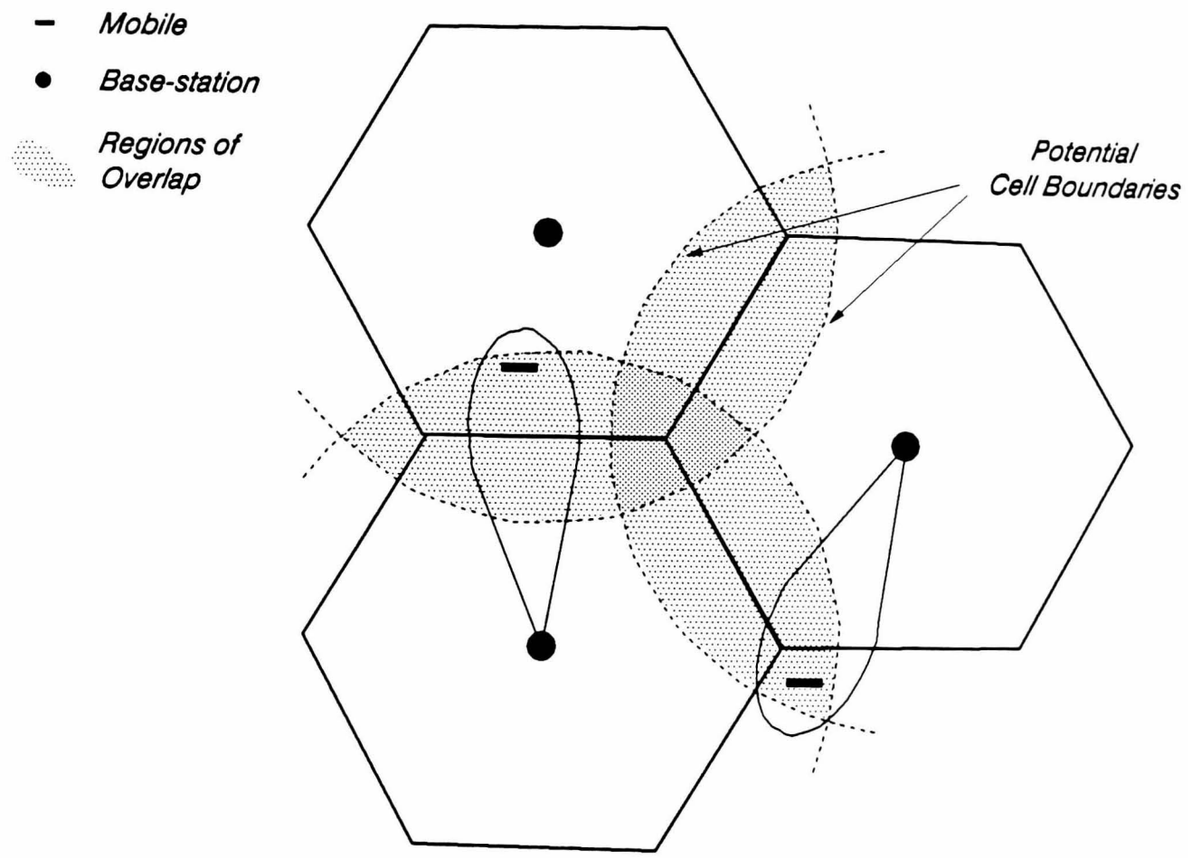

Figure 8.3: Overlapping cell boundaries.

When the base-station is estimating the angle of arrival of the active mobiles, the resulting spatial spectrum would also reveal any sources of potential co-channel interference (as shown in the computer simulations of chapter 5). Hence, if the azimuth direction of the wanted mobile approaches an interfering source, the base-station could reassign channels to prevent a drop in the received signal-to-interference ratio, thus avoiding a degradation in the quality of service, possibly leading to a lost call.

It is the intrinsic smartness of the proposed base-station that makes it so versatile, although intelligent antenna systems are not a new idea and

have been considered for numerous other applications. Sandler and Kokar [4] describe the use of an adaptive antenna in conjunction with an Artificial Intelligence system as an anti-jamming antenna for radar. Here the antenna has a wealth of stored data which is used to 'teach' the system about the various scenarios it will encounter. In this way it can adapt readily to every new situation as it presents itself and 'learn' from its mistakes. A similar proposal was put forward by Vannicola and Mineo [5] for a radar tracking antenna system for surveillance.

8.4 CONCLUDING REMARKS

The study presented here has considered a novel type of base-station antenna system for the future generation high capacity cellular and personal communication networks. The work has established the feasibility of such a scheme, although there is still much to be accomplished before it could be incorporated into a network. If the personal communications dream is to become a reality however, many new and innovative schemes will have to be given serious consideration by the network operators, and it is likely that the antenna array will play a crucial role in the future.

REFERENCES

[1]: D.R. Long, W.J. Whitmarsh and A. Bateman, *"Power Consumption Considerations for Future Personal Communications Systems"*, 2nd International Conference on Communications Systems, Singapore, 5th - 9th Nov. 1990.

[2]: R.E. Fudge, *"European Initiatives for Road Traffic Management"*, CCIR Interim Working Party IWP8/13, Sept. 1988.

[3]: J. Gosch, *"Europe's Prometheus Project Fires Up"*, Electronics, April 1989, pp.54A-54D.

[4]: S.S. Sandler and M. Kokar, *"Intelligent Antennas"*, URSI International Symposium on Electromagnetic Theory, Budapest, Hungary, 1986, pp.159-161.

[5]: V.C. Vannicola and J.A. Mineo, *"Applications of Knowledge Based Systems to Surveillance"*, Proceedings of 1988 IEEE National Radar Conference, USA, 20th - 21st April 1988, pp.157-164.

APPENDIX A

ADAPTIVE ANTENNA ARRAY FUNDAMENTALS

The adaptive array consists of a number of antenna elements, not necessarily identical, coupled together via some form of amplitude control and phase shifting network to form a single output. The amplitude and phase control can be regarded as a set of *complex weights*, and is illustrated in figure A.1 as a *beamforming network*. If the effects of receiver noise and mutual coupling are ignored,the operation of an N element uniformly spaced linear array can be explained as follows. Consider a wavefront generated by a narrowband source of wavelength λ arriving at an N element array from a direction θ_m off the array broadside. If the antenna spacing is d, the *electrical phase shift* from element to element across the array can be expressed as

$$\phi_m = \frac{2\pi d}{\lambda} \sin \theta_m \qquad (A.1)$$

Assuming constant envelope modulation of the source located at θ_m, and taking the first element in the array as the phase reference, the signal at the output of each of the antenna elements can be expressed as

$$x_{nm}(t) = e^{j(\omega t+(n-1)\phi_m)} \qquad (A.2)$$

and the total array output in direction θ_m as

$$y_m(t) = \sum_{n=1}^{N} w_n \, e^{j(\omega t+(n-1)\phi_m)} \qquad (A.3)$$

where w_n represents the value of the complex weight applied to the output of the nth element.

The weights are generated by the *adaptive control processor* and the complexity of this unit depends entirely on the application and the degree of *a priori* knowledge of the signal environment that is available. If, for

example, the array is required to respond in a manner which does not depend on the received array data, the adaptive control processor can be dispensed with altogether and the weights calculated independently. Alternatively, the weights can be chosen based upon the statistics of the data received at the array, the aim being to optimise the beamformer response to reduce contributions from noise and other unwanted signals whilst maintaining reception of the wanted signal, i.e. *optimum beamforming*. The result can also be considered as *adaptive spatial filtering* and many algorithms have been developed for the calculation of the optimum beamformer weights (further details can be found elsewhere). Hence the array will accept a wanted signal from direction θ_1 and steer nulls towards interference sources located at θ_m, for $m \neq 1$. Likewise, the weighting network can be optimised to provide maximum gain in a specific direction, or directions. It can be shown that an N element array has N - 1 degrees of freedom giving up to N - 1 independent pattern nulls.

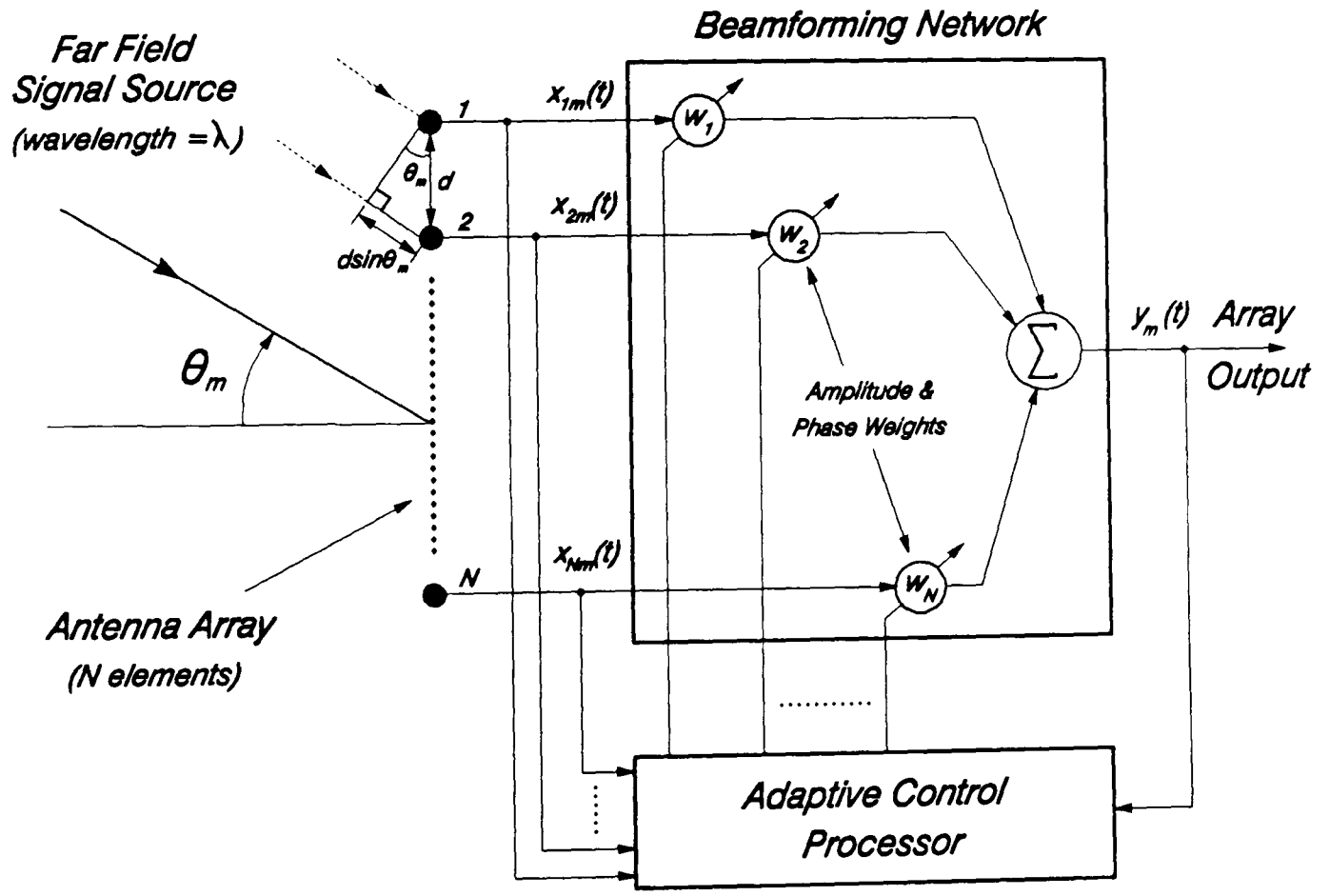

Figure A.1: An adaptive antenna array.

APPENDIX B

THE PERFORMANCE ENHANCEMENT OF MULTI-BEAM ADAPTIVE BASE-STATION ANTENNAS FOR CELLULAR LAND MOBILE RADIO SYSTEMS

Reprinted from:

IEEE Transactions on Vehicular Technology

Vol.VT-39, No. 1, February 1990.

The Performance Enhancement of Multibeam Adaptive Base-Station Antennas for Cellular Land Mobile Radio Systems

SIMON C. SWALES, MARK A. BEACH, DAVID J. EDWARDS, AND JOSEPH P. McGEEHAN, MEMBER, IEEE

Abstract—**The problem of meeting the proliferating demands for mobile telephony within the confinements of the limited radio spectrum allocated to these services is addressed. A multiple beam adaptive base-station antenna is proposed as a major system component in an attempt to solve this problem. This novel approach is demonstrated here by employing an antenna array capable of resolving the angular distribution of the mobile users as seen at the base-station site, and then using this information to direct beams toward either lone mobiles, or groupings of mobiles, for both transmit and receive modes of operation. The energy associated with each mobile is thus confined within the addressed volume, greatly reducing the amount of co-channel interference experienced from and by neighboring co-channel cells. In order to ascertain the benefits of such an antenna, a theoretical approach is adopted which models the conventional and proposed antenna systems in a typical mobile radio environment. For a given performance criterion, this indicates that a significant increase in the spectral efficiency, or capacity, of the network is obtainable with the proposed adaptive base-station antenna.**

I. Introduction

THE FREQUENCY SPECTRUM is, and always will be, a finite and scarce resource, thus there is a fundamental limit on the number of radio channels that can be made available to mobile telephony. Hence, it is essential that cellular land mobile radio (LMR) networks utilize the radio spectrum allocated to this facility efficiently, so that a service can be offered to as large a subscriber community as possible. Indeed, a major consideration of the second generation cellular discussions in both the US and Europe has focused on this point. However, present and proposed future generation cellular communication networks which employ either omnidirectional, or broad sector-beam, base-station antennas, will be beset with the problem of severe spectral congestion as the subscriber community continues to expand.

A measure often used to assess the efficiency of spectrum utilization is the number of voice channels per megahertz of available bandwidth per square kilometer [1]. This defines the amount of traffic that can be carried and is directly related to the ultimate capacity of the network. Hence, as traffic demands increase, the spectral efficiency of the network must also increase if the quality and availability of service is not to be degraded. At present this is overcome in areas with a high traffic density by employing a technique known as *cell splitting*. However, the continuing growth in traffic demands has meant that cell sizes have had to be reduced to a practical minimum in many city centers in order to maintain the quality of service. As well as increasing the infrastructure costs, the number of subscribers able to access these systems simultaneously is still well below the long-term service forecasts due to the reduced *trunking efficiency* of the network. This places great emphasis on maximizing the spectral efficiency, or ultimate capacity, of future generation systems, and thereby fulfilling the earlier promises of performance. There have already been significant developments in terms of spectral efficient modulation schemes, e.g., the proposed US narrow-band digital linear system [2], [3] and the second generation Pan-European cellular network [4]. Also, in the area of antenna technology, the use of fixed coverage directional antennas has been considered [5]. In particular, the use of fixed phased array antennas, with carefully controlled amplitude tapers and sidelobe levels for the enhanced UK TACS network (ETACS) [6], are currently under evaluation. However, the application of *adaptive antenna arrays* in civil land mobile radio systems has hitherto received little attention, in spite of the significant advances made in this field for both military and satellite communications.

In this paper a multiple beam adaptive base-station antenna is proposed to complement other solutions, such as spectrum efficient modulation, currently being developed to meet the proliferating demands for enhanced capacity in cellular networks. The feasibility of such a scheme is demonstrated, and a comparison made with existing conventional antennas in a realistic mobile radio environment. Geometrical and statistical propagation models are used and a unique insight is given into the benefits of utilizing adaptive base-station antennas in a cellular radio system. Finally, the concept of such a scheme is discussed and the integration of adaptive antenna array technology into a mobile communications environment considered.

II. Adaptive Antenna Arrays

An adaptive antenna array may be defined as one that modifies its radiation pattern, frequency response, or other parameters, by means of internal feedback control while the antenna system is operating. The basic operation is usually described in terms of a receiving system steering a *null*, that is, a reduction in sensitivity in a certain angular position, toward a

Manuscript received April 18, 1989. This work was supported by UK SERC.

The authors are with the Centre for Communications Research, Faculty of Engineering, University of Bristol, Bristol, B58 1TR, UK.

IEEE Log Number 9034227.

0018-9545/90/0200-0056$01.00

source of interference. The first practical implementation of electronically steering a null in the direction of an unwanted signal, a jammer, was the Howells–Applebaum sidelobe canceller for radar. This work started in the late 1950's, and a fully developed system for suppressing five jammers was reported in open literature in 1976 by Applebaum [7]. At about the same time Widrow [8] independently developed an approach for controlling an adaptive array using a recursive least squares minimization technique, now known as the LMS algorithm. Following the pioneering work of Howells, Applebaum, and Widrow, there has been a considerable amount of research activity in the field of adaptive antenna arrays, particularly for reducing the jamming vulnerability of military communication systems. However, to date, there has been little attention to the application of such techniques in the area of civil land mobile radio.

Adaptive antenna arrays cannot simply be integrated into any arbitrary communication system, since a control process has to be implemented which exploits some property of either the wanted, or interfering, signals. In general, adaptive antennas adjust their directional beam patterns so as to maximize the signal-to-noise ratio at the output of the receiver. Applications have included the development of receiving systems for acquiring desired signals in the presence of strong jamming, a technique known as *power inversion* [9]. Systems have also been developed for the reception of frequency hopping signals [10], [11], TDMA satellite channels [12] and spread spectrum signals [13]. Of particular interest for cellular schemes is the development of adaptive antenna arrays and signal processing techniques for the reception of multiple wanted signals [14].

A. Fundamentals of Operation

The adaptive array consists of a number of antenna elements, not necessarily identical, coupled together via some form of amplitude control and phase shifting network to form a single output. The amplitude and phase control can be regarded as a set of *complex weights*, as illustrated in Fig. 1. If the effects of receiver noise and mutual coupling are ignored, the operation of an N element uniformly spaced linear array can be explained as follows. Consider a wavefront generated by a narrow-band source of wavelength λ arriving at an N element array from a direction θ_k off the array boresight. Now taking the first element in the array as the phase reference and letting d equal the array spacing, the relative phase shift of the received signal at the nth element can be expressed as

$$\Psi_{nk} = \frac{2\pi d(n-1)}{\lambda} \sin \theta_k. \tag{1}$$

Assuming constant envelope modulation of the source at θ_k, the signal at the output of each of the antenna elements can be expressed as

$$x_{nk}(t) = e^{j(\omega t + \Psi_{nk})} \tag{2}$$

and the total array output in direction θ_k as

$$y_k(t) = \sum_{n=1}^{N} w_n e^{j(\omega t + \Psi_{nk})} \tag{3}$$

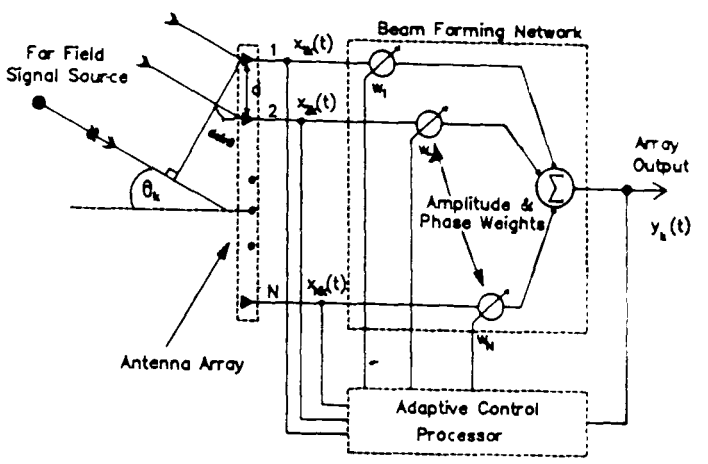

Fig. 1. An adaptive antenna array.

where w_n represents the value of the complex weight applied to the output of the nth element. Thus by suitable choice of weights, the array will accept a wanted signal from direction θ_1 and steer nulls toward interference sources located at θ_k, for $k \neq 1$. Likewise, the weighting network can be optimized to steer beams (a radiation pattern maxima of finite width) in a specific direction, or directions. It can be shown [15] that an N element array has $N-1$ degrees of freedom giving up to $N-1$ independent pattern nulls. If the weights are controlled by a feedback loop which is designed to maximize the signal-to-noise ratio at the array output, the system can be regarded as an *adaptive spatial filter*.

The antenna elements can be arranged in various geometries, with uniform line, circular and planar arrays being very common. The circular array geometry is of particular interest here since beams can be steered through 360°, thus giving complete coverage from a central base-station. The elements are typically sited $\lambda/2$ apart, where λ is the wavelength of the received signal. Spacing of greater than $\lambda/2$ improves the spatial resolution of the array, however, the formation of grating lobes (secondary maxima) can also result. These are generally regarded as undesirable.

B. Adaptive Antenna Arrays for Cellular Base-Stations

Multiple beam adaptive antenna arrays have been considered by Davies *et al.* [16] for enhancing the number of simultaneous users accessing future generation cellular networks. It is suggested that each mobile is tracked in azimuth by a narrow beam for both mobile-to-base and base-to-mobile transmissions, as shown in Fig. 2. The directive nature of the beams ensures that in a given system the mean interference power experienced by any one user, due to other active mobiles, would be much less than that experienced using conventional wide coverage base-station antennas. It has already been stressed that high capacity cellular networks are designed to be interference limited, so the adaptive antenna would considerably increase the potential user capacity.

This increase in system capacity of the new base-station antenna architecture was evaluated [17] by considering the spatial filtering properties of an antenna array. The results show that this type of base-station antenna could increase the spectral efficiency of the network by a factor of 30 or more. These results were obtained for a hypothetical fast frequency hopping

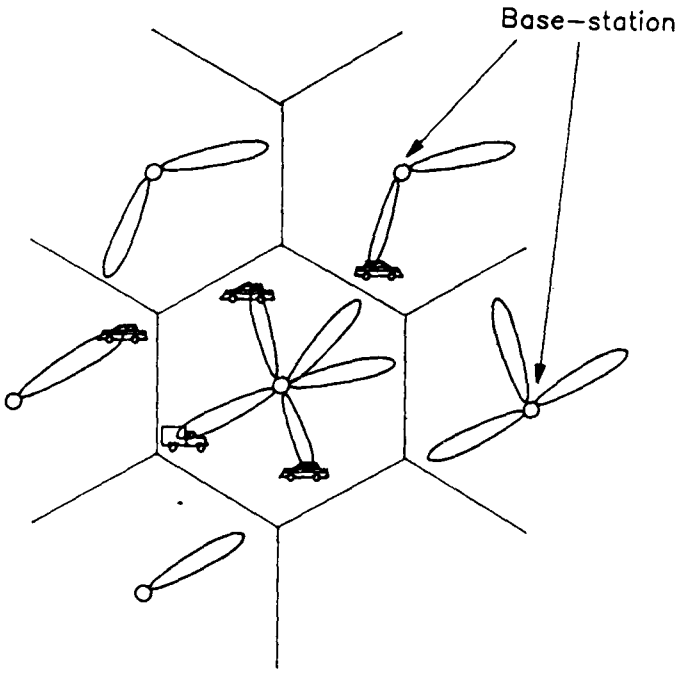

Fig. 2. Tracking of mobiles with multiple beams.

code division multiple access cellular network [18], assuming uniform user distribution and complete frequency reuse for the omnidirectional antenna case, i.e., adjacent cells are co-channel cells. Complete frequency reuse is then assumed for each of the beams formed by the adaptive array, i.e., adjacent beams are co-channel beams. Further, it was shown that a similar enhancement of efficiency can be obtained for either an idealized multibeam antenna, or a realizable 128 element circular array [19].

It was recognized in the analysis, but not fully assessed, that this approach would greatly increase the level of co-channel interference. It was, therefore, suggested that this problem could be overcome using dynamic channel allocation to eliminate the so called *common zones*. This again introduces additional hand-offs, reducing the trunking efficiency and available capacity of the network, as the mobile circumnavigates the cell.

The only study previous to the work discussed above considering the use of an adaptive antenna array in land mobile radio was by Marcus and Das [20] in 1983. The analysis assumed that the base-station, or repeater, sites could be placed closer together if an antenna array formed 20 dB nulls toward co-channel sites. This effectively reduces the amount of co-channel interference at the output of the base-station as explained in Section II. It was suggested that in this system the beam steering information could be derived from the squelch tone injection which is presently used in the US FM land mobile radio.

In contrast with the null steering technique considered by Marcus and Das, here the ability of the adaptive array to steer radiation pattern maxima toward the mobiles is considered. In the limit it can be envisaged that individual beams will be formed towards each mobile as illustrated in Fig. 2. It has already been mentioned that adaptive antenna technology cannot be simply integrated into an arbitrary communication system, and at present no one particular modulation scheme, or access technique, has been selected for the third generation of cellular systems. However, some well-established trends are becoming apparent in the quest toward higher spectrally efficient modulation schemes [1] for the systems of the year 2000 and beyond. It is thus vital during the initial stages of research to develop antenna architectures which are, in essence, modulation scheme independent, so that a figure of merit can be obtained for the multibeam base-station antenna.

III. Reduction of Co-Channel Interference Using Adaptive Antennas

In this paper the integration of an idealized adaptive array into an existing cellular network is considered. In order to ascertain the benefits of this class of antenna system compared with that of conventional omnidirectional base-station antenna systems, the following network topology has been assumed.

1) A cellular network consisting of hexagonal cells, with channel reuse every C cells (C is the cluster size).

2) The base-station transmitters are centrally located within each hexagonal cell.

3) There is a *uniform distribution* of users per cell.

4) There is a *blocking probability* of B in all cells.

5) The omnidirectional base-station antenna has an ideal beam pattern, giving a uniform circular coverage.

6) The adaptive base-station antenna can generate any number, m, of ideal beams, with a beamwidth of $2\pi/m$, and a gain equal to the omni-antenna.

7) Each adaptive beam will only carry the channels that are assigned to the mobiles within its coverage area.

8) Any mobile (or group of mobiles) can be tracked by the adaptive base-station antenna.

9) The necessary base-station hardware is available to enable beamforming and tracking.

10) The same modulation scheme can be used with each antenna system.

The blocking probability of B in assumption 4) is the fraction of attempted calls that cannot be allocated a channel. If there are "a" *Erlangs* of traffic intensity offered, the actual traffic carried is equal to $a(1 - B)$ Erlangs. The Erlang is a measure of traffic intensity, and measures the quantity of traffic on a channel or group of channels per unit time. This gives an *outgoing channel usage efficiency* (or loading factor) [21] of

$$\eta = a(1 - B)/N \tag{4}$$

where N is the total number of channels allocated per cell.

Assumptions 6), 7), and 8) imply the deployment of a somewhat hypothetical adaptive antenna system. This approach can be justified since a uniform user population has been assumed for both categories of antenna system. It is recognized that the dynamic, nonuniform, user distribution will have a significant effect on the results presented here. This will be considered in a subsequent more rigorous study. Also, in the analysis which follows only the base-to-mobile link has been studied, however, it can be shown that the analysis is also valid for the mobile-to-base link.

Two different categories of co-channel interference models are used as the basis for the study presented here. The first is the geometrical model adopted by Lee [5], followed by a more rigorous statistical analysis [21]–[23].

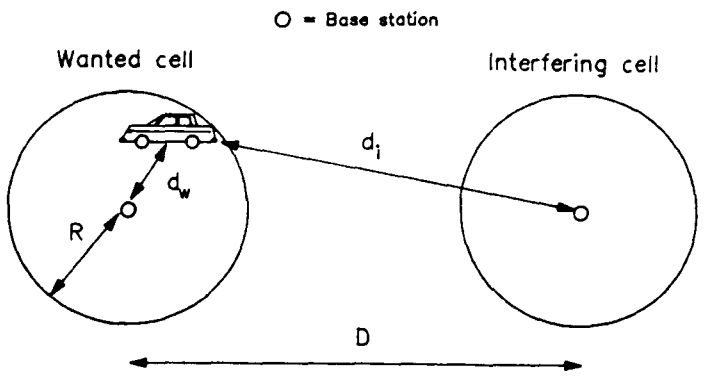

Fig. 3. Two co-channel cells.

IV. Geometrical Propagation Model

This approach considers the relative geometry of the transmitter and receiver locations, and takes into account the propagation path loss associated with the mobile radio channel.

A. One Co-Channel Cell

Consider one co-channel cell which forms part of a cellular network as shown in Fig. 3. By definition both the cells have the same channel allocation, and a reuse distance of D separating the base-station transmitters. The *co-channel reuse ratio* is defined as

$$Q = D/R. \tag{5}$$

This ratio has also been termed the *co-channel interference reduction factor* [5] since the larger it is (i.e., the further apart the cells) the less the co-channel interference for a given modulation scheme. The level of acceptable co-channel interference governs the value of this parameter and the overall spectral efficiency of the network.

The area mean signal level experienced at the mobile is assumed to be inversely proportional to the distance from the base-station raised to a power γ. With the advent of smaller cells, the propagation path loss is close to the free-space value [24], however, it is envisaged that the proposed base-station will initially operate in larger cells. Therefore, as a starting point for the comparison to follow, the commonly used approximation that the received signal power is inversely proportional to the fourth power of range will be used [25]. Hence, the area mean signal level (in volts) received from the wanted base-station at a mobile a distance d_w from the transmitter is

$$m_w = k/d_w^2. \tag{6}$$

Similarly, the area mean signal level from the interfering base-station transmitter at a distance d_i is

$$m_i = k/d_i^2 \tag{7}$$

assuming in each case identical radiated transmitter powers and signal propagation constants, as denoted by the constant k.

Co-channel interference will occur when the ratio of the received wanted signal envelope, s_w, to the interfering signal envelope, s_i, is less than some *protection ratio*, p_r, i.e.:

$$s_w \leq p_r s_i. \tag{8}$$

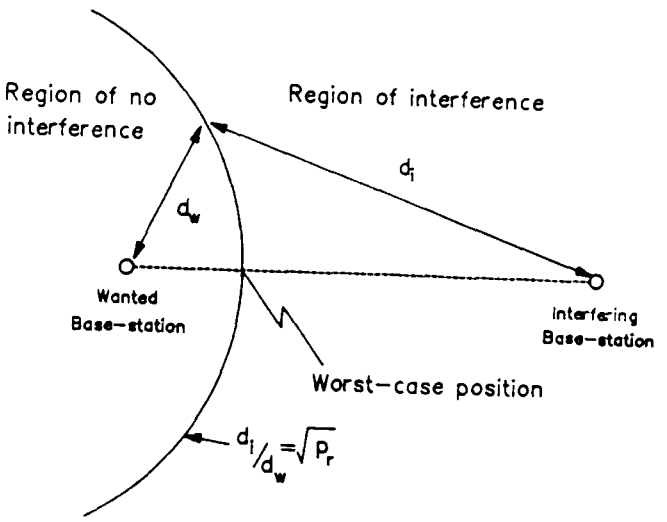

Fig. 4. Contour defining interference regions.

The protection ratio is defined by the modulation scheme employed [1]. Considering only the propagation path loss, the received signal envelopes are equal to the area mean signal levels, hence:

$$\frac{s_w}{s_i} = \frac{m_w}{m_i} = \frac{d_i^2}{d_w^2} \leq p_r. \tag{9}$$

So, for a given protection ratio, a locus given by

$$d_i/d_w = \sqrt{p_r} \tag{10}$$

can be drawn. This defines a region where no interference will occur, and where it will always occur, as illustrated in Fig. 4. For the worst-case position, which is in a direct line between the transmitters as shown, the co-channel reuse ratio is

$$Q = D/R = 1 + d_i/d_w = 1 + \sqrt{p_r}. \tag{11}$$

For a given protection ratio and modulation scheme, this defines the minimum spacing between co-channel cells in order to avoid interference, and the maximum spectral efficiency obtainable.

In this discussion it is assumed that the same modulation scheme is employed for both antenna systems under evaluation. This implies that the protection ratio and reuse distances are identical in both cases. Therefore, there would appear to be no apparent benefit from employing adaptive antenna technology at the base-station site. However, the occurrence of co-channel interference is a statistical phenomena. Hence, when comparing omni- and adaptive antennas, it is necessary to introduce the concept of the *probability of co-channel interference* occurring, i.e., $P(s_w \leq p_r s_i)$. This is often called the *outage probability*, which is the probability of failing to obtain satisfactory reception at the mobile in the presence of interference.

If the cells are considered to be identical, i.e., have equal blocking probabilities, then on average, there will be $N\eta$ active channels in each cell (η is as defined in (4)). So, in the case of the omnidirectional antenna, given that the wanted mobile is already allocated a channel, the probability of that channel being active in an interfering cell is the required outage

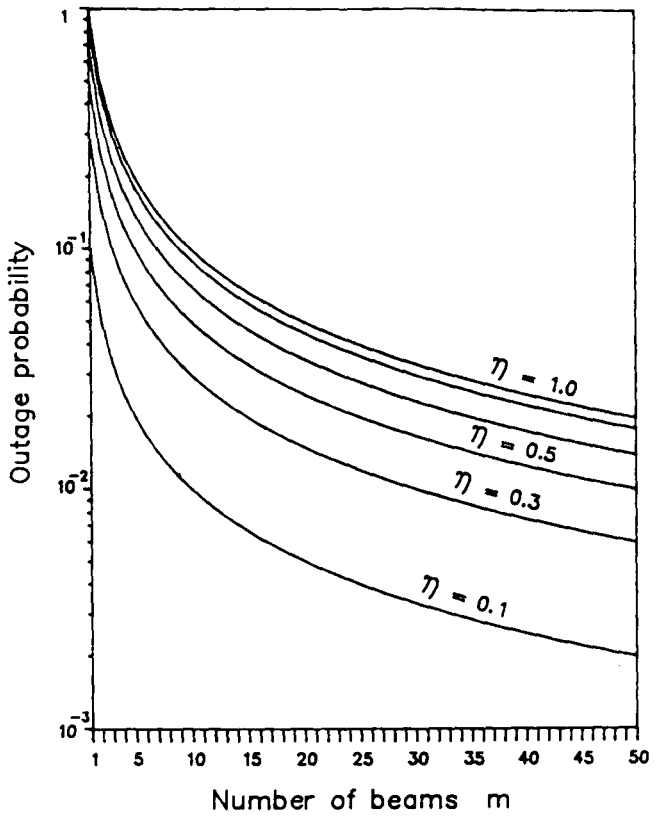

Fig. 5. Outage as a function of the number of beams.

probability. Hence, when the wanted mobile is in the region of co-channel interference the outage probability is given by

$$P(s_w \leq p_r s_i) = \frac{\text{number of active channels}}{\text{total number of channels}} = \frac{N\eta}{N} = \eta. \tag{12}$$

Now consider the case of the adaptive antenna as previously described, with m beams per base-station providing coverage of the whole cell, and with $N\eta/m$ channels per beam, given a uniform distribution of users. The same regions of co-channel interference can be defined, however, when the wanted mobile is within the region where co-channel interference may occur, the outage probability is reduced. The wanted mobile is always covered by at least one beam from the co-channel cell, hence, the outage probability is equal to the probability that one of the channels in the aligned beam is the corresponding active co-channel[1] and is given by

$$P(s_w \leq p_r s_i) = \frac{\text{number channels per beam}}{\text{total number of channels}} = \frac{N\eta/m}{N} = \frac{\eta}{m} \tag{13}$$

where the omnicase is given by $m = 1$. These results are presented graphically in Fig. 5, and show the strong influence of the number of beams, m, on the outage probability. The influence of the loading factor, η, is as expected, i.e., the less the loading, the fewer the number of active channels, and hence, a reduced chance of co-channel interference. This assumes that there are still m beams formed even though there are only

[1] The "active co-channel" is the channel that has also been allocated to the wanted mobile.

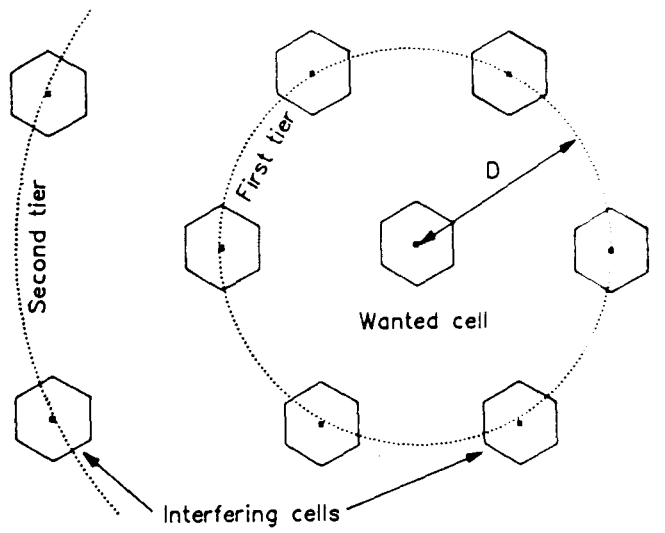

Fig. 6. Hexagonal cellular layout showing tiers of interferers.

$a(1 - B)$ active channels (or users). This is only really valid if $a(1 - B) > m$ and that the users are uniformly distributed within the cell. If this were not the case, and the number of beams formed was less than m, the outage probability would be reduced even further since the wanted mobile will not be covered by a co-channel beam all the time. This situation will not be pursued further since this analysis can be regarded as *worst-case* situation.

B. Six Co-Channel Cells

The previous approach can now be simply extended to assess the effect of six co-channel interferers, i.e., the first tier of co-channel cells in a conventional cellular scheme as shown in Fig. 6. It is considered that further tiers of interferers will not significantly affect the results except when reuse distances become small. Equation (9) can now be rewritten for this more realistic representation of the cellular network

$$\frac{s_w}{s_I} = \frac{m_w}{m_I} = \frac{d_w^{-2}}{\sum_{i=1}^{n} d_i^{-2}} \leq p_r \tag{14}$$

where the total mean signal level from the interfering cells, m_I, is the sum of the mean level from each active cell. Thus in a fully loaded system, the number of active users is six (i.e., $n = 6$). If all the d_i are assumed to be equal and the wanted mobile is at the edge of a cell boundary, as for the case described in Lee [5], then the co-channel reuse factor can be expressed as

$$Q = [6(s_w/s_I)]^{1/\gamma}. \tag{15}$$

Subjective tests showed that over a mobile radio channel $s_w/s_I \geq 18$ dB (i.e., $p_R = 18$ dB) gave good speech transmission for a 25-kHz FM channel operation. A value of Q can now be calculated to define the minimum cluster size, C. Using simple geometry it would be possible to evaluate the actual s_w/s_I in the worst-case locations. From this, a contour may be drawn defining regions with and without interference. For both classes of antenna systems the outage probability is still zero within the contour (i.e., when $s_w/s_I > p_r$), but outside,

in the region of interference:

$$P(s_w \leq p_r s_I) = \left(\frac{\eta}{m}\right)^6 \tag{16}$$

where s_I is the total co-channel interference and the omnicase is given by $m = 1$. Since it is assumed that all m beams per cell are formed, there are six beams aligned onto the wanted mobile at any time. The outage probability within the region of interference is then found by considering the probability that the active co-channel is in each of these beams.

C. Analysis of Results

The use of adaptive multiple beam-forming base-stations would, based upon the analysis presented so far, appear to give an improvement in performance with regard to the reduction of the probability of co-channel interference. The improvement depends on the degree of adaptivity used, i.e., the number of ideal beams formed. However, the above approach is over simplistic and gives a rather optimistic view of the situation. Firstly, the beams are assumed to be ideal, giving an equal gain over the whole beamwidth. In practice this would not be the case. Also, a hypothetical situation could be envisaged where, if m is large enough to satisfy a given outage criterion,[2] it would appear that the ultimate reuse distance ($D/R = 2$) is possible for any modulation scheme. Hence, adjacent cells are co-channel cells, the radius of which is decided by the required coverage area of the base-station site. In spite of this though, the analysis has been useful in introducing some of the important factors that affect the performance of a mobile radio network which exploits frequency reuse as a means of increasing spectral efficiency.

V. Statistical Propagation Model

In the previous analysis only the path loss associated with the mobile radio environment was considered when calculating the level of co-channel interference. This was useful in demonstrating the principle benefits to be offered by adaptive antennas, although it is an over simplified approach and totally unrealistic of many land mobile radio environments. It was shown that a single contour defining regions of operation where co-channel interference would occur can be drawn, however, it is known that the signal levels fluctuate rapidly generating small isolated pockets of interference in an operational system. In some adverse environments these areas may be quite close to the base-station antenna.

There is seldom a line of sight path between the base-station and the mobile, and hence, radio communication is obtained by means of diffraction and reflection of the transmitted energy. This produces a complicated signal pattern causing the field strength to vary greatly throughout the cell, and the received signal at the moving mobile to fluctuate very rapidly. This is generally attributed to the superposition of two different classifications of signal fading phenomenon: *fast fading* (or just fading) due to the multipath nature of the received signal, and *slow fading* (shadowing), the slower variations of the received signal due to variations in the local terrain. In areas experiencing this type of signal variation, the area mean signal level is essentially constant. In order to model these propagation effects, the are included in a statistical fashion, the fading and shadowing described above being represented by Rayleigh and log-normal type distributions, respectively.

[2] If there are ten beams ($m = 10$) a 10% outage criterion could be satisfied in a fully loaded system (13).

A. One Co-Channel Cell

Various studies [26]–[28] have been undertaken to analyze co-channel interference originating from a single co-channel interfering cell in an attempt to characterize the mobile radio environment. In particular the rigorous analysis presented by French [22] has been adopted here. The fast fading is the rapid fluctuation of the signal level s about the local mean $\bar{s}$ ($\bar{s} = \langle s \rangle$), and is usually described by a Rayleigh type probability density function (pdf), i.e.:

$$P(s/\bar{s}) = \frac{\pi s}{2\bar{s}^2} \exp\left[-\frac{\pi s^2}{4\bar{s}^2}\right]. \tag{17}$$

Shadowing of the radio signal due to the terrain, i.e., by buildings and hills, causes the local mean level $\bar{s}$ to fluctuate about the area mean. It has been generally accepted that this variation is *log-normally* distributed about the area mean m_d, where $m_d = \langle \bar{s}_d \rangle$, the mean of $\bar{s}$ in decibels. (Note, a subscript "d" indicates that a signal is in decibels.) The area mean level is approximately proportional to the inverse of the distance from the base-station raised to the power γ, as described in Section IV-A. Hence, the log-normal shadowing pdf is given by

$$P(\bar{s}_d) = \frac{1}{\sqrt{2\pi}\,\sigma} \exp\left[\frac{-(\bar{s}_d - m_d)^2}{2\sigma^2}\right]. \tag{18}$$

The *standard deviation*, σ, describes the degree of shadowing. This parameter typically varies from 6 to 12 dB in urban areas, the larger value being associated with very built up inner city areas.

The combined pdf can now be expressed as

$$P(s) = \int_{-\infty}^{\infty} P(s/\bar{s}) \cdot P(\bar{s}_d)\, d\bar{s}_d. \tag{19}$$

By substituting $\bar{s} = 10^{\bar{s}d/20}$ (from $\bar{s}_d = 20 \log_{10} \bar{s}$) into (17), the combined pdf becomes

$$P(s) = \sqrt{\pi/8\sigma^2} \int_{-\infty}^{\infty} \frac{s}{10^{\bar{s}d/20}} \exp\left[\frac{\pi s^2}{4 \times 10^{\bar{s}d/20}}\right] \cdot \exp\left[\frac{-(\bar{s}_d - m_d)^2}{2\sigma^2}\right] d\bar{s}_d. \tag{20}$$

1) Outage Probability With Fading and Shadowing: The outage probability with fading and shadowing is derived in French [22] and the resulting integral is

$$P(s_w \leq p_r s_i) = \frac{1}{\sqrt{\pi}} \int_{-\infty}^{\infty} \frac{\exp(-u^2)}{1 + 10^{(z_d - 2\sigma u)/10}}\, du \tag{21}$$

where, $z_d = m_{dw} - m_{di} - p_R$, $\sigma = \sigma_w = \sigma_i$, and u is an internal variable.

In many situations it is possible to greatly reduce the fading, e.g., antenna diversity at the mobile, and a similar result to that above can be derived [22] for shadowing only. Note that the result in (21) is for the case of the omnidirectional base-station antenna.

2) Outage Probability with an Adaptive Antenna: The outage probability for an adaptive antenna can be simply expressed as

$$P(s_w \le p_r s_i, m) = P(s_w \le p_r s_i) \cdot \begin{pmatrix} \text{probability of an active co-channel} \\ \text{in the aligned beam} \end{pmatrix}$$

$$= P(s_w \le p_r s_i) \cdot \left(\frac{\eta}{m}\right) \tag{22}$$

i.e., the probability that the ratio of the wanted signal to the interfering signal is less than some protection ratio (21) and the probability that the aligned beam actually contains the active channel (13). Again, the outage probability is reduced by a factor m. This is illustrated graphically in Fig. 7. The loading factor is fixed at 70% ($\eta = 0.7$) and the fading and shadowing case is considered for $\sigma = 6$ dB. This represents a typical urban environment. These results have been obtained by solving (21) and (22) numerically with $m = 1$, 2, 4, 8, 16, and 32. Note that $m = 1$ gives the omnicase.

The outage probability varies as expected with z_d and, for the omnicase is consistent with French. Note, however, that for a given z_d the outage is reduced by a factor of m when an adaptive antenna is considered.

3) Calculation of the Reuse Distance: When the fading and shadowing characteristics of the mobile radio channel are considered, it can be shown that no definite boundary exists between regions of interference, and regions of no interference. Co-channel interference can even occur close to the wanted transmitter if, for example, the wanted signals fades and the interfering signal peaks as illustrated in Fig. 8. Now, since co-channel interference is a statistical phenomena, it can be described by contours of outage probability. Using the definition for z_d and (9) yields

$$\frac{d_i}{d_w} = \sqrt{zp_r} = \sqrt{10^{(z_d+p_R)/20}}. \tag{23}$$

So for a given z_d, protection ratio p_R, and outage probability, contours can be drawn as shown in Fig. 9. If an adaptive antenna is used, the value of each contour is reduced by a factor of m, hence, for a given outage criterion, the service area is increased.

This can be represented graphically by substituting (23) into (11) and expressing the co-channel reuse ratio as

$$Q = 1 + \sqrt{10^{(z_d+p_R)/20}}. \tag{24}$$

From this formula the outage probability against the reuse ratio for a given protection ratio can be obtained in a manner similar to that of French.

4) Calculation of the Cluster Size: In a cellular network with a hexagonal layout, the cluster size is related to the reuse

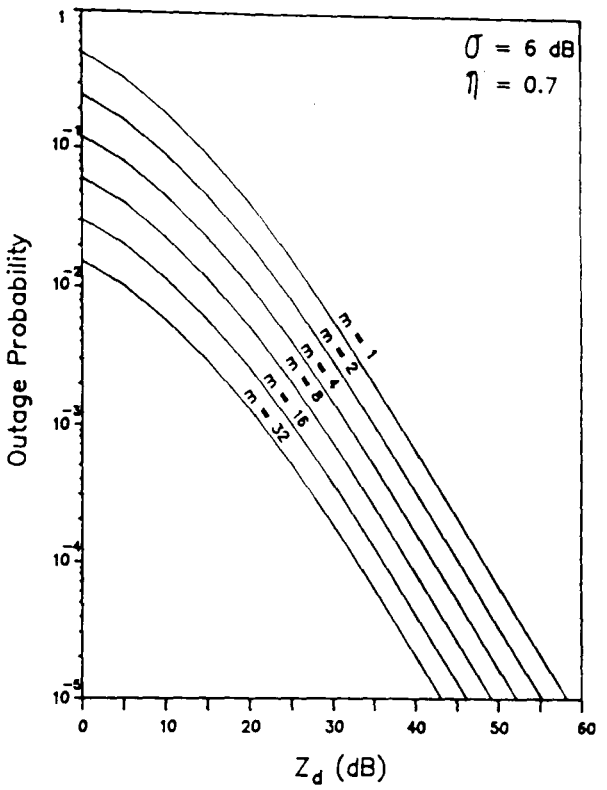

Fig. 7. Outage probability for one co-channel cell.

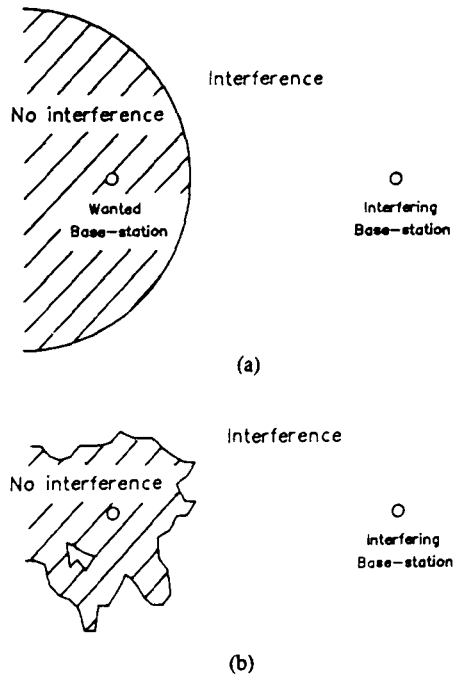

Fig. 8. Contour defining regions of interference. (a) With no shadowing or fading. (b) With shadowing and fading.

distance by

$$C = Q^2/3. \tag{25}$$

Note that only certain values of C are possible in a hexagonal cellular network [25], i.e., $C = (3, 4, 7, 9, 12, 13, 16, 19, 21, \cdots)$. Using (24) this can be expressed as

$$C = 1/3[1 + \sqrt{10^{(z_d+p_R)/20}}]^2. \tag{26}$$

Again the outage probability can now be evaluated for various cluster sizes for a given protection ratio.

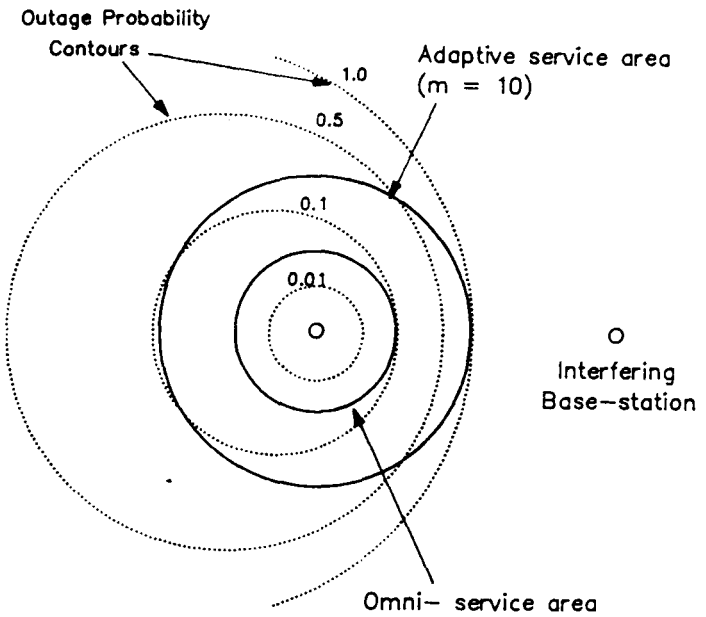

Fig. 9. Outage probability contours and service areas for a 10% chance of interference.

5) Calculation of Spectral Efficiency: To gain a more meaningful interpretation when comparing different system architectures in a cellular network, the spectral efficiencies [1] of the various schemes are usually considered. This gives an unbiased measure of spectrum utilization, and is usually expressed as the number of channels/MHz of bandwidth/km^2, i.e.,

$$\text{efficiency, } E = \frac{B_t/B_c}{B_t(CA)} = \frac{1}{B_c CA} \tag{27}$$

where

B_t total available bandwidth,
B_c channel spacing in megahertz,
C number of cells per cluster,
A cell area (km^2).

To enable a simple comparison to be made between omni- and adaptive antenna systems, it is necessary to assume that an identical modulation scheme will be employed in both cases. Thus $E \propto 1/C$, and the relative spectral efficiency can be expressed as

$$\frac{E_{\text{adapt}}}{E_{\text{omni}}} = \frac{C_{\text{omni}}}{C_{\text{adapt}}}. \tag{28}$$

Equation (22) was solved numerically and then the cluster size C, given by (26), was calculated for a fading and shadowing (6 dB variation) environment with a loading factor of 0.7. An outage criterion of 1% is used and, although this value is quite low, it serves to give some idea of the advantages that can be obtained by using this new class of base-station antenna. Two values of protection ratio, 8 and 20 dB, are considered in order to cover a variety of modulation schemes [1]. Then, using (28), the relationship between the relative spectral efficiencies was calculated for $m = 1, 2, 4, 8, 16$, and 32, and is shown in Fig. 11.

B. Six Co-Channel Cells

In order to present a more realistic comparison between omnidirectional and adaptive base-station antennas, it is necessary to consider interference originating from multiple co-channel cells. Several different studies [21], [29]–[31] have pursued this goal, but of particular interest is the work by Muammar and Gupta [23]. This has been adopted here since the analysis follows directly from the previous discussion. However, a few alterations have been necessary in order that a more meaningful comparison could be presented.

Fig. 6 shows the cellular layout of a mobile radio network for an arbitrary cell cluster size of C. It is recognized that there are many tiers of co-channel interferers present, but only the first, i.e., cells at a distance D from the wanted base-station, it considered here. This assumption was shown to be valid in similar studies [29], [31]. The wanted mobile in the central cell receives a signal envelope s_w from the wanted base-station. It also receives unwanted signals from the co-channel cells s_i, $i = 1, 2, \cdots, n$, where n is the number of active interfering co-channel cells (the maximum number being six in this case). The total co-channel interference is thus given by

$$s_I = \sum_{i=1}^{n} s_i. \tag{29}$$

When the wanted signal does not exceed this value by the protection ratio, co-channel interference will occur. In order to calculate the total probability of co-channel interference (or simply the outage probability), it is necessary to consider the probability of there being co-channel interference and n interfering co-channel cells. Using conditional probability theory this can be expressed as

$$P((\text{co-channel interference}) \cap (n \text{ active co-channels})) = P(s_w \le p_r s_I/n) \cdot P(n). \tag{30}$$

$P(n)$ is the PDF of n and $P(s_w \le p_r s_I/n)$ is the *conditional outage probability* (the probability of co-channel interference given that there are n active interfering cells). Hence, the total outage probability is given by

$$P(s_w \le p_r s_I) = \sum_n P(s_w \le p_r s_I/n) \cdot P(n) \tag{31}$$

since all possible values of n must be taken into account. Here only the first tier is considered, so the maximum number for n is six.

The pdf of the signal envelope s is as given by (20) and from here the conditional probability of co-channel interference for multiple interferers, when considering both fading and shadowing, can be derived. This result is simply quoted here without proof as details [23] can be found elsewhere.

$$P(s_w \le p_r s_I/n) = \frac{1}{2\pi} \int_{-\infty}^{\infty} dX \int_{-\infty}^{\infty} \left[1 - \exp\left(-\frac{\pi}{4K^2(X,u)}\right)\right] \cdot \exp\left(-\frac{(X^2+u^2)}{2}\right) du$$

where

$$20 \log_{10} K(X,u) = z_d + C \cdot \ln(4/\pi n^2) + \sigma X - \sigma_{NY} u - \frac{1}{4C}(\sigma_{NX}^2 - \sigma_{NY}^2) \tag{32}$$

and where σ^2_{NX} and σ^2_{NY} are defined by Muammar and Gupta [23]. The variable z_d is as defined previously, and u and X are internal variables. This integral can be solved using various numerical techniques and the results are presented later.

1) PDF of n, P(n): $P(n)$ is the probability that the number of active interfering co-channel cells is n and so if the channels are assumed independent and identically distributed, this has the form of a binomial pdf:

$$P(n) = \binom{6}{n} p^n (1-p)^{6-n} \tag{33}$$

where p is the probability of finding *one* interfering co-channel active. Using the loading factor η, as defined before, the probability p that a single co-channel cell has an active co-channel, given that the wanted mobile has been assigned that channel already, is

$$p = \frac{\text{number of active channels}}{\text{total number of channels}} = \frac{a(1-B)}{N} = \eta. \tag{34}$$

The *origination probability* [21], or the probability that n co-channel interfering cells are using the same channel as the wanted mobile, can then be expressed as

$$P(n) = \binom{6}{n} \eta^n (1-\eta)^{6-n}. \tag{35}$$

Hence, giving the total outage probability as

$$P(s_w \le p_r s_I) = \sum_n P(s_w \le p_r s_I/n) \cdot \binom{6}{n} \eta^n (1-\eta)^{6-n}. \tag{36}$$

This can now be calculated for a given outgoing channel usage efficiency over the range of z_d. Alternatively, as before, the outage probability can be considered against the co-channel reuse ratio Q, or the cluster size C.

2) Integration of Adaptive Antennas: With an omnidirectional antenna the probability of an active interfering co-channel cell was given by η, the outgoing channel usage efficiency or cell loading factor. Since it is assumed that at any one time all m beams per cell are formed, there will always be six beams aligned onto the wanted mobile. Hence, for the adaptive antenna:

$$p = \begin{pmatrix} \text{probability that the interfering co-channel is in the} \\ \text{beam pointing at the wanted mobile} \end{pmatrix}$$

$$= \frac{\text{number of active channels in beam}}{\text{total number of channels}}$$

$$= \frac{a(1-B)/m}{N} = \frac{\eta}{m}. \tag{37}$$

Hence, the *origination probability* is given by

$$P(n) = \binom{6}{n} \left(\frac{\eta}{m}\right)^n \left(1 - \frac{\eta}{m}\right)^{6-n}. \tag{38}$$

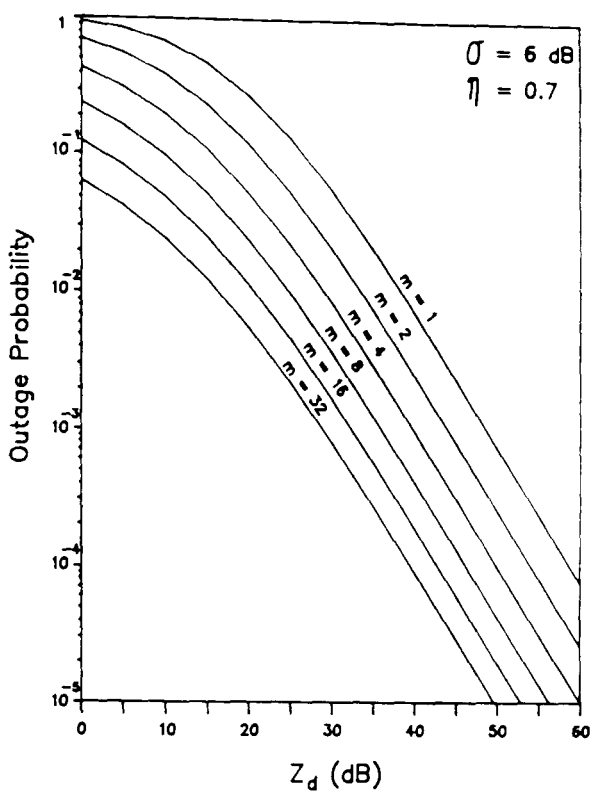

Fig. 10. Outage probability with six co-channel cells.

The overall outage probability can now be expressed as

$$P(s_w \le p_r s_I, m) = \sum_n P(s_w \le p_r s_I/n) \cdot \binom{6}{n} \left(\frac{\eta}{m}\right)^n \left(1 - \frac{\eta}{m}\right)^{6-n} \tag{39}$$

where the omnidirectional case is given for $m = 1$.

As before, when only one co-channel cell was considered, a comparison can now be made between the two base-station technologies. Fig. 10 shows the variation of the total outage probability against z_d. The case with both fading and shadowing is considered here, hence, the results are obtained by numerically solving (32) and applying (39) for $m = 1, 2, 4, 8, 16$, and 32. From (26) and (28) the cluster size and the relative spectral efficiency can now be calculated for a given outage criterion (1%), and is shown in Fig. 11. An outgoing channel usage efficiency of 0.7 and a log-normal shadowing standard deviation of 6 dB has been assumed. Protection ratios of 8 and 20 dB have also been considered.

3) Analysis of Results: It can be seen from Fig. 11 that for a given outage criterion and modulation scheme, the introduction of an adaptive array capable of forming eight tracking beams, into an existing network, would produce at least a threefold increase in efficiency. This can be equated to be three times the number of channels per megahertz per square kilometer, or simply as three times as many users in each cell. This result has been obtained by considering the co-channel interference originating from single and multiple co-channel cells. The propagation model employed here considers both the fading and shadowing characteristics of the mobile channel.

Although the application of power control of the individual tracking beams has not been considered to date, this may

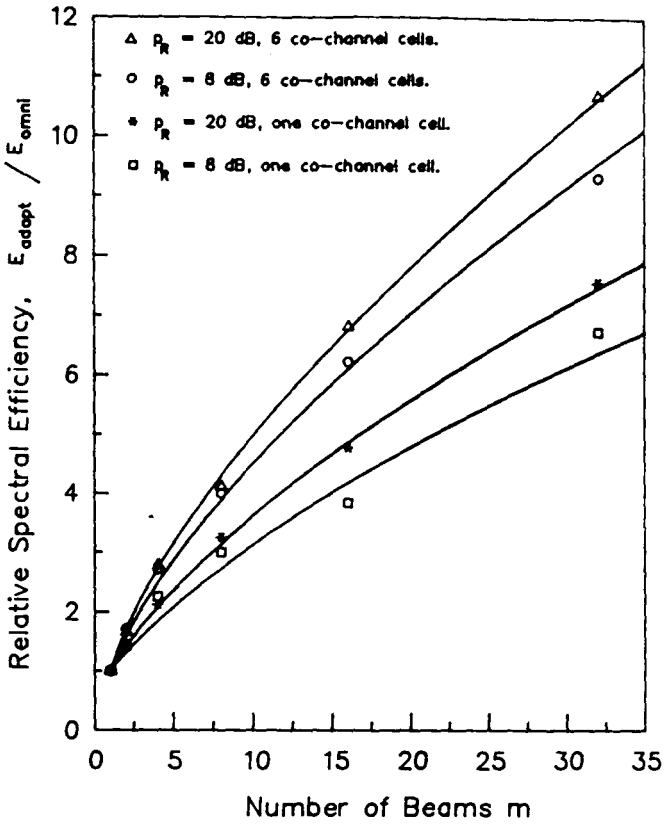

Fig. 11. Relative spectral efficiency as a function of the number of beams formed.

prove to be essential for future generation networks. It has been shown [21], [30] that base-station power control can substantially reduce co-channel interference for omnidirectional antenna systems. It can thus be envisaged that power control of the multiple beam adaptive base-station antenna would greatly reduce energy "overspill" into neighboring cells. The combination of the two adaptive techniques will be considered in a later study.

VI. The "Smart" Base-Station Antenna

Adaptive antennas operate by exploiting some property of the signal environment present at the array aperture [7], [8], and it is due to this ability that they are often aptly referred to as "smart" arrays [32]. In the previous theoretical analysis it was assumed that the base-station antenna could track any mobile, or group of mobiles, within its coverage area. Therefore, on reception, the array must be capable of resolving the angular distribution of the users as they appear at the base-station site. Armed with this knowledge, the base-station is then in a position to form an optimal set of beams, confining the energy directed at a given mobile within a finite volume. This concept can be further illustrated by considering the sequence of events illustrated in Fig. 12. The scenario depicted is realistic of many operational systems where there are lone mobiles, or groups of mobiles, dispersed throughout the cell. Using the spatial distribution of the users acquired by the array on reception, the antenna system can dynamically assign single narrow beams to illuminate the lone mobiles, and broad beams to the numerous groupings along major highways. It can be seen that by constraining the energy transmitted toward the mobiles, there are directions in which little or no signal is radiated. It is this phenomenon which gives rise to

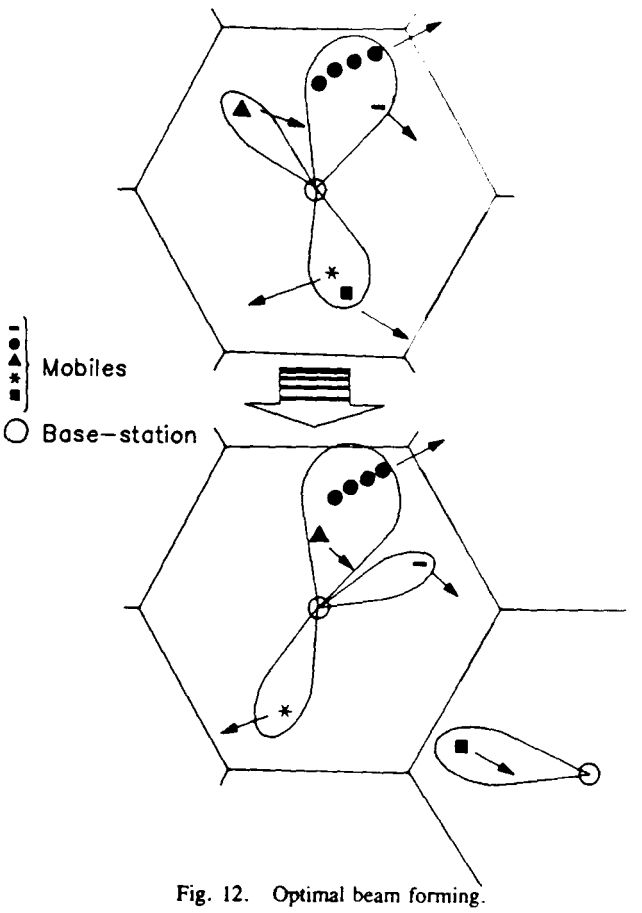

Fig. 12. Optimal beam forming.

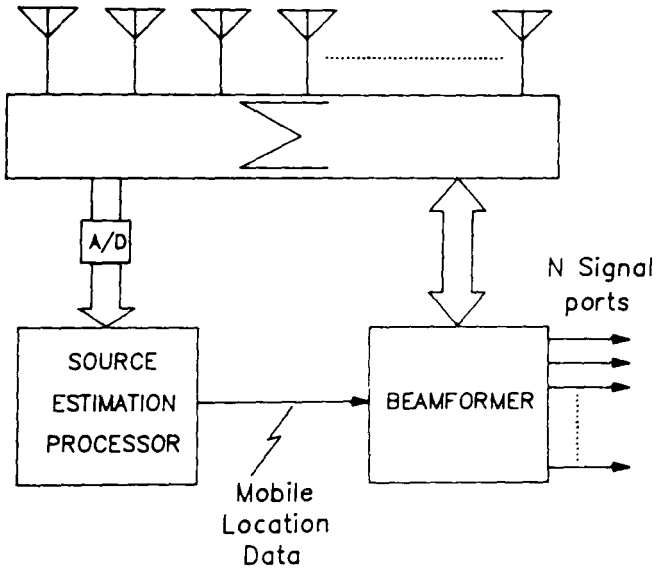

Fig. 13. The "smart" antenna.

the reduction in the probability of co-channel interference occurring in neighboring cells, and thereby increasing the spectral efficiency (or capacity) of the network as illustrated in the previous section.

The realization of such an adaptive base-station antenna requires an architecture capable of locating and tracking the mobiles, and a beam-forming network thus capable of producing the appropriate multiple independent beams. The former requirement can be broadly classified as that of a direction finding, or a spatial estimation problem. These two tasks are illustrated in Fig. 13 as a source estimation or direction find-

ing (DF) processor and a beamformer. In recent publications [33], [34] this concept was further extended to consider the implementation of such a base-station antenna. Also the results from some initial computer simulations were presented and these demonstrated the ability of the antenna array to resolve multiple mobile users in the signal fading conditions typical of the LMR scenario. Many of the popular *superresolution* DF algorithms used in radar were evaluated, and some beam-forming techniques which could generate the optimal beam set using the knowledge of the mobile distribution were discussed. Finally, a proposal was put forward for a fully adaptive base-station antenna test rig to demonstrate the principles of operation and show how such an antenna could be incorporated into the existing cellular network. The results of this work will form the basis for a future paper.

Intelligent antenna systems have also been considered for numerous other applications. Sandler and Kokar [35] have described the use of an adaptive antenna in conjunction with an artificial intelligence system as an antijamming antenna for radar. Here the antenna has a wealth of stored data which is used to "teach" the system about the various scenarios it will encounter. In this way it can adapt readily to every new situation as it is presented and "learn" from its mistakes. It is intended to exploit the synergy that exists between this application and that of the proposed cellular mobile radio base-station. Initially, the knowledge of the mobile locations within each cell could be utilized to provide an elegant hand-off mechanism as the mobiles cross cell boundaries. Also, combined with a knowledge of the local terrain and shadowing characteristics, it should be possible to extend this technique and provide a cellular network with dynamic cell boundaries. This would thus allow the optimal usage of the available system capacity.

VII. Discussion

The full potential of adaptive antenna technology in the future generation of ubiquitous portable communication networks is yet to be realized. The goal is to be able to provide universal pocket sized communications by the year 2000. This implies that the system must make very efficient use of the radio spectrum if it is to be made available to a large consumer base; thus making the portable equipment relatively cheap. Also, it is highly desirable that the portable communicator has a long duty cycle between battery recharging implying power efficient modulation. The role of adaptive antennas has already been discussed in terms of the former requirement, however, it must be emphasized that spectrum efficient modulation is still a vital parameter in the design of these systems. The potential enhancement of power efficiency obtainable using spatial filtering has not been fully assessed to date, and the merits of this technique in a rural service area are of particular interest.

The study presented here has demonstrated the feasibility of an adaptive base-station antenna for cellular communications networks. A comparison made between the conventional and proposed schemes has shown that a marked improvement in spectral efficiency and capacity can be obtained, e.g., an idealized eight beam antenna could provide a threefold increase in spectral efficiency. In addition to the other advantages that can be gained, as outlined in the previous section, the infrastructure costs incurred by this base-station antenna must also be considered. The majority of these costs are associated with the acquisition of the base-station site, construction of various buildings and antenna masts. When compared with existing schemes, such as cell splitting, the overall cost is less, since fewer base-station sites are required for an equivalent user capacity. Also, unlike the techniques of cell splitting and cell sectorization, the multiple beam adaptive array would not impair the trunking efficiency of the network.

Acknowledgment

We are extremely grateful to our colleagues at the Bristol University Centre for Communications Research for their stimulating intellectual support.

References

[1] H. Hammuda, J. P. McGeehan and A. Bateman, "Spectral efficiency of cellular land mobile radio systems," in *Proc. 38th IEEE Veh. Technol. Conf.*, Philadelphia, PA, pp. 616–622, June 15–17, 1988.

[2] J. A. Tarallo and G. I. Zysman, "Modulation techniques for digital cellular systems," in *Proc. IEEE Vehicular Technology Conf.*, pp. 245–248, June 15–17, 1988.

[3] J. Uddenfeldt, K. Raith and B. Hedberg, "Digital technologies in cellular radio," in *Proc. IEEE Vehicular Technology Conf.*, pp. 516–519, June 15–17, 1988.

[4] F. Lindell, J. Swerup and J. Uddenfeldt, "Digital cellular radio for the future," *The Ericsson Rev.*, no. 3, 1987.

[5] W. C. Y. Lee, "Elements of cellular mobile radio systems," *IEEE Trans. Veh. Technol.*, vol. VT-35, pp. 48–56, May 1986.

[6] P. C. Carlier, "Antennas for cellular phones," *Commun. Int.*, pp. 43–46, Dec. 1987.

[7] S. P. Applebaum, "Adaptive arrays," *IEEE Trans. Antennas Propagat.*, vol. AP-24, pp. 585–598, Sept. 1976.

[8] B. Widrow, P. E. Mantey, L. J. Griffiths, and B. B. Goode, "Adaptive antenna systems," *Proc. IEEE*, vol. 55, pp. 2143–2159, Dec. 1967.

[9] R. T. Compton, "The power inversion adaptive array: Concept and performance," *IEEE Trans. Aerospace Electron. Syst.*, vol. AES-15, pp. 803–814, 1979.

[10] L. Acar and R. T. Compton, "The performance of LMS adaptive array with frequency hopped signals," *IEEE Trans. Aerospace Electron. Syst.*, vol. AES-21, pp. 360–370, May 1985.

[11] K. Bakhru and D. J. Torrieri, "The maximum algorithm for adaptive arrays and frequency-hopping communication," *IEEE Trans. Antennas Propagat.*, vol. AP-32, pp. 919–928, Sept. 1984.

[12] R. T. Compton, R. J. Huff, W. G. Swarner, and A. A. Ksienski, "Adaptive arrays for communication systems: An overview of research at The Ohio State University," *IEEE Trans. Antennas Propagat.*, vol. AP-24, pp. 599–607, 1976.

[13] R. T. Compton, "An adaptive antenna in a spread spectrum communication system," *Proc. IEEE*, vol. 66, pp. 289–298, Mar. 1978.

[14] M. A. Beach, A. J. Copping, D. J. Edwards, and K. W. Yates, "An adaptive antenna for multiple signal sources," in *Proc. IEE Fifth Int. Conf. on Antennas and Propagation*, University of York, 1987.

[15] J. E. Hudson, *Adaptive Array Principles*, IEE Electromagnetic Wave Series No. 11. Stevenage, U.K.: Peter Peregrinus, 1981.

[16] Telecom Australia, "Base-station antennas for future cellular radio systems," Rev. Activities 1985/1986, pp. 41–43, 1985–1986.

[17] W. S. Davies, R. J. Lang, and E. Vinnal, "The challenge of advanced base station antennas for future cellular mobile radio systems," presented at IEEE Int. Workshop on Digital Mobile Radio, Melbourne, Australia, Mar. 10, 1987.

[18] G. R. Cooper and R. W. Nettleton, "A spread spectrum technique for high capacity mobile communications," *IEEE Trans. Veh. Techn.*, vol. VT-27, pp. 264–275, 1978.

[19] D. H. Archer, "Lens-fed multiple beam arrays," *Microwave J.*, pp. 171–195, Sept. 1984.

[20] M. J. Marcus and S. Das, "The potential use of adaptive antennas to increase land mobile frequency reuse," presented at *IEE 2nd Int. Conf. on Radio Spectrum Conservation Techniques*, CP224, Birmingham, UK, Sept. 6–8, 1983.

[21] K. Daikoku and H. Ohdate, "Optimal channel reuse in cellular land mobile radio systems," *IEEE Trans. Veh. Technol.*, vol. VT-32, pp. 217-224, Aug. 1983.
[22] R. C. French, "The effects of fading and shadowing on channel reuse in mobile radio," *IEEE Trans. Veh. Technol.*, vol. VT-28, pp. 171-181, Aug. 1979.
[23] R. Muammar and S. Gupta, "Co-channel interference in high capacity mobile radio systems," *IEEE Trans. Commun.*, vol. COM-30, pp. 1973-1978, Aug. 1982.
[24] J. H. Whitteker, "Measurements of path loss at 910 MHz for proposed microcell urban mobile systems," *IEEE Trans. Veh. Technol.*, vol. VT-37, pp. 125-129, Aug. 1989.
[25] W. C. Jakes, *Microwave Mobile Communications*. New York: Wiley, 1974.
[26] W. Gosling, "Protection ratio and economy of spectrum use in land mobile radio," *Proc. Inst. Elect. Eng.*, vol. 127, pt. F, pp. 174-178, June 1980.
[27] M. Hata, K. Kinoshita, and K. Hirade, "Radio link design of cellular land mobile communication systems," *IEEE Trans. Veh. Technol.*, vol. VT-31, pp. 25-31, Feb. 1982.
[28] A. G. Williamson, "Coverage, co-channel interference and outage probability calculations for mobile radio systems," in *Proc. IREE 20th Int. Electron. Convention and Exhibition*, Melbourne, pp. 224-227, Sept./Oct. 1985.
[29] D. C. Cox, "Co-channel interference considerations in frequency reuse small-coverage-area radio systems," *IEEE Trans. Commun.*, vol. COM-30, pp. 135-142, Jan. 1982.
[30] V. Palestini and V. Zingarelli, "Outage probability computation and cellular coverage for mobile radio," in *Proc. 37th IEEE Veh. Technol. Conf.*, Tampa Bay, FL, pp. 468-476, 1987.
[31] Y. S. Yeh and S. C. Schwartz, "Outage probability in mobile telephony due to multiple log-normal interferers," *IEEE Trans. Commun.*, vol. COM-32, pp. 380-388, Apr. 1984.
[32] W. F. Gabriel, "Adaptive arrays—An introduction," *Proc. IEEE*, vol. 64, pp. 239-272, Feb. 1976.
[33] S. C. Swales, M. A. Beach, and D. J. Edwards, "Multi-beam adaptive base-station antennas for cellular land mobile radio systems," in *Proc. 39th IEEE Veh. Technol. Conf.*, San Fransisco, CA, pp. 341-348, Apr. 29-May 3, 1989.
[34] S. C. Swales, M. A. Beach, D. J. Edwards, and J. P. McGeehan, "A multi-beam adaptive base-station antenna for cellular land mobile radio systems, in *Proc. 1989 IEEE Workshop on Mobile and Cordless Telephone Communications*, University of London, UK, pp. 55-61, Sept. 25-26, 1989.
[35] S. S. Sandler and M. Kokar, "Intelligent antennas," in *Proc. URSI Int. Symp. on Electromagnetic Theory*, Budapest, Hungary, pp. 159-161, 1986.

Simon C. Swales received the B.Eng. degree in electrical and electronic engineering from the University of Bristol, U.K., in 1987. He is currently engaged in postgraduate research at the University of Bristol, UK.

His research interests include the use of adaptive antennas arrays for future land mobile radio systems.

Mr. Swales is an Associate Member of the Institution of Electrical Engineers.

Mark A. Beach received the B.Sc. degree in electronic engineering from the University of York and the Ph.D. degree from the University of Bristol, UK, in 1983 and 1988, respectively.

He has worked for the Telecommunications Research Laboratories at the GEC Hirst Research Centre. He then joined the Department of Electrical and Electronic Engineering, University of Bristol, where he investigated various signal processing techniques for the control of adaptive antenna arrays operating in multiple signal source environments. Currently, he is a Lecturer in communications at Bristol University. His research interests include the development of novel antenna systems for both terrestrial and satellite land mobile communications systems and RF circuit techniques.

Dr. Beach is an Associate Member of the Institution of Electrical Engineers.

David J. Edwards received the B.Sc. degree in physics, the M.Sc. degree in the physics of materials and the Ph.D. degree from Bristol University, in 1972, 1973, and 1987, respectively.

He worked at British Telecom for 11 years, where he was engaged in research on communications, antennas, measurement techniques and instrumentation systems. In 1985, he joined the Department of Electrical Engineering, Bristol University, where he conducted research in the areas of communications and microwave techniques. Currently, he is with the Department of Engineering Science, Oxford University.

Dr. Edwards was awarded the Institution of Electrical Engineers Prize for Innovation in 1989. He is a member of the Institution of Electrical Engineers and a Fellow of the Royal Astronomical Society.

Joseph P. McGeehan (M'83) was born in Bootle, Merseyside, England, on February 15, 1946. He received the B.Eng. and Ph.D. degrees in electrical engineering from the University of Liverpool, England, in 1967 and 1972, respectively.

From 1970 to 1972 he held the position of Senior Scientist at the Allen Clark Research Centre, The Plessey Company Ltd., where he was primarily concerned with research into solid-state GaAs devices and their applications. In 1972 he was appointed Lecturer in Engineering at the University of Bath and promoted to Senior Lecturer in 1983, and led project teams conducting research into the application of signal processing techniques to linear modulation techniques for mobile radio communication systems and millimetric open waveguide techniques and systems. In 1985 he was appointed to the Chair of Communications Engineering in the Department of Electrical and Electronic Engineering at the University of Bristol and is Director of the Centre for Communications Research.

Dr. McGeehan is a member of the U.K. Study Group 8A of the International Radio Consultative Committee. He is the author of some 70 scientific papers. In recent years, he has served as a member of the U.K. Home Office (Directorate of Radio Technology) Working Group on comparative modulating techniques for mobile radio, was an advisor to the DTI Defence Spectrum Review Committee, and currently serves on a number of IEE Professional Committees.

APPENDIX C

THE BASIC SIGNAL MODEL

Consider a uniformly spaced linear array consisting of N ideal isotropic elements, with M plane waves incident onto the array. For the purpose of this analysis assume that all the incident plane waves are narrowband, with a carrier frequency f_c. Figure C.1 illustrates the case for a single plane wave incident at an angle of θ_m off the array broadside. Taking the first element in the array as the phase reference, the noiseless signal produced at the nth element by this wave, denoted as the mth plane wave, is

$$s_{nm}(t) = A_m cos\left[2\Pi f_c t + (n-1)2\Pi\left(d/\lambda\right)\sin(\theta_m) + \alpha_m\right] \qquad (C.1)$$

where n = 1,2,$\cdots$,N and m = 1,2,$\cdots$,M.

The parameters A_m and α_m denote the amplitude and phase of the signal measured at the first element (n = 1) which shall be referred to as the phase reference. The *electrical phase shift* from element to element along the array can be expressed as

$$\phi_m = \frac{2\Pi d}{\lambda} \sin \theta_m \qquad (C.2)$$

and if the the complex notation for narrowband signals is adopted, equation (C.1) can be represented by its complex amplitude as

$$s_{nm} = a_m \, exp\left[j(n-1)\phi_m\right] \qquad (C.3)$$

where, $a_m = A_m \, exp\left[j\alpha_m\right]$ denotes the complex amplitude of the signal measured at the first element.

The actual signal measured at the output of each element differs from the received signal given by equation (C.3), due to an additive noise component. This noise component is usually assumed to be a spatially and temporally white random process with zero mean and variance σ^2. Considering

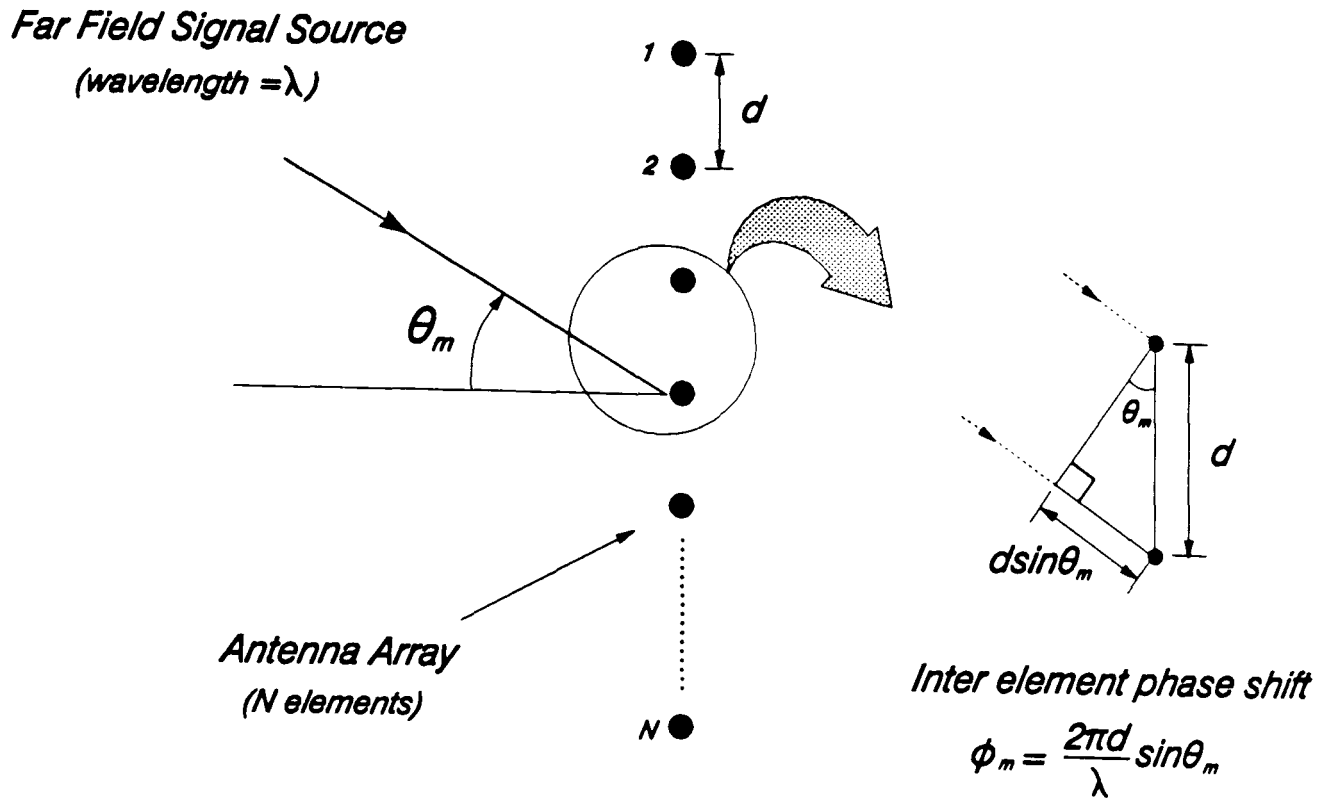

Figure C.1: Linear array with a single incident plane wave.

the M incident plane waves, the signal actually received at each element of the array can now be expressed as

$$x_n = s_n + v_n$$

$$= \sum_{m=1}^{M} s_{nm} + v_n$$

$$= \sum_{m=1}^{M} a_m exp\left[j(n-1)\phi_m\right] + v_n \qquad n=1,2,\cdots,N \qquad (C.4)$$

where v_n is the additive noise component. It is often easier to express this in the more compact matrix form as follows

$$\begin{bmatrix} x_1 \\ x_2 \\ \vdots \\ x_N \end{bmatrix} = \begin{bmatrix} s_1 \\ s_2 \\ \vdots \\ s_N \end{bmatrix} + \begin{bmatrix} v_1 \\ v_2 \\ \vdots \\ v_N \end{bmatrix}$$

or, more simply as

$$\mathbf{x} = \mathbf{s} + \mathbf{v} \qquad (C.5)$$

where, $\mathbf{x}$ is defined as the *observed signal vector*,

$\mathbf{s}$ is defined as the *received signal vector*,

$\mathbf{v}$ is defined as the *noise vector*.

The bold lower case letters are used to denote column vectors and bold upper case to represent matrices. The observed signal vector $\mathbf{x}$ represents a *snapshot* of data corresponding to a particular instant in time. These snapshots would normally occur at the Nyquist sampling rate, corresponding to the receiver bandwidth. Usually several independent measurements are made and equation (C.5) can be expressed as

$$\mathbf{x}(k) = \mathbf{s}(k) + \mathbf{v}(k)$$

$$= \mathbf{B}\mathbf{a}(k) + \mathbf{v}(k) \qquad k=1,2,\cdots,K \qquad \text{(C.6a)}$$

where K is the total number of snapshots taken and

$$\mathbf{a}(k) = \left[a_1(k),\ a_2(k),\ \cdots,\ a_M(k)\right]^T \qquad \text{(C.6b)}$$

is defined as the *signal-in-space* vector, and

$$\mathbf{B} = \begin{bmatrix} 1 & 1 & \cdots & 1 \\ exp(j\phi_1) & exp(j\phi_2) & \cdots & exp(j\phi_M) \\ exp(j2\phi_1) & exp(j2\phi_2) & \cdots & exp(j2\phi_M) \\ \vdots & \vdots & & \vdots \\ exp(j(N-1)\phi_1) & exp(j(N-1)\phi_2) & \cdots & exp(j(N-1)\phi_M) \end{bmatrix} \qquad \text{(C.6c)}$$

is defined as the *direction matrix*.

Using this set of data, temporal averaging may be used to improve the estimation of the angles of arrival (AOA) of the incident plane waves. It has been assumed in equation (C.6) that the source AOA's will not change significantly over the sampling period and so $\mathbf{B}$ is a slowly changing matrix. In contrast, the signal-in-space vector $\mathbf{a}(k)$ will generally vary rapidly with time, often unpredictably, and so it is modelled as a stochastic process. The *spatial correlation* matrix of the observed signal vector $\mathbf{x}$ is defined by

$$\mathbf{R} = E\left[\mathbf{x}(k)\mathbf{x}^{\dagger}(k)\right] \qquad \text{(C.7)}$$

where E is the expectation operator, and $\dagger$ denotes the complex conjugate transpose. This is also sometimes referred to as the *array covariance matrix*. Employing temporal averaging results in the sampled correlation or covariance matrix and this is defined as

$$\hat{\mathbf{R}} = \frac{1}{K}\sum_{k=1}^{K} E\left[\mathbf{x}(k)\mathbf{x}^{\dagger}(k)\right] \tag{C.8}$$

Substituting equation (C.6) into (C.7), and recognising that the signal-in-space vector $\mathbf{a}(k)$ and the noise vector $\mathbf{v}(k)$ are statistically independent, the spatial correlation matrix is given by

$$\mathbf{R} = E\left[\mathbf{B}\mathbf{a}(k)\mathbf{a}^{\dagger}(k)\mathbf{B}^{\dagger}\right] + E\left[\mathbf{v}(k)\mathbf{v}^{\dagger}(k)\right]$$

$$= \mathbf{B}\mathbf{R}_{a}\mathbf{B}^{\dagger} + \mathbf{R}_{v} \tag{C.9a}$$

where

$$\mathbf{R}_{a} = E\left[\mathbf{a}(k)\mathbf{a}^{\dagger}(k)\right] \tag{C.9b}$$

$$\mathbf{R}_{v} = E\left[\mathbf{v}(k)\mathbf{v}^{\dagger}(k)\right] \tag{C.9c}$$

$\mathbf{R}_{a}$ and $\mathbf{R}_{v}$ are defined as the spatial correlation matrices of the signal-in-space vector $\mathbf{a}(k)$, and the noise vector $\mathbf{v}(k)$ respectively. The structure of these matrices depends on the assumptions made about the signaling conditions. If all the elements of the noise vector $\mathbf{v}(k)$ are assumed to have a zero mean and an identical variance σ^2, then

$$\mathbf{R}_{v} = \sigma^{2}\mathbf{I} \tag{C.10}$$

where $\mathbf{I}$ is the identity matrix.

The structure of the spatial correlation matrix $\mathbf{R}_{a}$ depends whether there exists any correlation between the sources. If they are all uncorrelated or incoherent, $\mathbf{R}_{a}$ will be a diagonal matrix, i.e. all off-diagonal elements are zero. This will ensure that the spatial correlation matrix $\mathbf{R}$ is *Toeplitz*. On the other hand, if the sources are completely correlated or coherent, $\mathbf{R}$ is *non-Toeplitz*, and the received signal vector $\mathbf{s}$ is said to be spatially non-stationary.

APPENDIX D

FORMATION OF VECTOR d FOR KuTu ALGORITHM

The concept of signal and noise subspace eigenvectors of the array covariance matrix **R** was introduced in section 4.1.4 and the following matrices were formed

$$\mathbf{E}_S = \left[\mathbf{e}_1 \; \mathbf{e}_2 \; \cdots \; \mathbf{e}_M\right] \tag{D.1}$$

$$\mathbf{E}_N = \left[\mathbf{e}_{M+1} \; \mathbf{e}_{M+2} \; \cdots \; \mathbf{e}_N\right] \tag{D.2}$$

where $\mathbf{E}_S$ comprises of the M signal subspace eigenvectors and $\mathbf{E}_N$ comprises of the M-N noise subspace eigenvectors. $\mathbf{E}_S$ and $\mathbf{E}_N$ can then be partitioned as follows

$$\mathbf{E}_S = \begin{bmatrix} \mathbf{g}^T \\ \hdashline \mathbf{E}_S' \end{bmatrix} \tag{D.3}$$

$$\mathbf{E}_N = \begin{bmatrix} \mathbf{c}^T \\ \hdashline \mathbf{E}_N' \end{bmatrix} \tag{D.4}$$

where T denotes the transpose operation and **g** and **c** contain the first row of $\mathbf{E}_S$ and $\mathbf{E}_N$ respectively in column format. The rest of $\mathbf{E}_S$ and $\mathbf{E}_N$ are then included in the matrices $\mathbf{E}_S'$ and $\mathbf{E}_N'$. Since **d** is required to be orthogonal to the source direction vectors (equation (4.41)), it will lie in the noise subspace defined by $\mathbf{E}_N$ and consequently be orthogonal to the signal subspace eigenvectors. Hence, a vector **d** is required which satisfies the following equation

$$\mathbf{E}_S^{\dagger}\,\mathbf{d} = 0 \tag{D.5}$$

with † denoting the complex conjugate transpose. Substituting in equation (D.3) for $\mathbf{E}_S$, and remembering that the first element of **d** is set to

unity, it is possible to express equation (D.5) above as

$$\left[\begin{array}{c:c} \mathbf{g}^{*} & \mathbf{E}_{S}^{'\dagger} \end{array}\right] \left[\begin{array}{c} 1 \\ \hdashline \mathbf{d}^{'} \end{array}\right] = 0 \qquad \text{(D.6)}$$

with * denoting the complex conjugate operation. This can now be rewritten as follows

$$\mathbf{E}_{S}^{'\dagger}\,\mathbf{d}^{'} = -\mathbf{g}^{*} \qquad \text{(D.7)}$$

or, with a change of variable, more simply as

$$\mathbf{A}\,\mathbf{x} = \mathbf{b} \qquad \text{(D.8)}$$

Since **A** (which corresponds to $\mathbf{E}_{S}^{'\dagger}$) is a rectangular matrix of dimension M×(N-1) with rank(**A**) = M (M ≤ N-1), the solution to the above equation reduces to a *least squares problem*, i.e. finding a vector **x** which minimises the euclidean length of **Ax - b**. Kumaresan and Tufts employed the *pseudoinverse* approach [1] to this problem, i.e.

$$\mathbf{x} = \mathbf{A}^{+}\,\mathbf{b} \qquad \text{(D.9)}$$

where + denotes the pseudoinverse. The resulting N×1 vector **d** was shown to be given by

$$\mathbf{d} = \left[\begin{array}{c} 1 \\ \hdashline -\mathbf{E}_{S}^{'}\mathbf{g}^{*}/\left(1 - \mathbf{g}^{\dagger}\mathbf{g}\right) \end{array}\right] \qquad \text{(D.10)}$$

By exploiting the orthogonality that exists between the eigenvectors, it is possible to write

$$\mathbf{E}_{S}\mathbf{E}_{S}^{\dagger} + \mathbf{E}_{N}\mathbf{E}_{N}^{\dagger} = \mathbf{I} \qquad \text{(D.11)}$$

which can be expressed in the following form

$$\left[\begin{array}{c:c} \mathbf{g}^{T} & \mathbf{c}^{T} \\ \hdashline \mathbf{E}_{S}^{'} & \mathbf{E}_{N}^{'} \end{array}\right] \left[\begin{array}{c:c} \mathbf{g}^{*} & \mathbf{E}_{S}^{'\dagger} \\ \hdashline \mathbf{c}^{*} & \mathbf{E}_{N}^{'\dagger} \end{array}\right] = \mathbf{I} \qquad \text{(D.12)}$$

Hence,

$$\mathbf{c}^{\dagger}\mathbf{c} = 1 - \mathbf{g}^{\dagger}\mathbf{g} \tag{D.13}$$

$$\mathbf{E}_N'\mathbf{c}^{*} = -\mathbf{E}_S'\mathbf{g}^{*} \tag{D.14}$$

The alternative expression for **d** in terms of the noise subspace can now be written as

$$\mathbf{d} = \left[\frac{1}{\mathbf{E}_N'\mathbf{c}^{*} / \mathbf{c}^{\dagger}\mathbf{c}} \right] \tag{D.15}$$

REFERENCES

[1]: C.L. Lawson and R.J. Hanson, *"Solving Least Squares Problems"*, Prentice Hall, Inc., 1974.

APPENDIX E

SUMMARY OF ALGORITHMS FOR AOA ESTIMATION

Algorithm	Spatial Spectrum
Fourier Method (p 47)	$P_{FM}(\phi) = \mathbf{u}^{\dagger}\mathbf{R}\,\mathbf{u}$
Maximum Likelihood Method (p 51)	$P_{ML}(\phi) = \dfrac{1}{\mathbf{u}^{\dagger}\mathbf{R}^{-1}\mathbf{u}}$
Maximum Entropy Method (p 52)	$P_{ME}(\phi) = \dfrac{1}{\mathbf{u}^{\dagger}\mathbf{w}_o\mathbf{w}_o^{\dagger}\mathbf{u}}$
MUSIC Algorithm (p 57)	$P_{MU}(\phi) = \dfrac{1}{\mathbf{u}^{\dagger}\mathbf{E}_N\mathbf{E}_N^{\dagger}\mathbf{u}}$
JoDeG Algorithm (p 59)	$P_{JO}(\phi) = \dfrac{1}{\sum_{i=M+1}^{N} \frac{1}{\lambda_i} \lvert\mathbf{u}^{\dagger}\mathbf{e}_i\rvert^2}$
KuTu Algorithm (p 61)	$P_{KU}(\phi) = \dfrac{1}{\lvert\mathbf{u}^{\dagger}\mathbf{d}\rvert^2}$

The basic steering or weight vector **u** is defined as

$$\mathbf{u} = \left[\, 1 \;\; exp(j\phi) \;\; exp(j2\phi) \;\; exp(j3\phi) \;\; \cdots\cdots \;\; exp(j(N-1)\phi) \,\right]^{T}$$

APPENDIX F

CALCULATION OF MUTUAL IMPEDANCE MATRIX FOR AN ANTENNA ARRAY

The approach followed by Gupta and Ksienski [1] was adopted with the N element antenna array being represented by an N+1 terminal linear, bilateral network responding to an outside source as shown in figure F.1. Each of the N antenna ports is terminated in a known load impedance Z_L, and the driving source generator has an open circuit voltage V_g and an internal impedance Z_g. Hence, by applying Kirchoffs law the output voltage at each of the N antenna ports can be written as

$$\begin{aligned}
v_1 &= i_1 Z_{11} + \cdots + i_j Z_{1j} + \cdots + i_N Z_{1N} + i_s Z_{1s} \\
&\vdots \\
v_j &= i_1 Z_{j1} + \cdots + i_j Z_{jj} + \cdots + i_N Z_{jN} + i_s Z_{js} \\
&\vdots \\
v_N &= i_1 Z_{N1} + \cdots + i_j Z_{Nj} + \cdots + i_N Z_{NN} + i_s Z_{Ns}
\end{aligned} \qquad \text{(F.1)}$$

where Z_{ij} represents the mutual impedance between the ports i and j, i.e. between the antenna elements. The current at each of the antenna ports can then be expressed as

$$i_j = -\frac{v_j}{Z_L} \qquad j=1,\cdots,N \qquad \text{(F.2)}$$

If all the antennas are open circuited then $i_j = 0$ $(j=1,\cdots,N)$ and, from the expressions in equation (F.1), the antenna output voltage becomes

$$v_j = v_{oj} = i_s Z_{js} \qquad j=1,\cdots,N \qquad \text{(F.3)}$$

Substituting equations (F.2) and (F.3) into equation (F.1), and using vector and matrix notation, it is possible to write

$$\begin{bmatrix} \left(1 + \frac{Z_{11}}{Z_L}\right) & \frac{Z_{12}}{Z_L} & \cdots & \frac{Z_{1N}}{Z_L} \\ \frac{Z_{21}}{Z_L} & \left(1 + \frac{Z_{22}}{Z_L}\right) & \cdots & \frac{Z_{2N}}{Z_L} \\ \vdots & & & \vdots \\ \frac{Z_{N1}}{Z_L} & \frac{Z_{N2}}{Z_L} & \cdots & \left(1 + \frac{Z_{NN}}{Z_L}\right) \end{bmatrix} \begin{bmatrix} v_1 \\ v_2 \\ \vdots \\ v_N \end{bmatrix} = \begin{bmatrix} v_{o1} \\ v_{o2} \\ \vdots \\ v_{oN} \end{bmatrix} \qquad \text{(F.4)}$$

which can be expressed more compactly as

$$\mathbf{Z_o v} = \mathbf{v_o} \qquad \text{(F.5)}$$

where $\mathbf{Z_o}$ represents the normalised impedance matrix, and $\mathbf{v}$ and $\mathbf{v_o}$ are N×1 vectors representing the output voltages and open circuit voltages respectively. Hence, the output voltage across the array when mutual coupling is taken into account can be expressed as

$$\mathbf{v} = \mathbf{Z_o^{-1} v_o} \qquad \text{(F.6)}$$

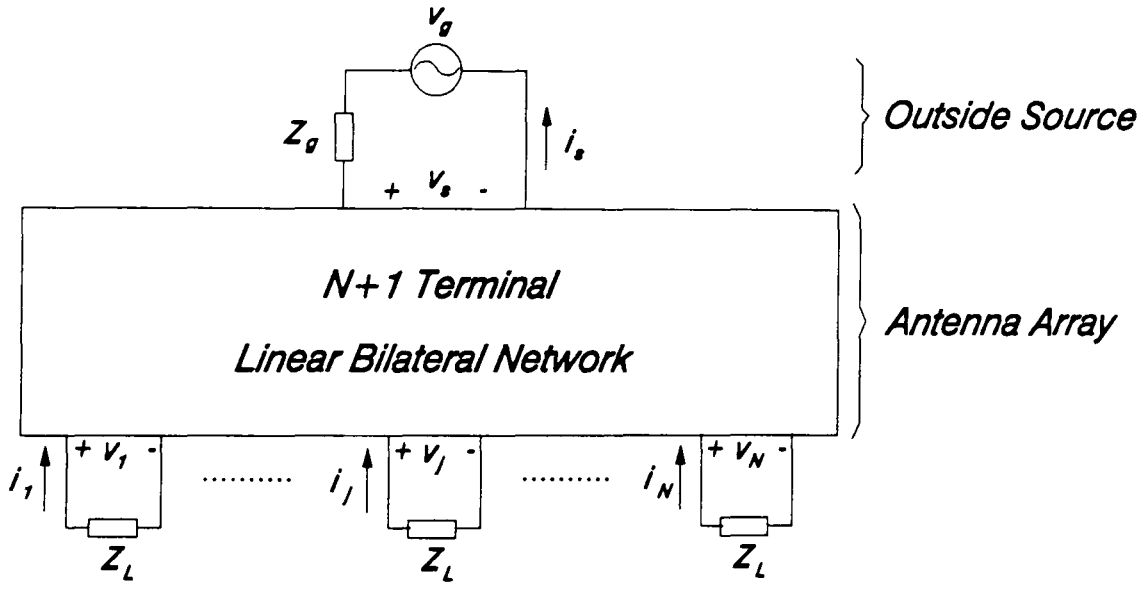

Figure F.1: Representation of an antenna array.

REFERENCES

[1]: I.J. Gupta and A.A. Ksienski, *"Effect of Mutual Coupling on the Performance of Adaptive Arrays"*, IEEE Transactions on Antennas & Propagation, Vol.AP-31, No.5, Sept. 1983, pp.785-791.

APPENDIX G

FORWARD/BACKWARD SPATIAL SMOOTHING FOR AOA ESTIMATION IN A DISCRETE MULTIPATH ENVIRONMENT

G.1 Coherent Signal Identification

The degree of correlation that exists between the signal sources incident onto the array is reflected directly in the structure of the array covariance matrix $\mathbf{R}_a$. Consequently, $\mathbf{R}_a$ will be diagonal and non-singular only if the signals are all uncorrelated. When they are only partially correlated, $\mathbf{R}_a$ will become non-diagonal but will remain non-singular, only becoming singular if any of the sources are fully correlated (or coherent). Hence, the presence of multipath reflections with a high degree of correlation with the wanted signal will strongly affect the performance of the DF techniques. In order to understand how this comes about, consider M sources incident onto an N element array as before, but let two of them be coherent, e.g. $a_2(k) = \rho a_1(k)$, where ρ is a complex scalar. The observed signal vector across the array is given by equation (C.6a) in Appendix C as

$$\mathbf{x}(k) = \mathbf{B}\mathbf{a}(k) + \mathbf{v}(k) \tag{G.1}$$

where k represents the sampling instant. $\mathbf{B}$ is the N×M direction matrix containing the direction vectors $\mathbf{b}(\theta_m)$ for each of the M sources incident onto the array, $\mathbf{a}(k)$ is the M×1 signal-in-space vector and $\mathbf{v}(k)$ contains the additive sensor noise. The array covariance matrix is then given by

$$\begin{aligned} \mathbf{R} &= E\left[\mathbf{x}(k)\cdot\mathbf{x}^{\dagger}(k)\right] \\ &= \mathbf{B}\mathbf{R}_a\mathbf{B}^{\dagger} + \mathbf{R}_v \end{aligned} \tag{G.2}$$

where $\mathbf{R}_v$ is the noise covariance matrix (often approximated by $\sigma^2\mathbf{I}$) and $\mathbf{R}_a = E\left[\mathbf{a}(k)\cdot\mathbf{a}^{\dagger}(k)\right]$ is the M×M source covariance matrix ($\dagger$ denoting the complex conjugate transpose operation). With two coherent sources however, the signal-in-space vector $\mathbf{a}(k)$, defined in equation (C.6b), can be written as the (M-1)×1 vector

$$\mathbf{a}(k) = \left[a_1(k),\ a_3(k),\ \cdots,\ a_M(k)\right]^T \qquad (G.3)$$

and, the direction matrix **B** as the N×(M-1) matrix

$$\mathbf{B} = \left[\left(\mathbf{b}(\theta_1) + \rho\mathbf{b}(\theta_2)\right),\ \mathbf{b}(\theta_3),\ \cdots,\ \mathbf{b}(\theta_M)\right] \qquad (G.4)$$

Hence, using the modified source vector given in equation (G.3) above, $\mathbf{R}_a$ can be written as a (M-1)×(M-1) non-singular matrix instead of a M×M singular matrix. This ensures that $\mathbf{BR}_a\mathbf{B}^\dagger$ will be of rank M-1 and, referring to the description of the eigenstructure DF techniques given in chapter 4, the smallest eigenvalue of **R** will have a multiplicity of N-(M-1) as opposed to (N-M) for the uncorrelated case. Hence the number of signals detected is reduced by one and, since only the direction vectors corresponding to $\{\theta_3, \cdots, \theta_M\}$ are in the so called signal subspace (no linear combination of two direction vectors will yield another valid direction vector), only these sources will successfully be resolved. In general terms, if there are M_c coherent sources out of the total M, application of any of the eigenstructure techniques will produce the incorrect result since, of the $(M-M_c)+1$ sources detected, only the $(M-M_c)$ bearings corresponding to the incoherent sources will be detected.

G.2 The Spatial Smoothing Technique

The principle behind the spatial smoothing technique is to preprocess the received data by partitioning the total array into subarrays, and to then form the overall array covariance matrix as the average of all the subarray covariance matrices. Consider splitting the complete N element array into L subarrays in both the forward and backward directions as depicted in figure G.1. If each subarray contains N_s elements, the total number of subarrays L satisfies the following expression

$$L = N - N_s + 1 \qquad (G.5)$$

The signal vector observed at each of the forward subarrays (denoted by the superscript f) is given by

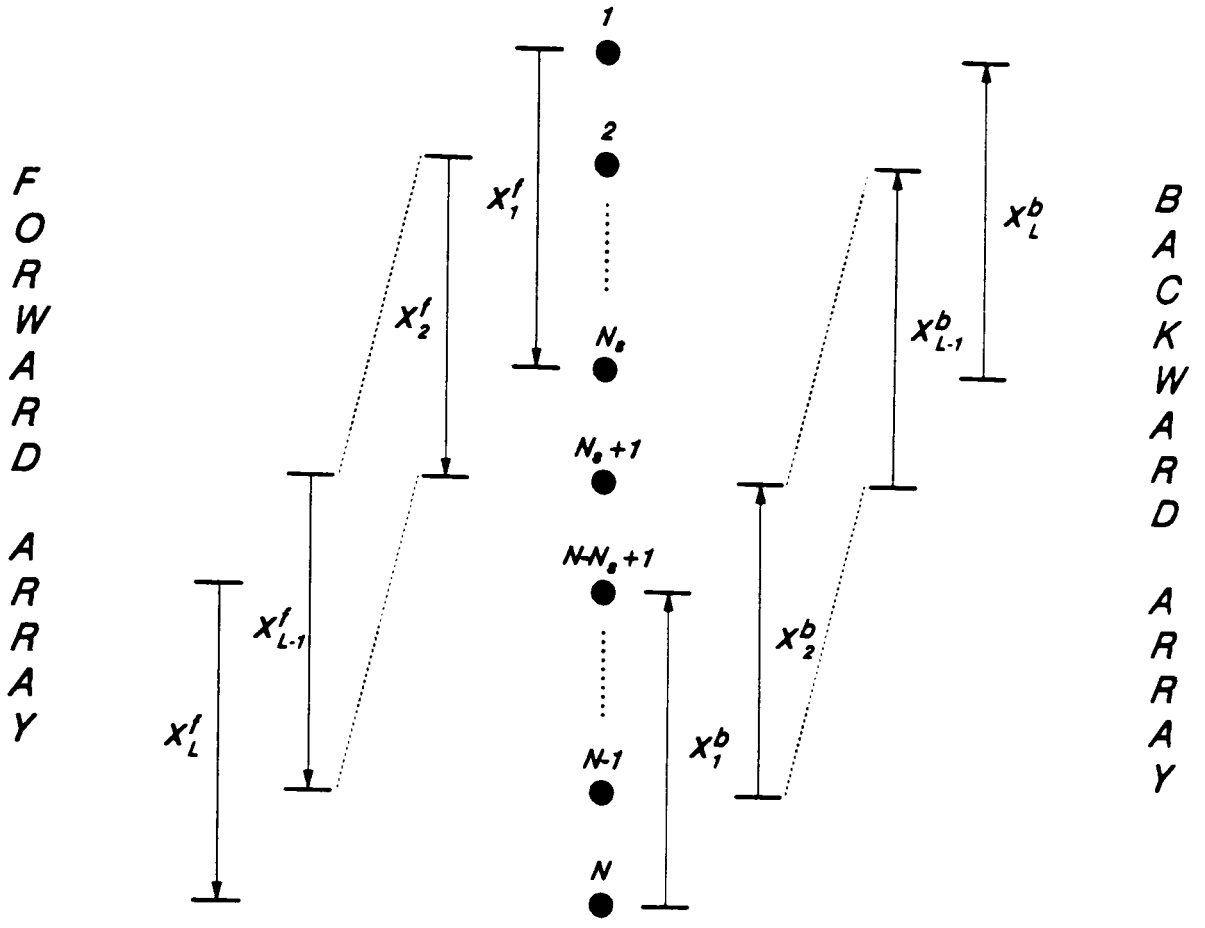

Figure G.1: Forward/backward subarraying.

$$\mathbf{x}_l^f(k) = \mathbf{B}\mathbf{D}^{l-1}\mathbf{a}(k) + \mathbf{v}_l(k) \qquad l=1,\cdots,L \tag{G.6}$$

where $\mathbf{D}^{l-1}$ denotes the (l-1)th power of the M×M matrix

$$\mathbf{D} = diag\left\{ \exp(j\phi_1)\ \exp(j\phi_2)\ \cdots\cdots\ \exp(j\phi_M) \right\} \tag{G.7}$$

Note that $\mathbf{B}$ is the $N_s \times M$ direction matrix defined now for the subarray, and multiplication of the signal vector $\mathbf{a}(k)$ by $\mathbf{D}^{l-1}$ ensures that the phase of each source is correct with respect to the phase reference (element number one in this case). The covariance matrix of the lth subarray then becomes

$$\begin{aligned} \mathbf{R}_l^f &= E\left[\mathbf{x}_l^f(k) \cdot \left(\mathbf{x}_l^f(k)\right)^\dagger \right] \\ &= \mathbf{B}\mathbf{D}^{l-1}\mathbf{R}_a\left(\mathbf{D}^{l-1}\right)^\dagger\mathbf{B}^\dagger + \mathbf{R}_v \end{aligned} \tag{G.8}$$

The forward only spatially smoothed covariance matrix is then the mean of the forward subarray covariance matrices and is expressed as

$$\mathbf{R}^f = \frac{1}{L}\sum_{l=1}^{L}\mathbf{R}_l^f$$

$$= \mathbf{B}\mathbf{R}_a^f\mathbf{B} + \sigma^2\mathbf{I} \qquad \text{(G.9)}$$

where the modified source covariance matrix is given by

$$\mathbf{R}_a^f = \frac{1}{L}\sum_{l=1}^{L}\mathbf{D}^{l-1}\mathbf{R}_a\left(\mathbf{D}^{l-1}\right)^{\dagger} \qquad \text{(G.10)}$$

An alternative approach is to consider the L backward arrays (denoted by the superscript b) illustrated in figure G.1. Hence, the complex conjugate of the observed signal vector for each array becomes

$$\mathbf{x}_l^b(k) = \mathbf{B}\mathbf{D}^{l-1}\left(\mathbf{D}^{N-1}\mathbf{a}(k)\right)^{*} + \mathbf{v}_l^{*}(k) \qquad l=1,\cdots,L \qquad \text{(G.11)}$$

and the covariance matrix of the lth backward subarray is given by

$$\mathbf{R}_l^b = E\left[\ \mathbf{x}_l^b(k)\cdot\left(\mathbf{x}_l^b(k)\right)^{\dagger}\ \right]$$

$$= \mathbf{B}\mathbf{D}^{l-1}\mathbf{R}_a^{'}\left(\mathbf{D}^{l-1}\right)^{\dagger}\mathbf{B}^{\dagger} + \mathbf{R}_v \qquad \text{(G.12)}$$

where

$$\mathbf{R}_a^{'} = \mathbf{D}^{-(N-1)}E\left[\mathbf{a}^{*}(k)\cdot\mathbf{a}^{T}(k)\right]\left(\mathbf{D}^{-(N-1)}\right)^{\dagger}$$

$$= \mathbf{D}^{-(N-1)}\mathbf{R}_a^{*}\left(\mathbf{D}^{-(N-1)}\right)^{\dagger} \qquad \text{(G.13)}$$

T and * denoting the transpose and complex conjugate operations in the normal way. Hence, in the same manner as for the forward only case, the backward spatially smoothed covariance matrix is given by

$$\mathbf{R}^b = \frac{1}{L}\sum_{l=1}^{L}\mathbf{R}_l^b$$

$$= \mathbf{B}\mathbf{R}_a^b\mathbf{B} + \sigma^2\mathbf{I} \qquad \text{(G.14)}$$

where the modified source covariance matrix is given by

$$\mathbf{R}_a^b = \frac{1}{L}\sum_{l=1}^{L} \mathbf{D}^{l-1}\mathbf{R}_a'\left(\mathbf{D}^{l-1}\right)^{\dagger} \qquad (G.15)$$

If the number of subarrays L is greater than or equal to the number of signals M ($L \geq M$), then the modified source covariance matrices $\mathbf{R}_a^f$ and $\mathbf{R}_a^b$, given in equations (G.10) and (G.15), will be non-singular regardless of the coherence of the signals (detailed proofs of this statement can be found in the referenced literature). Hence, by employing either the forward or backward spatial smoothing techniques, the eigenstructure DF algorithms can successfully resolve any coherent signal sources. The penalty for this improved resolution is a reduction in the available array degrees of freedom (DOF). Normally an N element array can successfully resolve up to N-1 uncorrelated signal sources but, by employing one of the above spatial smoothing techniques, this is reduced to a maximum of N/2 sources. This follows from the condition that $L \geq M$ and by recognising that the size of each subarray N_s must be at least one greater than the number of sources, i.e. $N_s \geq M+1$.

In order to increase the available degrees of freedom, the forward and backward subarray smoothing techniques can be combined as follows

$$\mathbf{R}^{fb} = \frac{\mathbf{R}^f + \mathbf{R}^b}{2}$$

$$= \mathbf{B}\mathbf{R}_a^{fb}\mathbf{B}^{\dagger} + \sigma^2\mathbf{I} \qquad (G.16)$$

where

$$\mathbf{R}_a^{fb} = \frac{1}{2}\left(\mathbf{R}_a^f + \mathbf{R}_a^b\right) \qquad (G.17)$$

gives the forward/backward smoothed source covariance matrix. It can be shown that the modified source covariance matrix, given by equation (G.17) above, will be non-singular regardless of the coherence of the M signal sources so long as $2L \geq M$. Hence, the array can potentially resolve up to 2N/3 signal sources. Table G.1 below includes a summary of all of the above results.

Smoothing Technique	Conditions	Available DOF
FORWARD	L ≥ M	N/2
BACKWARD	L ≥ M	N/2
F/B	2L ≥ M	2N/3

Table G.1: Properties of spatial smoothing techniques.

APPENDIX H

EXTENSION OF BASIC SIGNAL MODEL FOR MULTIPLE SOURCES IN AN FDMA COMMUNICATIONS SCHEME

In order to simulate an FDMA communications scheme, consider a number of narrowband sources M, each allocated a unique frequency $w_1,\cdots,w_M$ representing the communications channel. As before, the receiving array comprises of N elements, but now with a tapped delay line behind each element with P taps as shown in figure H.1 below.

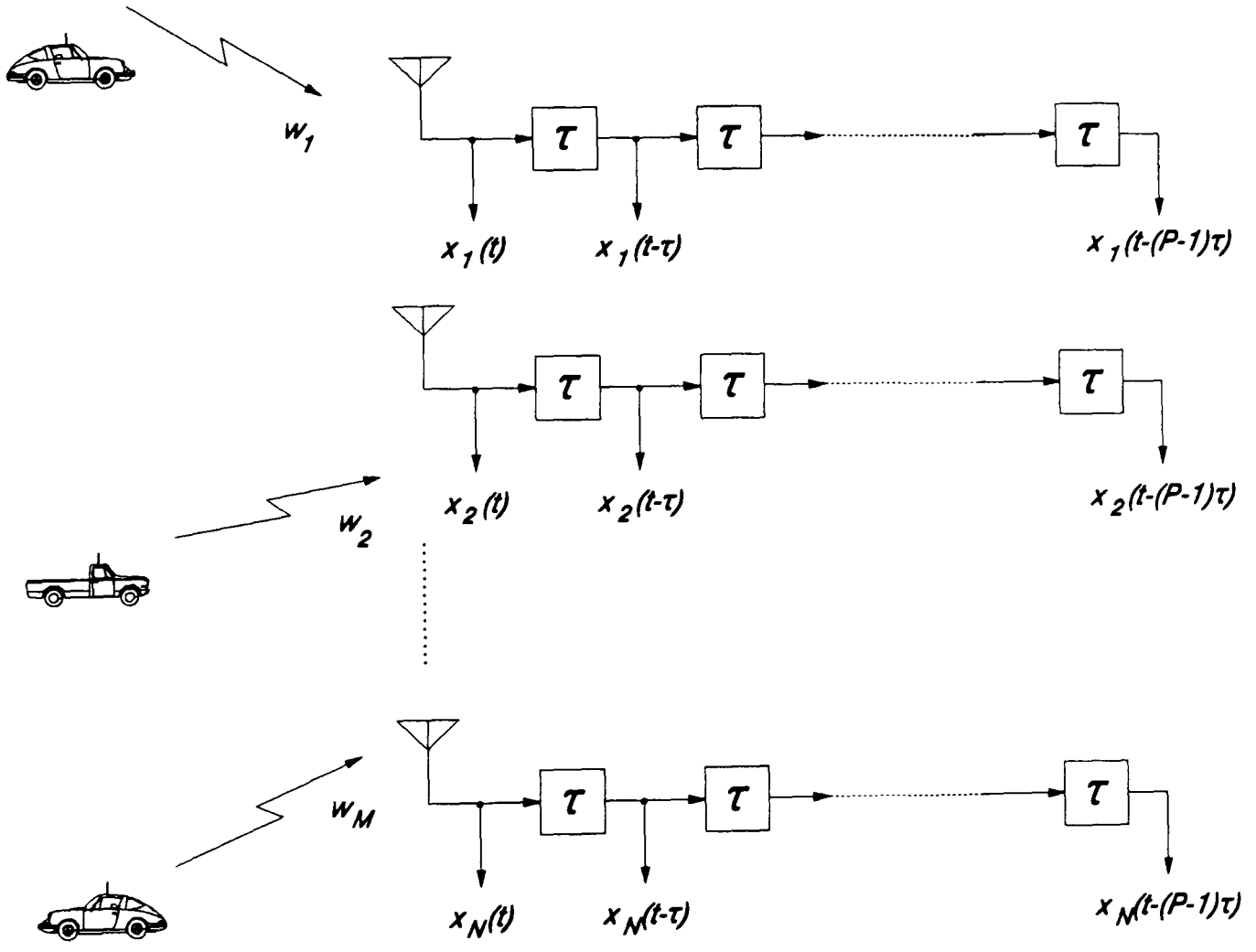

Figure H.1: An antenna array with a tapped delay line.

Using the notation already developed in Appendix C, the signal observed at the pth tap of the nth sensor can be expressed as

$$x_n\left(t-(p-1)\tau\right) = \sum_{m=1}^{M} s_{nm}\left(t-(p-1)\tau\right) + v_n\left(t-(p-1)\tau\right) \qquad \text{(H.1)}$$

where $s_{nm}(t)$ is the signal produced at the nth sensor by the mth source (defined in Appendix C, equation (C.1)) and $v_n(t)$ is the additive noise at the nth sensor. Adopting the complex notation as before, equation (H.1) can be expressed as

$$x_n\left(t-(p-1)\tau\right) = \sum_{m=1}^{M} a_m exp\left[j(n-1)\phi_m\right] exp\left[-j(p-1)w_m\tau\right] + v_n\left(t-(p-1)\tau\right) \qquad \text{(H.2)}$$

with the time delay represented as a phase shift (a valid approximation with narrowband sources). The inter element phase shift is defined by ϕ_m and, for a linear array with the elements spaced a distance d apart, is given by

$$\phi_m = \frac{2\Pi d}{\lambda_m} \sin \theta_m$$

$$= w_m \frac{d}{c} \sin \theta_m \qquad \text{(H.3)}$$

where c = speed of light. If it is assumed that the received signals are sampled simultaneously at time instants denoted by k (k = 1,···,K), each snapshot of data will consist of NP components $x_{np}(k)$ (n = 1,···,N; p = 1,···,P). Consider first of all only the components associated with the nth sensor and place them in a P×1 vector as follows

$$\mathbf{x}_n(k) = \mathbf{B}_n\mathbf{a}(k) + \mathbf{v}_n(k) \qquad \text{(H.4a)}$$

where $\mathbf{x}_n(k)$ and $\mathbf{v}_n(k)$ are the P×1 vectors

$$\mathbf{x}_n(k) = \left[x_n(t),\cdots,x_n\left(t-(p-1)\tau\right)\right]^T \qquad \text{(H.4b)}$$

$$\mathbf{v}_n(k) = \left[v_n(t),\cdots,v_n\left(t-(p-1)\tau\right)\right]^T \qquad \text{(H.4c)}$$

and $\mathbf{a}(k)$ is the M×1 signal-in-space vector

$$\mathbf{a}(k) = \left[\mathbf{a}_1(k), \cdots, \mathbf{a}_M(k)\right]^T \tag{H.4d}$$

$\mathbf{B}_n$ is the P×M direction matrix for the nth sensor and is given by

$$\mathbf{B}_n = \begin{bmatrix} exp\left(j(n-1)\phi_1\right) & \cdots & exp\left(j(n-1)\phi_M\right) \\ exp\left(j(n-1)\phi_1\right)exp\left(-jw_1\tau\right) & & exp\left(j(n-1)\phi_M\right)exp\left(-jw_M\tau\right) \\ \vdots & & \vdots \\ exp\left(j(n-1)\phi_1\right)exp\left(-j(P-1)w_1\tau\right) & \cdots & exp\left(j(n-1)\phi_M\right)exp\left(-j(P-1)w_M\tau\right) \end{bmatrix} \tag{H.4}$$

The N (P×1) vectors $\mathbf{x}_n(k)$ can now be placed in a single NP×1 vector, enabling the complete observed signal vector at sampling instant k to be written as

$$\mathbf{x}(k) = \mathbf{B}\mathbf{a}(k) + \mathbf{v}(k) \qquad k=1, \cdots K \tag{H.5a}$$

This is equivalent to equation (C.6a) given in Appendix C for the one dimensional case, except that $\mathbf{x}(k)$ and $\mathbf{v}(k)$ are now the NP×1 vectors

$$\mathbf{x}(k) = \left[\mathbf{x}_1(k), \cdots, \mathbf{x}_N(k)\right]^T \tag{H.5b}$$

$$\mathbf{v}(k) = \left[\mathbf{v}_1(t), \cdots, \mathbf{v}_N(k)\right]^T \tag{H.5c}$$

and $\mathbf{B}$ is the NP×M direction matrix

$$\mathbf{B} = \begin{bmatrix} \mathbf{B}_1 \\ \mathbf{B}_2 \\ \vdots \\ \mathbf{B}_N \end{bmatrix} \tag{H.5d}$$

where, as before, each column of $\mathbf{B}$ defines the NP×1 direction vector $\mathbf{b}\left(\theta_m, w_m\right)$ associated with each signal source. The covariance matrix is then given in the usual way by

$$\mathbf{R} = E\left[\mathbf{x}(k)\cdot\mathbf{x}^{\dagger}(k)\right] \tag{H.6}$$

which can be expressed as

$$\mathbf{R} = \mathbf{B}\mathbf{R}_{a}\mathbf{B}^{\dagger} + \mathbf{R}_{v} \tag{H.7a}$$

where

$$\mathbf{R}_{a} = E\left[\mathbf{a}(k)\cdot\mathbf{a}^{\dagger}(k)\right] \tag{H.7b}$$

$$\mathbf{R}_{v} = E\left[\mathbf{v}(k)\cdot\mathbf{v}^{\dagger}(k)\right] \tag{H.7c}$$

are the signal and noise covariance matrices respectively. If it is assumed that the noise is spatially and temporally white, with zero mean and variance σ^2, it can be represented, as before, by $\sigma^2\mathbf{I}$.

In order to simulate an FDMA scheme, the received signal vector for the mth source at the pth tap of the nth sensor can be written as

$$s_{nmp}(k) = a_{m}(k)\cdot exp\left[j\left((n-1)\phi_{m} - (p-1)w_{m}\tau\right)\right] \tag{H.8}$$

If the phase shift associated with each delay tap is equivalent to the phase shift between adjacent elements in an array when a signal at the centre frequency of the sources, w_o, is incident from $\theta = 90^{\circ}$, i.e.

$$w_{o}\tau = \frac{2\Pi d}{\lambda_{o}} = w_{o}\frac{d}{c}$$

$$\Rightarrow \quad \tau = \frac{d}{c} \tag{H.9}$$

then equation (H.8) can be rewritten as

$$s_{nmp}(k) = a_{m}(k)\cdot exp\left[j\left((n-1)w_{m}(d/c)sin\theta_{m} - (p-1)w_{m}(d/c)\right)\right]$$

$$= a_{m}(k)\cdot exp\left[jw_{m}(d/c)\left((n-1)sin\theta_{m} - (p-1)\right)\right] \tag{H.10}$$

Each source has a unique frequency channel allocation which can be expressed as a function of the centre frequency w_o of the system and the channel spacing

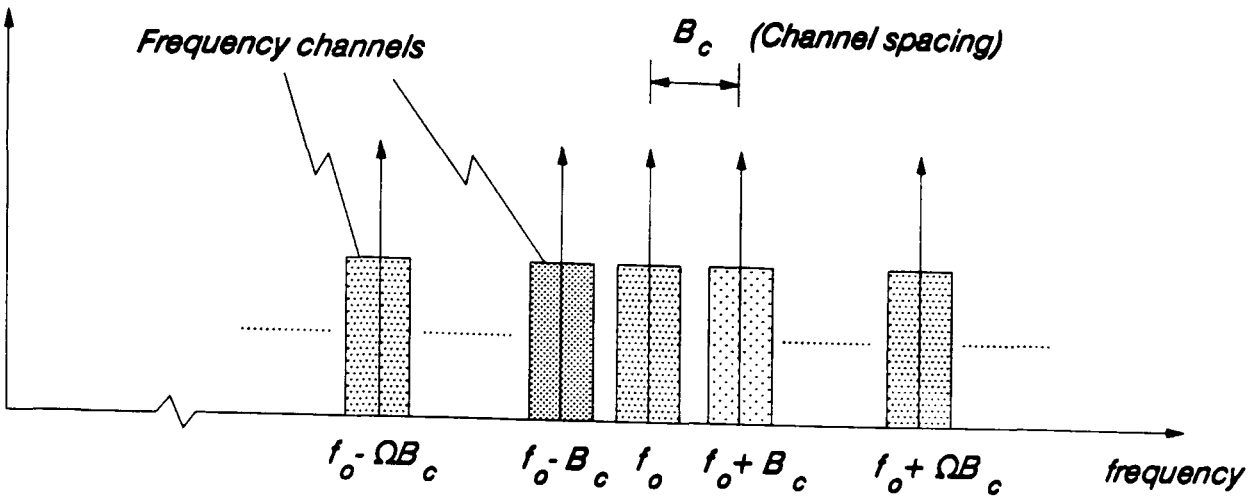

Figure H.2: Channel allocation for an FDMA type scheme.

$$w_m = w_o \pm \Omega 2\Pi B_c$$

$$= 2\Pi f_o \left(1 \pm \Omega \frac{B_c}{f_o}\right) \qquad \text{(H.11)}$$

where B_c is the channel spacing and Ω is the channel number as depicted in figure H.2. Hence equation (H.10) can be expressed as

$$s_{nmp}(k) = a_m(k) \cdot exp\left[j2\Pi f_o \left(1 \pm \Omega \frac{B_c}{f_o}\right)(d/c)\left((n-1)sin\theta_m - (p-1)\right)\right]$$

$$= a_m(k) \cdot exp\left[j\frac{2\Pi d}{\lambda_o}\left(1 \pm \Omega \frac{B_c}{f_o}\right)\left((n-1)sin\theta_m - (p-1)\right)\right] \qquad \text{(H.12)}$$

An FDMA type scheme can now be set up which is defined by the ratio of the channel spacing B_c to the centre frequency f_o. The inter element spacing d is usually expressed as a fraction of the wavelength at the centre frequency and is typically $0.5\lambda_0$.

The estimation of the eigenstructure of the sampled covariance matrix $\hat{\mathbf{R}}$ and the number of sources M proceeds as before for the algorithms described in section 4.1.4. The orthogonality of the noise subspace eigenvectors E_N with the source direction vectors is then exploited to form the spatial estimate, i.e.

$$P_{2D}(\phi,w) = \frac{|u^{\dagger}u|}{\frac{1}{NP-M}\cdot\sum_{i=M+1}^{N}|u^{\dagger}e_i|^2} \qquad \text{(H.13)}$$

where u is the ideal NP×1 steering vector and is given by

$$u = \begin{bmatrix} 1 \\ \vdots \\ exp\left(-j(P-1)w\tau\right) \\ exp\left(j\phi\right) \\ \vdots \\ exp\left(j\phi\right)exp\left(-j(P-1)w\tau\right) \\ \vdots \\ exp\left(j(N-1)\right) \\ \vdots \\ exp\left(j(N-1)\phi\right)exp\left(-j(P-1)w\tau\right) \end{bmatrix} \qquad \text{(H.14)}$$

The angles of arrival of the sources θ_m and their corresponding centre frequencies w_m are then determined by the highest peaks of the 2D function given in equation (H.13) above. In the paper of Wax *et al* [1], different estimators were also given, but for the purposes of this piece of work only the above estimate, corresponding to the "arithmetic mean metric" in [1], will be employed. The maximum number of sources that can be handled is NP-1, although the maximum number of co-frequency sources is N-1 as before.

REFERENCES

[1]: M. Wax, T.J. Shan and T. Kailath, *"Spatio-Temporal Spectral Analysis by Eigenstructure Methods"*, IEEE Transactions on Acoustics, Speech & Signal Processing, Vol.ASSP-32, No.4, Aug. 1984, pp.817-827.

APPENDIX I

CALCULATION OF SIGNAL-TO-NOISE RATIO AT RECEIVER INPUT

The ratio of the received signal power to the transmitted power defined in section 6.1 is given by

$$\frac{P_R}{P_T} = G_T G_R \left(\frac{\lambda}{4\pi R}\right)^2$$

$$= \frac{G_T G_R}{L_{FS}} \qquad \text{(I.1)}$$

where $L_{FS} = \left((4\pi R)/\lambda\right)^2$ is the free space loss. In reality additional losses are also present, therefore the total loss will be expressed as $L = L_{FS} \times L_A$, where L_A defines the additional losses. The ratio of the received signal power to the noise power in the receiver bandwidth can then be expressed as

$$\frac{P_R}{N} = \frac{P_T G_T G_R}{LkTB_{IF}} \qquad \text{(I.2)}$$

where the total noise power is given by

$$N = kTB_{IF} \qquad \text{(I.3)}$$

where k is the Boltzmann constant, B_{IF} is the noise equivalent bandwidth of the receiver as defined by the IF amplifier ($\cong$ 4 MHz), and T represents the total noise temperature at the receiver input. Figure I.1 shows a schematic of the receiver front end, and includes the relevant parameters for the calculation of the total noise temperature T. Each block has associated with it a signal gain (or loss when considering the cable), and an effective input noise temperature which defines the noise contribution to the signal of that block. The noise figure is another frequently used quantity which gives a measure of the degradation in the signal-to-noise ratio between the input and output of the device or network and is calculated directly from the noise temperature. The total noise temperature at the receiver input is calculated from the following equation [1]

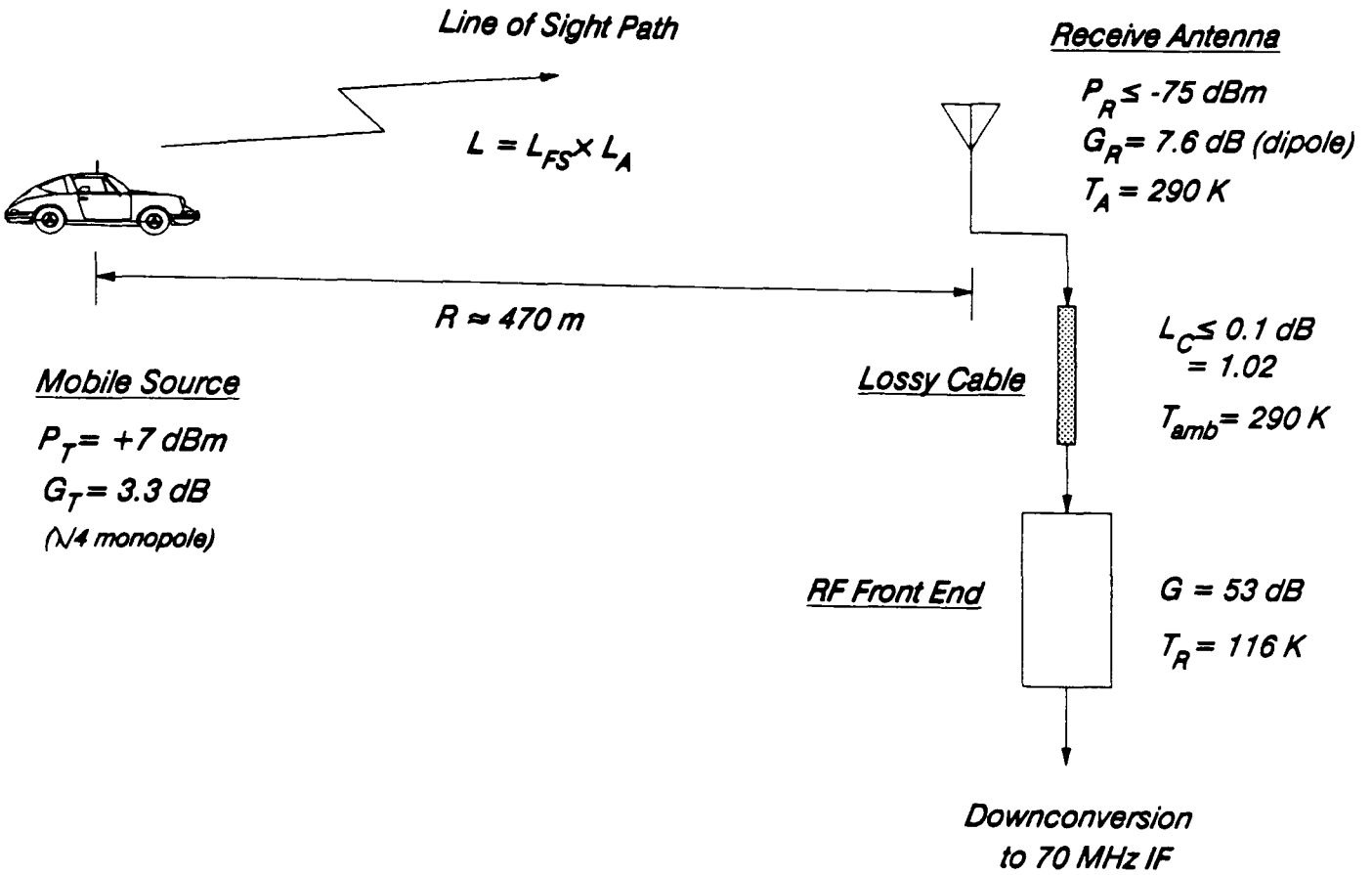

Figure I.1: Parameters for the calculation of the input SNR.

$$T = T_A/L_C + T_{amb}\left(1 - 1/L_C\right) + T_R \qquad (I.4)$$

where T_{amb} is the ambient temperature which will be close to 290 K in this case. L_C is the loss associated with the cable connecting the antenna to the LNA and, as can be seen from equation (I.4), has a strong influence on the overall noise performance of the receiver and so is ideally kept to a minimum. The noise figure for the RF front end of each channel was measured and the results are included in table 6.1 in section 6.1. As can be seen, Channel D has the worst noise performance with a noise figure of 1.5 dB, corresponding to an effective input noise temperature of 116 K. If it is assumed that the antenna temperature T_A is 290 K, the overall receiver noise temperature is calculated as

$$T = 283.5 + 6.5 + 116$$
$$= 406\ K \qquad (I.5)$$

From equation (I.2), the received signal power to noise power spectral density N_o (N/B_{IF}) can be expressed in decibels as

$$\left(\frac{P_R}{N_o}\right)_{dBHz} = 10log P_T G_T - 20log\frac{4\pi R}{\lambda} + 10log\frac{G_R}{T} - 10log L_A - 10log k \qquad (I6)$$

When the A/D converters are being driven with ±4 volts, the received signal power can be assumed to be approximately -75 dBm. Hence, combining the first four terms from equation (I.6) above and substituting in the value for the total noise temperature T, the signal power to noise power spectral density can be calculated as follows:

$$\left(\frac{P_R}{N_o}\right)_{dBHz} = \underset{10\log P_R}{-105} - \underset{10\log\frac{1}{T}}{26.1} + \underset{10\log k}{228.6} = 97.5 \text{ dBHz} \qquad (I.7)$$

Therefore, the received signal-to-noise ratio within the receiver bandwidth (set equal to the bandwidth of the IF stage, i.e. ≅ 4 MHz) is given as

$$SNR \cong 31 \text{ dB} \qquad (I.8)$$

If the digitisers are driven with a ± 4 volts signal, the received signal power is approximately -75 dBm and the corresponding thermal noise level within the IF bandwidth is then -106 dBm. This is rather an optimistic value since many additional losses have been ignored in the calculation. For a more thorough treatment of this subject please refer to the text of Maral and Bousquet [1].

REFERENCES

[1]: G. Maral and M. Bousquet, *"Satellite Communications Systems"*, John Wiley & Sons, 1986.

APPENDIX J

LIST OF PUBLICATIONS

1. S.C. Swales, M.A. Beach, D.J. Edwards and J.P. McGeehan, **"The Performance Enhancement of Multi-Beam Adaptive Base-Station Antennas for Cellular Land Mobile Radio Systems"**, IEEE Transactions on Vehicular Technology, Vol.VT-39, No.1, Feb. 1990, pp.56-67.

2. S.C. Swales, M.A. Beach and D.J. Edwards, **"Adaptive Antenna Arrays for Future Generation Cellular Communications Networks"**, IEE Sixth International Conference on Antennas & Propagation, ICAP89, University of Warwick, England, 4th - 7th April 1989, pp.312-325.

3. S.C. Swales, M.A. Beach and D.J. Edwards, **"Multi-Beam Adaptive Base-Station Antennas for Cellular Land Mobile Radio Systems"**, 39th IEEE Vehicular Technology Conference, San Francisco, USA, 1st - 3rd May 1989, pp.341-348.

4. S.C. Swales, M.A. Beach, D.J. Edwards and J.P. McGeehan, **"A Multi-Beam Adaptive Base-Station Antenna for Cellular land Mobile Radio"**, Proceedings of 1989 Workshop on Mobile & Cordless Telephone Communications, Kings College - University of London, England, Sept. 1989, pp.55-61.

5. S.C. Swales, M.A. Beach, D.J. Edwards and J.P. McGeehan, **"The Realisation of a Multi-Beam Adaptive Base-Station Antenna for Cellular Land Mobile Radio Systems"**, IEE Fifth International Conference on Mobile Radio & Personal Communications, MRPC89, University of Warwick, England, 11th - 14th Dec. 1989. (Not bound in proceedings.)

6. S.C. Swales and M.A. Beach, **"Direction Finding in the Cellular Land Mobile Radio Environment"**, IEE Fifth International Conference on Radio Receivers & Associated Systems, RRAS90, University of Cambridge, England, 23rd - 27th July 1990, pp.192-196.